

Novel Applications of Paleometabolomics and Stable Isotope
Ratios to Archaeobotanical Maize

Isabella Rose Gaffney

PhD

University of York

Chemistry

January 2022

Abstract

Understanding how crops responded to drought stress in the past is increasingly important due to climate change. This thesis explores applications of stable isotope ratio analysis and paleometabolomics to archaeological maize cobs from Tularosa Cave, New Mexico, cultivated during two different climate regimes (wet ca. 1800 cal BP and dry ca. 700 cal BP). Attenuated total reflectance Fourier-transform infrared spectroscopy and elemental analysis have shown that the archaeological samples have good preservation across the age range.

Archaeological maize cobs from Tularosa Cave were distinguished through $\delta^{15}\text{N}$ measurements of bulk material and individual amino acids (AAs). These findings complement previous paleogenomic analysis of Tularosa maize cobs suggesting selection for drought resistance-related genes.

Lyophilisation was shown to stabilise the maize extractable metabolome, increasing throughput and efficiency of extraction of the metabolome for analysis over more traditional tissue processing in liquid nitrogen. The lyophilisation approach was taken to explore the effect of drought upon the maize metabolome in a untargeted high resolution mass spectrometry (HRMS) metabolomics approach. It was shown that under ideal growing conditions, the biochemical make-up of the maize tissue types is different. However, under drought-stress conditions, the stress response dominates the metabolic profile. HRMS untargeted analysis showed differences in the extractable paleometabolomes of the two Tularosa maize populations. Statistical analysis reveals drought-stress biomarkers in the ancient maize metabolomes and direct evidence of increased sucrose production in the later population, possibly an indicator of adaptation to dry climate conditions.

The work presented in this thesis demonstrates the novel use of nitrogen isotope ratio analysis as a direct indicator for drought stress in archaeobotanical samples and paleometabolomics was used to test genomic inferences about the archaeological maize. Paleometabolomics can complement other 'omics techniques and may be used as a novel approach to study desiccated archaeological remains.

Table of Contents

Chapter 1.	Introduction.....	1
1.1	Introduction	2
1.2	Research Rationale	5
1.2.1	Domestication History of Maize	5
1.2.2	Maize Usage	8
1.2.3	Climate Change and Maize Production.....	10
1.2.4	Plant Responses to Stress and Drought	11
1.2.5	Archaeological and Environmental Context of Tularosa Cave.....	12
1.3	Previous Molecular Analyses of Archaeological Maize	18
1.4	Stable Isotope Ratios	22
1.4.1	Nitrogen Isotope Ratios.....	22
1.4.2	The Effect of Drought on Nitrogen Isotope Ratios.....	25
1.4.3	Compound-Specific Nitrogen Isotope Ratios	25
1.4.4	Oxygen Isotopes	26
1.4.5	Previous Studies of Ancient Maize Using Oxygen and Nitrogen Isotope Ratios.....	27
1.5	Metabolomics.....	30
1.5.1	Overview	30
1.5.2	Extraction Considerations.....	31
1.5.3	Primary and Secondary Metabolites	32
1.5.4	Drought Stress Response in Maize	33

1.5.5 Review of Relevant Previous Metabolomic Studies.....	34
1.5.5.1 Extraction Approaches.....	34
1.5.5.2 Metabolomics in Archaeology	35
1.5.5.3 Metabolomics in Studies of Modern Maize	36
1.6 Aim and Objectives	38
Chapter 2. Analytical Technology and Considerations.....	41
2.1 Analytical Technologies Used in Plant Metabolomics.....	42
2.2 Metabolomics Experiment Workflow	43
2.2.1 Study Design.....	43
2.2.2 Sample Collection and Pre-Treatment	43
2.2.3 Data Acquisition: High Performance Liquid Chromatography-Mass Spectrometry (HPLC-MS).....	44
2.2.4 Liquid Chromatography	45
2.2.5 Mass Spectrometry	45
2.2.6 Statistical Analysis.....	46
2.2.7 Identifying Small Molecules Using High Resolution High <i>m/z</i> Accuracy Mass Spectrometry	48
2.3 Mass Spectrometry	50
2.3.1 ESI 50	
2.3.1.1 Ion Evaporation Model (IEM):.....	51
2.3.1.2 Charge Residue Model (CRM):.....	52
2.3.2 Mass Analysers.....	53
2.3.2.1 Fourier Transform Ion Cyclotron Resonance (FTICR).....	53

2.3.2.2	Quadrupole Mass Analysers	56
2.3.2.3	Orbitrap.....	58
2.4	High Performance Liquid Chromatography.....	60
2.5	Analytical Technology and Software Used in Isotope Ratio Analysis	64
2.5.1	Considerations for Sampling.....	64
2.5.2	Isotope Ratio Mass Spectrometry (IR-MS)	64
2.5.3	Compound-Specific Isotope Ratio Mass Spectrometry	67
2.6	Summary	69
Chapter 3.	Stable Nitrogen Isotopes Reveal Archaeological Maize Adapted to Drought in Southwestern US	70
3.1	Abstract.....	71
3.2	Introduction (as in submitted paper)	71
3.3	Results.....	73
3.3.1	Plant Growth Experiments	73
3.3.2	$\delta^{15}\text{N}$ analysis of archaeological maize cobs from Tularosa Cave.....	75
3.3.3	$\delta^{15}\text{N}$ Analysis of Individual AAs from Archaeological Maize Cobs.....	78
3.3.4	Effects of Drought on the $\delta^{13}\text{C}$ Values of Modern and Ancient Maize	82
3.4	Discussion: Implications	85
3.5	Methods	89
3.5.1	Experimental Materials	89
3.5.2	Archaeological Materials.....	90

3.5.3 Bulk $\delta^{15}\text{N}$ Isotope Ratio Analysis	90
3.5.4 Preparation of Amino Acid Derivatives (N-acetyl-i-propyl esters)	91
3.5.5 Cellulose Extraction	92
3.5.6 Instrumental Analyses.....	93
Chapter 4. Metabolomic Approaches to Studying the Response to Drought Stress in Corn (<i>Zea mays</i>) Cobs	95
4.1 Abstract.....	96
4.2 Introduction (as in published paper).....	97
4.3 Results and Discussion	99
4.3.1 Effect of Lyophilisation on the Plant Metabolome	99
4.3.2 Effect of Drought Conditions upon the Extractable Maize Metabolome.....	103
4.3.2.1 Variation in the Extractable Metabolome of Plants Grown under Different Watering Conditions	103
4.3.2.2 Identification of Potential Drought Biomarkers.....	105
4.3.3 Drought-Stress Response Dominates Metabolome in Kernel and Inner Cob Tissues.....	111
4.4 Materials and Methods.....	113
4.4.1 Plant Material Description, Cultivation and Sampling	113
4.4.1.1 Extraction Condition Experiment	113
4.4.1.2 Drought Condition Experiment	113
4.4.2 Metabolite Extraction Method.....	114
4.4.3 Data Collection	114

4.4.4 LC–MS-Based Analysis of Metabolome.....	115
4.4.4.1 Liquid Chromatography Separation Method.....	115
4.4.4.2 Mass Spectrometry Methods	115
4.4.5 LC–MS/MS	116
4.4.5.1 Mass Spectrometry Methods	116
4.4.5.2 Data Handling and Analysis	116
4.4.5.3 Statistical Analysis.....	117
4.5 Conclusions	118
Chapter 5. Paleometabolomics Reveals Drought Stress Response	
in Archaeological Maize	120
5.1 Abstract.....	121
5.2 Introduction (as in submitted paper)	121
5.3 Results.....	124
5.3.1 Untargeted Metabolomic Analysis of Ancient Maize Extractable Metabolomes Reveals Variation Between Maize Phenotypes	124
5.3.2 Osmoprotectant disaccharides were revealed in archaeological maize.....	129
5.3.3 Features with High Identity Scores were Investigated by Compound Class	130
5.3.4 Drought-Related Metabolites Were Revealed in the Metabolome of Archaeological Samples.....	132
5.4 Discussion.....	136
5.5 Material and Methods	138
5.5.1 Archaeological Materials.....	138

5.5.2 Metabolite Extraction Method.....	138
5.5.3 Data Collection	139
5.5.4 LC-MS-Based Analysis of Metabolome	139
5.5.4.1 Liquid Chromatography Separation Method.....	139
5.5.4.2 HILIC Separation Method	139
5.5.5 Mass Spectrometry Methods	140
5.5.6 LC–MS–MS.....	140
5.5.6.1 Mass Spectrometry Methods.....	140
5.5.6.2 Data Handling and Analysis.....	141
5.5.6.3 Statistical Analysis.....	141
Chapter 6. Assessment of the Effect of Diagenesis on Archaeological Maize Samples: Artificial Ageing Experiments.....	143
6.1 Introduction.....	144
6.2 Results and Discussion	146
6.2.1 Assessing the Preservation of the Tularosa Maize	146
6.2.1.1 ATR-FTIR of Archaeological and Modern Aged Maize Shows Limited Changes on Comparison with Modern Unaged Maize.....	147
6.2.1.2 Elemental Analysis of Archaeological and Modern aged Maize Shows Limited Changes Due to Ageing Processes	150
6.2.2 Bulk Isotope Ratios of Artificially Aged Samples	151
6.2.3 Amino Acid Composition Analysis.....	153
6.2.3.1 Amino acid Composition Analysis	153

6.2.3.2	Amino Acid Racemisation Analysis of Tularosa Maize Shows Increased Asx D/L and Glx D/L with Age	156
6.2.3.3	Artificially Aged Maize Samples Show No Change in Amino Acid Isotope Ratios Compared to a Modern Lyophilised Sample	157
6.2.4	The Effect of Ageing on the Extractable Maize Metabolome.....	158
6.2.5	The Effect of Ageing on Drought-Related Metabolites was Investigated.....	160
6.3	Conclusions	161
6.4	Material and Methods	162
6.4.1	Experimental Samples	162
6.4.2	Archaeological Samples	162
6.4.3	Attenuated Total Reflectance Fourier-Transform InfraRed Spectroscopy.....	163
6.4.4	LC-MS Metabolome Extraction.....	163
6.4.4.1	Data Collection.....	163
6.4.5	LC-MS-Based Analysis of Metabolome.....	164
6.4.5.1	LC-MS Mass Spectrometry Methods.....	164
6.4.5.2	Data Handling and Analysis	164
6.4.5.3	Statistical Analysis.....	165
6.4.6	LC-MS-MS.....	165
6.4.6.1	Mass Spectrometry Methods	165
6.4.7	Amino acid analysis.....	165

6.4.7.1	Acid Hydrolysis and Amino Acid Recovery	165
6.4.7.2	RP-HPLC of Amino Acids.....	166
6.4.8	Stable Isotope Ratio and EA (Carbon and Nitrogen) of Bulk Maize Cob Powder.....	167
Chapter 7.	Conclusions and Future Research.....	168
7.1	Summary	169
7.2	Recommendations for Future Research.....	171
7.2.1	Strategies to Protect Crops During Modern Day Climate Change	171
7.2.2	Use of Oxygen and Carbon Cellulose Isotope Ratios to Test for Drought Stress.....	172
7.2.3	Control Experiments for Amino Acid Isotope Ratios	172
7.2.4	Effect of Different Burial Environments on Archaeobotanical Metabolome and Isotope Ratios.....	173
7.2.5	Effect of Different Cooking Techniques on Archaeobotanical Metabolome and Isotope Ratio Values ..	173
7.2.6	Use of Metabolomics for Other Archaeobotanical Remains and Other Human/Animal Remains as a Complement to Other `Omics Techniques	174
Appendix.....		175
List of Abbreviations.....		243
References.....		246

List of Tables

Table 3.1: Mean average AA $\delta^{15}\text{N}$ values from inner maize cob samples.

Numbers in brackets represent one standard deviation associated with triplicate analytical replicate measurements for AA $\delta^{15}\text{N}$ values and replicate precision for duplicate experimental replicates of bulk $\delta^{15}\text{N}$ values. 80

Table 4.1: Summary of data on all possible identifications of drought-related biomarkers of maize. Possible identifications were assigned using compound databases (Metlin, LipidBlast, ChemSpider, Progenesis MetaScope). * Indicates the data were scaled. The p -val between the well-watered and severe drought conditions is quoted. All features are level 3 Schymanski identifications¹²⁹. 110

Table 5.1: Table showing features with the highest loadings in PC1.

*Scaled data. All features are level 3 Schymanski identifications¹²⁹. .. 128

Table 5.2: Summary of data on all proposed identifications of drought-related biomarkers in archaeological maize extracts. Possible identifications were assigned using compound databases (Metlin, LipidBlast, ChemSpider, Progenesis MetaScope). The p -val between the 700 BP and 1800 BP maize are quoted. * Metabolite identification confirmed with a standard. FA = formic acid. All features are level 3 Schymanski identifications¹²⁹. 134

Table 6.1: Table showing molar ratios (O:C, H:C, C:N) of archaeological maize and modern maize heated at 50 °C and 70 °C 150

Table 6.2: Table showing molar ratios of C:N of modern maize heated at 70 °C comparing two analysers. 151

Table 6.3: Table showing $\delta^{15}\text{N}$ and $\delta^{13}\text{C}$ values of artificially aged maize... 152

Table 6.4: Summary of data on proposed identifications of drought-related biomarkers in modern artificially aged maize. Proposed identifications were assigned using compound databases (Metlin, LipidBlast, ChemSpider, Progenesis MetaScope). All features are level 3 Schymanski identifications ¹²⁹	160
--	-----

List of Figures

Figure 1.1: Diagram of a maize plant. The tassel, ear, silk and roots are labelled.....	5
Figure 1.2: (A) Morphology of teosinte and maize plants and (B) differences in ear architecture, taken from ¹⁵	7
Figure 1.3: Map showing location of Tularosa Cave.....	14
Figure 1.4: Examples of corn recovered from Tularosa Cave (from Martin <i>et al.</i> ⁷).	15
Figure 1.5: Stalagmite records from Carlsbad Cavern (BC2 red) and Hidden Cave and (HC1 blue). The growth for each year is given as band thickness (mm); 10-year moving average applied. The dates of the 1850 and 750 assemblages are marked on the graph as green and yellow diamonds.....	16
Figure 1.6: Figure from da Fonseca <i>et al.</i> ⁶ representing gene trees using PBS distance for the genes <i>dehyd1A</i> and <i>su1</i>	19

Figure 1.7: Simplified schematic of nitrogen uptake, adapted from Szpak <i>et al.</i> ⁶³ . Fractionation factors are labelled in blue: (1) Ammonium volatilisation. It has been found that this process concentrates ¹⁵ N in the remaining ammonium labelled [*] NH ₄ ⁺ ⁵⁹ . (2) Nitrification. The biological oxidation of ammonia into nitrate. ⁵⁹ (3) Uptake of NO ₃ ⁻ causes negligible fractionation ⁶⁴ . (4) Uptake of [*] NH ₄ ⁺ is associated with nitrogen fractionation. The extent of the fractionation depends on the source concentration of [*] NH ₄ ⁺ ^{60,64} . (5) NO ₃ ⁻ assimilation into organic nitrogen. The reduction of NO ₃ ⁻ to [*] NH ₄ ⁺ is associated with a fractionation of nitrogen isotopes ⁶⁵ . (6) [*] NH ₄ ⁺ assimilation occurs in the root and is associated with fractionation of N isotopes. (7) NO ₃ ⁻ can also be moved to the shoot to be assimilated. This results in fractionation of N isotopes. This is because the NO ₃ ⁻ pool has been depleted in ¹⁵ N via assimilation of N into organic N in the root. (8) NO ₃ ⁻ assimilation into organic N in the leaf. (9) Organic N can be moved between the root and the shoot with no fractionation of N isotopes.	24
Figure 1.8: Diagram summarising oxygen isotope fractionation in plants.	27
Figure 1.9: 'Omics technologies in combination offer a comprehensive understanding of biological systems.	31
Figure 1.10: Classification of primary and secondary metabolites (image adapted from www.vivadifferences.com ¹⁰⁰).	33
Figure 2.1: Typical metabolomics experiment workflow. Image created using BioRender.com.	42
Figure 2.2: Schematic of an ESI source.	51
Figure 2.3: Ion evaporation model of gas-phase ion production in ESI.	51

Figure 2.4: Charge residue model of gas-phase ion production in ESI.....	52
Figure 2.5: Diagram of an FTICR cell, the purple arrows show the direction of motion of the ions.	54
Figure 2.6: Diagram of a quadrupole mass analyser, showing opposite rods electrically connected. Blue rods are positive charged and brown are negatively charged.....	56
Figure 2.7: Simplified diagram of Orbitrap mass analyser (adapted from http://planetorbitrap.com).	58
Figure 2.8: Schematic of the Thermo Scientific Orbitrap Fusion™ Tribrid™ (Adapted from http://planetorbitrap.com).	59
Figure 2.9: Diagram illustrating how the analytes elute from an LC column at different rates, dependent upon their physicochemical properties. The analytes (represented by colours and shapes in the diagram) indicate components with different physiochemical properties resulting in different elution times due to interactions with the column.....	61
Figure 2.10: Diagram showing the separation of ions in an IR-MS instrument.	66
Figure 3.1: Graph displaying the $\delta^{15}\text{N}$ (‰) values of modern maize grown under different watering conditions. Each point represents a duplicate mean measurement, sample uncertainty is quoted in Appendix 2. Dark blue dots represent well-watered control, medium blue dots represent drought at three-leaf stage and pale blue dots drought at the three-leaf and grain-fill stages. (a) B73 kernel samples, (b) B73 inner cob samples, (c) B73 kernels samples and (d) B76 inner cob samples. All samples were measured in duplicate and the means calculated and corrected using standards.....	75

- Figure 3.2: Box plots of $\delta^{15}\text{N}$ (‰) values of Tularosa maize cobs. Samples date from 1800 BP (blue circles) and 700 BP (yellow circles), means are shown as black circles.77
- Figure 3.3: Graph displaying the $\delta^{15}\text{N}$ (‰) kernel and inner cob values of each sample. Samples from the 1800 BP (ovoid) and 700 BP (cylindrical) time periods are blue and yellow circles respectively. Correlation line for each time period is shown.78
- Figure 4.1: Characteristic base peak ion chromatogram for an LNE sample obtained using a T3 column coupled to high-resolution mass spectrometry (LC–HRMS) to allow the retention and separation of metabolites with a broad range of polarities..... 100
- Figure 4.2: PCA plots showing the scores for the first two principal components obtained using untargeted metabolomic analysis of different extraction conditions for *Zea mays* coloured by experimental group (green, purple and grey represent LNE, LC and LRT, respectively) (a) for the positive-ion-mode; (b) and for the negative-ion-mode. The data have been scaled to unit variance and QC corrected. 101
- Figure 4.3: PCA plots showing the scores for the first two principal components obtained using untargeted metabolomic analysis of drought-stressed and well-watered control plants, coloured by watering conditions for *Zea mays* for (a) positive-ion-mode kernel extracts; (b) negative-ion-mode kernel extracts; (c) positive-ion-mode inner cob extracts and (d) negative-ion-mode inner cob extracts. The data have been scaled to unit variance and QC corrected. 105
- Figure 4.4: Data analysis workflow for the identification of key features in mass spectrometric data. 107

Figure 4.5: Figure showing relative abundances of m/z features (a) 279.1238 (b) 143.0349 (c) 480.3075 and (d) 520.3398. Blue, yellow and red diamonds represent well-watered, moderate drought and severe drought conditions respectively. ANOVA p -vals are indicated.	108
Figure 4.6: Product ion spectrum of m/z 279.124 at 9.52 min.	109
Figure 4.7: PCA plots showing the scores for the first two principal components obtained for the untargeted metabolomic analysis coloured by watering conditions for <i>Zea mays</i> for (a) the positive-ion-mode and (b) the negative-ion-mode. The data have been scaled to unit variance and QC corrected for both cases.	112
Figure 5.1: PCA plots showing the scores for the first two principal components obtained using untargeted metabolomic analysis of <i>Zea mays</i> cob extracts coloured by sample age (yellow and blue represent 1800 BP and 700 BP respectively) (A) for the positive-ion-mode; (B) and for the negative-ion-mode datasets. The data have been scaled to unit variance and QC corrected.	125
Figure 5.2: Volcano plot, green dots show features (i.e. metabolites) with significant adjusted p -values (<0.05) and fold change > 1.5 between 700 BP and 1800 BP Tularosa maize extracts. Blue dots show metabolites with non-significant adjusted p -values. Red lines to show adjusted p -value cut-off of 0.05, and black lines show fold changes < 0.5 or > 1.5	126
Figure 5.3: Figure showing the relative abundances of the feature with m/z 377.085 for the two maize varieties, where yellow and blue diamonds refer to 1800 BP and 700 BP samples respectively. Lines indicate averages across sample groups. Level 1 Schymanski identification ¹³⁰	130

Figure 5.4: (A) Heatmap of the abundance of metabolites (log transformed) aggregated by compound class. (B) Boxplots of abundances of different compound classes of metabolites (carbohydrates, lipids, organic acids, peptides, phytochemicals, vitamins and cofactors and unidentified (NA)). 1800 BP and 700 BP groups are coloured yellow and blue respectively. 131

Figure 5.5: PCA biplot showing the scores for the first two principal components obtained for features with accurate m/z values corresponding to known drought related features selected from untargeted metabolomic analysis of archaeological *Zea mays*, coloured by age (yellow and blue represent 1800 BP and 700 BP respectively). Loadings of features are represented by red arrows, where the length of the arrow is proportional to the loading. 133

Figure 6.1: ATR-FTIR scans of (A) modern unheated sample (0 weeks) and (B) modern sample heated at 70 °C for 16 weeks..... 148

Figure 6.2: ATR-FTIR scans of Tularosa maize samples (A) 151, 700 BP and (B) 81, 1800 BP. 149

Figure 6.3: The amino acid concentrations of eight maize cobs found in Tularosa Cave. 1800 BP and 700 BP maize age groups are represented by yellow and blue coloured bars respectively. Green bar represents modern lyophilised maize samples. Error bars represent one standard deviation of triplicate experimental replicates..... 153

Figure 6.4: The AA % composition of eight Tularosa cave maize samples. Modern lyophilised maize in green. Error bars represent the standard deviation (1σ) of triplicate experimental replicates..... 155

- Figure 6.5: Figure plotting the racemisation of Asx D/L versus Glx D/L. Archaeological samples from Tularosa Cave (700 BP and 1800 BP) are marked as green circles and red squares respectively. Modern samples that were heated at 50 °C for 1, 2, 3, 4, 5, 6, 7, 8 days are marked as purple triangle, star, cross, circle, diamond and square respectively. Control sample (not heated) is marked in blue..... 156
- Figure 6.6: $\delta^{15}\text{N}_{\text{AA}}$ values normalised to $\delta^{15}\text{N}_{\text{Glx}}$ from maize inner cob samples. Red squares and black circles represent a sample aged at 70 °C for one week and a modern control. Black dotted line, $y=0$. Error bars represent the standard deviation associated with triplicate analytical measurements. Black dotted line, $y=0$ 158
- Figure 6.7: PCA plots showing the scores for the first two principal components obtained using untargeted metabolomic analysis of *Zea mays* cob extracts coloured by weeks spent in 70 °C oven. Red, green blue, yellow turquoise and purple diamonds represent 0, 1, 2, 4, 8, and 16 weeks respectively. 159

Acknowledgements

I would like to express my sincere gratitude to my supervisors Jane Thomas-Oates and Oliver Craig whose encouragement, support and guidance has seen me through this PhD. Special thanks go to Jane whose enthusiasm, commitment and support is inspirational. I would also like to especially thank J. Brett Sallach for his guidance and friendship.

Thank you to Ryan Morrison for growing the maize samples, the Museum of Natural History for providing the archaeological samples and to Helen Grant for hosting me at the Centre for Ecology and Hydrology. I would like to thank Ed Bergström, Matt von Tersch and Helen Talbot for their technical support and good humour.

The JTO group and BioArCh members past and present have made this journey a pleasure. Thanks for all the laughter and fun in the lab and also at the pub... Particular thanks go to Dr Burns, Dr Sallach and Dr Lundy for being hilarious and inspiring.

I would like to thank my family, whose support has always been unwavering and for which I am always grateful. Thank you to my friends for sticking with me through this and listening to me complain about MS and pretending to care - especially Holly and Alice! Finally, thank you Ally for being there for me every step of the way.

Declaration

Throughout the writing and construction of this thesis I received guidance and support from my supervisors, Prof. Jane Thomas-Oates and Prof. Oliver E. Craig. I also received guidance from Prof. Julie Wilson and Dr Brett Sallach for the work presented in Chapter 4. Mark Halsall (MChem project student on a project that I devised and supervised) collected data which are included in Chapters 3 and 6. Dr. Ryan Morrison grew samples used in Chapters 3, 4 and 6. Chapters 3, 4 and 5 have been written as papers for international peer-reviewed journals. These papers have been reworked, so that they are presented in a consistent style for this thesis.

Chapter 3: Is in review with the journal ‘Scientific Reports’. Co-authors are: Logan Kistler, Mark Halsall, Helen Talbot, Ryan Morrison, Matthew von Tersch, Nathan Wales, Jane Thomas-Oates, Oliver E. Craig.

Co-author contributions are as follows:

Conceptualisation, J.T.-O., O.E.C and I.G.; experiments I.G, M.H, R.M, M.V.T., H.T. software, I.G.; validation, I.G.; formal analysis, I.G., M.H.; investigation, J.T.-O., I.G., O.E.C.; resources, J.T.-O., O.E.C., R.M. and L.K.; data curation, I.G.; writing—original draft preparation, I.G.; writing—review and editing, I.G., O.E.C, J.T.-O., L.K., N.W. visualisation, I.G.; supervision, J.T.-O. and O.E.C; project administration, J.T.-O. ; funding acquisition, J.T.-O.

Chapter 4: Has been published: ‘Gaffney, I., Sallach, J. B., Wilson, J., Bergström, E., & Thomas-Oates, J. (2021). Metabolomic Approaches to Studying the Response to Drought Stress in Corn (Zea mays) Cobs. *Metabolites*, 11(7), 438.’

Co-author contributions are as follows:

Conceptualisation, J.T.-O. and I.G.; experiments I.G., J.B.S. and E.B.; software, I.G. and J.W.; validation, I.G.; formal analysis, I.G. and J.W.; investigation, J.T.-O. and I.G.; resources, J.T.-O.; data curation, I.G.; writing—original draft preparation, I.G.; writing—review and editing, I.G., J.B and J.T.-O.; visualisation, I.G.; supervision, J.T.-O.; project administration, J.T.-O. ; funding acquisition, J.T.-O.

Chapter 5: Submitted to the journal ‘Plants’. Co-authors are:

Isabella Gaffney, Oliver E. Craig, Nathan Wales, Logan Kistler, Edmund Bergström and Jane Thomas-Oates.

Co-author contributions are as follows:

Conceptualisation, J.T.-O., O.E.C and I.G.; experiments I.G, E.B software, I.G.; validation, I.G.; formal analysis, I.G.; investigation, J.T.-O., I.G., O.E.C.; resources, J.T.-O., O.E.C. and L.K.; data curation, I.G.; writing—original draft preparation, I.G.; writing—review and editing, I.G., O.E.C, J.T.-O., L.K., N.W. visualisation, I.G.; supervision, J.T.-O. and O.E.C; project administration, J.T.-O. ; funding acquisition, J.T.-O.

I hereby declare that this thesis is my original work, except where otherwise acknowledged, and that it has not been submitted previously for a degree at this or any other University. All sources are acknowledged as References.

Isabella Gaffney

Chapter 1. Introduction

1.1 Introduction

Drought stress is a pressing issue faced by modern arable farmers globally. Maize, rice and wheat contribute 30% of calories to more than 4.5 billion people, including to those from some of the poorest countries in the world¹. Maize is also an essential animal feed and is used to produce biofuel². Maize agriculture in the present-day Southwestern United States has historically faced sparse and unreliable levels of precipitation, resulting in several pan-regional droughts in the last 2000 years³⁻⁵. The research described in this thesis comprises investigations of the effects of drought stress on the maize metabolome and the isotopic composition of maize. Specifically, both modern maize plants grown under experimental watering conditions, as well as archaeological maize samples from Tularosa Cave were examined, as they offer a unique proxy for future droughts.

Plants are frequently subjected to biotic and abiotic stress events and due to their sessile nature, plants are under constant pressure to adapt to such stresses. Water deficit is an abiotic stress that can adversely affect plant growth and crop yield. In combination with often associated high temperatures and radiation, drought is the most important environmental constraint imposed upon plant survival^{6,7}. This is a pressing issue as modern-day climate change makes periods of drought more likely⁸.

Plants can adapt to changing weather conditions via the process of homeostasis, which is the state of steady internal, physical, and chemical conditions maintained by living systems, within certain pre-set limits. Homeostasis allows for a degree of perturbation from the optimum to encompass general daily and seasonal change. However, water deficit, when the plant requires more water than is available, is classed as stress and falls outside the normal range of metabolism that is maintained homeostatically. When a plant experiences water deficit, it is affected in the short term in

several ways. Primarily, its metabolic pathways are disrupted, which can trigger metabolic pathways which produce metabolites that protect against drought stress ⁹.

This thesis focuses on studies of the adaptation of maize to past environmental conditions. Maize (*Zea mays*. L) is the top food crop grown globally and is highly adaptable to different growing environments¹⁰. However, drought is a major factor limiting crop yields of maize¹¹ and climate change is threatening food security in many tropical areas⁸ due to increased periods of drought^{1,12,13}.

This thesis describes investigations of ancient maize from Tularosa Cave in New Mexico. The site was occupied by a Native American culture in two main occupational phases. Direct radiocarbon dating of maize cobs has revealed two temporally distinct periods of occupation: older (1830 - 1719 BP, 95.4% CI) and younger (771 - 681 BP, 95.4% CI)¹⁴. The cave is very dry, and many artifacts are well preserved including desiccated samples of maize which derive from the full span of the cave's occupation.¹⁵ The region is known to have undergone periods of drought at the time of the cave's occupation^{5,16}. These maize samples therefore represent a unique opportunity to investigate the effects of drought upon a valuable food crop over a large time-span, impossible to recreate in laboratory or greenhouse experiments. By studying the effects of drought upon these maize remains we can use the data to understand the potential effects of future droughts and hope to mitigate their impact.

Water stress has been previously investigated using isotope ratio mass spectrometry^{17,18}. $\delta^{18}\text{O}$ ¹¹ and $\delta^{13}\text{C}$ ¹⁹ signatures (see Section 2.5.2 for information on isotope ratio calculations) showing enrichment in the heavy isotope can be correlated to periods of drought. Williams *et al.*¹⁷ have shown that reliable oxygen isotope data can be acquired from measuring isotope ratios in cellulose extracted from archaeological maize cobs, and can be

correlated to the conditions in the plant's growing environment, specifically the source water which was used to water the plants. In the work described in this thesis, the use of various isotope ratios was investigated for their suitability as drought indicators. $\delta^{18}\text{O}$ data were collected from maize cellulose, and bulk $\delta^{15}\text{N}$ and single-compound $\delta^{15}\text{N}$ data were also investigated.

Water stress causes disruption to a plant's metabolic pathways, so changes in the metabolome can be a good indicator that the plant is under stress²⁰. In the work described in this thesis the metabolomes of modern drought-stressed maize (grown under experimentally controlled watering conditions) and the Tularosa archaeological maize were investigated using metabolomic techniques.

1.2 Research Rationale

1.2.1 Domestication History of Maize

Maize is a thick-stemmed annual grass which can grow between one and four meters tall. Maize has both male and female reproductive organs on the same plant (Figure 1.1).

The male reproductive organ (the tassel) produces pollen.

The female reproductive organ (the ear) contains the ovules.

Each kernel in a maize ear is derived from an individual ovule, and each kernel is genetically distinct. The

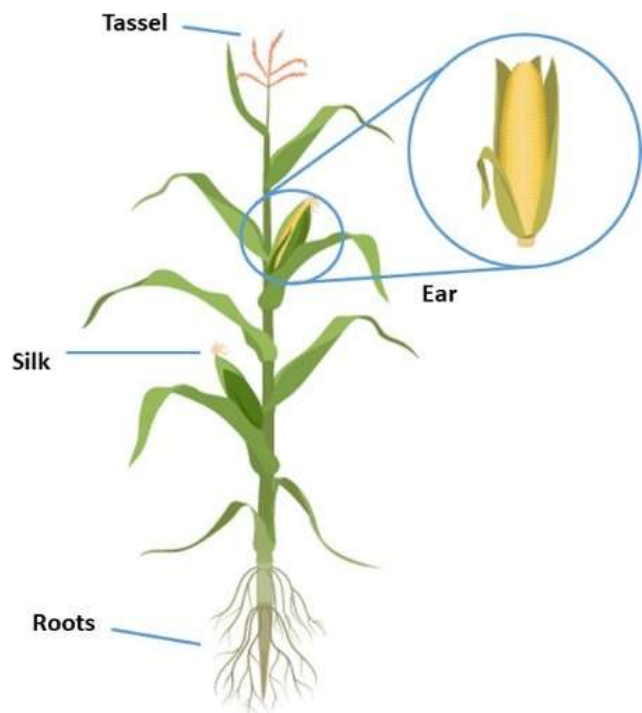


Figure 1.1: Diagram of a maize plant. The tassel, ear, silk and roots are labelled.

tassel and the ear are typically separated by up to a meter²¹. Pollen is captured by silks found on the end of the ear. The silks brush the pollen against the ovules to facilitate fertilization. In the wild, pollen is spread by the wind, allowing cross-pollination of plants. Maize fixes carbon during photosynthesis following the C4 pathway. C4 refers to the four- carbon molecule, oxaloacetate, that is the first molecule produced during this process. C4 plants are more tolerant of drought and high temperatures than C3 carbon fixing plants²². Modern maize has been domesticated over many thousands of years from the plant Balsas teosinte* (*Z. mays parviglumis*).

* Teosinte is the species that modern-day maize evolved from.

There are several wild species of teosinte^a and they are all native to Mesoamerica[†].

Recent archaeological and ancient deoxyribonucleic acid (DNA) research by Kistler *et al.*²³ suggests that the maize domestication process started in what is now Southern Mexico approximately nine thousand years ago and partially domesticated maize was brought to South America approximately 6500 years ago. Kistler *et al.* found that teosinte was fully domesticated in Mexico and Southern America over the course of several thousand years. Ancient DNA evidence suggests that partially domesticated teosinte had spread into what is the modern-day U.S. Southwest by approximately 4000 years ago. Within the last 1000 years fully domesticated varieties of maize emerged from different domestication centres, such as highland Mexico and Central America and the Andes and Pacific coast of South America. Dispersal to different domestication centres occurred before domestication traits were fixed, resulting in wide genetic variation in modern maize varieties.

Phenotypically, modern maize is very distinguishable from ancestral teosinte (summarised from Stitzer & Ross-Ibarra²⁴). Morphological changes are generally associated with increased yields or ease of harvesting. Teosinte plants are branched, with multiple ears per branch, whereas maize plants are unbranched, which allows easier access to the fruit (Figure 1.2A). Maize has larger fruits than teosinte, resulting in bigger yields.. Maize has

[†] Mesoamerica is broadly defined as the area that is home to the Mesoamerican civilization, which comprises a group of peoples with close cultural and historical ties. The heartland of Mesoamerica is Southern Mexico, but extended to include central Mexico to Northern Costa Rica.

paired mature spikelets[‡], whereas in a teosinte ear only a single spikelet matures. This results in twice as many seeds being formed in maize than teosinte.

Maize also has multiple ranks of kernels in the ear, whereas teosinte only has two, again producing more seeds in maize. Teosinte fruit is protected by a tough tissue called the outer glume (Figure 1.2B); maize fruits are exposed, once the outer husk is removed, making harvesting easier. Maize also has non-disarticulating rachis; this means the rachis is rigid and non-shattering, whereas the teosinte rachis disarticulates upon maturity. This makes maize dependent on human intervention for seed dispersal, as the seeds remain upon the cob which is advantageous for harvesting.

The genomic regions responsible for the morphological structure of maize relating to domestication have been identified²⁵. The paired spikelets are associated with gene variants on chromosomes 1 and 3. The interactions are complex as the loci are dependent on the presence of other genes. Also, the loci appear to affect more than one phenotypic trait, such as plant architecture. The ranks of the ears are mostly controlled by the gene *Zea*

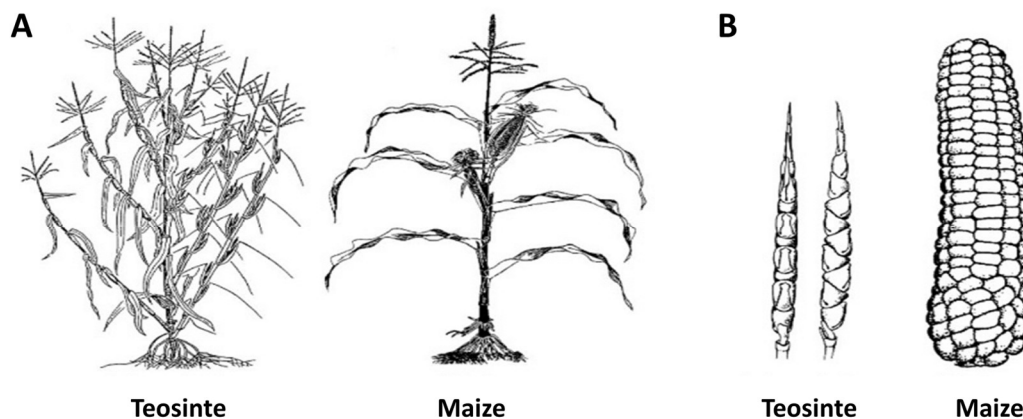


Figure 1.2: (A) Morphology of teosinte and maize plants and (B) differences in ear architecture, taken from¹⁵.

[‡] A spikelet is a short branch on which flowers are borne.

floricaula leafy2 (*zfl2*). Rachis shattering, or disarticulation, is associated with *Zea agamous-like1* (*zagl1*). Glume architecture and hardening are thought to be controlled by the gene *teosinte glume architecture1* (*tga1*). Finally, plant architecture is controlled by *teosinte branched1* (*tb1*)²⁶.

Domestication impacts most on the genes that control morphology and physiology. It is mutually beneficial for the domesticated species and the domesticator. Maize is well adapted for its ecological niche and well adapted to its growing environment.

1.2.2 Maize Usage

Maize was an extremely valuable commodity to early Mesoamerican cultures. According to ancient Mayan legend, humans were even created from maize²⁷. The oldest known evidence of maize has been found in the Central Balsas region of Mexico. Starch grain and phytolith evidence of teosinte was identified on stone grinding tools and stone flakes dating to 8700 BP found in the Xihuatoxtla shelter²⁸. Xihuatoxtla is a small cave shelter seasonally occupied by small groups of people for several weeks at a time. There is evidence that people were planting maize at the fertile edges of nearby lake Laguna Tuxpan during the dry season, when water levels were low. This strategy was probably an important aspect of their seasonal settlement cycles.

Genetic data also point to the Balsas river valley in Mexico as the site where maize was domesticated from teosinte^{29,30}. Archaeological phytolith evidence suggests that squash was domesticated around the same time²⁸. Population genetics comparison of maize and teosinte showed multiple centres for selection and a recent genetic bottleneck causing loss in genetic diversity during domestication. Following domestication, there is evidence of gene flow from teosinte to maize having improved maize's adaptation to

different climates³¹⁻³⁴. Other early evidence for maize comes from two rock shelters in Arizona and western New Mexico; these sites are notable for the diversity of their settings (upland and lowland). The fact that maize occurs almost concurrently in these different sites suggests that the ancient landrace(s) were tolerant of a wide range of environmental conditions³⁵.

Today there are several types of maize:

Sweet corn: Sweet corn is the variety of maize typically consumed by humans. It has a higher sugar content than starch content. It is harvested prematurely before the sugars can be converted into starch.

Dent corn: Dent corn, or field corn is the type of maize predominantly grown. It has a higher starch content than sweetcorn and is usually used to feed livestock, and to produce corn syrup and ethanol.

Popcorn: Popcorn is another variety of maize consumed by humans. It has a tough outer glume and a small amount of starch.

Flour corn: Flour corn is ground into flour to make baked foods.

Flint corn: Flint corn is similar to dent corn, but can be coloured yellow, orange, red, white and black, rather than just yellow. It is primarily used to make a coarse cornmeal.

1.2.3 Climate Change and Maize Production

A study by Jones and Thornton¹² indicates that there will be an overall reduction of 10 % in maize production in Africa and Latin America by 2055 due to climate change. The study used modelling to predict the yield of maize crops in Africa and Latin America. However, the results of the simulation show a highly variable pattern of risk, with some areas much more at risk than others. An analysis by Lobell *et al.*⁸ assessed the climate change adaptation needs for at-risk crops in 12 food insecure regions. Lobell *et al.* found that Southern African maize was most at risk from climate change and in need of adaptive measures. Cairns *et al.*³⁶ also identified sub-Saharan Africa as an at-risk area. A study (Southworth *et al.*³⁷) focused on the effect of climate change on the production of maize in the midwestern United States found variable results. An overall reduction in crop production was predicted. However, this varied depending on where the maize was grown, and which hybrid was used.

By 2050 the global population is predicted to have increased by an additional 3.5 billion individuals. Production of maize, wheat and rice will need to increase by 70 % by 2050 to feed this growing population³⁶; currently, 800 million people still experience poverty and hunger every year. Current climate change predictions show that agricultural production in general will be negatively impacted in the forthcoming years³⁸. There is a huge impetus to make adaptations to crops to maintain food security in impoverished regions of the world, or risk increased global hunger. This PhD project has looked at the adaptations of ancient maize to historical drought; which may be used to inform strategies that could be used to protect crops during modern day climate change.

1.2.4 Plant Responses to Stress and Drought

Due to their sessile nature, plants are adaptable to biotic and abiotic stresses. When a plant experiences drought a complex system of mechanisms is triggered, ultimately resulting in a series of responses designed to conserve resources and energy. The stomata are closed, and the leaves are rolled to prevent water loss by evapotranspiration, which in turn has the effect of inhibiting photosynthesis. Plants may be subject to slowly developing water shortage or more rapid dehydration. Different rates of desiccation can trigger different physiological responses ⁶.

When water deficit develops slowly, the plant has the option to escape desiccation by shortening its life cycle. This involves the successful completion of reproduction before water stress becomes too severe and ovules must be aborted. This means a high growth rate, utilising resources whilst they remain available; this is a useful strategy for plants growing in arid conditions ³⁹. Many plants also discard older leaves, allowing the nutrients in the older leaves to be recycled into the younger ones ⁶.

Further long-term acclimatisation responses to drought include turgor maintenance, which can be achieved in a variety of ways. Water loss can be minimised by stomatal closure, means to change leaf configuration, for example upturned leaves avoid excessive sunlight which prevents excessive heating and therefore water loss. Other mechanisms, such as increased root area, maximise the amount of water being taken up⁴⁰. Conversion of complex storage carbohydrates to small, soluble mono-, di- and oligo- saccharides can also change the osmotic potential, helping maintain tissue water potential⁴¹. Several other metabolic pathways are also employed to maintain turgidity⁴².

Short term responses to urgent stress generally involve minimising water loss (stomatal closure) and metabolic responses to limit dehydration damage. Whilst stomatal closure is one of the first responses to drought, as it is the most obvious way to prevent water loss, it can be difficult to assess the

details of this mechanism. This is because plant stomata are sensitive to light intensity, CO₂ concentration, and plant leaf water status, so they can be responding to a combination of factors at any time.

In this PhD project, the archaeological samples are mostly inner cob material with some kernel material; therefore the metabolic processes that occur in these tissues are focused upon. The samples are also fully mature fruits and in maize the effects of drought stress are reflected in kernel material^{43,44}.

1.2.5 Archaeological and Environmental Context of Tularosa Cave

Maize agriculture in the American Southwest has historically struggled against the issues of drought stress due to sparse and unreliable levels of precipitation, resulting in several pan-regional droughts in the last 2000 years^{4,5,45}. Various agricultural interventions have been adopted to mitigate the effects of drought, such as canal irrigation and lithic mulching⁴⁶. The oldest irrigation system in the Southwestern region (Tuscon, Arizona) dates to 2,680-2,260 BP⁴⁷. Since then canals have been constructed with variable intensity and complexity, reaching a peak during the Hohokam culture of Arizona in the 14th century AD⁴⁸. The covered channels were used to channel water from less arid mountainous regions to dryer areas.

Maize agriculture in Southwestern North America however has much longer antiquity than these drought management agricultural practices. Genetic^{23,29} and phytolith²⁸ evidence (Section 1.2.2) suggests that while the initial stages of maize domestication from the wild plant teosinte occurred once (in the Balsas River basin area of Mexico beginning around 9000 years ago, Section 1.2.2), several lineages separated before domestication traits were fixed.

Domestication pressures on the maize continued outside of the initial domestication area, resulting in several semi-domesticated divergent maize populations, some of which evolved into modern maize under

anthropogenic pressures. Maize arrived in the modern-day Southwestern United States around 4,100 years before present^{14,35}.

Maize was an important food crop and was integral to the rise of agriculture and therefore complex societies in Mesoamerica. Corn, beans and squash were key components of the Mesoamerican diet and cornerstones to agriculture. Corn has the advantages that it can be stored a long time and can also be ground into flour to make tortillas.

The samples examined in this project originate from Tularosa Cave in New Mexico (Figure 1.3). The peoples who occupied the cave are from the Southwestern Mogollon culture. The Mogollon culture was an early agricultural society which was active from approximately 3400 - 500 BP. They lived in the mountainous region of Southwestern New Mexico and Southeastern Arizona. They depended upon rainfall, floodwaters and stream diversion to irrigate their crops. The Mogollon, the Ancestral Pueblo peoples, and the Hohokam were the three major farming complexes in the southwest United States. All three were notable for geographic expansion, population growth and pueblo architecture. Pueblo architecture includes great cliff dwellings which could be up to four stories tall. Aridity in the Southwestern region put stresses on the societies and many of the largest settlements were abandoned by the late 14th century⁴⁹.

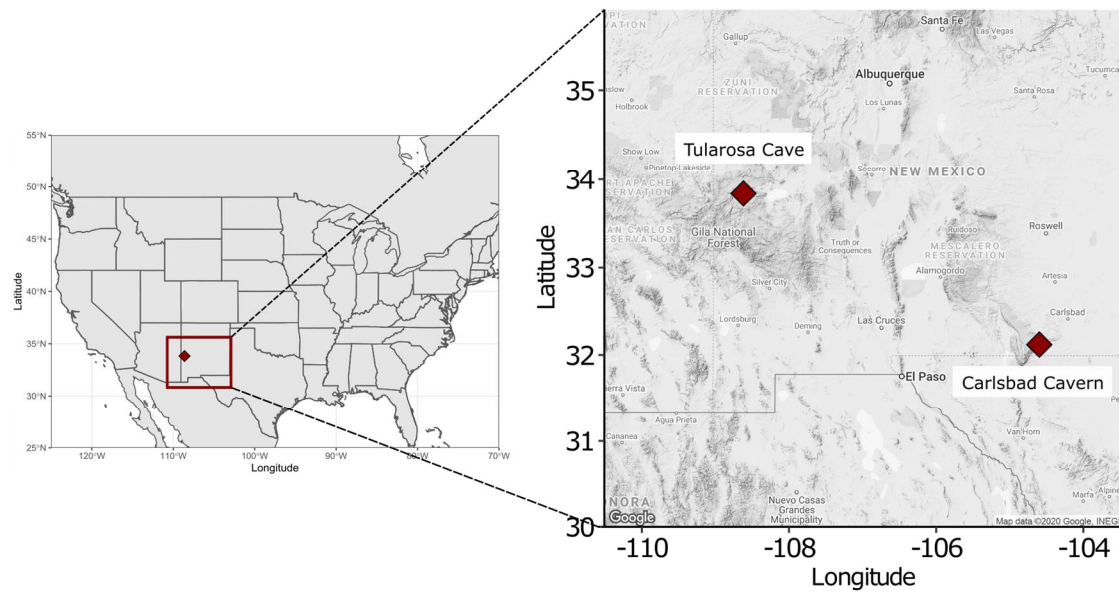


Figure 1.3: Map showing location of Tularosa Cave.

Tularosa Cave was excavated in 1950 by Martin *et al.*¹⁵ and housed a large collection of artifacts relating to the Mogollon Native American culture. The site was excavated in 12 lots of 20 cm layers which were dated according to the pottery culture excavated within. The cultures are: San Francisco, George Town and Pine-Lawn. Layers with no pottery were designated 'pre-pottery'. Due to the arid nature of the local environment, many of the finds were exceptionally well preserved, among them two human burials which were desiccated, and so 'mummified'. The plant remains in this cave were extensive and well preserved; 30,000 samples of maize were recovered (Figure 1.4). The maize dates from between 1,850 to 740 Cal BP.¹⁴

Phenotypically, the older maize is significantly different from the younger; it is also notably different from modern landraces. The early maize cobs (1850 – 1750 BP) are 'ovoid-shaped' (described in previous literature as pineapple-shaped¹⁴), short in length with a thick mid-section and small kernel form, consisting of 10-12 kernels. In contrast, the later corn (900 - 700 BP) is

'cylindrical' in shape with a thin mid-section and 8-10 rows of larger kernels. It is possible that these two morphologically distinct sets of maize are evidence for an adaptation to climate change. Genetic evidence from these maize cobs¹⁴ suggests that the maize was adapting to selective pressures.

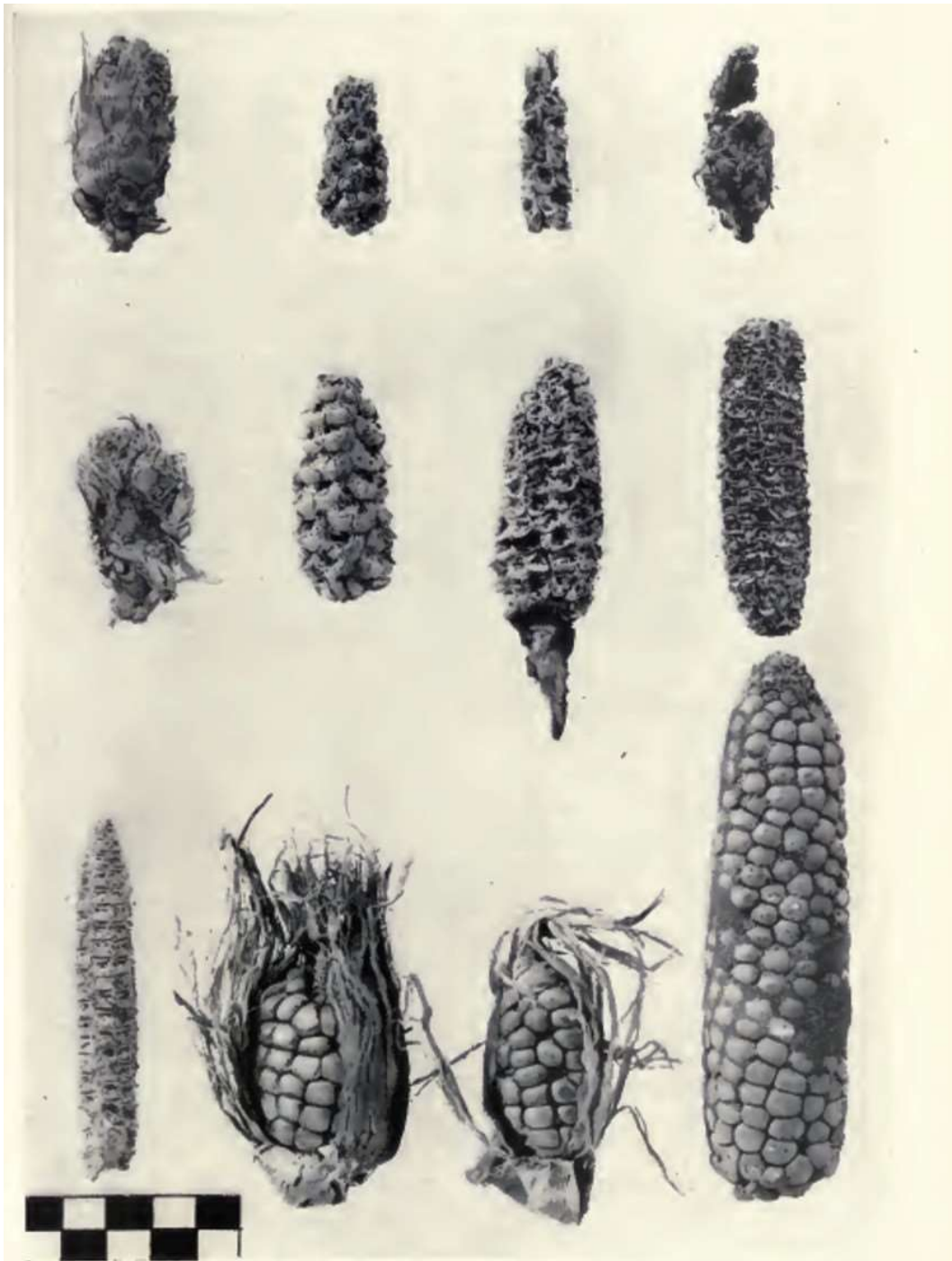


Figure 1.4: Examples of corn recovered from Tularosa Cave (from Martin *et al.*⁷).

The Tularosa assemblage offers a unique opportunity to investigate the effect of drought on maize, as a proxy for modern day climate change. With the maize grown during the earlier occupation being phenotypically significantly different from the more recent maize, it is possible that these two morphologically distinct sets of maize look different due to adaptation to climate change. Examples of the corn recovered from Tularosa Cave can be seen in Figure 1.4 and in Appendix 1.

Seven samples in this study have been radiocarbon dated to two temporally distinct periods: older (1830 - 1719 BP, 95.4% CI) and younger (771 - 681 BP, 95.4% CI)¹⁴. These periods are thought to correlate to two well-defined occupations of Tularosa Cave^{14,50}. Stalagmite records^{5,51} from caves in the Sacramento Mountains, New Mexico, show that during the earlier occupation of Tularosa Cave (2000 - 1700 BP) the annual precipitation was higher than at present and the more recent occupation (700 - 800 BP) was a time of severe drought. Figure 1.5 is drawn from annual stalagmite band

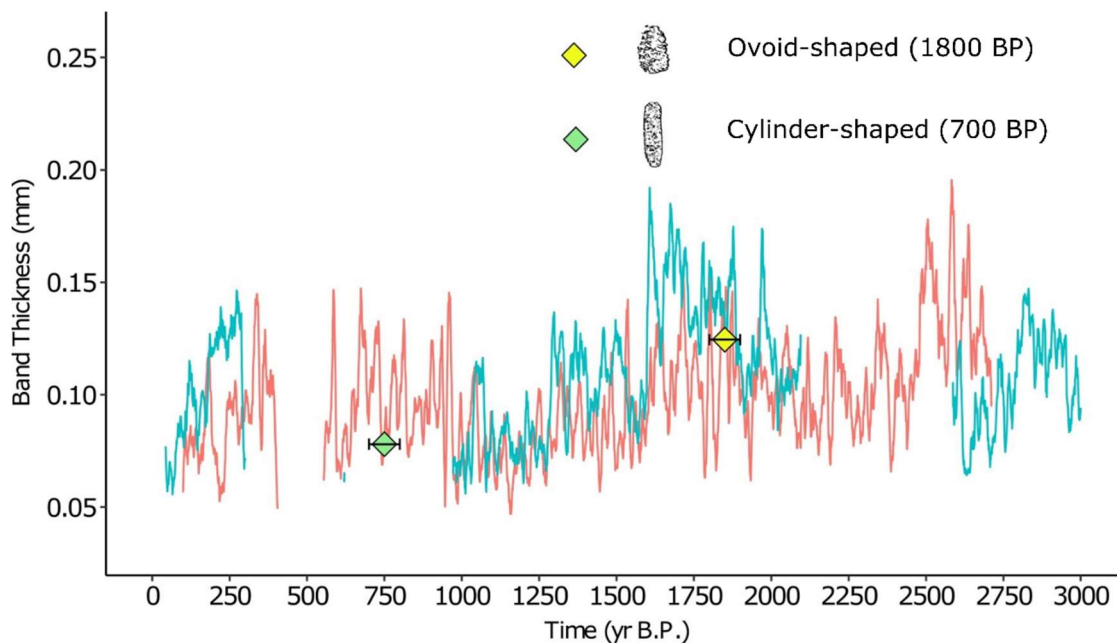


Figure 1.5: Stalagmite records from Carlsbad Cavern (BC2 red) and Hidden Cave and (HC1 blue). The growth for each year is given as band thickness (mm); 10-year moving average applied. The dates of the 1850 and 750 assemblages are marked on the graph as green and yellow diamonds.

thickness data and U/Th chronology for two stalagmites (BC2 and HC1) from Carlsbad Cavern and Hidden Cave (30 km southwest of Carlsbad Cavern, approximately 400 km from Tularosa Cave, Figure 1.3), New Mexico⁵¹.

Previous studies have correlated the oxygen isotopic signatures of maize to those of the source or soil water in order to find the growing location of the samples. For example, Williams *et al.*¹⁷ used the $\delta^{18}\text{O}$ of maize cellulose to identify the source water used for maize production in the arid Southwest of America. It is notable that some of the samples in the Williams *et al.* study were charred which has greatly affected the $\delta^{18}\text{O}$ value. Charred samples have a $\delta^{18}\text{O}$ value of more than 15 ‰ higher than uncharred samples. Charring-related enrichment in the heavier isotope, resulting in a higher $\delta^{18}\text{O}$ ‰ value is probably caused by fractionation during heating, resulting in the lighter isotopes being driven off preferentially. The samples from Tularosa are remarkable for their exceptional preservation through desiccation, so fractionation in these samples should be more simply related to stomatal conductance (rate of water vapor exiting the leaf through the stomata) than in the charred samples. Several further studies have attempted to use various stable isotope analysis approaches to identify the provenance of maize cobs⁵²⁻⁵⁸, although none have used stable isotope data to act as an indicator for drought stress.

Climate evidence from the Tularosa occupation periods suggests that drought was prevalent and severe^{5,16} and can be used as a proxy for future climate change, which is important due to the growing concerns caused by modern day climate change⁵⁹. It is imperative to protect the food security of future generations; given the fact that maize is the most important staple globally, it is crucial to understand the effects on it of drought. An important research question of this research relates to the investigation of the effects of drought on this important food crop. Tularosa cave is an important

archaeological site, from which were excavated many exceptionally well preserved archaeobotanicals including desiccated maize cobs, 89 of which have been obtained for examination in this PhD project. These samples are known to cover a 1,500 year period during which the New Mexico region underwent periods of severe drought¹⁶. Whilst the region benefits from a well-defined paleoclimate record indicating extended periods of low precipitation⁵, there is no existing direct evidence that the plants were directly exposed to drought. Comparison of drought and adaptation to it by a plant could never be attempted experimentally (via greenhouse or field experiments) over the time frame of a typical PhD. Access to the Tularosa Cave assemblage allows an otherwise impossible study of drought stress to be carried out.

1.3 Previous Molecular Analyses of Archaeological Maize

Studies of the Tularosa maize cobs conducted prior to the start of this project have focused on the recovery and analysis of ancient DNA and ancient RNA. The success of these studies (see below) is evidence of the exceptional preservation of these maize samples; if labile molecules such as DNA and especially RNA have survived, this encourages optimism that other biomolecules, such as ancient metabolites, may also have been preserved.

Da Fonseca *et al.*¹⁴ used the Tularosa samples in a broad discussion to identify the route maize took to arrive in the Southwestern USA. Da Fonseca *et al.* compared the nuclear DNA of the Tularosa corn to that of modern landraces. The Tularosa maize is split into two temporally distinct populations. The older ancestral population consists of individuals approximately 1800 years old (SW2K), while the other individuals are approximately 700 years old (SW750). The results showed that maize most likely entered the Southwestern USA 4000 years ago from Mexico via a

highland route. Population genetic analysis was also used to identify adaptation loci relevant to drought resistance.

Figure 1.6 shows gene trees constructed from population branch statistic (PBS) distance, which is a measure of the dissimilarity between the ancient landraces (SW750 and SW2K) and teosinte (*Z. m. parviglumis*), for the genes most strongly selected between the two populations: *su1* and *dehyd1A*. Both these genes are of interest in the context of the work described in this thesis, as they are associated with drought resistance. *dehyd1A* is a dehydration-

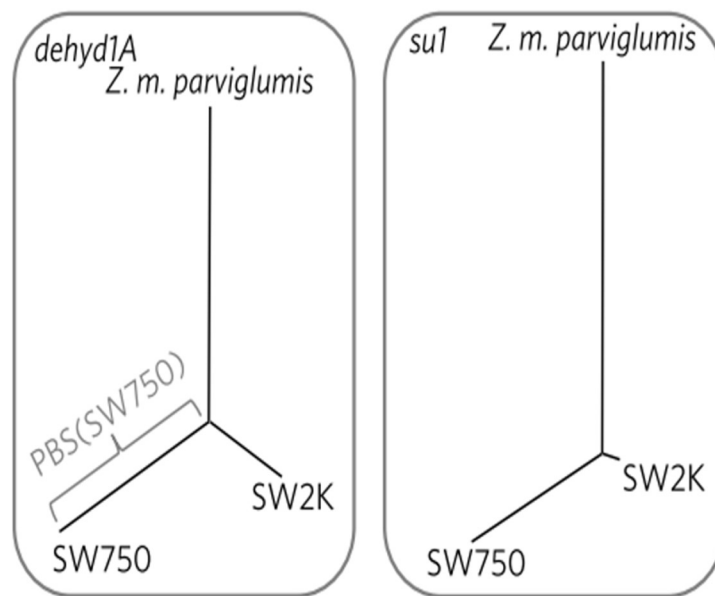


Figure 1.6: Figure from da Fonseca *et al.*⁶ representing gene trees using PBS distance for the genes *dehyd1A* and *su1*.

responsive element-binding protein shown in a previous study (Liu *et al.* 2013) to be upregulated in maize seedlings as a response to drought conditions. Diversity at *su1* was found to be reduced more than 60 % between the 2000-year-old samples and the 750-year-old samples which means that the allele was under selection during that period. This gene is responsible for the storage of non-structural starches such as soluble mono- or oligo- saccharides. This gene has been linked to maize flour consumption, as flour requires a high content of soluble starch. An alternative hypothesis

is that an increase in soluble mono- or oligo- saccharides compared to starches helps to regulate the osmotic potential when water is scarce, maintaining the plant's turgor, and thus structural integrity. This finding suggests there may also be molecular evidence for such changes in the metabolome of the Tularosa maize.

Other genes investigated by da Fonseca *et al.*¹⁴ are notable due to their implications regarding domestication, include *zagl1* and *ba1*. These genes relate to shattering and crop architecture respectively. These are both domestication features strongly selected for by human harvesting, as it is easier to harvest the kernels when the plants grow linearly on a single stalk and the kernels do not shatter randomly, but rather stay on the stalk. A third gene, *gi*, was identified and is associated with the regulation of flowering - a further desirable trait in the domestication of plants. It is advantageous to have plants flowering at the same time, so the harvest can be collected in one go.

Another study by Jaenicke-Despres *et al.*⁶⁰ which used the maize collection from Tularosa (and several other sites in Mexico) concentrates on three genes involved in aspects of plant domestication: plant architecture, storage protein synthesis, and starch production. *tb1* is a gene responsible for the unbranched maize architectures, *pb1* is responsible for the prolamin box binding factor - the protein involved in the expression of seed storage kernels - and *su1*. The report does not clarify the part of the cob sampled, but it is most likely the kernel. The DNA sequences were reconstructed from several clones from the amplification products, and these were compared to the sequences of modern maize landrace and teosinte alleles. The results were independently verified at two separate laboratories. The results showed that by 4400 years ago, domestication selection had substantially homogenised

the allelic diversity (up to a three-fold reduction) at three gene loci. This shows that domestication had a profound effect upon the genetic diversity of maize very early in the domestication process. A further example of ancient DNA analysis has been performed on samples from El Gigante cave in Honduras⁶¹. That report has similar results to the findings of Jaenicke-Despres *et al.*⁶⁰, finding that by approximately 4000 BP many domestication traits were fixed.

Fordyce *et al.*⁶² extracted the ancient ribosomal RNA from six kernels (aged approximately 750 BP) of maize. These samples originate from a site in Arizona called Turkey House ruin. The study concluded that maize kernels are a potential source of refuge for ancient genetic material due to the tough nature of the kernel and the fundamental role of RNA in seed germination⁶³. The similarity in burial condition, age and morphology of the Tularosa Cave samples to the samples studied by Fordyce *et al.* (2013) makes it seem feasible that ancient RNA may also be preserved in the Tularosa samples, and encourages optimism that metabolites may also be preserved.

In summary, a range of genetic evidence shows that genes that correlate with domestication are also consistent with adaptation to drought. It is possible that due to the excellent preservation of the Tularosa samples, metabolic evidence of drought may also be obtainable, which would be the first time this technique has been used for to study abiotic stress in ancient plant material. In this thesis I describe my investigations of the ancient maize metabolome for drought adaptations and also considered stable isotope ratio data for their potential to provide markers of past drought.

1.4 Stable Isotope Ratios

1.4.1 Nitrogen Isotope Ratios

Nitrogen is absorbed by plants through the soil. Fractionation of the nitrogen isotopes in plants is complicated by the presence and effect of nitrogen-fixing microorganisms and varying levels and types of nitrogen sources in the soil.

The levels and types of nitrogen sources vary naturally but can also be affected by anthropogenic factors such as addition of fertilisers (for information on isotope fractionation calculations see Section 2.5.2).

Nitrogen acquisition in plants is summarised by Miller and Cramer⁶⁴. Briefly, complex organic nitrogen-containing molecules are broken down into NH_4^+ by microbes and fungi in the soil. NH_4^+ may be oxidised to NO_3^- via nitrification. In anaerobic conditions and warm temperatures nitrate can be turned into nitrogen-containing gases, such as N_2O ⁶⁵. Inorganic nitrogen in the soil can become immobilised into organics by microbes and the situation is further complicated by symbiotic relationships between plants and mycorrhizae and rhizobia⁶⁶.

There are many factors which cause natural variation in the nitrogen isotopic composition of plants. At a local level these include: the form of the N being assimilated (N_2 , NH_4^+ , NO_3^-); the pathway used (direct uptake or following microbial uptake and transfer to the plant); the location of nitrogen assimilation (root or shoot); and the plant part sampled (leaf, root, fruit).

Isotopic fractionation of nitrogen also occurs as a result of biochemical fractionation (enzymatic discrimination between the isotopes) as the nitrogen is converted into organic nitrogen and further metabolised.

Many plants and especially legumes can also acquire nitrogen via symbiotic relationships with mycorrhizal fungi and rhizobial bacteria. Mycorrhizae tend to reduce the $\delta^{15}\text{N}$ value of the plant, as the fungi retain the isotopically heavier nitrogen⁶⁷. The type of mycorrhizae also affects the magnitude of the

resulting depletion of ^{15}N in the plant. Arbuscular mycorrhizae (AMs), the most common type of mycorrhiza, tend to lower the $\delta^{15}\text{N}$ value of the plant tissue by an average of 3.2 ‰ with respect to that of plants without AM symbionts.⁶⁸ The local climate can also affect the $\delta^{15}\text{N}$ signature. More arid sites tend to see a higher plant $\delta^{15}\text{N}$ value than wetter sites⁶⁹. There is some evidence that $\delta^{15}\text{N}$ plant signatures also fluctuate seasonally, possibly due to ammonium volatilisation^{68,69}. Ammonium volatilisation in the soil can enrich the ammonium in the heavier isotope by approximately 40 ‰⁷⁰. However, climate will also effect the type of mycorrhizae and rhizobia present, which will in turn effect the $\delta^{15}\text{N}$ signature of plants.

Finally, anthropogenic effects can have a large impact on $\delta^{15}\text{N}$ signatures. Fertilised plants exhibit an enrichment in ^{15}N (due to the ^{15}N enrichment of manure), which can be variable, depending upon the type of fertiliser used⁷¹. The intensity of fertilisation also affects $\delta^{15}\text{N}$ values⁷². Tillage (mixing of soil using plough technologies) also disrupts $\delta^{15}\text{N}$ isotope signatures, as the $\delta^{15}\text{N}$ values of soil profiles vary with depth⁷³. Therefore, disrupting the soil column changes the $\delta^{15}\text{N}$ value of plants growing in that soil. The factors influencing fractionation of nitrogen isotopes within the soil and root are summarised in Figure 1.7 (adapted from Szpak *et al.*⁷⁴). The figure shows that in warm conditions, ammonium volatilisation causes enrichment of ^{15}N (Figure 1.7, step 1). The biological oxidation of ammonia to form nitrates causes depletion of ^{15}N (Figure 1.7, step 2). Certain conditions (anaerobic, warm) cause the denitrification of nitrates. Uptake of nitrates results in minimal fractionation (Figure 1.7, step 3), but uptake of ammonium causes reduction of $\delta^{15}\text{N}$ values (Figure 1.7, step 4), the extent of which varies depending on source ammonium concentration. The assimilation of nitrates and ammonium into organics causes a depletion in ^{15}N (Figure 1.7, steps 5, 6 and 8). Movement of nitrates to the shoot before assimilation results in a

depletion of ^{15}N (Figure 1.7 step 7). Organic N can be moved between the root and the shoot with no fractionation of N isotopes (step 9).

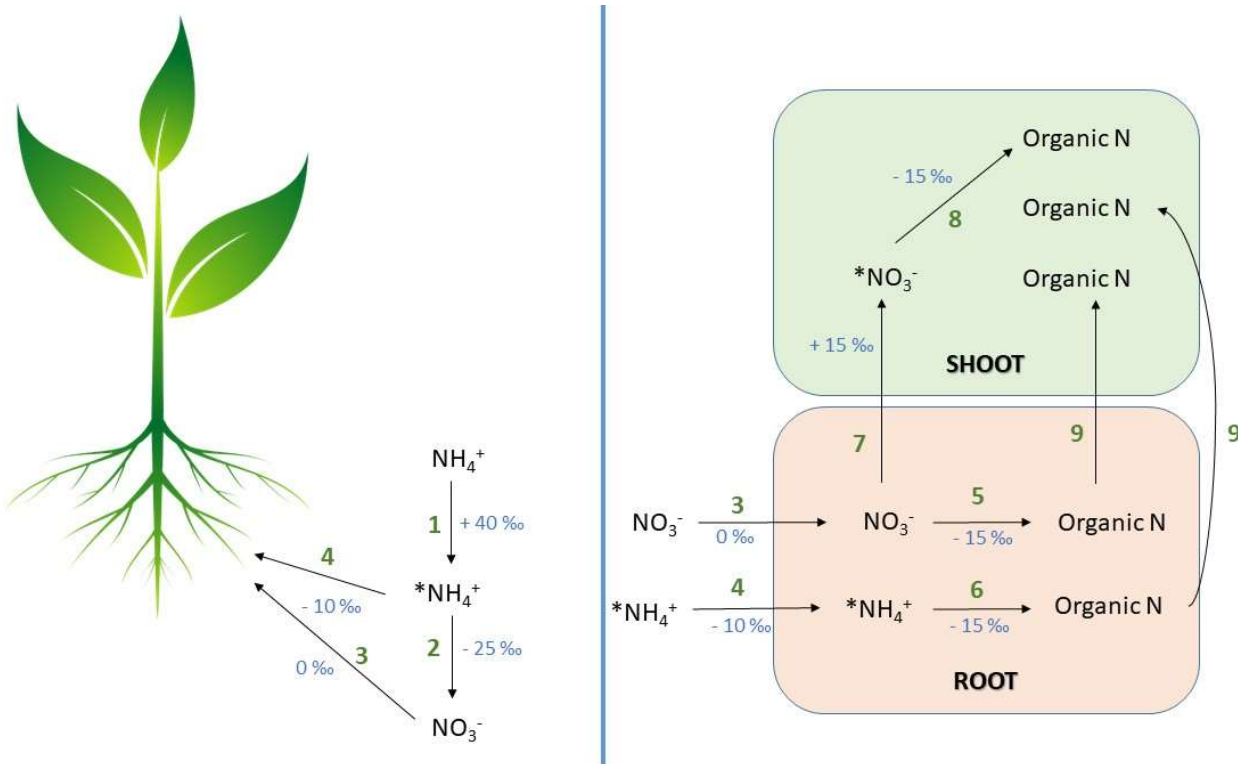


Figure 1.7: Simplified schematic of nitrogen uptake, adapted from Szpak *et al.*⁶³. Fractionation factors are labelled in blue: (1) Ammonium volatilisation. It has been found that this process concentrates ^{15}N in the remaining ammonium labelled $^*\text{NH}_4^+$ ⁵⁹. (2) Nitrification. The biological oxidation of ammonia into nitrate.⁵⁹ (3) Uptake of NO_3^- causes negligible fractionation⁶⁴. (4) Uptake of $^*\text{NH}_4^+$ is associated with nitrogen fractionation. The extent of the fractionation depends on the source concentration of $^*\text{NH}_4^+$ ^{60,64}. (5) NO_3^- assimilation into organic nitrogen. The reduction of NO_3^- to $^*\text{NH}_4^+$ is associated with a fractionation of nitrogen isotopes⁶⁵. (6) $^*\text{NH}_4^+$ assimilation occurs in the root and is associated with fractionation of N isotopes. (7) NO_3^- can also be moved to the shoot to be assimilated. This results in fractionation of N isotopes. This is because the NO_3^- pool has been depleted in ^{15}N via assimilation of N into organic N in the root. (8) NO_3^- assimilation into organic N in the leaf. (9) Organic N can be moved between the root and the shoot with no fractionation of N isotopes.

1.4.2 The Effect of Drought on Nitrogen Isotope Ratios

Drought conditions cause ammonium volatilisation in the soil, enriching in the heavier (^{15}N) isotope and thus increasing the $\delta^{15}\text{N}$ value of ammonium in the soil. In drought conditions it has been found that AMs help the host plant to withstand drought stress by inducing a wide array of effects in plants such as root elongation, improvement of nutrient uptake and increasing resistance to abiotic stresses^{75,76}. The nitrogen is predominantly assimilated into the root via AMs. AMs deplete the ^{15}N in the soil and retain the heavier isotope, resulting in a depletion in the heavier isotope in the plant root.⁷³ Evaporative enrichment may also occur when small volatile nitrogen-containing compounds diffuse out through open stomata, causing an increase in the heavier nitrogen isotopes in the leaf tissues. Translocation from the senescent parts (old leaves) may also enrich ^{15}N in fruits⁷³, this is due to the losses of volatiles in leaves which results in enrichment in ^{15}N .

1.4.3 Compound-Specific Nitrogen Isotope Ratios

In order to understand the complex expression of plant bulk $\delta^{15}\text{N}$ signatures it can be revealing to look at the isotopes at a compound-specific level. Since the main contributor to bulk N content is protein, analysis of the individual amino acids' (AAs) nitrogen isotope signatures can further understanding of the biochemical processes that contribute to the overall bulk $\delta^{15}\text{N}$ signature⁷⁷.

This compound-specific approach can be used to interrogate the metabolic processes of plants and is achieved by examining the stable nitrogen isotope ratios of individual amino acids ($\delta^{15}\text{N}_{\text{AA}}$). Amino acids are released by acid hydrolysis of proteins present in plant remains and derivatised for gas chromatography-combustion-isotope ratio mass spectrometry (GC-C-IR-MS). Previously this approach has shown that $\delta^{15}\text{N}_{\text{AA}}$ values of modern cereal grains and rachis were largely attributed to metabolic pathways involved in

their biosynthesis and catabolism and that manuring resulted in consistent ^{15}N -enrichments of all amino acids⁷⁸. The latter shows that the application of manure does affect the metabolic routing of nitrogen into cereal grain, but that such external factors affect all amino acids similarly^{78,79}. Styring *et al.*⁷⁹ also found that growing conditions and climate across two growing sites (annual rainfall 727 mm compared to 483 mm) do not result in significant differences in the relative $\delta^{15}\text{N}$ values of different AAs in barley and bread wheat grains, although some differences were noticed in the rachis.

Styring *et al.*⁷⁹ also related $\delta^{15}\text{N}_{\text{bulk}}$ and $\delta^{15}\text{N}_{\text{AA}}$ values within bone collagen, using a mass balance equation. A strong correlation was found between the $\delta^{15}\text{N}_{\text{bulk}}$ and $\delta^{15}\text{N}_{\text{AA}}$ values, $r = 0.93$. There was an offset of approximately 2 ‰ between measured $\delta^{15}\text{N}_{\text{bulk}}$ and the calculated $\delta^{15}\text{N}_{\text{bulk}}$ values determined by summing the component $\delta^{15}\text{N}_{\text{AA}}$ values, likely due to the missing values for those AAs that cannot be analysed using GC-C-IR-MS (see Section 2.5.3).

1.4.4 Oxygen Isotopes

Oxygen is taken up by plants in the form of water through the roots. The oxygen isotopic signature ($\delta^{18}\text{O}$) highly correlates with that of the source water at the root¹⁷. As the water travels from the root to the leaf no biochemical fractionation occurs^{**}, however some fractionation will occur due to thermodynamics⁸⁰. Once in the leaf, fractionation also occurs due to thermodynamic processes. The lighter oxygen isotope, ^{16}O , is more likely to evaporate and diffuse out of the stomata than ^{18}O . This results in 'evaporative enrichment' of the heavier isotope in the leaf tissues (Figure 1.8).

^{**} Enzymes discriminate between isotopes, which may result in a depletion or enrichment in the heavier isotope depending on the enzyme.

Biochemical fractionation occurs due to the enzymatic processes associated with photosynthesis and glucose metabolism. If the leaf experiences lots of heat radiation, then more ^{16}O will be lost than ^{18}O . The oxygen atoms (from the water) become fixed in cellulose due to photosynthesis and subsequent metabolism of the glucose produced. Therefore, a higher $\delta^{18}\text{O}$ is observed if cellulose has been fixed when a plant has experienced high temperatures⁸¹. In this manner $\delta^{18}\text{O}$ values can be correlated to environmental conditions.

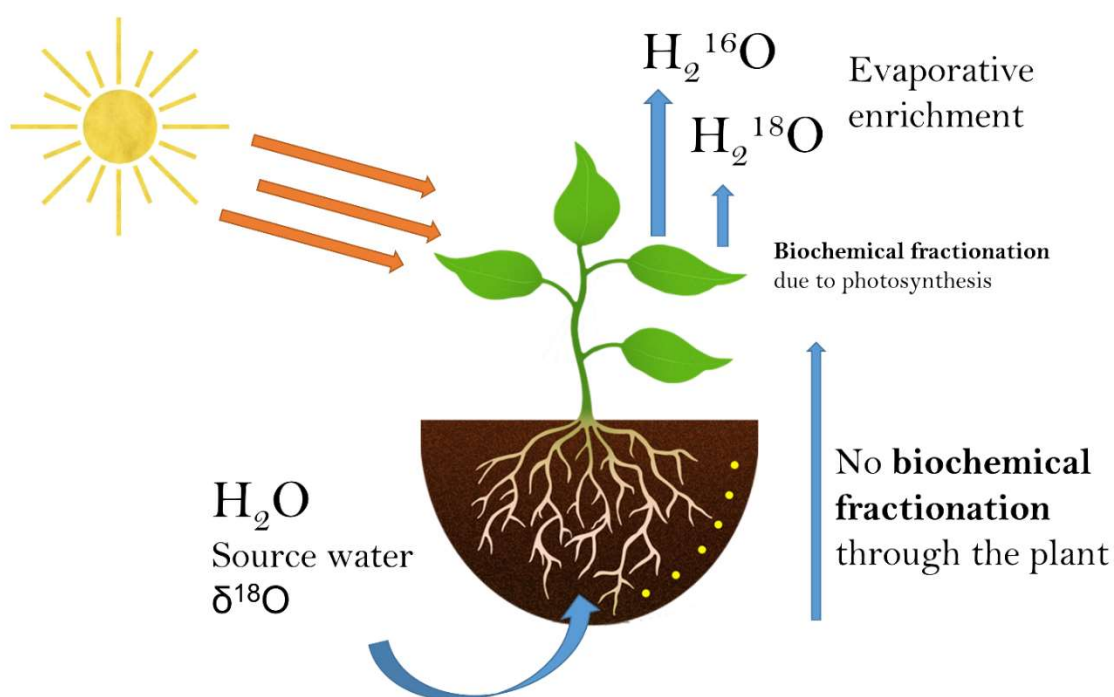


Figure 1.8: Diagram summarising oxygen isotope fractionation in plants.

1.4.5 Previous Studies of Ancient Maize Using Oxygen and Nitrogen Isotope Ratios

Previous studies have correlated the oxygen isotopic signatures of maize to those of source or soil water in order to identify the growing location of the samples. Williams *et al.*¹⁷ used the $\delta^{18}\text{O}$ of maize cellulose to identify the source water used for ancient maize production in the arid Southwest of America. They tested the hypothesis that source water variation in $\delta^{18}\text{O}$ is

related to $\delta^{18}\text{O}_{\text{cellulose}}$ in a series of control experiments using experimentally grown maize grown under the same conditions, to control for evaporative enrichment. Having proven that the $\delta^{18}\text{O}_{\text{water}}$ value is retained in the cellulose $\delta^{18}\text{O}$ signature, they used these data to match the $\delta^{18}\text{O}$ isotope signature of the cob cellulose of archaeological samples with those of potential water sources.

Whilst this correlation worked well with the control experimental samples analysed by Williams *et al.*¹⁷, it is difficult to know how robust this is in relation to the archaeological samples tested by these researchers because the ancient water sources are not available, although, an estimation of fractionation due to evaporative enrichment was incorporated into the model. It is notable that some of the samples in the Williams *et al.* study were charred which is likely to have greatly affected the $\delta^{18}\text{O}$ values (Section 1.4.4). This charring-related enrichment is probably caused by fractionation during heating, resulting in the lighter isotopes being driven off preferentially.

Understanding $\delta^{15}\text{N}$ signatures in archaeological samples is complex, due to diagenesis which can occur in the plant following death, as well as the many factors that can result in fractionation (Sections 1.4.1 and 1.4.2). Many archaeological samples of plant materials are preserved due to charring. Fraser *et al.*⁸² found that the heating of various cereal grains and pulses (wheat grain, pea, broad bean and lentil) at 230 °C for 24 h can cause an enrichment in ^{15}N that increases the $\delta^{15}\text{N}$ value by around 1 ‰. This is most probably due to the preferential loss of isotopically lighter ^{14}N -containing volatiles. Styring *et al.*⁸² showed that the heating of modern einkorn grain at 230 °C for 24 h also resulted in an increase of 1 ‰. FTIR and solid-state ^{13}C NMR showed that the heating of modern einkorn grains resulted in Maillard reactions between proteins and starch, producing high molecular weight melanoidins. Solid-state ^{13}C NMR of ancient charred einkorn grains showed that they retained a similar proportion of N to the 24 h-charred modern

einkorn grains, suggesting that the amino acid nitrogen in the ancient grains was retained in stable melanoids, which are resistant to degradation.

Fraser *et al.*⁸² also reported that burial (for up to 2 years) had little effect on the $\delta^{15}\text{N}$ values of charred botanical remains. However, most archaeological samples are buried for several hundred years or more, so it is possible that burial does have an effect on the isotopes over such long time periods.

However, the work presented here focusses on uncharred remains.

A study by DeNiro and Hastorf⁸³ suggested that the $\delta^{15}\text{N}$ signatures of prehistoric plants that were not charred are generally 10-20 % more positive than their modern counterparts. This study suggests that this is a result of diagenesis. However, a more modern study by Metcalfe and Mead⁸⁴ suggests that maize samples analysed by DeNiro and Hastorf were possibly fertilized by seabird guano which can produce extremely high plant $\delta^{15}\text{N}$ signatures⁷⁴. Metcalfe and Mead found that a range of uncharred plant remains (mostly trees) from the Early Holocene have similar $\delta^{15}\text{N}$ signatures to their modern counterparts. However, they recommend the use of FTIR or other structure analysis techniques to assess the level of diagenesis in samples with altered $\delta^{15}\text{N}$ signatures.

A study by Amundson *et al.*⁶⁹ has shown that, globally, soil $\delta^{15}\text{N}$ values tend to be higher than plant $\delta^{15}\text{N}$ signatures. Therefore, it is possible that leaching of organics from the soil into buried ancient plant material could cause an enrichment of the plant ^{15}N levels during burial. Volatilisation of nitrogen-containing compounds over the long term could result in an increase in $\delta^{15}\text{N}$ values, as Admussen *et al.* found that increasing annual temperatures and decreasing rainfall led to an increase in soil and plant $\delta^{15}\text{N}$ values.

The ancient maize from Tularosa is extremely well preserved, not charred and is desiccated. The isotope ratios of the two sets of samples of different ages (and climate conditions) can thus conveniently be compared to determine whether drought signatures can be inferred.

1.5 Metabolomics

1.5.1 Overview

Metabolomics is a powerful tool for investigating the entire chemical profile of a biological sample. Metabolites and their levels are of particular interest when investigating genetic influences or environmental changes, as they can be regarded as the final response of an organism to genetic or environmental perturbations⁸⁵. Metabolomics has previously been used to understand the stress response from drought^{9,86–88} and salinity^{89,90} in experimentally-grown modern maize. A detailed description of metabolomics workflows and the instrumentation used is provided in chapter 2.

Metabolomics can be used to complement the other `omics techniques (genomics, transcriptomics, and proteomics, Figure 1.9) and in combination with these techniques it can help us understand complex molecular processes in biological material (for example^{91,92}). Metabolomics, unlike other `omics techniques does not depend on organism-specific genome information for data analysis and interpretation⁹³.

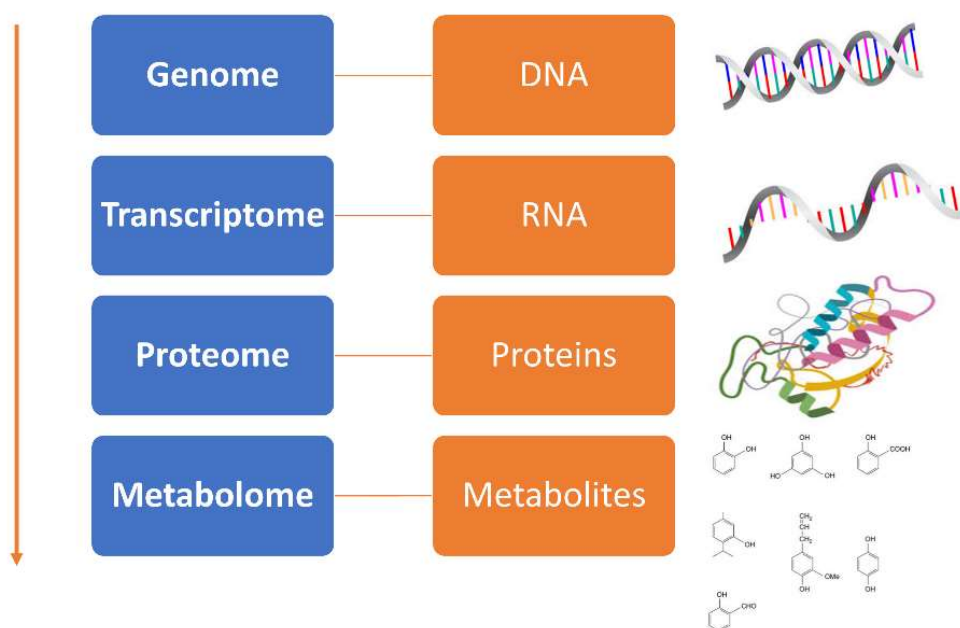


Figure 1.9: 'Omics technologies in combination offer a comprehensive understanding of biological systems.

1.5.2 Extraction Considerations

Metabolomics approaches in general consider the extractable metabolites; therefore extraction protocol plays an important role in the types of molecules included in the analysis. Published methods in plant metabolomics most often work with fresh material processed under cold conditions, although this can pose significant practical challenges. Samples are generally immediately frozen in liquid nitrogen and stored at -80 °C to inactivate enzymatic processes. However, weighing plant material kept frozen in liquid nitrogen can be difficult due to several practical considerations such as electrostatic charging, and condensation onto frozen tissue in damp atmospheres which can cause variation in the tissue weights (due to condensed water). Lyophilising the samples prior to homogenisation removes water from the sample, which inactivates enzymes and potentially

stabilises the metabolome⁹⁴. However, few studies have considered the effect of lyophilising plant material as a means to stabilize the metabolome^{95,96}.

1.5.3 Primary and Secondary Metabolites

The metabolite pool of a plant tissue is made up of a wide range of metabolites with diverse physicochemical properties, ranging from ionic inorganics to amino acids, and hydrophobic lipids. Plant metabolites are classified into primary and secondary metabolites⁹⁷ (Figure 1.10), although some metabolites can be classed as both a primary and secondary metabolite.

Primary metabolites are fundamental for plant growth and development.

Primary metabolites are usually directly involved in normal growth, development, and reproduction, and they often perform an intrinsic function. Examples of primary metabolite classes include lipids and nucleic acids. Such compounds are often those found concentrated in seeds (such as maize kernels) and vegetative storage organs.

Secondary metabolites are organic compounds that aid the organism in normal growth and development, and are compounds derived from primary metabolites. Secondary metabolites usually have an important ecological function, such as adaptations to environmental stresses⁹⁸, or serve as chemical defences against predators. Examples include: phenolics and alkaloids⁹⁹.

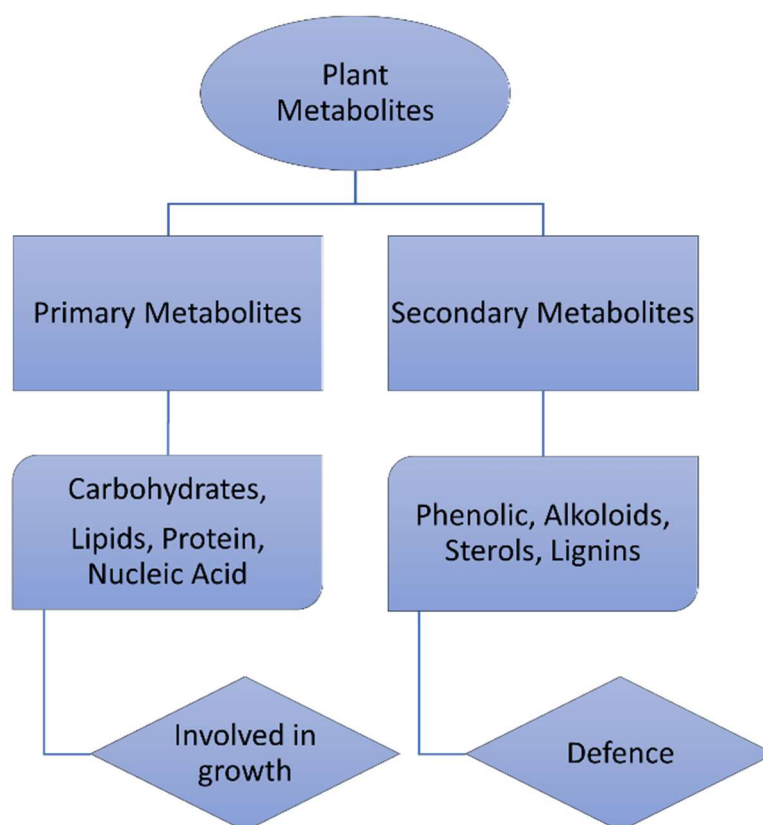


Figure 1.10: Classification of primary and secondary metabolites (image adapted from www.vivadifferences.com¹⁰⁰).

1.5.4 Drought Stress Response in Maize

The maize cob provides the growing seed with nutrients including proteins, oils and starch. Hence, lipids, amino acids, and soluble carbohydrates are expected to be the major components of a kernel extract. It has been shown that increases in the levels of osmoprotectants, such as mono-, di- and oligo-saccharides, polyols and some quaternary ammonium compounds such as taurine are a common adaptive measure to water stress across a range of cells and tissues; their accumulation accompanies drought stress⁹. Amines, mono-, di- and oligo- saccharides and sugar alcohols can act as stabilising agents to macromolecules such as proteins; these molecules help proteins to maintain their hydration state and hence their structure^{88,101}.

Hormones are important mediators of plant responses to stress. For example, abscisic acid (ABA) is heavily implicated as a controller of stomatal closure

when water deficiency is detected in the roots¹⁰². Plant hormones can be found in most plant tissues including the fruit¹⁰³. A large reduction in intracellular CO₂, such as occurs during drought (due to stomatal closure¹⁰⁴), can result in over-reduction in the electron transport chain and produce reactive oxygen species (ROSs) that may initiate photo-oxidation. Accumulated ROSs can act as secondary messengers in hormone-mediated events. The intracellular concentrations of ROSs are controlled by antioxidants, which include ascorbate and glutathione⁶. For B73, a drought-susceptible modern maize cultivar, drought stress has been shown to cause an accumulation of simple sugars and polyunsaturated fatty acids and a decrease in amines, polyamines and dipeptides, together with an increase in accumulation of ROSs and the fungal product aflatoxin⁴³.

1.5.5 Review of Relevant Previous Metabolomic Studies

1.5.5.1 Extraction Approaches

Hamid *et al.*⁹⁵ investigated the effects of freeze-drying compared with oven-drying of material on the metabolite profiles of three different types of edible brown seaweed; it was found that freeze-drying resulted in the ability to extract higher metabolite concentrations than did oven-drying. A previous study by Oikawa *et al.*⁹⁶ has shown that freeze-drying of plant tissue following grinding can be used to stabilise metabolites. Oikawa *et al.* found that in *Arabidopsis* freeze-drying had no effect on the concentration of plant hormones, when compared to keeping samples frozen, except for on salicylic acid, the concentration of which in the resulting extracts was increased following freeze-drying. They also tested pear fruit, in which plant hormone concentrations were found to slightly decrease in freeze-dried samples when compared to frozen samples. It is clear that the effect of freeze-drying should be tested on maize, as the few results there are, are inconsistent between species and tissue types.

The archaeological maize from Tularosa Cave is totally desiccated, so the effect of lyophilization as a way to stabilize the metabolome is of interest. If desiccation can stabilize the metabolome effectively, then metabolites, and perhaps even a drought signature in the maize extract may be preserved in the archaeological samples. If lyophilisation does stabilise the metabolome, it could prove to be a very convenient development for application in metabolomic studies of fresh modern samples as well as paleobotanical material.

1.5.5.2 *Metabolomics in Archaeology*

Metabolomic techniques have been used in a small number of studies of archaeological samples in recent years, although the number is fast growing indicating a vibrant area of application in archaeological sciences. When metabolomic approaches are used to analyse ancient biological systems, we would like to suggest it can be referred to as paleometabolomics.

Metabolomics has been used in the analysis of the stomach content of the Iceman, a 5,300-year old European glacier mummy¹⁰⁵. This study took a multi-omics approach to gain insight into the nutritional habits of the Iceman. The microscopic and molecular data found evidence of three components in the Iceman's last meal: fat and game meat from ibex and red deer, supplemented with cereals from einkorn. Other studies have used metabolomics to distinguish closely related plant species found in residues of ancient pipes¹⁰⁶ and tobacco mixture usage by ancient Mayans¹⁰⁷. To the author's knowledge, paleometabolomics has not been used to infer the physiological status of ancient plants before.

1.5.5.3 Metabolomics in Studies of Modern Maize

Whilst there has been minimal use of metabolomics in an archaeological context, there are many studies profiling metabolites under drought conditions in modern maize grown under experimental conditions. Rohlig *et al.*⁸⁷ investigated the differentiation in metabolite profiles of maize due to genetics and environment. Differentiation due to wet and dry growing conditions was possible on the basis of the metabolite profiles of kernel extracts.

Rohlig *et al.* samples were obtained from randomised field plots, and for each cultivar, three field replicates were analysed in triplicate. The kernel frozen in liquid nitrogen to inhibit metabolic processes, and ground and dried. Polar and apolar metabolites were extracted, using methanol:water and dichloromethane (DCM) respectively. The lipid extract (apolar metabolites) was trans-methyl esterified and the polar extract was fractionated prior to gas chromatography-mass spectrometry (GC-MS).

Over 300 distinct analytes were detected, of which 167 were identified. Four different growing regions were used in their study; of them one was characterised by dry, sandy soil, whereas the others had wet clay/loam soil. Principal components analysis (PCA) of the GC-MS results reveals that in two of the three growing seasons the metabolite profile of the plants grown in the drier region can be clearly separated from those of plants grown in the others, for a variety of metabolite classes.

A study by Witt *et al.*⁸⁸ was designed to test the metabolic and phenotypic responses of greenhouse-grown maize to experimentally controlled drought stress. Polar and non-polar metabolites were extracted by shaking different plant tissues in water at 70 °C for 15 minutes. The apolar metabolites were removed by adding chloroform, and the chloroform layer was then discarded. The polar analytes in the aqueous phase were analysed by GC-MS. This study focuses on the different metabolic responses to drought of

different tissue types. Several tissue types were sampled, including the ear and husk. PCA revealed that the tissue types are distinguishable by their metabolite profiles and that the cob in this study had a distinctive metabolite profile (identified by comparison of product ion data to a database).

Witt *et al.* (2012) reported that leaf blades were the most informative plant tissue to use if the aim is to diagnose drought stress. However, leaf tissue rarely survives archaeologically, and the inner cob material is much more plentiful in Tularosa Cave archaeological assemblages than other maize material. Witt *et al.* conclude that the ears, being short-duration organs, only grow if they are fully hydrated, thus are relatively inert metabolically, compared with leaf tissue. However, slight increases in some metabolites, particularly in soluble carbohydrates, were detected in the ear. Metabolites that showed the largest responses to drought stress across all tissues were: xylose, vanillic acid, methionine, putrescine, proline, histidine, β -alanine and phosphoric acid.

A study by Harrigan *et al.*⁸⁶ studied the metabolite profile of the grain (kernels) of seven maize hybrids grown in the field under well-watered and drought conditions. This study focuses on water restriction during grain-fill^e. Water restriction at this stage in the growing process is the time most likely to affect metabolites in the cob¹⁰⁸. The samples were ground and oven-dried (130 °C for 2 h). and the hexane extraction protocol of Harrigan *et al.*⁹ was followed for metabolite extraction. Fatty acids were trans-esterified using acetyl chloride/methanol, extracted into hexane and analysed using GC-MS. Polar metabolites (amino acids, organic acids and sugars) were analysed following separate extractions. These polar analytes were separated and analysed using reversed-phase high performance liquid chromatography-mass spectrometry (HPLC-MS). Glutamic acid and histidine were found to increase when water was restricted during grain-fill. Glucose was found to be lowest if water was restricted during the grain-fill period, and highest if

water was restricted during the vegetative growing period. The organic acids saccharopine and malic acid increased (compared to the control) if water stress was applied during grain-fill, as did glycine, betaine and glycerol.

The molecules identified by Harrigan *et al.* that are relevant to drought stress in maize kernels include sugars, alcohols and amines and organic acids. No fatty acids were specifically identified as changing. Therefore, the apolar molecules in the kernel matter were less informative of drought effects than the analytes identified in the polar extracts. This is intuitive as the most obvious effect drought has upon a plant is water loss, and the resulting metabolic pathways utilised by plants involve the release of osmolytes (polar molecules) to protect turgidity¹⁰⁹.

1.6 Aim and Objectives

The overarching aim of this PhD project was to examine the effects of drought stress on the maize metabolome and the isotopic composition of maize. Specifically, both modern maize plants grown under experimental watering conditions, as well as archaeological maize samples from Tularosa Cave were examined, as the latter offer a unique proxy for future droughts this is due to the extreme drought conditions in the time-period these maize cobs were grown. To achieve the aim of this thesis the following specific objectives were identified:

- To test whether nitrogen isotope ratios are affected by drought stress and can be used to distinguish maize grown under different climate regimes (chapter 3).
- To test whether amino acid nitrogen isotope ratios are affected by drought stress and can be used to distinguish maize grown under

different climate regimes (chapter 3).

- To test whether oxygen and carbon cellulose isotope ratios are affected by drought stress and can be used to distinguish maize grown under different climate regimes (chapter 3).
- To develop and apply a method to use untargeted metabolomic approaches (chapter 4) to investigate changes in plant metabolites under drought stress in maize grown under experimentally controlled watering conditions using lyophilized inner cob and kernel material.
- To use the methods developed (described in chapter 4) to carry out untargeted and targeted analyses of drought-stress related metabolites in archaeological maize extracts (chapter 5)
- To use laboratory ageing experiments to understand how age and desiccation may have affected isotope ratios and metabolite preservation in the archaeological maize samples (chapter 6).

Chapter 2 details the analytical techniques and instrumentation used in the work described in this thesis. Chapter 3 presents the results of bulk nitrogen isotope ratio analyses of experimentally drought stressed maize, analysing both the inner cob and kernels, with the goal of applying this approach to identify direct indicators of drought in archaeobotanicals. The results of bulk nitrogen isotope ratio analyses of the maize from Tularosa Cave are presented here. Nitrogen isotope ratios of amino acids were used to distinguish between metabolic and external causes of bulk ^{15}N enrichment. Chapter 3 further details the results of oxygen isotope ratio analysis of

cellulose from experimentally drought-stressed maize and the Tularosa archaeological samples.

Chapter 4 describes a method developed to extract drought-related metabolites from both experimentally drought-stressed maize and the Tularosa maize for analysis by HPLC-MS. The effect of lyophilisation on stabilising metabolites was investigated. The results of untargeted metabolomics experiments on drought treated modern maize and the Tularosa archaeological maize are presented here.

In chapter 5 untargeted metabolomics experiments have been used to identify differences in the metabolomes of the archaeological maize and then to target detection of drought-related metabolites in the Tularosa maize. Ageing experiments (Chapter 6) were used to help interpret how the metabolites may have changed with diagenesis to help deconvolute the effects of diagenesis from those of drought.

Chapter 7 contains an overview of the results and attempts to integrate them, and presents recommendations for future work.

Chapter 2. Analytical Technology and Considerations

2.1 Analytical Technologies Used in Plant Metabolomics

Metabolomics describes the high-throughput analyses of complex metabolite mixtures from biological systems such as plant extracts¹¹⁰. Metabolomics provides a biological 'endpoint', for example markers associated with a particular disease, treatment or defence mechanism. Other 'omics technologies (transcriptomics, proteomics, genomics) describe what may happen.

There are many types of analytical approaches, although more recently these seem to depend increasingly on mass spectrometry. This analysis can require the use of multiple mass spectrometry platforms to achieve a comprehensive coverage of metabolites. In this section, the metabolomics workflow will be discussed: experimental design, sample preparation, instrumentation, and statistical data analysis. A schematic outlining a typical metabolomics workflow can be seen in Figure 2.1. Whilst GC-MS and liquid chromatography-mass spectrometry (LC-MS) are both commonly used, the work described in this thesis used LC-MS approaches, and so those will be the focus of this section.

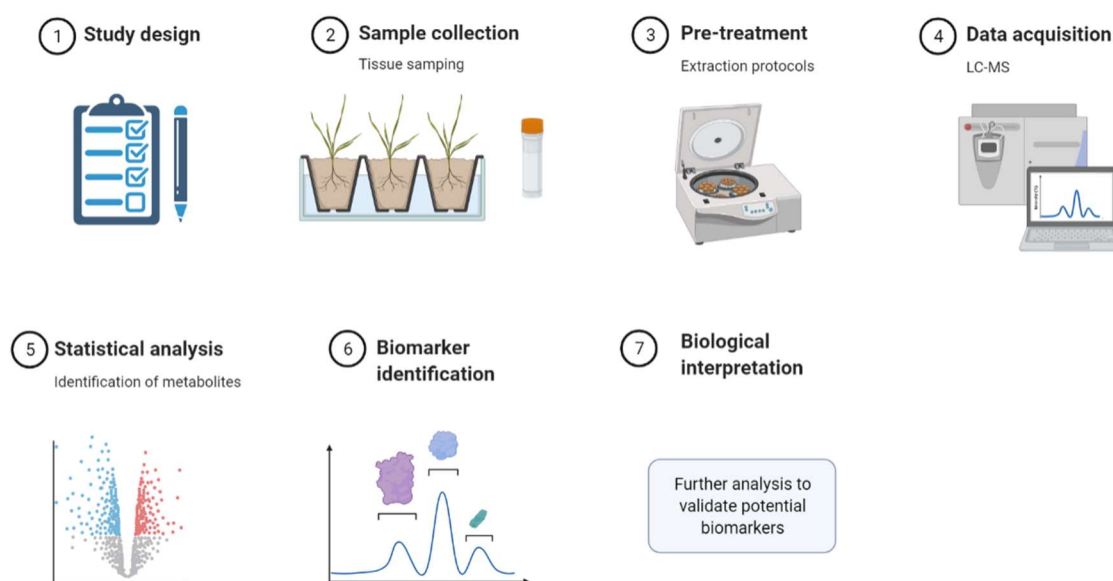


Figure 2.1: Typical metabolomics experiment workflow. Image created using BioRender.com.

2.2 Metabolomics Experiment Workflow

2.2.1 Study Design

Metabolomics experiments can follow one of two approaches, a targeted or untargeted approach. Untargeted metabolomic studies involve the profiling of many low-molecular-weight organic metabolites, in an effort to identify diagnostic changes in metabolites due to different conditions, such as abiotic stress, to which the metabolome is sensitive¹¹¹. Untargeted experiments allow the visualisation of changes in both known and unknown metabolites across different conditions. This type of experiment can be described as hypothesis generating (for example see ¹¹²). Following an untargeted study, the metabolites can be annotated using tandem mass spectrometry (MS/MS) – usually based on product ion analyses – to gather structurally informative fragmentation information, and using this to search a range of metabolite databases. Targeted metabolomics (hypothesis driven) involves the detection and quantification of specific metabolites using known amounts of authentic reference standards.

2.2.2 Sample Collection and Pre-Treatment

When setting up targeted and untargeted metabolomics experiments it is important to carefully consider the experimental design to achieve truly comparable analyses, and thus generate reliable and reproducible results¹¹³. In a metabolomics experiment biological replicates are required to represent the total population which is being studied to account for biological variation. Consideration of how many replicates is used must be balanced with the availability of replicate material and the time and resources available for the analyses.

2.2.3 Data Acquisition: High Performance Liquid Chromatography-Mass Spectrometry

Liquid chromatography separation coupled to a mass spectrometer is a powerful way to investigate the plant metabolome, in both targeted⁸⁶⁻⁸⁸ and untargeted analyses^{112,114}. HPLC is frequently used to separate complex biological mixtures. A wide range of analyte classes can be analysed using HPLC-MS, such as polar analytes, lipids and thermo-labile analytes (without derivatisation). This versatility makes HPLC a good choice for metabolomic analysis. MS can be used to measure the relative abundances of different elemental isotopes in a sample (elemental mass spectrometry) or to generate fragment ions characteristic of the structures of compounds, and/or to quantify known compounds (organic mass spectrometry).

To obtain the most reproducible and comparable series of data from an LC-MS separation it is advisable to run several (ideally 20) quality control (QC) injections at the start of the run to condition the column¹¹⁵. A QC is typically made up of pooled sample and is used to monitor the performance of the instrument run. This is important to reduce retention time drift between runs and to equilibrate the column to the type of sample being analysed by masking certain binding sites. It is also a possibility that the MS optics and electronics may heat up at the start of data acquisition, and therefore require several injections to reach equilibrium¹¹⁶⁻¹¹⁸.

It is advised that QC injections are also inserted throughout the run (every 5 to 10 sample injections); this serves to check the data remain reproducible throughout the run. They can also be used to correct for batch drift during statistical analysis. Blank solvent injections should also be periodically included to check for carryover on the system. The samples are typically injected in a randomised order, to reduce the effects of instrument drift. Technical replicates (multiple injections of the same sample) are often used to check for instrument reproducibility. Several batches of randomised

technical replicates can be ran, and they can be used to minimise batch drift¹¹⁹.

2.2.4 Liquid Chromatography

Generally, the most commonly used separation methods for metabolomic studies are reversed phase and hydrophilic interaction liquid chromatography (HILIC)¹²⁰. Reversed-phase column stationary phases are generally made up of silica particles covalently bonded to hydrophobic alkyl chains, such as a C18 functional group^{121–123}. HILIC can retain more polar compounds¹¹⁸. The bonded stationary phase for HILIC is made up of a zwitterionic functional group with a net charge of zero (made of two functional group with opposing charges). HILIC is thought to work by the hydrophilic partitioning of compounds into the water rich stationary phase sequestered by the zwitterionic compounds, and also weak electrostatic interactions¹²⁴. Recently, T3 columns have become popular, and have found applications in plant metabolomics^{106,125}. T3 columns, similarly to C18 columns, are made up of silica particles covalently bonded to hydrophobic alkyl chains, but they also have some polar functional groups attached, so that these columns can retain both polar and some apolar compounds. T3 columns serve as a good compromise between C18 and HILIC by saving both time and sample by avoiding the need for separate HILIC and RP analyses¹²⁶.

2.2.5 Mass Spectrometry

Liquid chromatography (LC) is typically coupled to MS in metabolomics applications. Mass spectrometry is a powerful analytical tool in which chemical species are ionised and sorted based on their mass to charge (m/z) ratios. Before the compounds enter the mass analyser, they are ionised.

Electrospray ionisation (ESI) is a soft ionisation technique; ions are produced with low internal energies, so generally do not fragment during the ionisation process¹²⁷. Structural information can be gathered from MS/MS analysis, such as product ion analyses, often coupled with collision-induced dissociation (CID)^{128–130}.

There are many designs of instruments that can be used for LC-MS and MS/MS analyses. High m/z resolution and high m/z accuracy instruments, such as the Orbitrap family of instruments and Fourier transform ion cyclotron resonance (FTICR) instruments, offer some of the best performance for metabolomic analyses (as used in Chapters 4, 5 and 6). A detailed description of MS instrumentation is provided in Section 2.3 and liquid chromatography in Section 2.4.

2.2.6 Statistical Analysis

Once the raw LC-MS or MS/MS data files are obtained, the next step involves spectral processing. There are many different software packages which can be used to help process the raw data; in the work described in this thesis the software Progenesis QI™ was used¹³¹ and the process, involving peak-picking, spectral alignment and normalization, is briefly described below.

Progenesis QI aligns the chromatographic runs, compensating for small between-run variations that may arise during the chromatography. One run is chosen as the alignment reference against which the remaining runs are aligned, and the alignment can be performed automatically or manually. Alignment vectors connect the location of a feature (identified by its retention time and m/z value) in the reference run with the equivalent feature in the run that is being aligned.

An experimental design can be created to group together samples that have received the same treatment or are of the same sample class. Next, features,

with their intensities, across all the runs are identified through a peak-picking/alignment procedure. In order to ensure consistency, all the features found across the full range of runs are collected together into a merged or aggregate data set; overlapping features can be distinguished. Several parameters, such as peak width and feature intensity, can be employed at this stage to reduce or increase the number of peaks picked. This can be helpful to reduce the size of extremely large datasets.

Progenesis can be configured to recognise protonated, ammoniated, sodiated and other molecules of the same species from a user-specified list of expected charge-bearing species for the ionisation mode used. By recognising each of the different charged species for a single component, the intensities of all the differently-charged ions from the same compound can be included in the intensity calculation, improving the chances of detection and the accuracy of representation of that feature's abundance. The data are normalised by calculating a scalar multiplier which is applied to each feature abundance measurement. Each run can be normalised to a run selected as the normalisation reference. This is important so that features can be compared across different runs correcting for experimental and technical variation and statistical bias.

In order to understand how the component abundances are changing across the different experimental groups being compared, statistics are generated for each component. ANOVA provides a statistical test to determine if the means between two or more groups are all equal^{132,133}. The ANOVA p -value is calculated to help understand if variance between the abundance of a feature in two experimental groups is significant. A small p value (less than 0.05) implies statistical significance. Setting a threshold of p less than 0.05 means that 5 % of the values may be false positives. To overcome the likelihood of false positives due to multiple testing, multiple testing correction approaches can be used, such as the q -value (adjusted p values)

which is calculated using a false discovery rate (FDR) approach or the Benjamini–Hochberg correction¹³⁴

Further statistical tests are typically carried out at this point. In metabolomics data analysis workflows, both univariate and multivariate statistical methods can be employed^{134,135}. In the work described in this thesis, Matlab was used to carry out the statistical analysis using the package ‘metabolab’¹³⁶. The data can be ‘de-zeroed’ at this point. This means features that are not detected in a certain minimum percentage of runs are removed from the dataset. The data can also be batch corrected to compensate for retention time drift, using the behaviour of the repeated QCs to enable this correction. Unsupervised principal components analysis (PCA) can provide a summary of all the variables (in the case of metabolomics m/z , t_R and intensity) by finding the correlation between variables. In this manner, similarities and differences between the samples can be found. The reproducibility of the instrumental analysis can be determined by examining how tightly the QC sample data cluster. Good reproducibility will result in tight clustering of the QC data in the PCA plot. Supervised methods, such as partial least squares-discriminant analysis (PLS-DA), can be used for classification/discrimination purposes, allowing inference of those variables that maximise the discrimination between the predefined sample groups^{134,137}.

2.2.7 Identifying Small Molecules Using High Resolution High m/z Accuracy Mass Spectrometry

Following untargeted metabolomics experiments, a list of candidate masses and retention times is identified. Alternatively, candidate analytes can also be identified from reports in the literature. It is possible to begin to propose candidate assignments of features for which accurate masses and thus elemental compositions are known, and that appear to be discriminatory between sample classes. An integrated approach that gathers metabolite

information such as the m/z , product ion profiles, and retention time profiles, and then matches this information with that obtained from reference compounds, literature, and spectral databases is typically used¹³⁸.

A range of different possible levels of identification has been proposed by Schymanski *et al.*¹³⁰.

- Level 1. Confirmed structure: MS, product ion data, t_R reference standard.
- Level 2a. Probable structure: MS, product ion data
- Level 2b. Probable structure: MS, product ion data, diagnostic experimental context.
- Level 3. Tentative candidate(s): Probable structure: MS, product ion data, diagnostic experimental context.
- Level 4. Unequivocal molecular formula: MS isotope/molecular species
- Level 5. Exact mass: MS

Level 1 is the ideal situation, where the proposed structure has been confirmed by reference to an authentic standard with matching MS, product ion data, and retention time. Level 2a can be used when there is no suitable reference standard, but the MS and product ion data match library spectral data. Level 2b is when MS and product ion data indicate only one possible structure for the molecule, but no literature or reference standard is available to validate the assignment. Level 3 indicates that MS and product ion data point to several possible structures, with the correct structure being speculative. Level 4 describes a situation where the exact elemental formula can be assigned using MS, isotopes and charge-bearing species, but there are no fragment data that can be used to assign a possible structure. Finally, level 5 is an exact mass, but further information such as isotope patterns is lacking, meaning that a formula cannot be assigned confidently.

2.3 Mass Spectrometry

Organic mass spectrometry is the primary means of identifying metabolites used in the studies described in this thesis. A mass spectrometer comprises a sample inlet, an ionisation source, a mass analyser which separates and measures the m/z of the resulting ions, and a detector. Usually, a computer is used to control the instrument and to record the data.

2.3.1 ESI

Before entering the mass analyser the sample must be ionised, making the analytes manipulable using electric and magnetic fields. In ESI, the analytes are introduced in the liquid phase at atmospheric pressure, useful when liquid chromatography is coupled to MS. ESI has been described in detail by Bruins¹³⁹. Nanospray ionisation is a development of ESI for performing analysis with limited sample volumes, or fragile analytes. Nanospray only requires very low volumes (μL) of very low concentration sample solutions (nmol/mL).

Figure 2.2 shows a schematic of an ESI source. The solvent (containing dissolved analytes) flows through a capillary to which a voltage is applied. Depending on the resulting charge on the analytes, they are either attracted to or repelled by the charged capillary walls. In positive-ion-mode, negatively charged species are removed by discharging against the positively charged capillary walls, while positively charged ions are repelled by the capillary walls and each other. In the negative-ion-mode, this is reversed. Often formic acid is added to the solvent to provide protons to aid the formation of positive ions. The charged liquid exiting the capillary forms a Taylor cone and when repulsion of the like charges exceeds the Rayleigh

limit^{††} the cone ‘explodes’, budding into droplets and the nebulising gas (N₂) helps form an aerosol. Drying gas can be used to aid solvent evaporation.

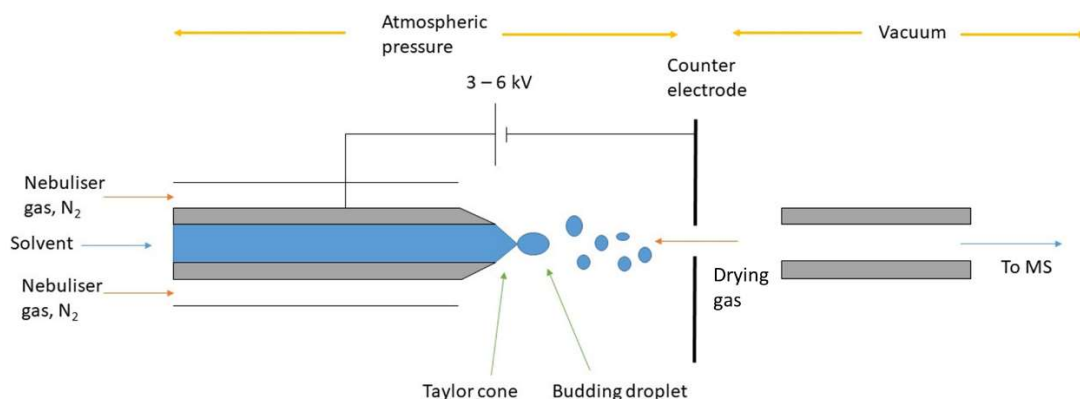


Figure 2.2: Schematic of an ESI source.

There are two mechanisms by which the ions in the droplets formed by this process are thought to arrive in the gas phase: the ion evaporation model and the charge residue model.

2.3.1.1 Ion Evaporation Model (IEM):

The IEM suggests that as the solvent evaporates the gas phase ions are ejected individually from the droplet due to charge repulsion when the droplet has reached sufficient charge density, as shown in Figure 2.3. There is evidence that this model is accurate for smaller (in)organic molecules¹⁴⁰.

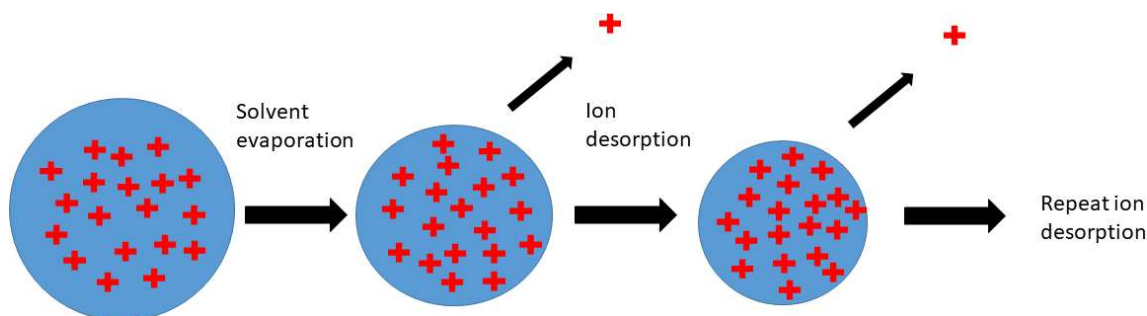


Figure 2.3: Ion evaporation model of gas-phase ion production in ESI.

^{††} The maximum amount of charge a liquid droplet can carry.

2.3.1.2 Charge Residue Model (CRM):

The CRM is similar to the IEM, but in this model, as the solvent evaporates, the droplets undergo multiple rounds of solvent evaporation and droplet 'explosion'. As solvent evaporates from the droplets they reduce in size and their charge density increases. When the charge density reaches the Rayleigh limit the droplets become unstable and explode into smaller droplets, which then continue to shrink due to solvent evaporation until just one desolvated gas-phase ion remains from each droplet (Figure 2.4). There is evidence this mechanism is accurate for higher molecular weight molecules, such as proteins¹⁴¹. According to the CRM, all of the charge carried by a droplet can reside after solvent evaporation on a single ion. The radius of the smallest droplet is equal to the ion radius with one extra monolayer of solvent and is constrained by the Rayleigh limit. Comparison of the ion charge (z) with the Rayleigh limit in the study by Fernandez de la Mora¹⁴¹ suggests that for larger ions, gas-phase ion production proceeds by the CRM.

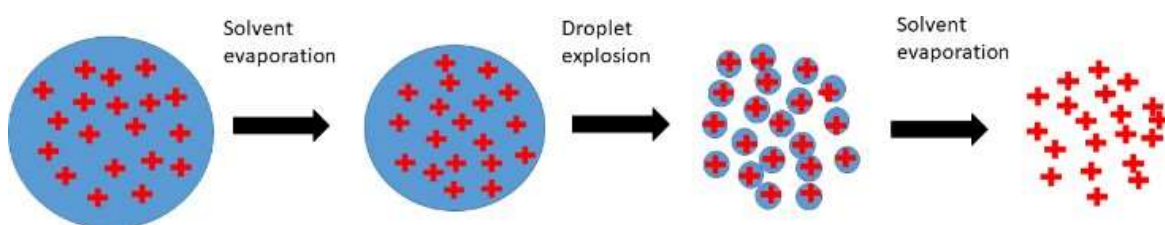


Figure 2.4: Charge residue model of gas-phase ion production in ESI.

2.3.2 Mass Analysers

Following ionization, the analytes are separated according to their m/z in the mass analyser.

2.3.2.1 Fourier Transform Ion Cyclotron Resonance

FTICR-MS is a technique that has excellent m/z accuracy and m/z resolution (described by Marshall *et al.*¹⁴²). FTICR works on the principle that ions traveling at low velocity in a strong magnetic field can be trapped in cyclotron motion, as described by Equation 2.1. The frequency at which the ions circle in their cyclotron motion is proportional to their m/z . All ions of the same m/z have the same cyclotron frequency, independent of their kinetic energies. The mass of the ions can be determined from the measured frequency of the cyclotron motion.

$$\omega = \frac{zB}{m2\pi}$$

Equation 2.1

ω = cyclotron frequency

z = charge on ion

m = mass of ion

B = magnetic field strength

In an FTICR instrument, ions are trapped in a Penning trap which at its simplest is essentially a small box, usually several centimetres in diameter, consisting of three sets of orthogonally arranged pairs of parallel plates: the trapping plates, excitation plates and detection plates (Figure 2.5). The ions are injected into the trap along the axis of the magnetic field (produced by a superconducting magnet) and are trapped into cyclotron motion by the magnetic field.

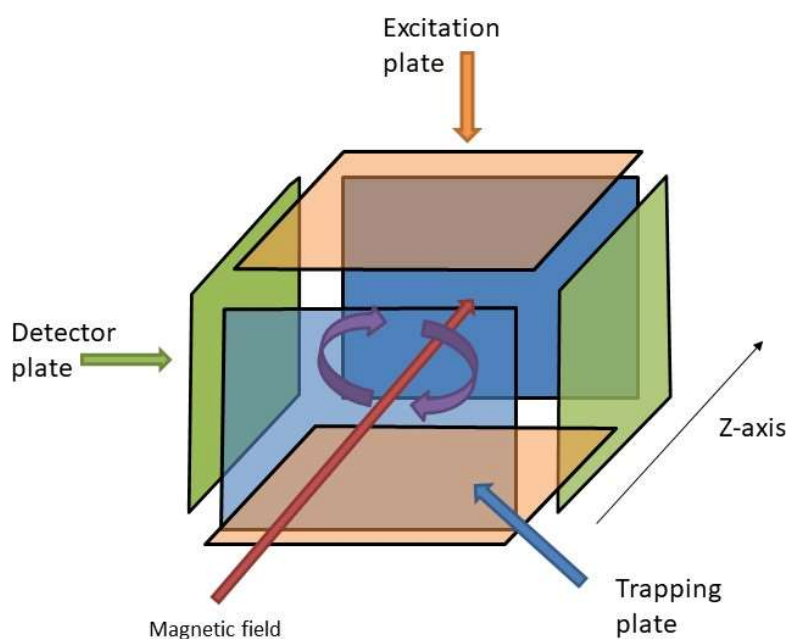


Figure 2.5: Diagram of an FTICR cell, the purple arrows show the direction of motion of the ions.

Trapping plates are positioned perpendicular to the magnetic field and a small voltage is applied across them, to prevent the ions from escaping the trap. The electric field generated by the trapping potential causes a radial force to be exerted on the ion. This results in a magnetron rotation. The magnetron and trapping frequency (due to the axial electric field created by the trapping plates) are very small, post excitation (see below), compared to the cyclotron frequency.

The cyclotron radius of an ion is usually too small to enable the ions to be detected by the detector plates, because the ions do not travel close enough to the detector plates to induce an image current. To be able to detect ions, their cyclotron radius needs to be enlarged, so that they circulate close to the detector plates. This is achieved by applying an excitation voltage at their resonant frequency - for a range of m/z values, a range of resonant frequencies is required. When the excitation voltage is applied the radii of the ion's cyclic paths are increased (due to the extra kinetic energy). This has the added effect of bringing all the ions into phase. This is important because the current induced by one ion at a detector plate traveling offset by 180° from another ion cancels out the current induced by the other ion.

During an FTICR-MS experiment, a range of frequencies is scanned over the excitation plates; this is known as chirp or a frequency sweep. This results in coherent packets of ions of particular m/z ratios becoming excited, as their respective resonant frequency is reached, and traveling in cyclotron motion of a particular radius. When the packets travel past the detector plates an image current is induced. The current can be measured many times as the ions orbit the Z-axis (Figure 2.5) and averaged, increasing the resolution of the m/z determination. The Penning trap is kept under ultra-high vacuum to reduce collisions within the trap between ions and neutral molecules, which may cause a loss of energy and coherence of the ion packet.

As the ions cycle, an image current is generated at the detector plates. The image current is very complex, as ions of different m/z travel with different frequencies. The image is collected in the time domain and is converted to a mass spectrum using Fourier transformation.

2.3.2.2 Quadrupole Mass Analysers

A quadrupole can be used as a scanning or static mass analyser. In scanning mode, the instrument is set up to allow ions of sequential m/z to travel stably through the quadrupole; ions with m/z values that have unstable trajectories hit the poles or pass

between them and are lost. In scanning mode, the quadrupole has a relatively low duty cycle, because only one m/z value at a time is transmitted stably through the rods to the detector as the mass range is scanned. In static mode, the quadrupole has excellent duty cycle, and is set to transmit one m/z or small m/z range only. The quadrupole consists of four hyperbolic or circular rods held parallel to each other and electrically connected in opposite pairs, Figure 2.6¹⁴³. Potentials are applied by supplying radio frequency (RF) and direct current (DC) voltages. One pair of rods has a positive DC potential applied to them and the other has a negative DC potential applied. Ions are introduced at one end of the quadrupole, travel the length of the quadrupole and are detected at the opposite end (or into another device, such as another mass analyser).

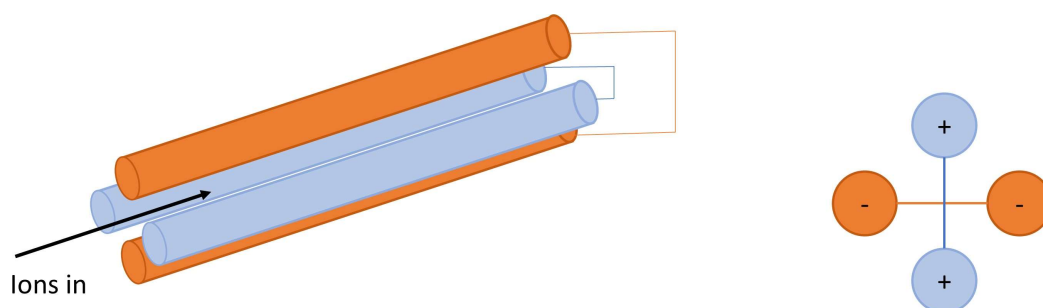


Figure 2.6: Diagram of a quadrupole mass analyser, showing opposite rods electrically connected. Blue rods are positive charged and brown are negatively charged.

As positive ions enter the quadrupole they are repelled by the positively charged rods, keeping the ions in the centre of the quadrupole. The polarity of the voltage applied is mostly positive but switches briefly to negative due to the RF component of the applied potential, which means the sign of the

potential is constantly changing. When this happens, the ions will change direction because they are now being repelled by that rod but attracted by the oppositely charged pair of rods, which attract the positive ions.

Ions with m/z values below the stable m/z hit the rods and are discharged before the rods return to positive polarity and can repel them away again. Higher m/z ions are also attracted to the rods, but remain stable as the polarity switches back before the ion can react, due to their higher inertia. In this manner the positive rods act as a low mass filter, that removes low m/z ions but allows through high m/z species.

Conversely the negatively charged rods act as high mass filters. Positively charged ions are attracted to the negative rods. When the rods briefly change polarity to positive the higher m/z ions are repelled by the rods, but are not repelled back to the middle of the rods due to their inertia, and so have an unstable trajectory and are lost. Ions with m/z s below the stable m/z are repelled back to the middle of the quadrupoles and so are able to follow a stable trajectory. Ions can only be transmitted through the mass analyser if they are stable to both the high and low mass filters^{‡‡}. In order to record a mass spectrum, the magnitudes of the RF and DC voltages applied to the poles are scanned. Stable ions of different m/z are permitted through the filter sequentially in this manner. To record an entire mass spectrum, the range of stability is scanned across the entire m/z range, making a measurement at each step.

The quadrupole can also be operated in fixed mode; this is when the RF and DC applied potentials are kept constant in order to transmit ions of a particular m/z . Or it can be set to oscillate between several different potentials to select several m/z ions in turn. The quadrupole can also be used as a

^{‡‡} High mass filter is when larger m/z ions are discharged on the rods. Low mass filter is when low m/z ions are discharged on the rods.

collision cell. In this instance, only RF is applied, while DC voltage is not applied (so moving all ions into the stable region). Ions are accelerated into the collision cell, which is pressurised with inert gas with which the ions collide, causing them to undergo collision induced dissociation (CID).

2.3.2.3 Orbitrap

The Orbitrap mass analyser consists of three electrodes. The two outer, cup-shaped grounded electrodes face inwards and are secured by a central, insulating ring. The third electrode, a spindle-like central electrode, holds the trap together and aligns it via dielectric end-spacers¹⁴⁴. Ions are injected (tangentially to the radius of the spindle electrode) into the volume between the central and outer electrodes (Figure 2.7).

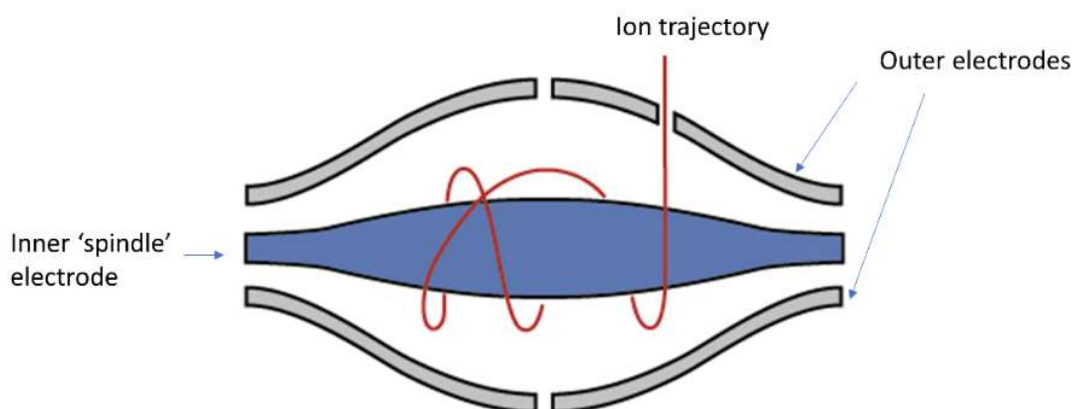


Figure 2.7: Simplified diagram of Orbitrap mass analyser (adapted from <http://planetorbitrap.com>).

The ion source is external to the trap. Capturing ions from the source is performed using 'electrodynamic squeezing' (in the C-trap – Figure 2.8), where ions experience an increase in electric field strength as they enter the trapping field. The outer electrodes remain at a fixed potential while the potential on the central electrode is ramped down (for positive ions). Ions entering the field cannot escape and are trapped by the trapping potential.

Voltage is then applied across the central and outer electrodes, inducing a radial electric field which bends the ion trajectory toward the central electrode while tangential velocity creates an opposing centrifugal force. Under the correct conditions, ions can be induced to orbit the spindle and the ion trajectory assumes the shape of a complicated spiral. When ions start their motion at the correct energy and radius, stable trajectories result. Unlike in an FTICR, the resulting cyclic frequency of the ions is dependent on the kinetic energy of the ions.

The axial electric field caused by the conical shape of the electrodes pushes ions toward the widest part of the trap, bringing the particles into phase and initiating harmonic axial oscillations. The outer electrodes are used as detection plates for an induced image current which is Fourier-transformed, similarly to in FTICR, and then converted into a mass spectrum.

Figure 2.8 shows a schematic of the Orbitrap instrument used in the work presented in this thesis: the Orbitrap Fusion Tribrid. Most Orbitrap-containing instruments are hybrid quadrupole-Orbitrap instruments, in

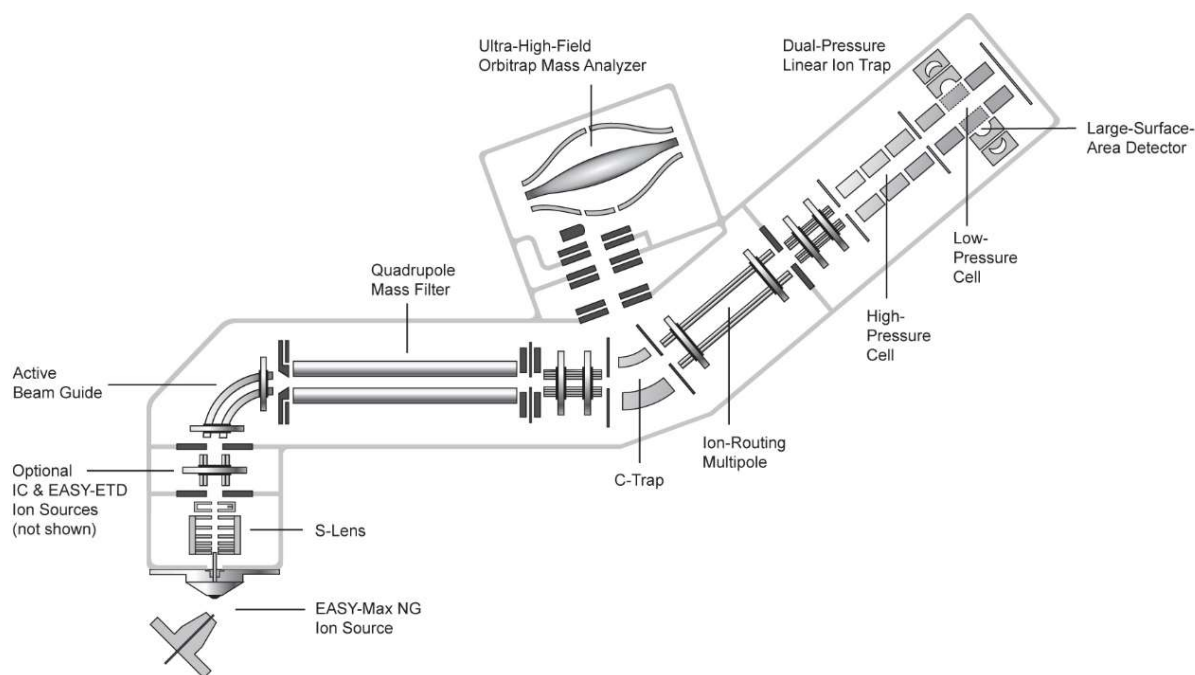


Figure 2.8: Schematic of the Thermo Scientific Orbitrap Fusion™ Tribrid™ (Adapted from <http://planetorbitrap.com>).

which ion fragmentation occurs in the higher energy collisional dissociation (HCD) cell (marked as ion-routing multipole in Figure 2.8) or at lower energies in the linear ion trap. Afterwards, the subsequent fragments are accelerated and cooled down in the C-trap¹⁴⁵, where a high radiofrequency (RF) voltage retains the fragment ions. Subsequently, these fragment ions are injected and separated inside the Orbitrap mass analyser based on their frequencies. Alternatively the product ions can be injected into the ion trap which increases the instrument's duty cycle, but decreases the resolution of the product ion spectra.

2.4 High Performance Liquid Chromatography

High performance liquid chromatography (HPLC) is a separation technique. The basic theory of chromatography is that the analyte mixture is carried by a mobile phase through a column containing a stationary phase. The analyte mixture becomes separated depending on the interaction of each analyte with the stationary phase which is determined according to their physicochemical properties. HPLC is often coupled to a mass spectrometer. HPLC is advantageous over direct injection into a mass spectrometer as it can be used to separate complex mixtures before they enter the ionisation source. Reducing the complexity of mixtures entering the ion source (as in HPLC) results in reduced charge competition in the ion source. Another advantage of using HPLC is that it can be possible to separate isomers¹⁴⁶.

Analyte mixtures are loaded onto the top of the column in solution in the liquid phase (mobile phase). The column is packed with stationary phase material and in many separations the analytes partition between the stationary and mobile phases. Analytes are retained on the column to varying degrees according to their partitioning behaviour, resulting in them moving through the column at different speeds and eluting with different retention times (Figure 2.9). The partitioning of an analyte (A) between the

mobile and stationary phases can be described as an equilibrium (equation 2.2). Analytes with a higher partitioning constant (K_d) (equation 2.3) spend more time in the stationary phase, and hence have a longer retention time.

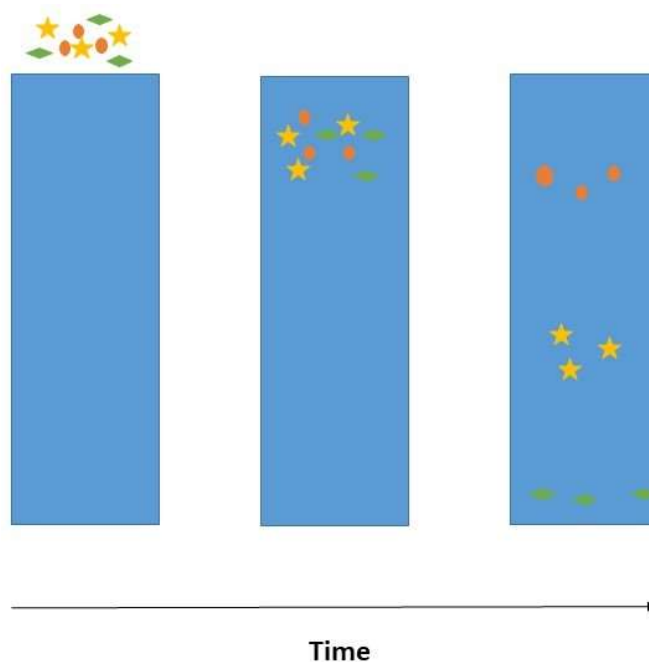
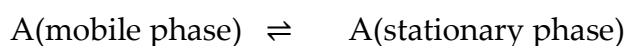


Figure 2.9: Diagram illustrating how the analytes elute from an LC column at different rates, dependent upon their physicochemical properties. The analytes (represented by colours and shapes in the diagram) indicate components with different physiochemical properties resulting in different elution times due to interactions with the column.



A = Analyte

Equation 2.2

Where the partition constant is described as:

$$K_d = \frac{[A_{\text{stationary phase}}]}{[A_{\text{mobile phase}}]}$$

Equation 2.3

The efficiency of chromatographic separation is determined by the theoretical plate height. Plate height is the length of column required for one equilibration event of analyte partitioning between mobile and stationary phase. The more theoretical plates a column possesses, the more separation events it can host and thus the more efficient the separation, so it is important to minimise plate height if separation is to be maximised. However, in practice it is often a compromise between separation and column length and time. Flow rate of the mobile phase through the column is linked to the theoretical plate height through the van Deemter equation (equation 2.4).

$$H = A + \frac{B}{u} + Cu$$

H = plate height

A = eddy diffusion

B = longitudinal diffusion

C = mass transfer

u = mobile phase flow rate

Equation 2.4

As can be seen in equation 2.4, to minimise plate height (H), A , B/u and Cu should be minimised. Eddy diffusion (A) refers to the multiple paths that analyte molecules may take as they proceed down a column packed with particles; because the paths may be different lengths the band corresponding to a single component is broadened, so reducing separation efficiency. Small particle size column packing can help reduce this band broadening by reducing the potential differences in path lengths. However, use of small particles increases the resistance to solvent flow. Efficient systems can be achieved using very small particles (1.7 – 5 μm) but need solvent pressures up to 400 bar.

Longitudinal diffusion (B) is caused by diffusion of analytes spreading along the column as they travel down it and can also cause band broadening. Increasing the mobile phase flow rate (u) reduces band broadening due to longitudinal diffusion, as the analytes are pushed through the column more quickly, so the opportunities for diffusion are reduced. The mass transfer term (C) arises because it takes a certain amount of time for the analytes to partition between the mobile and stationary phases. If the mobile phase velocity is too high then analyte in the mobile phase moves ahead of analyte in the stationary phase, resulting in band broadening. Therefore, in order to minimise H , a compromise must be made in mobile phase flow rate to allow enough time for separation events to take place, without compromising separation due to band broadening.

Several factors can be used to improve column efficiency including using a mobile phase gradient. When using reversed phase chromatography, this usually involves starting with low and moving to high organic content over the course of the separation. This speeds up the elution of hydrophobic compounds, so reducing the opportunity for longitudinal diffusion to cause band broadening and reduce efficiency. Other factors that may improve LC

separation efficiency include optimising the material and size of the column packing material, and the column internal diameter.

2.5 Analytical Technology and Software Used in Isotope Ratio Analysis

2.5.1 Considerations for Sampling

When preparing samples for isotope ratio mass spectrometry it is imperative that they are completely dry, so the samples are lyophilised. The samples are homogenised by grinding, in order to make the sample taken representative of the bulk.

2.5.2 Isotope Ratio Mass Spectrometry (IR-MS)

Very slight variations in the ratios of isotopes can be measured using an IR-MS. The IR-MS the intensities of the different stable isotopes of targeted elements and enables the ratio of the intensities of heavy isotopes to light in a given sample to be compared with that of a standard. The differences in ratios are expressed with the δ notation, in units of per mille (‰). Equation 2.5 gives the stable isotope ratio equation:

$$\delta X = \frac{R_{sample} - R_{standard}}{R_{standard}} * 1000$$

Equation 2.5

where R = the intensity of the heavier/intensity of the lighter isotope, so $^{15}\text{N}/^{14}\text{N}$ for nitrogen, $^{18}\text{O}/^{16}\text{O}$ for oxygen, and $^{13}\text{C}/^{12}\text{C}$ for carbon. The standard against which samples are compared is atmospheric N_2 , which is assigned a δ value of 0 ‰ for nitrogen, and Vienna PeeDee Belemnite (VPDB) for carbon (assigned a δ value of 0 ‰) and Vienna Standard Mean Ocean Water (VSMOW) for oxygen.

Isotope fractionation occurs via two processes: kinetic and equilibrium isotope fractionation. Heavier isotopes of the same element form stronger bonds to other atoms than does the lighter isotope (larger zero-point vibrational frequency)¹⁴⁷. The kinetic isotope effect derives from the difference in energy required to break a bond containing a heavier isotope when compared with the lighter isotope; more energy is required to break a bond with a heavier isotope. Isotopologues^s of the same molecule react at different rates if in the rate limiting step a bond involving an isotopic bond is broken or formed. The equilibrium isotope effect occurs because more energy is required to dissociate the bond of a heavier isotopologue than a lighter one.

In an isotope ratio measurement, the samples are first homogenised and combusted in a 1000 °C furnace in the presence of oxygen, chromium oxide and silvered copper oxide to remove oxides. All carbon in the sample is converted by combustion to CO_2 . Nitrogen-containing compounds are converted to N_2 gas and different oxides of N, denoted NO_x . The resultant gases are carried by a helium stream and passed through a copper oxide reduction unit, which converts NO_x products to N_2 . N_2 and CO_2 are then separated using a GC column before the entering the IR-MS; N_2 elutes first followed by CO_2 .

N₂ and CO₂ are ionized in the ion source by electron ionization. The ions are then accelerated into a flight tube, then separated by their different m/z values in a magnetic field; the ions are deflected into circular paths whose radii are proportional to their m/z values (Figure 2.10).

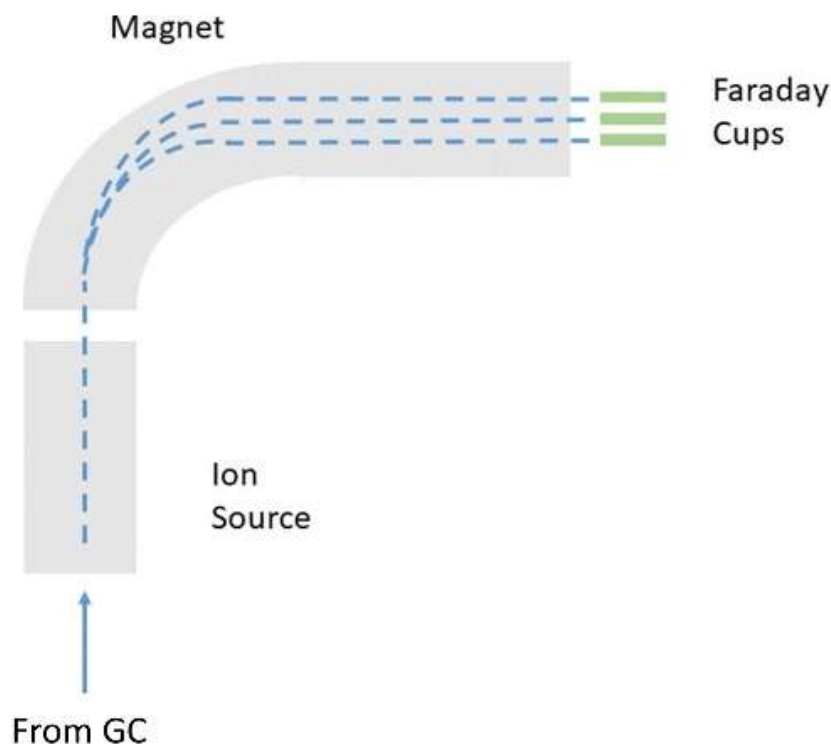


Figure 2.10: Diagram showing the separation of ions in an IR-MS instrument.

The different m/z species are collected in Faraday cups, each cup collecting a different isotope. The Faraday cups are positioned to receive ions of m/z s 28, 29 and 30 for N₂ and 44, 45 and 46 for CO₂. A Faraday cup is a conductive cup designed to catch charged particles in a vacuum. The resulting current can be measured and used to determine the number of ions hitting each cup. The ratios of signals from each cup determine the isotope ratio for the samples. The mass analysers described in the mass spectrometry section (2.3) cannot be used for these measurements as they are not able to determine accurately enough the very small differences in isotopic signal intensities that

these analyses demand, because the signal to noise ratios are not good enough, however some recent progress is being made in the use of Orbitrap-based instruments to measure isotope ratios for components of complex mixtures¹⁴⁸.

Several replicates are often required for accuracy, and replicate precision. Sample uncertainty is also measured. Samples with high uncertainty are generally removed from an experiment's dataset. Accurate weighing of the samples is important to calculate δX values and X% values. Standards with known δX values are used to monitor instrumental performance. They are injected every 6-10 samples in a sequence. The quality control of a sequence is monitored by assessing the variation in the measurements obtained for standards throughout the run, the standard measurements are corrected and sample δX values are calibrated to the known standard measurements. Typical standards for a carbon and nitrogen isotope ratio experiment include fish gelatine, sugar cane and caffeine, for each of which, standardised isotope ratios have been determined. When measuring oxygen isotope ratios sucrose, sugar cane, benzoic acid and cellulose can be used.

2.5.3 Compound-Specific Isotope Ratio Mass Spectrometry

In order to rationalise the expression of bulk $\delta^{15}\text{N}$ signatures, it is useful to investigate the $\delta^{15}\text{N}$ values for the molecular components that contribute to the bulk signal⁷⁷. For $\delta^{15}\text{N}$, the main N-containing species is protein, and so breaking down protein to its constituent amino acids (AAs) and measuring the $\delta^{15}\text{N}$ of each can allow a deeper understanding of the complex biochemical processes that contribute to the sample's bulk $\delta^{15}\text{N}$ value. Compound-specific isotope analysis is carried out using GC-C-IR-MS.

Protein is extracted from the source material, and hydrolysed to its constituent AAs. The amino acids are derivatised and separated using gas

chromatography. The separated amino acids are then combusted on-line and the resultant gases are then introduced into an IR-MS as described above (Section 2.5.2).

Typically, protein is split into its constituent amino acids by acid hydrolysis; commonly 6 M HCl with heating (110 °C for 24 h). The acid-hydrolysis reaction with 6 M HCl results in the addition of water to each covalent peptide bond and results in constituent AAs, with some exceptions.

Tryptophan, serine and threonine can be destroyed during the reaction and the sulfur-containing amino acids cysteine and methionine cannot be reliably measured due to partial destruction of the amino acids. Lysine is reactive with reducing sugars and can produce Maillard products. Ala-Ala, Ile-Ile, Val-Val, Val-Ile, Ile-Val, and Ala-Val linkages have been found to be resistant to hydrolysis, but this can be solved by increasing the length of the hydrolysis procedure¹⁴⁹. Asparagine and glutamine side chain amides are hydrolysed to acids to form aspartic acid and glutamic acid, respectively.

Following hydrolysis, contaminating lipids are removed using solvent extraction; often hexane is used for this purpose. When the samples have been filtered they are derivatised, so they can be analysed using GC-C-IR-MS. Esterification and acetylation are optimal derivatization strategies for GC analysis¹⁵⁰.

Amino acid standards are used during a compound specific IR-MS experiment. An international standard is made using alanine, glycine, valine, norleucine is also typically used. The $\delta^{15}\text{N}$ values measured are calibrated to the international standard using a calibration curve and then drift corrected to norleucine. Typically, samples are analysed in triplicate and the international standard mixture can be injected every three runs to monitor instrument performance.

2.6 Summary

The background to this PhD have been explored in Chapter 1 and the instrumentation and approaches used have been surveyed and discussed in Chapter 2. The research results that these first two chapters underpin follow. Briefly, Chapter 3 presents the results of bulk and individual amino acid nitrogen isotope ratio analyses of experimentally drought stressed maize and archaeological maize from Tularosa Cave are presented here. Oxygen isotope ratio analysis of cellulose from experimentally drought-stressed maize and the Tularosa archaeological samples are also included in this chapter.

In Chapter 4 the effect of lyophilisation on stabilising metabolites was investigated. The results of untargeted metabolomics experiments on drought treated modern maize and the Tularosa archaeological maize are presented here. In chapter 5 the metabolome of the Tularosa maize is investigated; including drought-related metabolites. Ageing experiments (Chapter 6) were used to help interpret how the metabolites may have changed with diagenesis to help deconvolute the effects of diagenesis from those of drought. Finally, Chapter 7 contains an overview of the results and recommendations for future work.

Chapter 3. Stable Nitrogen Isotopes Reveal Archaeological Maize Adapted to Drought in Southwestern US

In review at Scientific Reports as 'Stable nitrogen isotopes reveal archaeological maize adapted to drought in Southwestern US'.

3.1 Abstract

Understanding how crops have responded to drought stress in the past is becoming increasingly important due to climate change. Here we explore the utility of nitrogen isotope ratio data ($\delta^{15}\text{N}$) to identify varieties of maize grown under different hydrological regimes. Archaeological maize cobs from Tularosa Cave, New Mexico, cultivated during two different climate regimes (wet ca. 1800 cal BP and dry ca. 700 cal BP) were distinguished through $\delta^{15}\text{N}$ measurements of bulk material and individual amino acids. The results show that farmers successfully cultivated maize during severe drought conditions, implying their crops had adapted to the drier climate. These findings complement previous paleogenomic analysis of Tularosa maize cobs suggesting selection for drought resistance-related genes. Adaptation of crops to climate change took many centuries resulting in extant landraces that could be advantageous to modern producers.

3.2 Introduction

Drought stress is a pressing issue faced by modern arable farmers globally. Maize, rice and wheat contributes 30% of calories to more than 4.5 billion people, including to those from some of the poorest countries in the world¹. Maize is also an essential animal feed and increasingly used as a biofuel. Maize agriculture in the present-day Southwestern United States has historically faced sparse and unreliable levels of precipitation, resulting in several pan-regional droughts in the last 2000 years³⁻⁵. Various technologies have been adopted to mitigate the effects of drought, such as canal irrigation and lithic mulching^{46,47,48}.

Here we used the exceptional archaeobotanical record at Tularosa Cave, New Mexico¹⁵ (Figure 1.3), to examine the effect of drought on maize. At this site, a large assemblage of ancient maize cobs is exceptionally well preserved

due to desiccation and provides a unique opportunity to examine the effect of drought on maize through chemical, isotopic, and genetic analyses of preserved biomolecules. Direct radiocarbon dating of maize cobs has revealed two temporally distinct periods of occupation: older (1830 - 1719 BP, 95.4% CI) and younger (771 - 681 BP, 95.4% CI)¹⁵¹. Through deoxy DNA analysis, two genetically discrete groups were identified corresponding to the periods of occupation, with the older population ancestral to the younger⁵⁰, although the limited sample size of radiocarbon and genomic analysis does not preclude outliers. Records of stalagmites from caves in the Sacramento Mountains, New Mexico, show that during the earlier occupation of Tularosa Cave the annual precipitation was higher than at present, and that the more recent occupation was in a time of severe drought (Figure 1.4⁵); tree-ring data also show that this region experienced drought during the mid-1200s AD^{4,152,153}. The early maize cobs are described as 'pineapple-shaped'¹⁵¹, referred to in this text as 'ovoid-shaped', short in length with a thick midsection and small kernel form, consisting of 10–12 rows of kernels. The later corn is described as 'cylindrical' in shape with a thin midsection and 8–10 rows of larger kernels. It is hypothesized that the morphologically distinct sets of maize reflect an adaptation to climate change. Genomic analysis of these samples^{60,151} has shown that loci associated with drought tolerance (*dehyd1A*) and sugar content (*ae1* and *su1*) in the later cylindrical-shaped maize cobs might have undergone episodes of selection between the earlier and later occupation phases at Tularosa. Yet direct evidence that the maize was able to withstand the harsher, drier conditions so far has not been forthcoming.

Here, we determined experimentally how the $\delta^{15}\text{N}$ values of modern maize respond to drought conditions, and then measured both $\delta^{15}\text{N}$ in bulk tissue and single amino acids from samples from both the earlier and later occupations of Tularosa Cave. Nitrogen in the form of nitrate and

ammonium is absorbed by plants from the soil. Various biotic and abiotic processes cause isotopic fractionation resulting in variations in $\delta^{15}\text{N}$ ⁶⁴. It has been noted that plants grown in arid locations and during drier seasons tend to have higher $\delta^{15}\text{N}$ values than those grown in comparatively wetter conditions ^{68,154}. We also investigated the potential value of both bulk and cellulose carbon isotope data in understanding drought stress to complement the $\delta^{15}\text{N}$ studies.

3.3 Results

3.3.1 Plant Growth Experiments

To test how bulk nitrogen isotopes vary in response to aridity, we experimentally grew maize under drought and well-watered conditions for isotopic analysis. Two inbred lines of maize, B73 which is drought susceptible, and B76 which is drought resistant¹⁵⁵, were selected. The maize was grown to maturity and grain-fill in three different conditions: well-watered control, moderate drought (2 weeks' drought at the three-leaf stage) and severe drought (two weeks' drought at the three-leaf stage and a further week at the grain-fill stage). The bulk nitrogen isotope ratios of inner cob material (pith) were measured using IR-MS. Nitrogen is utilised differently in the inner cob and the kernel^{156,157}, due to different metabolic requirements across tissue types, so the kernels were separated from the inner cob. Table Appendix 2 shows the %N and $\delta^{15}\text{N}$ signatures for each sample, and Figure 3.2 shows plots of %N versus $\delta^{15}\text{N}$ for the kernel and inner cob samples from the B73 and B76 lines.

It is striking how low the drought-susceptible B73 inner cob %N is in the well-watered control group (mean 0.35 %) when compared with the moderate (1.79 %) and severe drought (3.16 %) groups (Figure 3.1b, Table Appendix 2, Wilcoxon rank sum, $p=0.0061$). Similarly, there is an increase in the $\delta^{15}\text{N}$ values in the B73 inner cob drought-treated groups, when compared

with the well-watered treatment (Figure 3.1b). The well-watered samples have a mean $\delta^{15}\text{N}$ value of -6.26 ‰; samples that experienced drought in the three-leaf growing stage had the highest mean $\delta^{15}\text{N}$ value of -3.69 ‰ and samples that experienced drought at both the three-leaf and grain-fill stages had a mean $\delta^{15}\text{N}$ signature of -4.33 ‰. The pattern of heavy isotope enrichment with drought stress is also seen in the drought-tolerant B76 inner cob samples (Figure 3.1d).

The kernel $\delta^{15}\text{N}$ signatures however show a more complicated picture. The drought-tolerant B76 maize kernels showed a slight increase in mean $\delta^{15}\text{N}$ value over well-watered values for both drought regimes (Figure 3.1c). The well-watered samples have an average $\delta^{15}\text{N}$ signature of -4.42 ‰ and samples that experienced drought at both the three-leaf and grain-fill stages had average $\delta^{15}\text{N}$ signatures of -2.68 ‰. The drought-susceptible B73 kernel data (Figure 3.1a) show depletion of ^{15}N due to drought stress; the well-watered samples have an average $\delta^{15}\text{N}$ value of -2.16 ‰ and samples that experienced drought at both the three-leaf and grain-fill stages had $\delta^{15}\text{N}$ signatures of -4.50 ‰. As expected^{68,154}, $\delta^{15}\text{N}$ signatures are increased in response to drought conditions, except in B73 kernels. The data presented here show that the bulk $\delta^{15}\text{N}$ signatures in experimental plants are affected by water availability, and so the $\delta^{15}\text{N}$ values of the ancient maize samples were examined to test for drought stress evidence in their $\delta^{15}\text{N}$ signatures.

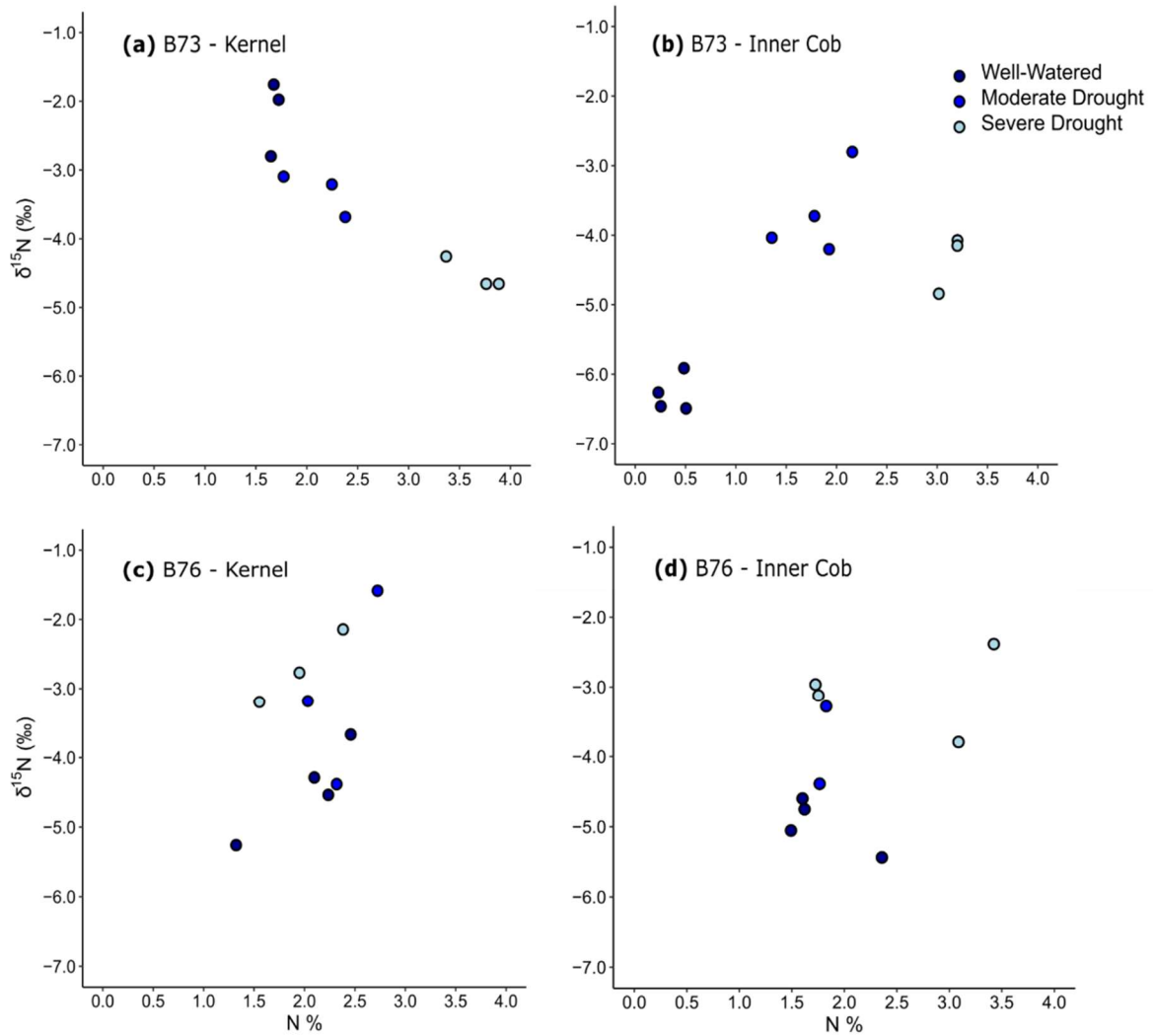


Figure 3.1: Graph displaying the $\delta^{15}\text{N}$ (‰) values of modern maize grown under different watering conditions. Each point represents a duplicate mean measurement, sample uncertainty is quoted in Appendix 2. Dark blue dots represent well-watered control, medium blue dots represent drought at three-leaf stage and pale blue dots drought at the three-leaf and grain-fill stages. (a) B73 kernel samples, (b) B73 inner cob samples, (c) B76 kernels samples and (d) B76 inner cob samples. All samples were measured in duplicate and the means calculated and corrected using standards.

3.3.2 $\delta^{15}\text{N}$ analysis of archaeological maize cobs from Tularosa Cave

Ninety-five samples of maize cobs from Tularosa Cave were sampled. The maize falls into two morphologically distinct groupings, cylindrical-shaped

and ovoid-shaped. Nine of the Tularosa maize samples have been radiocarbon dated and the dates suggest that the maize falls into two temporally distinct periods: older (1830 - 1719 BP, 95.4% CI) and younger (771 - 681 BP, 95.4% CI)^{50,151} (henceforth referred to as 1800 BP and 700 BP). Prior to analysis, the cobs were separated into the inner cob (pith) and outer cob material, which consists of a mixture of cellulose-rich cob tissue, cupules, and kernel material¹⁵⁸, henceforth referred to as 'outer cob'.

Our data show that the $\delta^{15}\text{N}$ values measured in the maize samples are stratified according to their age and morphology. The Tularosa Cave cobs from the later period (700 BP) show higher bulk $\delta^{15}\text{N}$ values than the Tularosa Cave cobs from the earlier period (1800 BP). Samples shown to have been grown in the relatively wet conditions of the cave's early occupation phase showed significantly lower $\delta^{15}\text{N}$ values than those grown in the relatively drier conditions of the later phase (Figure 3.2; Mann-Whitney test $p = 3.673.0^{15}\text{e-11}$

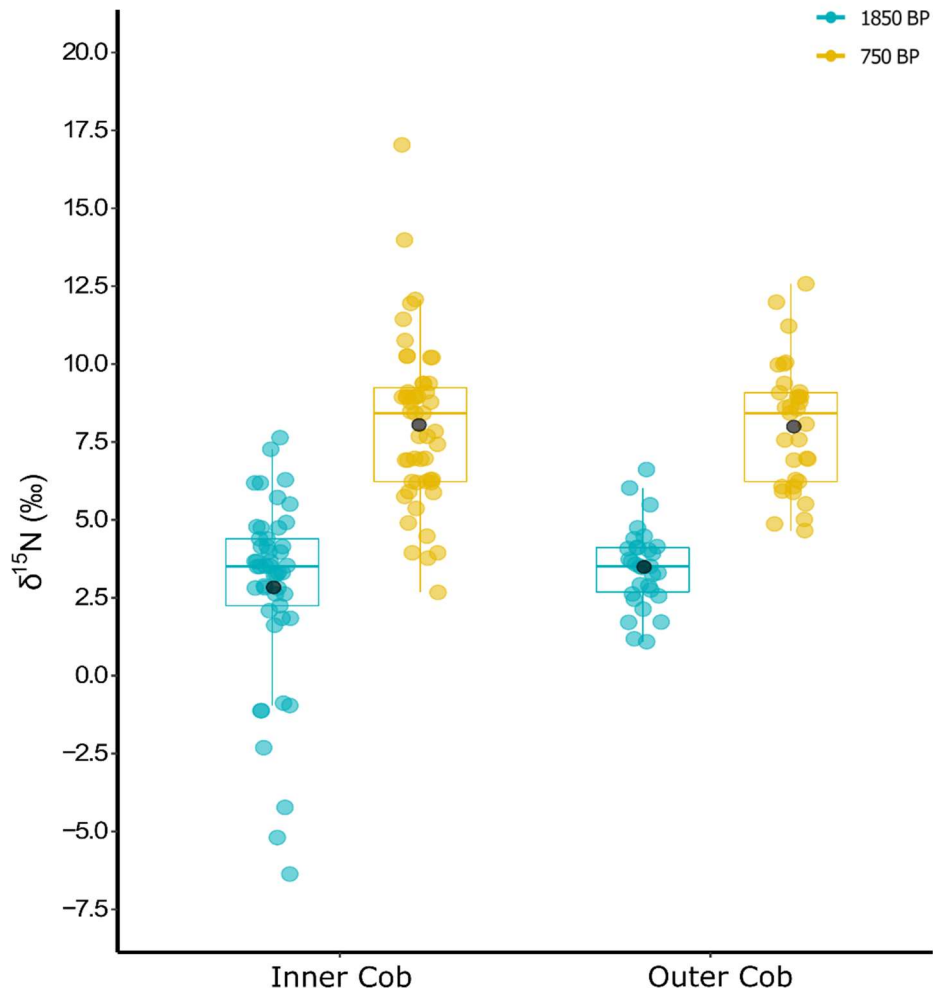


Figure 3.2: Box plots of $\delta^{15}\text{N}$ (‰) values of Tularosa maize cobs. Samples date from 1800 BP (blue circles) and 700 BP (yellow circles), means are shown as black circles.

for inner cob samples; $p = 4.223\text{e-}11$ for outer cob, data in Appendix 3 for outer cob and Appendix 4 for inner cob). These results support the hypothesis that drier growing conditions result in higher $\delta^{15}\text{N}$ values. $\delta^{15}\text{N}$ signatures from the inner cob sections are much more variable than those of the outer cob material, especially in the earlier cobs. The inner cob $\delta^{15}\text{N}$ values tend to reflect more enrichment in ^{15}N than those from the outer cob material from the same sample (Figure 3.2, Figure 3.3), as is also seen in our experimental plant drought data. The N% showed no trend in these data (see Appendix 3 and 4).

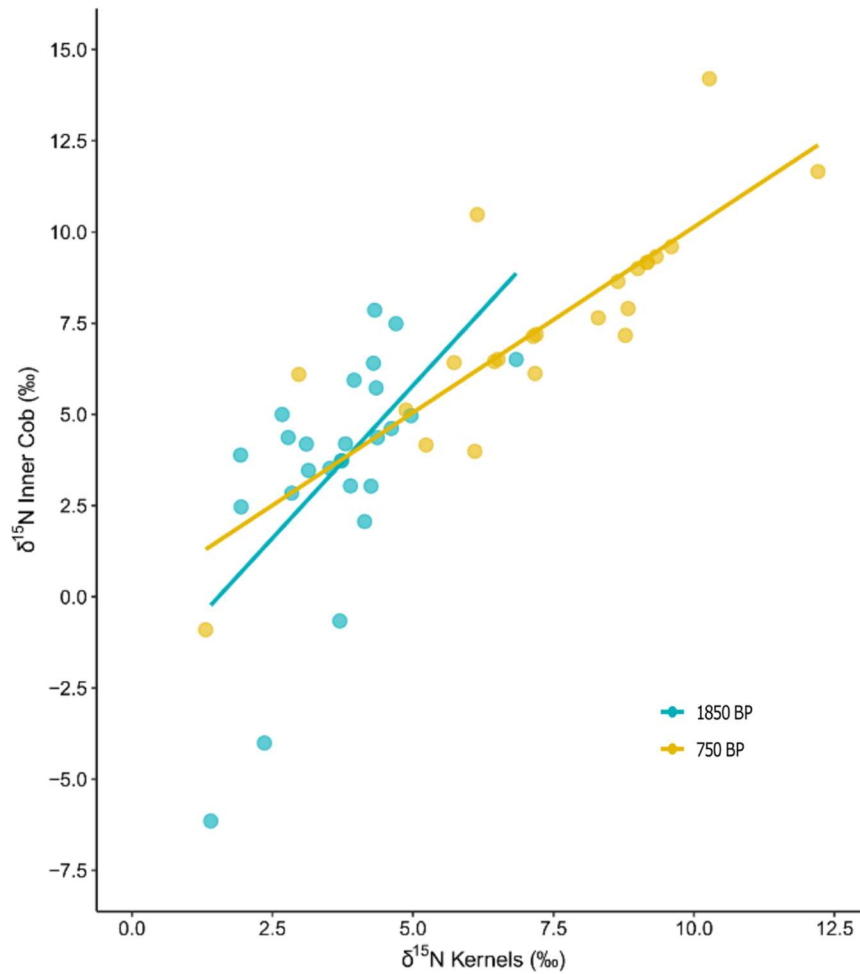


Figure 3.3: Graph displaying the $\delta^{15}\text{N}$ (‰) kernel and inner cob values of each sample. Samples from the 1800 BP (ovoid) and 700 BP (cylindrical) time periods are blue and yellow circles respectively. Correlation line for each time period is shown.

3.3.3 $\delta^{15}\text{N}$ Analysis of Individual AAs from Archaeological Maize Cobs

The isotope ratios of individual amino acids were investigated and compared with the bulk values. Amino acids were extracted from five maize cobs, two samples from 1800 BP (TL81, TL82) and 700 BP (TL123, TL151) and a modern lyophilised sample, and analysed using gas chromatography-combustion-isotope ratio mass spectrometry (GC-C-IR-MS). This approach can be used to interrogate the metabolic processes of plants by examining the stable nitrogen isotope ratios of individual amino acids ($\delta^{15}\text{N}_{\text{AA}}$). Amino acids are released by acid hydrolysis of protein present in plant remains and

derivatised for GC-C-IR-MS (see Section 3.5.4). Previously this approach has shown that $\delta^{15}\text{N}_{\text{AA}}$ values of modern cereal grains and rachis were largely attributed to metabolic pathways involved in their biosynthesis and catabolism⁷⁹ and that manuring resulted in consistent ^{15}N -enrichments of all amino acids⁷⁸. These studies^{78,79} demonstrate that the application of manure does affect the metabolic routing of nitrogen into cereal grain, but that such external factors affect all amino acids similarly^{78,79}. Styring *et al*⁶⁶ also found that growing conditions and climate across two growing sites (annual rainfall 727 mm compared to 483 mm) did not result in significant differences in the relative $\delta^{15}\text{N}$ values of different AAs in barley and bread wheat grains, although their rachis values were different, suggesting that rachis AA $\delta^{15}\text{N}$ values are more sensitive than grain values to differences in growing conditions.

Here, we were able to measure $\delta^{15}\text{N}$ values for 13 amino acids with reasonable baseline separation (Figure 3.4). Figure 3.5a shows the fractionation of nitrogen isotopes for amino acids normalised to Glx. In the hydrolysis process the amino acids asparagine and glutamine are irreversibly converted into aspartic acid and glutamic acid respectively, therefore asparagine and aspartic acid are collectively labelled Asx and glutamine and glutamic acid are collectively labelled Glx.

Table 3.1: Mean average AA $\delta^{15}\text{N}$ values from inner maize cob samples. Numbers in brackets represent one standard deviation associated with triplicate analytical replicate measurements for AA $\delta^{15}\text{N}$ values and replicate precision for duplicate experimental replicates of bulk $\delta^{15}\text{N}$ values.

Sample	AA $\delta^{15}\text{N}$ value (‰)													
Identification	Gly	Ser	Glx	Ala	Asx	Pro	Hyp	Val	Leu	Ile	Thr	Lys	Phe	Bulk
123	4.5	-0.9	5.4	2.4 (0.9)	3.5	7.7	4.0	3.4	0.3	0.2	-3.1	-0.3	15.0	6.5 (1.5)
	(1.2)	(2.0)	(1.5)		(1.2)	(0.2)	(5.5)	(1.6)	(1.0)	(3.7)	(1.7)	(1.0)	(2.6)	
151	7.2	2.4	7.1	5.0 (0.2)	7.6	8.6	3.5	4.3	2.2	1.6	-0.8	1.3	¹⁵ 7	9.2 (0.1)
	(0.4)	(0.8)	(0.4)		(1.0)	(0.5)	(6.2)	(0.2)	(0.6)	(2.7)	(0.6)	(1.7)	(2.0)	
81	2.7	-0.9	1.0	1.1 (0.8)	3.3	7.0	0.1	2.1	-1.0	0.1	-5.2	0.1	10.4	2.7 (0.1)
	(1.2)	(1.7)	(0.2)		(2.0)	(1.3)	(0.1)	(1.2)	(2.1)	(0.1)	(1.2)	(0.1)	(1.3)	
82	2.3	-1.3	0.4	-0.3	3.5	7.3	1.8	3.4	-0.2	2.4	-5.0	-2.1	9.9	3.7 (0.6)
	(0.3)	(0.2)	(0.7)	(0.7)	(0.7)	(0.2)	(3.7)	(1.5)	(0.5)	(3.6)	(1.9)	(2.5)	(1.6)	
Modern	10.9	4.6	8.3	5.8 (1.6)	8.7	12.8	-0.6	4.8	5.1	-0.6	0.5	1.0	17.7	7.8 (0.2)
Reference	(1.0)	(1.8)	(1.5)		(0.2)	(2.5)	(0.1)	(2.0)	(1.7)	(0.1)	(1.4)	(1.4)	(1.2)	

Figure 3.5b shows the fractionation of the amino acid nitrogen isotopes which are not normalised. The $\delta^{15}\text{N}$ value of Glx is a product of the net flux of N entering and leaving the Gln and Glu pools and is a reflection of the bulk plant tissue $\delta^{15}\text{N}$ value⁶⁶. Normalising to Glx eliminates fractionation changes in $\delta^{15}\text{N}$ due to external N and therefore reflects metabolic fractionation⁶⁶. Figure 3.5a shows that the amino acid $\delta^{15}\text{N}$ values of the 1800 BP group are all similarly increased relative to $\delta^{15}\text{N}_{\text{Glx}}$ compared to the 700 BP group with the notable exception of phenylalanine (Phe). Phe is comparatively enriched in both groups compared to the $\delta^{15}\text{N}_{\text{Glx}}$ values.

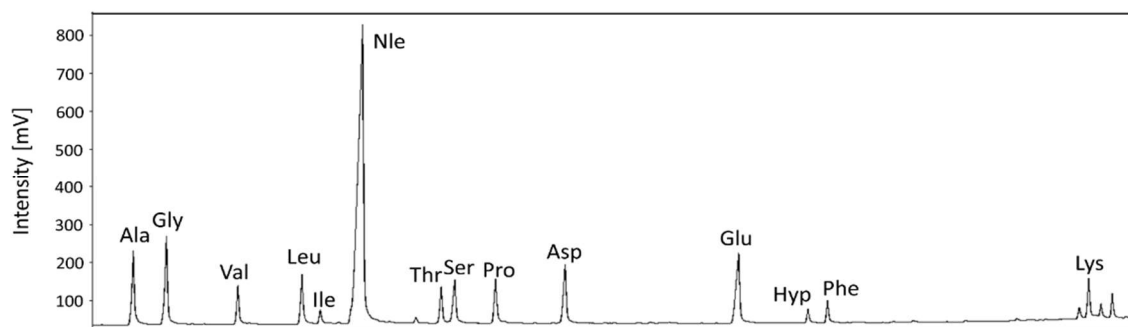


Figure 3.4: GC-C-IR-MS chromatogram displaying the separation of N-acetylated-isopropyl esters of derivatised AA in Tularosa maize cob sample TL151. AAs abbreviated to their three letter codes. Nle represents norleucine a non-proteinaceous amino acid internal standard.

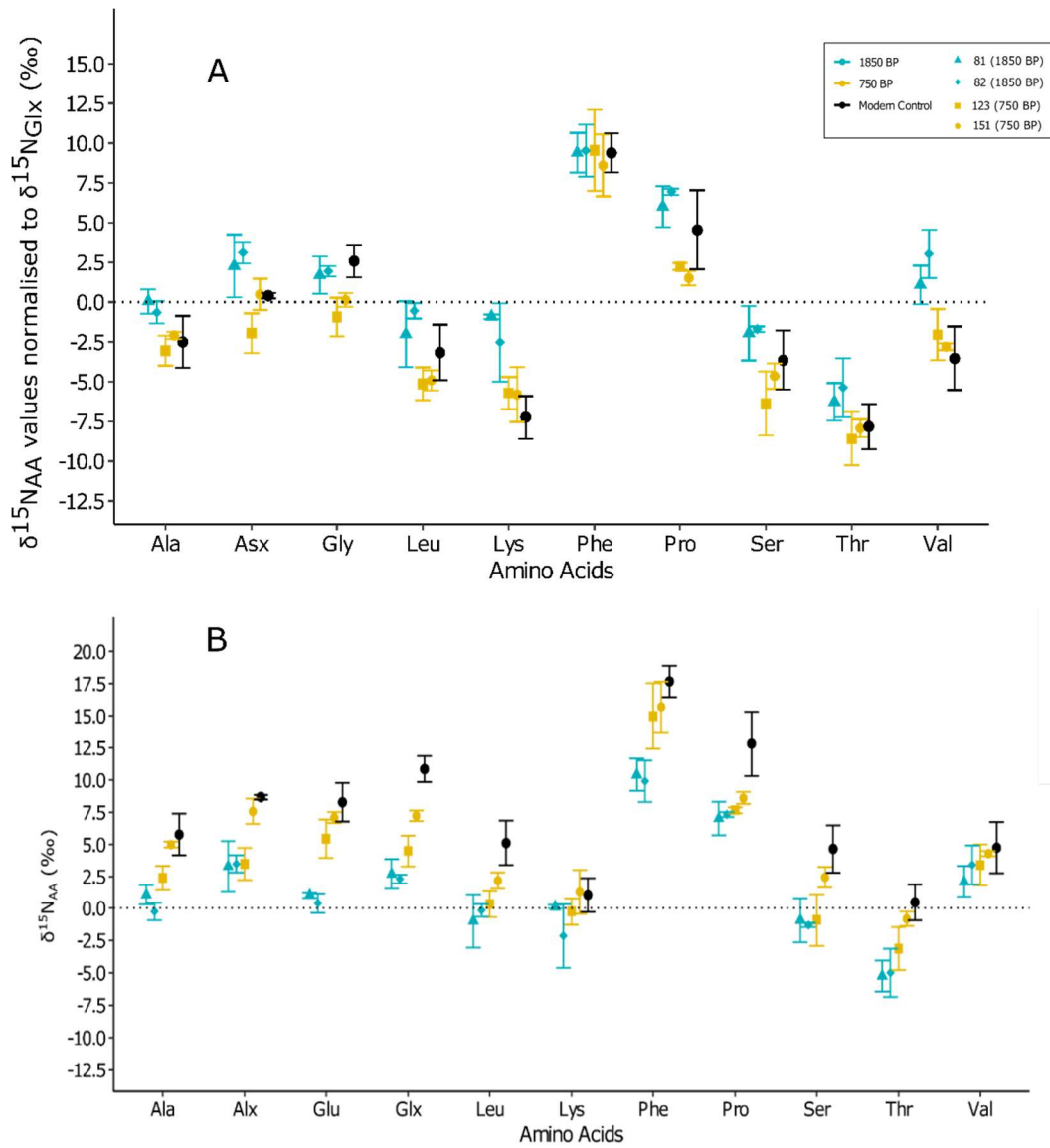


Figure 3.5: (A) $\delta^{15}\text{N}_{\text{AA}}$ values normalised to Glx from maize inner cob samples detailed in Table 1. Blue triangles and diamonds represent samples TL81 and TL82 respectively (1800 BP), yellow squares and circles represent samples TL123 and TL151 respectively (700 BP) and black circles represent the modern control. Black dotted line, $y=0$. Error bars represent the standard deviation associated with triplicate analytical measurements. (B) $\delta^{15}\text{N}_{\text{AA}}$ values which are not normalised.

3.3.4 Effects of Drought on the $\delta^{13}\text{C}$ Values of Modern and Ancient Maize

Drought conditions caused small depletions in bulk ^{13}C in B76 maize inner-cob material (well-watered $\delta^{13}\text{C}$ mean = $-13.29 \text{ ‰} \pm 0.52$, severe drought $\delta^{13}\text{C}$

mean = $-13.97 \text{ ‰} \pm 0.02$, data in Appendix 5). This suggests that the drought conditions have caused the stomata to close, causing fractionation of the carbon isotopes due to enzymatic effects to become evident. Changes in fractionation were not observed in the B73 variety under drought conditions suggesting that this drought-tolerant variety is able to maintain open stomata and continue photosynthesis under drought conditions (Figure 3.6).

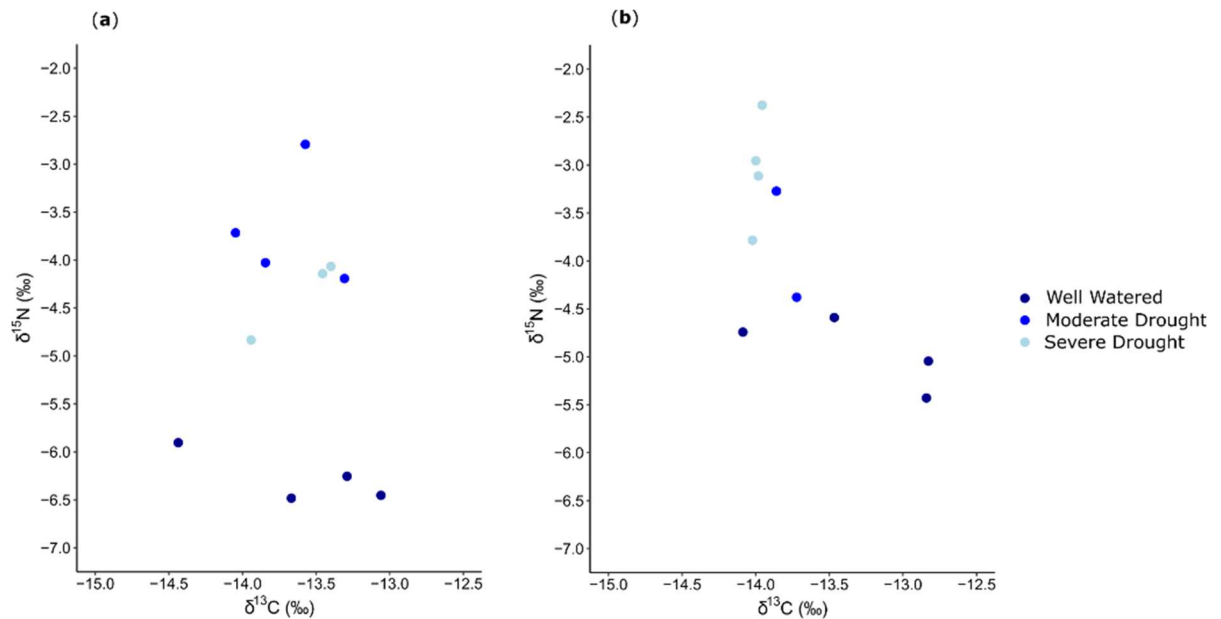


Figure 3.6: Graphs displaying the $\delta^{15}\text{N}$ (‰) and $\delta^{13}\text{C}$ (‰) inner cob values of each sample. A. B73 samples and B. B76 samples

A slight depletion in bulk ^{13}C is observed (Figure 3.8) in the more recent archaeological samples, when compared with the older, Figure 3.7 (1850 BP $\delta^{13}\text{C}$ mean = $-9.34 \text{ ‰} \pm 0.70$, 750 BP $\delta^{13}\text{C}$ mean = $-10.21 \text{ ‰} \pm 0.75$, p -value = 1.67×10^{-5}).

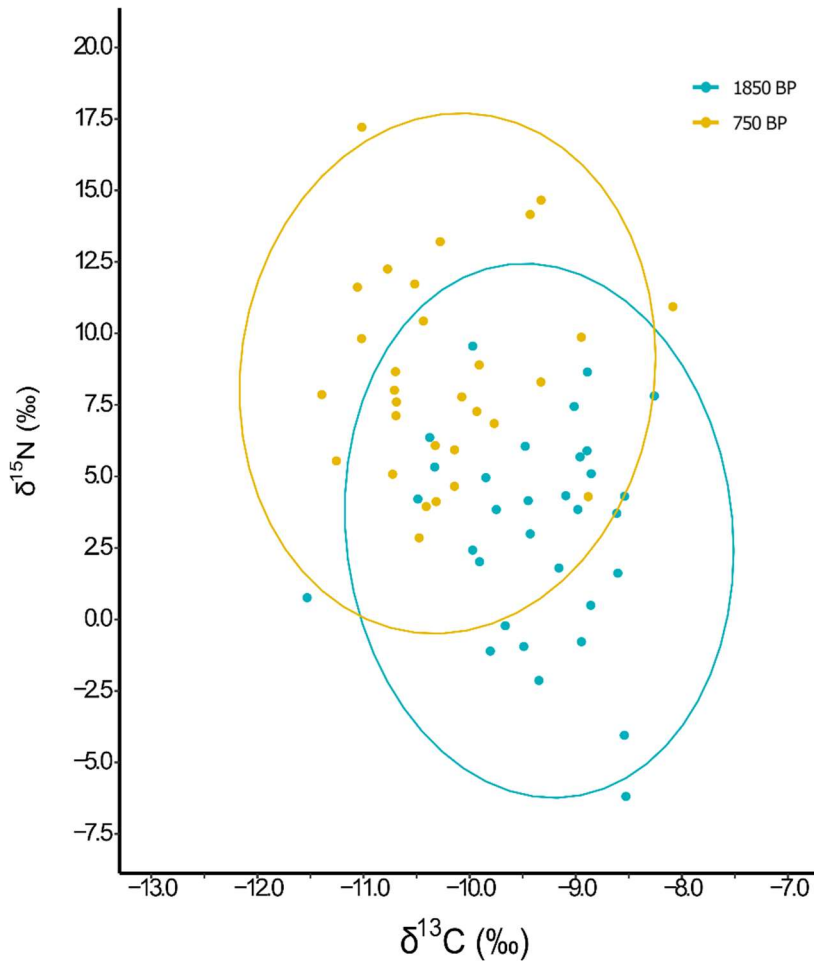


Figure 3.7: Graph displaying the bulk $\delta^{15}\text{N}$ (‰) and $\delta^{13}\text{C}$ (‰) inner cob values of each sample. Ellipses are drawn with 95% confidence level for a multivariate t-distribution. Samples date from 1800 BP (blue circles) and 700 BP (yellow circles)

This trend is not observed when analysing the cellulose extracted from a selection ($n = 14$) of the archaeological samples (Figure 3.8); however overall, there is a trend between the bulk $\delta^{13}\text{C}$ values and the $\delta^{13}\text{C}_{\text{cellulose}}$ values (correlation coefficient = 0.46). The $\delta^{13}\text{C}_{\text{cellulose}}$ values are enriched in ^{13}C when compared with the bulk measurement (Figure 3.8, data in Appendix 6).

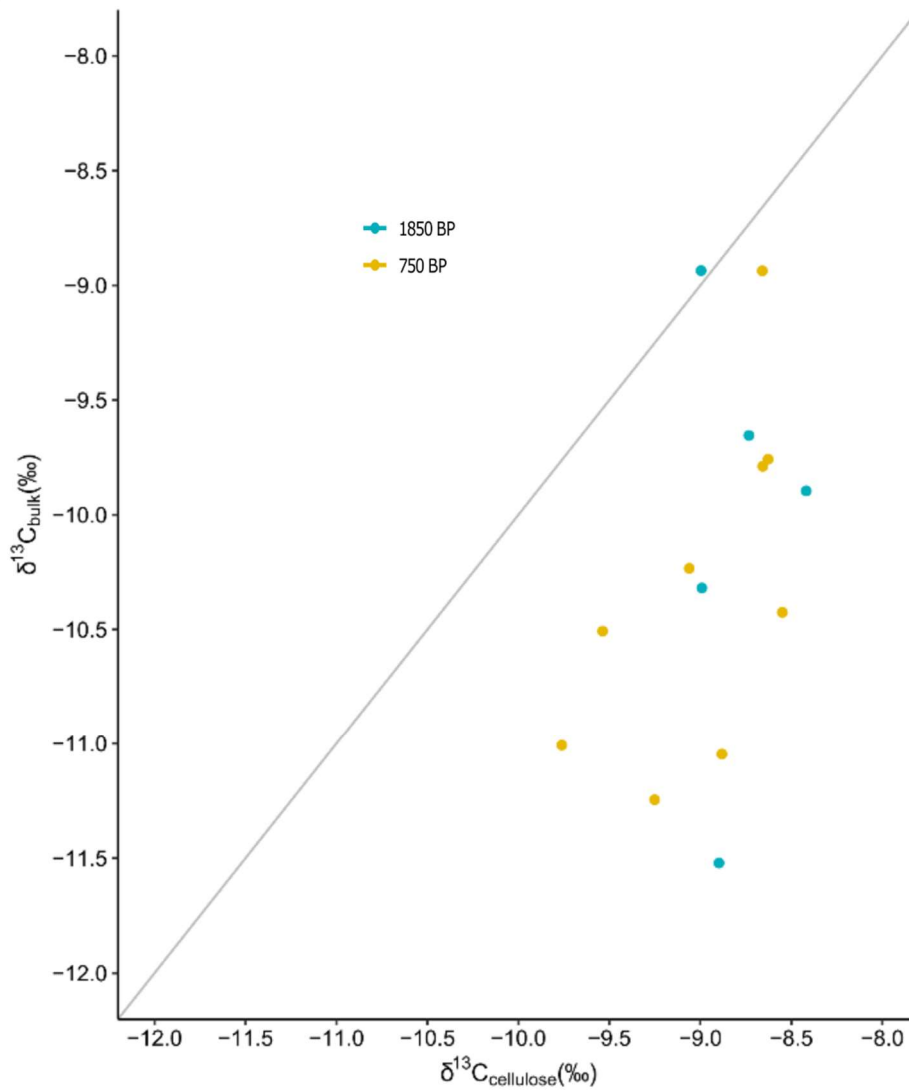


Figure 3.8: Graph displaying the bulk $\delta^{13}\text{C}_{\text{cellulose}} (\text{‰})$ and $\delta^{13}\text{C}_{\text{bulk}} (\text{‰})$ inner cob values of each sample. Samples from the 1850 BP (ovoid-shaped cobs) and 750 BP (cylindrical cobs) time periods are blue and yellow circles respectively. Grey line is $y=x$.

3.4 Discussion: Implications

Compound-specific analysis of individual amino acids from the archaeological tissues has shown that for each individual amino acid the isotopic fractionation is similar in both later and earlier cobs (Figure 3.6), with samples from the 700 BP time period displaying an enrichment effect with respect to the earlier material across all amino acids, most pronounced

in the Glx and Phe. This similarity in fractionation is strong evidence that the enrichment in ^{15}N in the later cobs is not due to changes in individual amino acid metabolism, but to external environmental factors. One potentially confounding reason for the difference in the $\delta^{15}\text{N}$ between the two occupational phases at Tularosa Cave could be due to changes in soil quality or fertilisation rather than changes in aridity. Styring *et al.*⁶⁷ noted manuring increases the bulk $\delta^{15}\text{N}$ values of cereal grain but does not affect the metabolic routing of nitrogen into cereal grain amino acids, so that the enrichment effect due to drought stress cannot be distinguished from that from manuring. However, the application of animal manure to fields is not known to have been practised by pre-colonial indigenous farmers in the southwest; the only available domesticated animals were turkeys and dogs¹⁵, however the use of wood ash and urine as manure has been documented¹⁵⁹.

A more parsimonious explanation is related to changes in aridity. The modern-day experimental data showed that both the B73 and B76 inner cobs were enriched in ^{15}N when grown under drought conditions. This is most probably due to evaporative enrichment of ammonia in the soil. The kernels as well as the inner cobs of the drought-tolerant B76 variety also displayed ^{15}N enrichment with drought stress (B76 inner cob showed enrichment of 1.9 ‰ between well-watered and severe drought groups). The modern experimental samples were not manured, so the effect of nitrogen enrichment must be due to drought conditions. The bulk $\delta^{15}\text{N}$ values in the Tularosa assemblage mirrors this pattern (an enrichment of 5.1 ‰ between assemblages), indicating they experienced drought stress, and therefore developed some measure of drought tolerance.

A number of mechanisms could cause an increase in the $\delta^{15}\text{N}$ values of maize due to drought stress. Firstly, ammonium volatilisation in the soil can enrich the ammonium in the heavier isotope by approximately 40 ‰⁷⁰. Secondly, in drought conditions it has been found that arbuscular mycorrhiza (AM) help

the host plant to withstand drought⁷⁵. Nitrogen is predominantly assimilated in the root via AM. AM depletes the ^{15}N in the soil resulting in an enrichment of the heavier isotope in NO_3^- in the root⁷³. Also, evaporative enrichment may occur when small volatile nitrogen-containing compounds diffuse out through stomata, causing an increase in the heavier nitrogen isotopes in the leaf tissues and translocation from the senescent parts of plants (old leaves) also may enrich ^{15}N signatures in fruits⁷³. Finally, drought-induced changes in plant metabolism may have an effect on their $\delta^{15}\text{N}$ signatures⁷⁹.

Similarly, the climate record shows that the later cobs experienced a period of pan-regional drought⁴, causing human population loss in this region. *Dehyd1A* is a dehydration responsive element-binding protein shown in a previous study¹⁶⁰ to be upregulated in maize seedlings as a response to drought conditions. Diversity at *su1* was found to be reduced more than 60 % between the 1800 year old samples and the 700 year old samples at Tularosa Cave. This gene is responsible for the storage of non-structural starches as soluble low molecular mass carbohydrates¹⁶¹. Low molecular mass carbohydrates such as sucrose, trehalose and fructose are implicit in osmotic regulation, which is important when water is scarce, helping to maintain the plant's structural integrity¹⁶². However, the *su1* gene may have arisen because of human selection due to culinary preferences, as it is also implicit in the pasting properties of maize flour used for making tortillas. However, when the stable isotope measurements of maize cobs are also considered, it is more likely that these genes were under selection at least largely as a consequence of the environmental conditions. Therefore, we conclude that these attributes would be desirable in modern maize varieties given the current climate emergency.

In cases where source water $\delta^{18}\text{O}$ information is available, $\delta^{18}\text{O}_{\text{cellulose}}$ may be used to infer environmental conditions, as evaporative enrichment causes lighter isotopes to evaporate preferentially. Carbon isotope ratios showed a

depletion in ^{13}C under drought conditions in the modern drought-resistant samples (B76) and ancient samples, however the effect is slight (less than 1 ‰). There was no depletion seen in the drought-susceptible modern samples. This suggests that a decrease in $\delta^{13}\text{C}$ signatures represents an adaptation to drought stress in the ancient samples. Some studies have found drought stress causes an accumulation of ^{13}C in leaf material¹⁶³. If taken in combination with nitrogen and oxygen isotope data then carbon isotope ratios could be a possible indicator of drought tolerance in archaeological plants, however further study is needed. Other studies of modern plant tissues subject to drought conditions have shown a depletion in ^{13}C in maize tissue, and therefore in $\delta^{13}\text{C}$ signatures, which is further complicated by the availability of nitrogen sources¹⁶⁴ and the drought tolerance of the maize variety¹⁹.

To conclude, climate data and genetic analysis provide a strong case that bulk ^{15}N enrichment is caused by drought stress in this instance. Climate records can show us that crops were cultivated during periods of drought, but cannot tell us whether this stress was mitigated by anthropogenic practises such as irrigation. The technique used here is a direct indicator that the plants experienced drought stress, but survived and adapted, allowing us to more confidently attribute specific genetic adaptations to drought ¹⁵¹.

Measuring bulk $\delta^{15}\text{N}$ can therefore be used to monitor the effects of changing climatic conditions directly in well-preserved archaeobotanical remains.

Understanding how humans have adapted their agricultural practices in the past, and how maize has responded genetically to past climate change, could contribute a vital perspective to present-day food security during the current climate crisis.

3.5 Methods

3.5.1 Experimental Materials

Maize plants, B73 variety (GRIN accession number: PI 550473, developed at Iowa State University, drought-susceptible) and B76 variety (GRIN accession number: PI 550483 developed at Iowa State University, drought-tolerant), were grown at the Warwick University Phytobiology Facility in a climate-controlled greenhouse. Plants were grown at 28 °C day/20 °C night in a 16-h light/8-h dark cycle with a light intensity of 230 $\mu\text{E m}^{-2} \text{s}^{-1}$. Seeds were germinated in three-inch diameter pots containing peat-based soil. Soil water content was measured at regular intervals during drought stress using a Professional Soil Moisture Meter (Lutron Electronic Enterprise Co., LTD., Taipei, Taiwan) to ensure drought conditions were successfully applied. The plants were split into three groups, outlined in Table 3.2. Drought conditions were applied during two growth stages, three-leaf and grain-fill (BBCH principal growth stage 1 and 8, respectively¹⁶⁵). Drought conditions consisted of withholding water for one week, which resulted in soil water content between 0 and 1% (Appendix 8). Non-sterilised soil was used, and reverse osmosis water was used to water the plants. Cobs were harvested for analyses when the cobs were fully ripe and were immediately frozen in liquid nitrogen and stored at -80 °C.

Table 3.2: Table showing the watering conditions for each plant growth condition group.

Condition Group	Details
Well-watered	Samples were well watered for the duration of the experiment
Moderate drought	Drought stressed for two one-week periods, the first week starting at the three-leaf stage (approximately 4 weeks after seeding). The plants were watered for a further week and then droughted for another one-week period
Severe drought	Drought stressed as described for moderate drought conditions and then for a further two weeks during grain-fill (approximately 14 weeks after seeding)

3.5.2 Archaeological Materials

95 archaeological samples of maize were analysed. The maize was excavated from Tularosa Cave, New Mexico by Martin *et al.*¹⁵. Some of the samples used in this study have previously been radiocarbon dated¹⁵¹. The maize samples correspond to two temporally distinct occupations, one at approximately 1800 BP (1830 - 1719 BP, 95.4% CI, n=49) and the other at ~ 700 BP (771 - 681 BP, 95.4% CI, n=51). The older samples have an 'ovoid' morphology and the more modern samples have a 'cylindrical' shaped morphology.

3.5.3 Bulk $\delta^{15}\text{N}$ Isotope Ratio Analysis

If the samples were visibly contaminated, they were washed using acetone and then methanol. Samples were then ground and archaeological and modern maize inner cob powder samples were weighed in duplicate (2 mg) using an MT5 6 dp micro balance (METTLER TOLEDO, Ohio, USA) into tin capsules, which were analysed by elemental analysis-IR-MS in a GSL analyser coupled to a 20-22 mass spectrometer (Sercon, Crewe, UK). Isotope

ratios were calculated as $\delta^{15}\text{N}$ versus atmospheric N_2 by comparison with standards calibrated against IAEA-N-1 and N_2 .

3.5.4 Preparation of Amino Acid Derivatives (N-acetyl-i-propyl esters)

An international standard for isotope ratio mass spectrometry studies of AA was prepared, consisting of alanine, glycine, valine, leucine, norleucine, aspartic acid, glutamic acid, and phenylalanine ($2000 \text{ ng } \mu\text{L}^{-1}$, in 0.1 M HCl). An internal standard was made by adding a solid bovine collagen standard (4 mg) to a scintillation vial with norleucine standard ($100 \text{ } \mu\text{L}$, $2000 \text{ ng } \mu\text{L}^{-1}$) and HCl (0.01 M , 1 mL). All reagents and standards were provided by Sigma.

Dry archaeological and modern maize inner cob powders were weighed (20 mg) into 2 mL hydrolysis vials. Norleucine standard solution ($50 \text{ } \mu\text{L}$, $5000 \text{ ng } \mu\text{L}^{-1}$, in 0.1 M HCl) was added to each sample along with HCl (6 M , $200 \text{ } \mu\text{L}$) and heated at 110°C for 24 h , then allowed to cool to room temperature. The hydrolysate from the hydrolysis vials was pipetted into individual Nanosep filters (Nanosep® Centrifugal Devices supplier) ($4.5 \text{ } \mu\text{m}$) along with HCl (0.1 M , $200 \text{ } \mu\text{L}$) and vortexed (20 s). The samples were then centrifuged (12298 RCF , 60 s , Nanosep® centrifugal device). The filtration process was repeated once, with a further $200 \text{ } \mu\text{L}$ HCl (0.1 M), to yield a yellow solution derived from acid hydrolysed maize sample, which was transferred into clean 1 mL Reacti-Vials™ (Thermo-Fisher).

Lipids were extracted from the clean hydrolysate solutions by pipetting on hexane: DCM (c.a. 0.5 mL , $3:2$, v:v) and vortexing (20 s) and removing the organic layer, repeating a further twice. The solutions were blown to dryness under N_2 . The derivatisation procedure followed is from¹⁶⁶. The AAs were isopropyl esterified in 1 mL of acidified isopropanol solution (1.85 M , prepared by the addition of 2 mL of acetyl chloride to 8 mL of dry isopropanol in an ice bath, $4:1$, v:v) at 100°C for 1 h . The reaction was terminated by placing the reaction tubes in a freezer (-20°C , 5 min). The

solutions were blown to dryness under N₂. DCM was added (2 × 0.25 mL) and evaporated at room temperature to remove excess reagents. AA *i*-propyl esters were then treated with 1 mL of a mixture of acetic anhydride, triethylamine and acetone (1:2:5, v/v/v; 10 min, 60 °C). The reagents were evaporated under a gentle stream of nitrogen at room temperature and dissolved in 2 mL ethyl acetate. 1 mL of saturated NaCl solution was added, and, with vortexing, was used to effect phase separation. The organic phase was collected and dried under nitrogen at room temperature. Residual water was removed by addition and evaporation of successive 1 mL aliquots of DCM. The derivatised AAs were redissolved in ethyl acetate (300 µL) and stored at -20°C until required for analysis.

Isoleucine, hydroxyproline and tyrosine were omitted from further measurements due to their relatively high standard deviations of the $\delta^{15}\text{N}$ measurements (Table 3.1). In order to consider the fractionation due to AA metabolism, the $\delta^{15}\text{N}$ values were normalised to that of Glx ($\Delta^{15}\text{Glx}$) where $\Delta^{15}\text{Glx} = \delta^{15}\text{N}_{\text{AA}} - \delta^{15}\text{N}_{\text{Glx}}$. This is to account for differences caused by the $\delta^{15}\text{N}$ of the source inorganic nitrogen (NO₃⁻ and NH₄⁺) entering the plant⁷⁷.

3.5.5 Cellulose Extraction

The method used to extract cellulose from maize was adapted from Azubuike *et al.*¹⁶⁷ and Staff *et al.*¹⁶⁸ Azubuike *et al.* specifically extracted α -cellulose from maize cobs and Staff *et al.* from wooden archaeological samples. If the samples were visibly contaminated, they were washed using acetone and then methanol. Modern samples were freeze dried; all samples were then ground. The samples (100 mg) were placed first in 5 mL HCl (1 M) and heated (20 min, 80 °C) and ultrasonicated to remove sedimentary and contaminant carbonates. The samples were filtered and washed three times each with 3 mL deionised water, then placed in 3 mL NaOH (0.2 M) and heated (20 min, 80 °C) and ultrasonicated to remove organic contaminants. The NaOH was replaced until on sonication it remained colourless. The

samples were washed three times each with 3 mL deionised water and then placed in 5 mL HCl (1 M) and ultrasonicated (1 h, 80 °C) to remove adsorbed atmospheric CO₂. The samples were washed with 3 mL deionised water three times, then bleached with 3 mL NaClO₂ (5 %, wt/vol, pH 3) for approximately 30 min to remove lignins. The samples were rinsed in deionised water until the water was neutral, assessed using indicator paper, and the resultant cellulose was freeze-dried prior to analysis. The carbon and oxygen isotope ratios were measured by weighing 0.5 - 1.0 mg of cellulose (two replicates) and the ¹²C:¹³C ratios determined using IR-MS.

3.5.6 Instrumental Analyses

Chromatographic separations of AA derivatives were performed using a Trace Ultra 1310 gas chromatograph (Thermo Fisher, Bremen, Germany) equipped with an Agilent DB-35 custom column (60 m 320 µm x 0.50 µm; J&W Scientific Technologies, Folsom, CA, USA). The GC was interfaced to a Delta V Plus isotope ratio mass spectrometer (EI, 100 eV, three Faraday cup collectors for *m/z* 28, 29 and 30) and a flame ionisation detector (temperature 250°C; hydrogen flow 35 mL min⁻¹; air flow 350 mL min⁻¹; make-up gas off) via a GC isolink II interface (Cu/Ni combustion reactor held at 1000°C) both from Thermo Fisher, Bremen, Germany. Samples were injected (2 µL for standards and 1 µL for samples) using a split/splitless injector operated in splitless mode at 240°C with a 3.5 s pre-injection dwell time. Helium (ultra-high purity grade) at a flow rate of 1.4 mL min⁻¹ was used as the carrier gas. The oven temperature of the GC started at 40 °C (held for 5 min), then increasing by 15°C min⁻¹ to 120°C, then by 3°C min⁻¹ to 180°C, then by 1.5°C min⁻¹ to 210°C, then by 5°C min⁻¹ to 280°C. The final temperature was maintained for 8 min. A cryogenic trap was employed to remove CO₂ from the oxidised and reduced analyte.

All the δ¹⁵N values are reported relative to reference N₂ of known nitrogen isotopic composition, previously calibrated against the AIR international

isotope standard ($\delta^{15}\text{N} = 0$, $^{15}\text{N}/^{14}\text{N} = 0.003865$), introduced directly into the ion source in nine pulses at the beginning and three at the end of each run. The $\delta^{15}\text{N}$ values measured were calibrated to an international standard using a calibration curve (see Appendix) and then drift corrected so that the internal standard norleucine was set to its known $\delta^{15}\text{N}$ value (14.47 ‰). Each reported value is a mean of triplicate $\delta^{15}\text{N}$ determinations. The AA standard mixture, of known $\delta^{15}\text{N}$ values, was analysed every three runs in order to monitor instrument performance. The standard calibration curve can be found in Appendix 7.

The standard deviations of the $\delta^{15}\text{N}$ values of AAs within the maize samples should be as low as possible, ideally < 0.2 ‰; in this work standard deviations of triplicate measurements varied from 0.1 ‰ to 2.0 ‰ (Table 3.1), likely due to the low concentration of nitrogen ions detected in the IR-MS.

Chapter 4. Metabolomic Approaches to Studying the Response to Drought Stress in Corn (*Zea mays*) Cobs

Published in Metabolites as 'Metabolomic Approaches to Studying the
Response to Drought Stress in Corn (*Zea mays*) Cobs.'

4.1 Abstract

Metabolomics is a technique that allows for the evaluation of the entire extractable metabolite profile of a plant, for example, using high-resolution mass spectrometry (HRMS) and can be used to evaluate plant stress responses, such as those due to drought. Metabolomic analysis is dependent upon the efficiency of the extraction protocol. Currently, there are two common extraction procedures widely used in metabolomic experiments, those that extract fresh plant tissue snap frozen and processed in liquid nitrogen, or extraction from dried plant tissues. Here, we evaluated the two using untargeted metabolomics to show that lyophilisation can stabilise the maize (*Zea mays*) extractable metabolome, increasing throughput and efficiency of extraction over the more traditional processing in liquid nitrogen. Then, we applied the lyophilisation approach to explore the effect of drought upon the maize metabolome in an untargeted HRMS metabolomics approach. Metabolomics revealed differences in the metabolome of mature maize having undergone three drought conditions imposed at two critical development stages (three-leaf stage and grain-fill stage); moreover, this difference was observed across two tissue types (kernel and inner cob/pith). It was shown that under ideal conditions, the biochemical make-up reflected in the metabolome of the tissue types is different. However, under stress conditions, the stress response dominates the metabolic profile. Drought-related metabolites known from other plant systems have been identified and metabolomics has revealed potential novel drought-stress indicators in our maize system.

4.2 Introduction

Maize (*Zea mays*. L) is one of the most important food crops produced globally and is highly adaptable to different growing environments. However, drought is a major limiting factor to crop yields of maize, and climate change is threatening food security^{8,13,169} due to increased periods of drought. Southern African maize has been identified as particularly at risk⁸.

Metabolomics is a powerful tool for investigating all metabolites of a biological sample. Metabolites and their levels are of particular interest when investigating genetic influences or environmental changes, as they can be regarded as the final response of an organism to genetic or environmental perturbations⁸⁵. Metabolomics has previously been used to study stress from drought^{9,43,87,88,170} and salinity^{89,90} in maize.

The maize cob provides the growing seed with nutrients including proteins, oils and starch¹⁰¹. Hence, lipids, amino acids, sugars and carbohydrates are expected to be the major components of a kernel extract. It has been shown that increases in the levels of osmoprotectants, such as mono-, di- and oligosaccharides, polyols and some quaternary ammonium compounds are a common adaptive measure to water stress across a range of plants; their accumulation accompanies drought stress⁹. Amines, mono-, di- and oligosaccharides and sugar alcohols can act as stabilising agents to macromolecules such as proteins; these molecules help proteins to maintain their hydration state and hence their structure^{88,170,171}.

Hormones are also important in plant responses to stress. For example, the plant phytohormone abscisic acid (ABA) is heavily implicated in the response to various stressors, such as drought, radiation and salt stress^{102,172}. Phytohormone signalling can trigger the production of secondary metabolites whose primary function is to scavenge reactive oxygen species, which protects the plant from lipid peroxidation; for a full review see

Jogawat *et al.*¹⁷³. For B73, a drought-susceptible modern maize cultivar, drought stress has been shown to cause an accumulation of simple sugars and polyunsaturated fatty acids and a decrease in amines, polyamines and dipeptides, together with an increase in the accumulation of ROSs and the fungal product aflatoxin⁴³. The accumulation of simple sugars is thought to be due to protection against oxidative stress, by osmoregulation or through ROS scavenging. Polyunsaturated fatty acids have been shown to regulate the stomatal aperture in response to drought stress¹⁷⁴. An increase in ROSs occurs when a plant is under drought stress and hydroperoxidation of polyunsaturated fatty acids can result in oxylipin production which can exacerbate aflatoxin contamination (see¹⁷⁵).

Metabolomics approaches consider the extractable plant metabolites, and therefore the extraction protocol plays an important role in the types of molecules included in the analysis. Literature methods most often work with fresh material processed under cold conditions (for example⁸⁷), and this can pose significant challenges. Samples are generally immediately frozen in liquid nitrogen and stored at -80°C ^{176,177} to inactivate enzymatic processes. However, weighing plant material kept frozen in liquid nitrogen can be difficult due to several practical considerations such as electrostatic charging, and condensation onto frozen tissue in damp atmospheres which can cause variation in the tissue weights following drying. Lyophilising the samples prior to homogenisation removes water from the sample, which inactivates enzymes and potentially stabilises the metabolome⁹⁴. Few studies have considered the effect of lyophilising plant material as a means to stabilise the plant metabolome^{95,96} and no studies have considered its impact on metabolomic studies of an agriculturally significant crop, such as maize.

The first objective of this study was to assess the robustness of two steps of the plant tissue extraction process. First, we compared the efficiency of lyophilisation and grinding tissue with a more traditional approach of

grinding fresh-frozen tissue in liquid nitrogen. Next, we tested the necessity of cold room (4 °C) conditions during the solvent (70:30 methanol:water) extraction step; the effects of cold vs. room temperature extraction following lyophilisation were also considered. Our results were used to validate a safe, efficient, robust and reproducible extraction method (extraction condition experiment). The second objective was to use this method to evaluate the influence of drought stress upon mature corn cobs from plants having undergone three different watering regimes (drought condition experiment). The third objective was to test whether drought markers could be identified in fresh, desiccated samples before attempting extraction of the desiccated archaeological maize using an updated HILIC and RP separation approach^{120,178} with the availability of new column chemistries such as T3 column (Section 2.2.4). And finally, it was important to assess whether the drought stress markers were reflected in the inner cob material as the Tularosa material is predominantly made up of inner cob material, and the inner cob has not been studied for this purpose.

4.3 Results and Discussion

4.3.1 Effect of Lyophilisation on the Plant Metabolome

The effect of lyophilisation on the extractable plant metabolome was investigated using untargeted liquid chromatography–mass spectrometry (LC–MS). Metabolites were extracted from maize cob tissue using three different extraction methods. In one set of samples, fresh tissue was ground and extracted under liquid nitrogen (LNE), another set was lyophilised, ground and extracted in the cold (4 °C) (LC), and a third group was lyophilised, ground and extracted at room temperature (LRT). The water content of samples was $69.0 \pm 7.5\%$, as described in Appendix 8.

A chromatographic separation method was designed so a wide range of feature polarities could be examined. Atlantis® T3 columns are reversed-phase C18 columns that provide balanced retention of polar and hydrophobic molecules. Application of such a column using a high polar to high organic solvent concentration gradient allowed good retention and separation of metabolite classes (Figure 4.1). A wide range of metabolite classes was extracted from the maize tissue using methanol:water extraction; polar metabolite classes such as disaccharides and amino acids were first to elute, followed by organic acids and lipids. Figure 4.1 shows a characteristic chromatogram of a sample from the LNE group. Chromatograms from the LC and LRT sample groups can be seen in Appendix 9.

It is difficult to distinguish visually between samples groups based upon the base peak chromatograms, hence statistical techniques were used to assess the data.

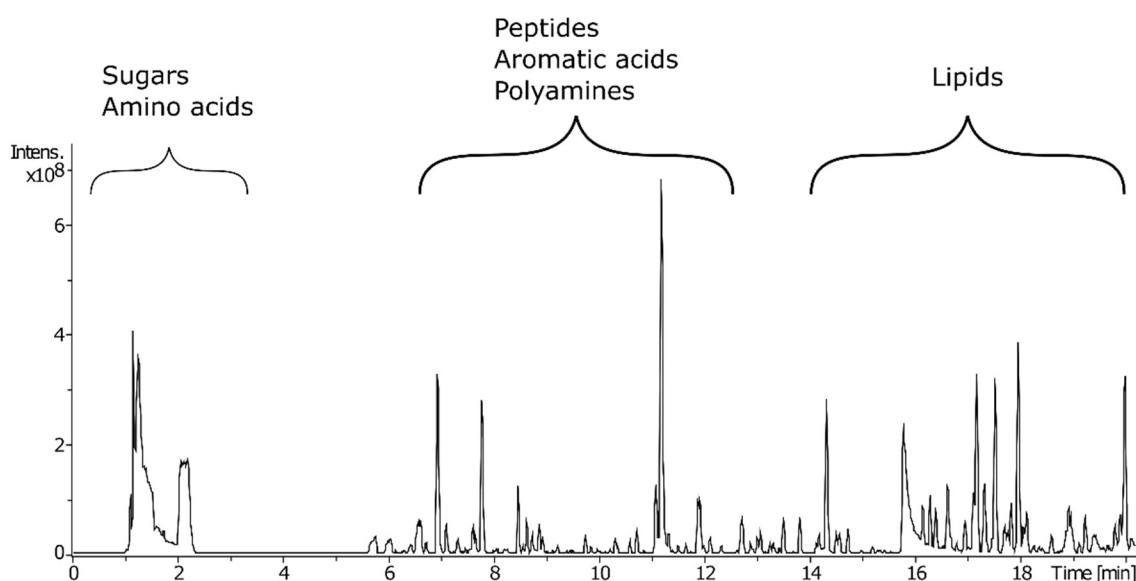


Figure 4.1: Characteristic base peak ion chromatogram for an LNE sample obtained using a T3 column coupled to high-resolution mass spectrometry (LC–HRMS) to allow the retention and separation of metabolites with a broad range of polarities.

To test whether there are differential effects of freeze-drying on extracted maize metabolites, an untargeted study of methanol:water-soluble

metabolites was performed to identify features that change due to the different tissue extraction protocols used. Datasets of full-scan positive-ion-mode and full-scan negative-ion-mode LC–MS data, collected using a Bruker solariX FTICR–mass spectrometer (FTICR–MS), were investigated using principal components analysis (PCA), a multivariate unsupervised statistical technique. Figure 4.2 shows the PCA scores plots for all replicate injections of samples generated using the three different extraction conditions being compared: LNE (green diamonds), LC (purple diamonds) and LRT (grey diamonds) for the positive- and negative-mode data.

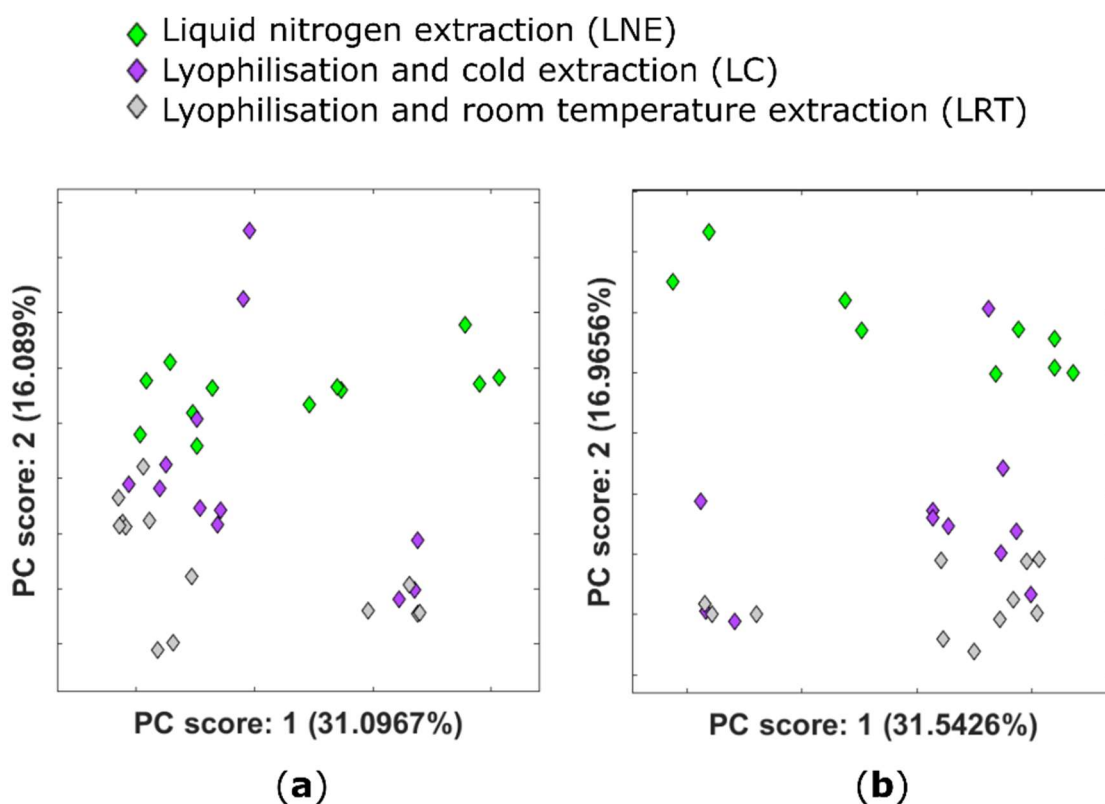


Figure 4.2: PCA plots showing the scores for the first two principal components obtained using untargeted metabolomic analysis of different extraction conditions for *Zea mays* coloured by experimental group (green, purple and grey represent LNE, LC and LRT, respectively) (a) for the positive-ion-mode; (b) and for the negative-ion-mode. The data have been scaled to unit variance and QC corrected.

Examination of PC1 for both scan polarities revealed that the majority of variance is across biological replicates. PC2 in both instances primarily shows

variation due to extraction conditions. Once lyophilised, extraction in either cold or room temperature conditions had a small effect on the extractable metabolome, with more variance across the LC group than LRT. Extraction conditions therefore did not account for the majority of variance in metabolite profiles acquired in either the positive (Figure 4.2a) or negative-ion-mode (Figure 4.2b).

Using liquid nitrogen or lyophilisation to stabilise the extractable metabolome of maize cob tissues seems to have limited impact on the extractable metabolome based on the PCA results. Both the extraction protocols (liquid nitrogen and lyophilisation) have been used to stabilise the extractable metabolome in previous metabolomic studies (for example^{87,179}). Using liquid nitrogen to stabilise the extractable metabolome is well established, but cumbersome and requires access to specific facilities. Accurately weighing samples whilst the samples are frozen using liquid nitrogen is challenging. First, LNE relies on the assumption that water content is consistent between samples, but the moisture content of samples in this experiment had a standard deviation of $\pm 7.5\%$ which is considerable. Variability in the water content can be reduced by thorough grinding of samples, distributing the water crystals more evenly throughout the sample, but this can be difficult to achieve with some biological materials, including maize cobs. Second, the electrostatic nature of frozen material and condensation from the damp atmosphere on to the sample can make weighing samples accurately difficult. Lyophilising samples prior to extraction can avoid some of these issues as dry masses can be more efficiently weighed whilst not requiring access to liquid nitrogen except to snap freeze the tissue or a cold room.

Very few studies have compared the effects of extraction following lyophilisation versus freezing under liquid nitrogen in plant material⁹⁶. Studies that have been conducted have shown that freeze-drying can be used

to stabilise metabolites, including plant hormones⁸⁴. Hamid *et al.*⁹⁵ compared freeze-drying and oven-drying as techniques to stabilise the metabolome of seaweed, and concluded that freeze-drying yielded higher metabolite concentrations than oven-drying. However, Hamid *et al.*⁸³ did not directly compare lyophilisation and liquid nitrogen extraction. Zhu *et al.*¹⁸⁰ have shown that freeze-drying milk to produce milk powders has a limited effect on the milk metabolites; this study also showed stability in the metabolome when stored at either 4 or -20 °C, but storage at room temperature resulted in significant changes. Cheng *et al.*¹⁸¹ suggest using lyophilised faecal samples, rather than fresh frozen samples. Our data have shown that lyophilisation can stabilise the extractable maize metabolome and resolves the issues around weighing variability across tissue samples in this experiment. The effect of drying methods on the metabolome should be tested across a wider range of different biological species and tissue types. Investigating the effect of desiccation on the metabolome has additional value when considering archaeobotanical samples. These samples are often well preserved through natural desiccation and considering the effect desiccation has on the metabolome may offer fruitful insight into the physiological conditions under which ancient plants were grown, with obvious relevance for studies of past climates.

4.3.2 Effect of Drought Conditions upon the Extractable Maize Metabolome

4.3.2.1 Variation in the Extractable Metabolome of Plants Grown under Different Watering Conditions

An untargeted study of methanol:water-soluble maize metabolites was performed to identify features that undergo changes due to drought conditions and also between kernel and inner cob tissue. Two datasets of

full-scan positive- and negative-ion-mode LC–MS data were investigated.

Maize was grown under three different watering conditions: a well-watered control; moderate drought; and severe drought (see Section 3.5.1). Cobs were harvested at maturity in all cases.

The tissue samples were lyophilised and extracted in a cold room using the methanol:water extraction protocol. The LC extraction protocol was chosen for two reasons. The data from the extraction conditions experiment had shown that lyophilisation stabilised the extractable metabolome as effectively as liquid nitrogen extraction. The cold room extraction was chosen because at the time of sample processing, it was not yet clear what effect room temperature extraction has upon more labile molecules, and therefore the more cautious approach was taken. Considering the results of the extraction condition experiment, either LC or LRT would have been appropriate.

PCA (Figure 4.3) shows very distinct clustering by watering conditions for extracts of both kernels and inner cob tissue. Multivariate analysis also showed a tight clustering of QC samples (not shown), which indicates that the differences in watering regimes account for the differentiation between groups rather than instrumental variation throughout the run. Figure 4.3 shows that separation in PC1 is characterised by differences between well-watered and drought conditions. Separation in PC2 is characterised by differences between moderate and severe drought conditions. This implies a different metabolic response to drought stress when it is applied at the three-leaf and grain-fill stages of plant development. Positive-ion-mode data show strong separation of drought conditions for both kernels and inner cob tissue, as do negative-ion-mode inner cob data. Clustering is less strong for severe drought-treated kernel negative-ion-mode data (Figure 4.3b, red diamonds).

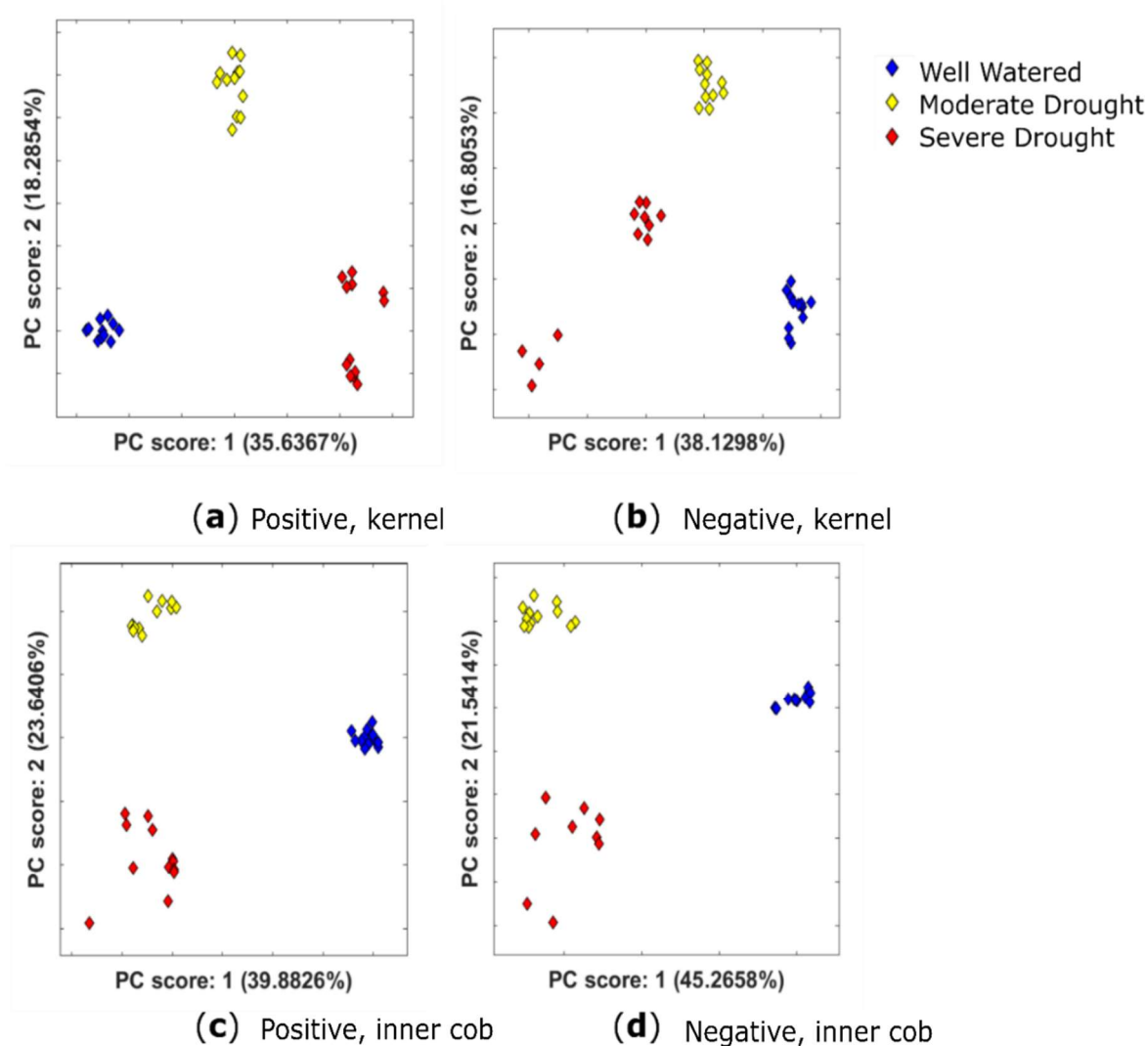


Figure 4.3: PCA plots showing the scores for the first two principal components obtained using untargeted metabolomic analysis of drought-stressed and well-watered control plants, coloured by watering conditions for *Zea mays* for (a) positive-ion-mode kernel extracts; (b) negative-ion-mode kernel extracts; (c) positive-ion-mode inner cob extracts and (d) negative-ion-mode inner cob extracts. The data have been scaled to unit variance and QC corrected.

4.3.2.2 Identification of Potential Drought Biomarkers

Multivariate analysis shows that PC1 is characterised by differences between well-watered and drought conditions (Figure 4.3) for both tissue types for positive- and negative-ion-mode data. Therefore, the largest loadings of PC1 were investigated as potential drought biomarkers.

ANOVA tests were conducted on peak intensities of features identified as having the largest loadings in PC1. Molecular formulae were obtained from the FTICR–MS data using the ‘SmartFormula’ function of Bruker’s DataAnalysis software and checked using Progenesis QI. An internal lock-mass calibration was carried out on the positive-ion-mode samples in order to improve mass error ($\leq 1\%$ ppm). Information about all key features (m/z , t_R , molecular formulae, ANOVA 1-way p -values (p -val)) are presented in Appendix 10. Where possible, HCD product ion spectra were obtained using a Thermo™ Orbitrap™ Fusion™ instrument for key features and the fragmentation patterns were interrogated against compound databases (Metlin, LipidBlast, ChemSpider, Progenesis MetaScope) in order to assign possible identifications. Table 4.1 displays information about key features where a possible identification has been assigned. For an identification to be accepted, the Progenesis fragmentation score was required to be greater than 50. The data analysis workflow is outlined in Figure 4.4. An example figure showing the relative abundances of the top four highest loadings can be found in Figure 4.5.

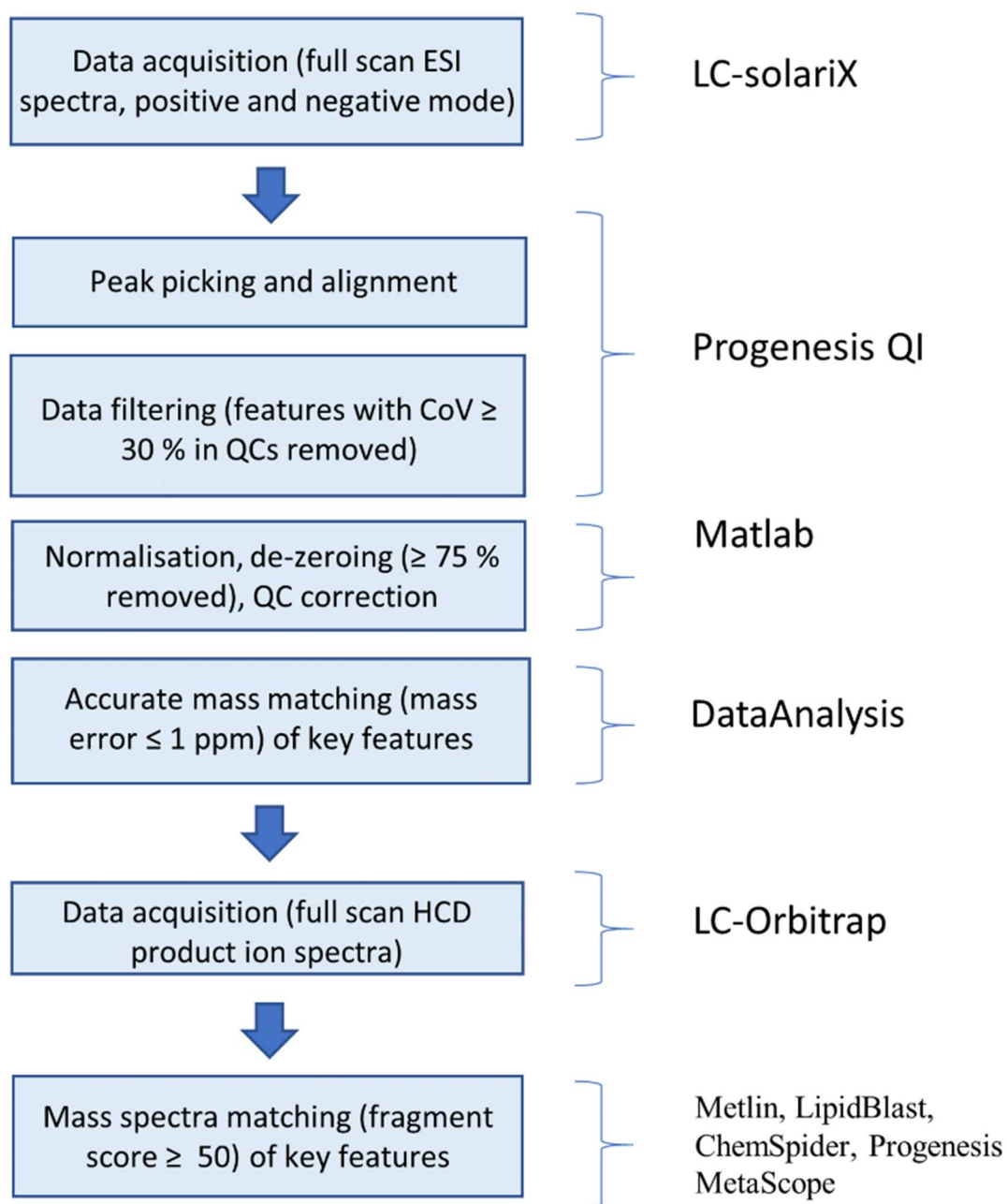


Figure 4.4: Data analysis workflow for the identification of key features in mass spectrometric data.

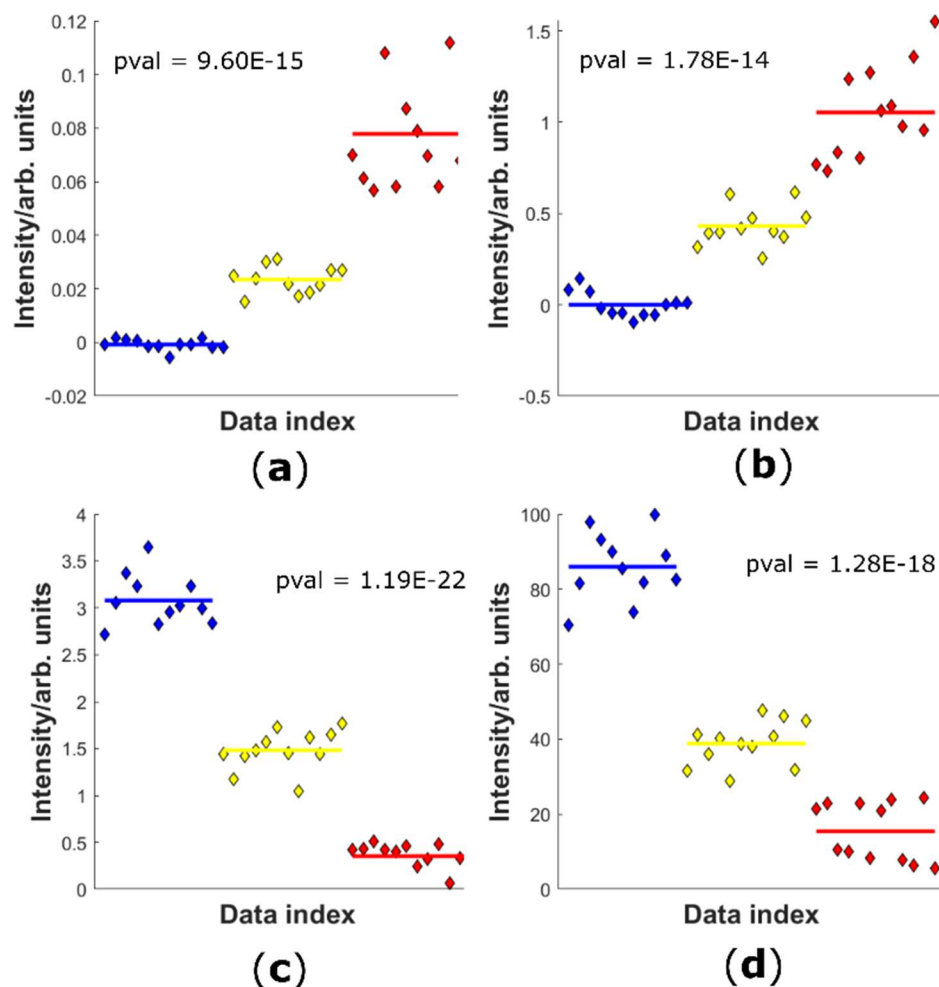


Figure 4.5: Figure showing relative abundances of m/z features (a) 279.1238 (b) 143.0349 (c) 480.3075 and (d) 520.3398. Blue, yellow and red diamonds represent well-watered, moderate drought and severe drought conditions respectively. ANOVA p -vals are indicated.

A feature with m/z 279.124 eluting at a retention time (t_R) of 9.52 min was tentatively identified as neophaseic acid (neoPA) (product ion spectrum in Figure 4.6). The feature was identified by Progenesis as hydroxyabscisic acid, but following examination of Zhou *et al.*¹⁸², the feature was re-assigned as the isomeric neoPA. NeoPA is a metabolite of the phytohormone ABA which is formed following the oxidation of the 9-methyl group of ABA^{182,183}. ABA is one of the most common stress signals to appear in plant organs in response to drought conditions^{172,173,182,184}. ABA was detected in the drought-treated samples in this study. However, it was not included in further analysis because it had a coefficient of variation (CoV) score greater than 30%.

Oxidation of ABA causes inactivation of the hormone and neo-PA is considered biologically inactive. Neo-PA has been detected in drought-stressed barley seedlings¹⁸² and its detection here in drought-stressed maize tissue suggests a role in the abiotic stress response.

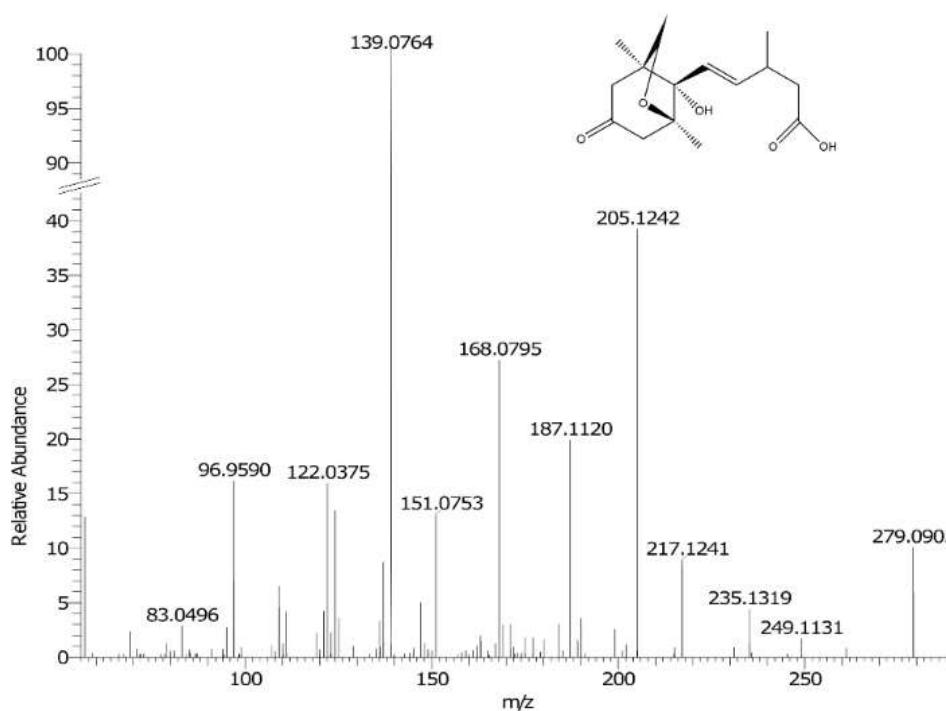


Figure 4.6: Product ion spectrum of m/z 279.124 at 9.52 min.

The molecular formulae of several phospholipids (m/z : 480.3075, 520.3398, 522.3556, 540.3305) were also tentatively identified. Drought stress is known to have an impact on the metabolism of membrane lipids and can cause changes in the membrane lipid composition^{160,185}. Phospholipids can act as signalling precursors and molecules which regulate plant growth and development, and response to environmental factors, such as drought stress^{186,187}.

Table 4.1: Summary of data on all possible identifications of drought-related biomarkers of maize. Possible identifications were assigned using compound databases (Metlin, LipidBlast, ChemSpider, Progenesis MetaScope). * Indicates the data were scaled. The *p*-val between the well-watered and severe drought conditions is quoted. All features are level 3 Schymanski identifications¹³⁰.

Tissue Type	Scan Mode	m/z	<i>t_R</i>	Molecular Species	MF	ppm	<i>p</i> -val	Possible Identification	Fragmentation Score
K	N *	279.1238	9.52	[M – H] [–]	C ¹⁵ H ₂₀ O ₅	–0.04	9.60 × 10 ^{–15}	Hydroxyabscisic acid or Neophaseic acid (neoPA)	50.1 *
K	N *	143.0349	3.88 and 3.89	[M – H] [–]	C ₆ H ₈ O ₄	0.30	1.78 × 10 ^{–14}	Methyl itaconate	58.5
K	P *	480.3075	18.87	[M + H] ⁺	C ₂₃ H ₄₆ NO ₇ P	–0.21	1.19 × 10 ^{–22}	PE(18:1/0:0)	55.1
K	P	520.3398	17.75	[M + H] ⁺	C ₂₆ H ₅₀ NO ₇ P	–0.10	1.28 × 10 ^{–18}	PC(18:2/0:0)	88.8
K	P	522.3556	18.99	[M + H] ⁺	C ₂₆ H ₅₂ NO ₇ P	–0.46	2.42 × 10 ^{–16}	PC(18:1/0:0)	78.4
IC	N	540.3305	18.51	[M + FA – H] [–]	C ₂₄ H ₅₀ NO ₇ P	0.37	1.81 × 10 ^{–8}	Lysolecithin	63.5

4.3.3 Drought-Stress Response Dominates Metabolome in Kernel and Inner Cob Tissues

Two datasets of full-scan positive and negative-ion-mode LC–FTICR–MS data were investigated to compare the metabolomes of the kernel and inner cob. The growing conditions and data handling are described in Sections 3.5.1 and 4.4). PCA analysis (Figure 4.7) shows clustering of the kernel and inner cob severe drought samples (red diamonds and stars) and clustering of the kernel and inner cob moderate drought samples (yellow diamonds and stars). However, well-watered kernels and inner cob samples did not cluster together (blue diamonds and stars).

Watering conditions cause more variance in both sets of drought-treated samples (moderate and severe drought) than tissue type. During optimum growing conditions (well-watered), there is a clear difference in the biochemical composition of the two tissue types as indicated by separate and distinct clusters. However, when drought stress is introduced, there is less divergence between the two tissues. This shows that the drought-stress response was dominant over tissue-specific metabolism across the two tissue types. In severely stressed plants, kernel material can be limited since kernels tend not to develop well under severe stress¹⁸⁸, but inner cob material is more likely to be available and these data show it contains useful abiotic stress signals.

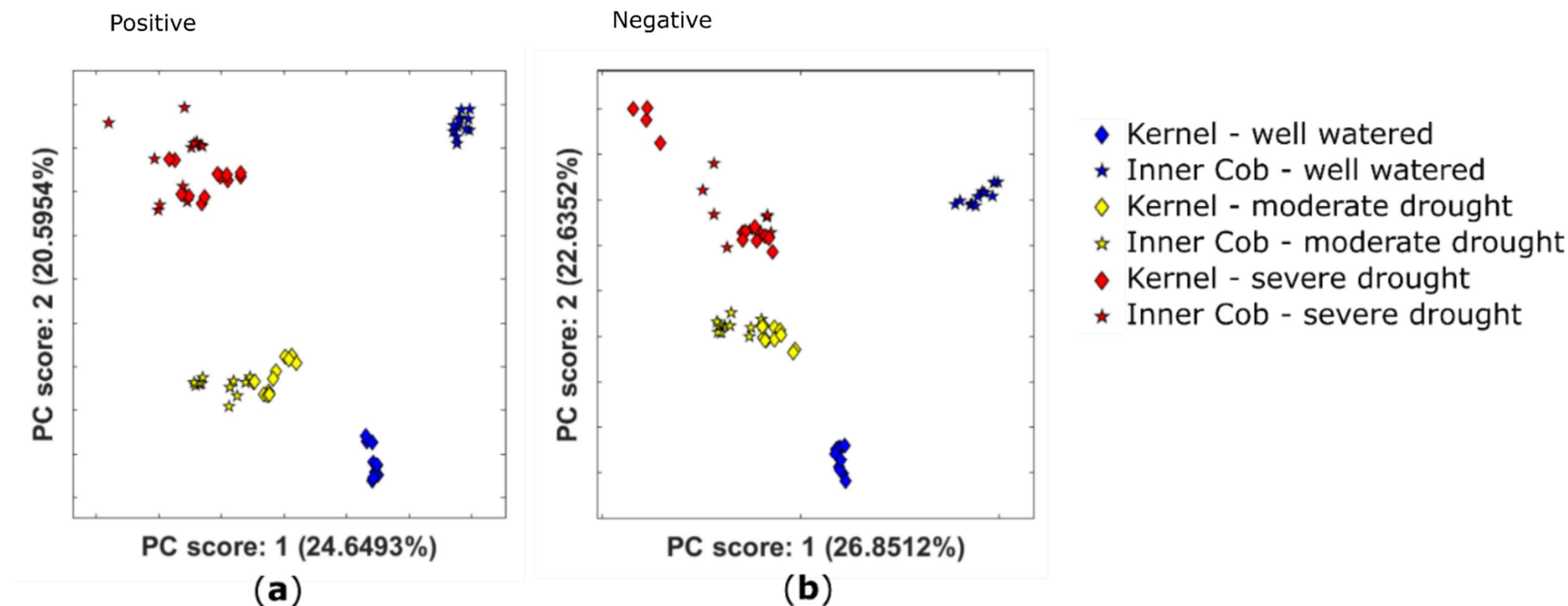


Figure 4.7: PCA plots showing the scores for the first two principal components obtained for the untargeted metabolomic analysis coloured by watering conditions for *Zea mays* for (a) the positive-ion-mode and (b) the negative-ion-mode. The data have been scaled to unit variance and QC corrected for both cases.

4.4 Materials and Methods

4.4.1 Plant Material Description, Cultivation and Sampling

4.4.1.1 Extraction Condition Experiment

Four biological replicates of B73 corn were investigated. Three sample preparation conditions were compared. The inner central section of each cob was sampled in each condition (1 g). The following extraction conditions were used: liquid nitrogen extraction (LNE), the samples were ground and weighed whilst kept frozen using liquid nitrogen; lyophilised cold (LC), lyophilised maize ground at room temperature and extracted at 4 °C, and lyophilised room temperature (LRT), lyophilised maize ground at room temperature and extracted at room temperature.

For LC and LRT conditions, the samples were lyophilised and three extraction replicates were weighed ($5.00 \text{ mg} \pm 0.09$). For the LNE condition, three extraction replicates were weighed ($16.12 \text{ mg} \pm 1.2$, moisture content 68.95%).

4.4.1.2 Drought Condition Experiment

Experimental details in Section 3.5.1.

Prior to extraction, samples were lyophilised and the kernels were separated from the inner cob. For each cob, a central section of pith (1 g) was ground. For each kernel sample, 5 randomly selected kernels were ground together. Three extraction replicates were prepared ($5 \text{ mg} \pm 0.05 \text{ mg}$) for each tissue and from each biological replicate (2 per sample group).

4.4.2 Metabolite Extraction Method

The plant material was extracted with methanol:water (70:30, *v/v*, 100 μ L). The extraction process consisted of shaking at 31 RCF for 30 min in dark conditions, followed by centrifugation at 28413 RCF for 10 min. The supernatant was transferred to a clean tube, dried using a vacuum concentrator (whilst kept cool) and reconstituted in methanol:water (70:30, *v/v*, 100 μ L) and subsequently analysed using HPLC–FTICR–MS. For the LNE and LC conditions, the samples were kept at 4 °C during extraction and for the LRT condition, the samples were extracted at room temperature. All samples were extracted in the cold room for the drought conditions experiment.

4.4.3 Data Collection

In the extraction condition experiment, three extraction replicates were taken for each condition and two technical replicates were taken for each extract. For analysis by LC–MS, the sample injections were separated into three semi-randomised batches containing one technical replicate from each extract. QCs composed of a pooled aliquot of 5 μ L from each sample were injected at the start of the experiment (20 injections) to equilibrate the column. A QC and a blank were injected after every five sample injections.

For the drought condition experiment, three extraction replicates were taken for each condition and two technical replicates were taken for each sample. Data collection was the same as that described in the paragraph above.

4.4.4 LC-MS-Based Analysis of Metabolome

4.4.4.1 *Liquid Chromatography Separation Method*

HPLC-MS was carried out using an Agilent 1200 HPLC fitted with an Atlantis® T3 column (Waters, cortecs 2.7 μm , 3 \times 150 mm); the column temperature was maintained at 25 °C. The HPLC was coupled to an electrospray FTICR mass spectrometer (Bruker solariX XR 9.4T). The mobile phase was composed of water (A) and acetonitrile (B) both with 0.1% (*v/v*) formic acid, and the following gradient was used: 5% B increasing linearly to 95% over 22 min and held for 2 min. B was then returned to 5% over 0.33 min and held for 5.33 min to allow column equilibration. The flow rate was 300 $\mu\text{L}/\text{min}$ and the injection volume was 5 μL .

4.4.4.2 *Mass Spectrometry Methods*

Positive-ion-mode: The LC methods are described in Section 4.4.4.1. A Bruker solariX XR 9.4T mass spectrometer was operated over the *m/z* range 57.75–2000.00 with an ESI source. Analytes were detected in the positive-ion-mode using the following MS parameters: the dry gas flow was 7.0 L/min; the dry gas temperature was 200 °C, the source voltage was 4000 V and the nebuliser gas pressure was 2.0 bar.

Negative-ion-mode: The LC methods are as described in Section 4.4.4.1. A Bruker solariX XR 9.4T was operated in the negative-ion-mode over the *m/z* range 57.75–2000.00 with an ESI source. Analytes were detected in the negative-ion-mode using the following MS parameters: dry gas flow was 7.0 L/min; the dry gas temperature was 200 °C and the source voltage was 4000 V. To optimise ionisation, the nebuliser gas pressure was 2.0 bar (0–6 min), 1.5 bar (6–12 min), 1.3 bar (12–21 min), 1.0 (21–25 min), 1.5 (15–26 min), 1.8 (26–27.5 min) and 2.0 bar (27.5–30 min).

4.4.5 LC-MS/MS

4.4.5.1 Mass Spectrometry Methods

The LC methods are as described in Section 4.4.4.1. An Orbitrap™ Fusion™ MS was operated in the positive-ion-mode and the negative-ion-mode with the following parameters. The m/z range was 85–1000 with an ESI source. Analytes were detected in the positive-ion-mode using the following MS parameters: the ion transfer temperature was 325 °C; the vaporiser temperature was 350 °C; the sheath gas was 50 (arb); the aux gas was (arb) 10; time between master scans was 1 s; the isolation window was 1.6; the collisional energy was stepped and the HCD collision energies (%) were 20, 35, and 60.

4.4.5.2 Data Handling and Analysis

For the extraction conditions experiment, Progenesis QI (Waters, Milford, MA, USA), a dedicated software package for processing LC-MS data, was used for alignment and peak picking. Bruker .d files were imported into Progenesis in centroid mode. The runs were aligned and alignment was accepted if within 80% of the reference run. Experimental groups were used as described in Section 4.4.1.1.

At the peak picking stage, the following parameters were set to reduce the volume of data to allow the computer to process it. Peaks with a t_R of less than 1 min were excluded as being within the void and peaks with a t_R greater than 21 min were excluded on the basis of poor separation during the column wash phase. A minimum peak width of 0.05 min was set. The list of expected charge-bearing species $[M]^+$, $[M + H]^+$, $[M + 2H]^{2+}$, $[2M + H]^+$, $[M + K]^+$ and $[M + Na]^+$ for the positive-ion-mode and $[M - H]^-$, $[M + Cl]^-$, $[M - 2H]^{2-}$, $[M + FA - H]^-$, $[2M - H]^-$ and $[M - H_2O - H]^-$ for the negative-ion-mode were chosen for consideration, as they would arise from the same compound. In the raw data 23,178 and 16,044 features were identified in the

positive and negative-ion-modes, respectively. Features with a coefficient of variation greater than 30% in QC injections were excluded from further analysis.

The settings for Progenesis QI were the same for the drought experiment as in the extraction condition experiment, unless stated. Experimental groups were used as outlined in Section 4.4.1.2. At the peak picking stage, the following parameters were set to reduce the volume of data to allow the computer to process it. Peaks with a t_R of less than 1 min were excluded as being within the void and peaks with a t_R greater than 21 min were excluded on the basis of poor separation during the column wash phase. In the raw data, 4912 and 11,531 features were identified in the positive and negative-ion-modes, respectively.

4.4.5.3 *Statistical Analysis*

For the extraction condition experiment, statistical tests were conducted using the programming environment MATLAB (Mathworks, Natick, MA, USA) using the package 'metabolab'. The data were normalised using the total ion count, de-zeroed at a rate of 75% and QC corrected. 8483 and 10,715 features were included in the analysis (positive and negative-ion-modes, respectively). Data were scaled to unit variance for PCA. For each feature, one-way analysis of variance (ANOVA) was used to test the statistical significance of differences between groups with Benjamini–Hochberg adjustment to correct for multiple testing.

Statistical tests were carried out as described in the paragraph above for the drought conditions experiment. Following data filtering, 1105 and 2191 features were included in the positive and negative analyses, respectively.

4.5 Conclusions

This study has shown that lyophilising plant material is an effective way to stabilise the extractable plant metabolome in maize and is as effective as extracting under liquid nitrogen. Lyophilisation is thus an adequate alternative to the more challenging, resource-intensive and potentially hazardous liquid nitrogen processing techniques. This observation has the potential to improve sample processing efficiencies which can be a bottle neck in metabolomics workflows. However, the effect of desiccation on labile molecules such as phytohormones and the utility of cold room extractions following lyophilisation require further study (in this study CoV was too high for confident interpretation of phytohormones). The lyophilisation extraction technique also has useful applications to archaeobotanical studies where archaeological plant tissues have been naturally preserved via desiccation.

Divergence in the metabolomic profiles of the experimentally drought-stressed maize studied here occurs with the onset of drought stress at the three-leaf stage. Drought stress at the grain-fill growth stage indicated a further divergence from the metabolome of well-watered plants. Differences in response to drought stress were also observed in two plant tissues, kernels and inner cob. It was shown that the drought-stress response was dominant across both tissue types and that inner cob material can be a useful source of information when no kernel data can be obtained. Untargeted metabolomic profiling is clearly a powerful tool to better understand the biochemical mechanisms maize employs to cope with drought stress.

Finally, the LC-MS method demonstrated in this chapter confirms its utility for analysis of polar and apolar compounds in the same separation using the T3 column, which is useful in optimising instrument time and sample. This can be useful for analysing drought-stressed material, as cobs and kernels

develop poorly, making such material limited, but especially for Tularosa
maize material which although an unusually plentiful assemblage is
nonetheless limited and precious.

Chapter 5. Paleometabolomics Reveals Drought Stress Response in Archaeological Maize

Submitted for consideration for publication in Plants as 'Paleometabolomics
Reveals Drought Stress Response in Archaeological Maize.'

5.1 Abstract

The metabolome is the global collection of low molecular weight metabolites produced by systems. Metabolomics studies can provide a direct functional insight into an organism's cellular activity and physiological status.

Paleometabolomics is, by extension, the study of metabolomes of ancient samples. Here we explore the metabolomes of ancient maize cobs from Tularosa Cave in New Mexico, corresponding in age to human occupations during two different climate regimes (wet ca. 1800 cal BP and dry ca. 700 cal BP). Untargeted high-resolution liquid chromatography-mass spectrometry showed differences in the extractable paleometabolomes of the two archaeological populations, and multivariate statistical analysis revealed drought stress biomarkers in the ancient maize metabolomes. Direct evidence of increased sugar production was found in the later population, possibly an indicator of adaptation to dry climate conditions.

5.2 Introduction (as in submitted paper)

Drought stress is an increasingly important issue faced by modern arable farmers globally¹⁸⁹. Maize agriculture in the present-day Southwestern United States has historically faced sparse and unreliable levels of precipitation, resulting in several pan-regional droughts in the last 2000 years^{4,5,45}. Drought stress can threaten food security, especially in developing countries^{8,190}. A better understanding of how humans have adapted their agricultural practices in the past, and how ancient crops have adapted to abiotic stress, is crucial in protecting current global food security. Maize, together with rice and wheat, contributes 30% of calories to more than 4.5 billion people, including to those from some of the poorest countries in the world¹.

Metabolomics is an approach for analysing and comparing the metabolomes of biological samples⁸⁵. The metabolites are extracted, and untargeted liquid chromatography-mass spectrometry data (using high resolution mass spectrometry if available) collected. Supervised and unsupervised statistical approaches can be used to elucidate differences between sample populations, providing a global insight into cellular activity and physiology. Many such studies have shown the effect of abiotic stressors such as drought upon the extractable maize metabolome ^{86–90,98,191}.

Metabolomics has been utilised in some studies of archaeological samples in recent years and such ‘paleometabolomics’ studies are a fast growing and exciting area of interest in archaeological sciences. Metabolomics has been used in the analysis of the stomach content of the Iceman, a 5,300-year old European glacier mummy ¹⁰⁵, in a multi-omics approach to gain insight into the nutritional habits of this individual. The microscopic and molecular data found evidence of three components in the Iceman’s last meal: fat and game meat from ibex and red deer supplemented with cereals from einkorn. Other studies have used metabolomics to distinguish closely related plant species found in residues of ancient pipes ¹⁰⁶, and tobacco mixture usage in ancient Mayans ¹⁰⁷. A recent paper has used metabolomics to study the evolutionary divergence of modern maize from its wild ancestor teosinte ¹⁹². The study found 461 metabolites diverged due to selection. To the authors’ knowledge, paleometabolomics has not yet been used to infer the physiological status of ancient plants.

Tularosa Cave in New Mexico (Figure 1.3) is home to an impressive assemblage of archaeological materials, excavated in 1952 ¹⁵. The extensive collection of maize cobs has two phenotypically distinct varieties. One variety has been described ‘ovoid-shaped’, short in length with a thick midsection and small kernel form, consisting of 10–12 kernels. In contrast, the other is described as ‘cylindrical’ in shape with a thin midsection and 8–

10 rows of larger kernels¹⁴. Radiocarbon dating has found that ovoid-shaped cobs date to 700 BP and ovoid-shaped cobs to 1800 BP. These two periods correspond to two separate human occupations of Tularosa Cave during two different climate regimes (wet ca. 1800 cal BP and dry ca. 700 cal BP). This assemblage is of interest, as the area had undergone extreme droughts across the later occupation and between the occupations and can provide insight into how the maize adapted to the extreme climate conditions. Records of stalagmites from caves in the Sacramento Mountains, New Mexico, show that during the earlier occupation of Tularosa Cave the annual precipitation was higher than at present, and that the more recent occupation was in a time of severe drought (Figure 5.1b⁵); tree-ring data are also consistent with this region experiencing drought during the mid-1200s AD^{4,152,153}. Gaffney *et al.* (paper in review, Chapter 3) have suggested, that stable isotope data provide evidence of drought markers.

It is possible that the two morphologically distinct sets of maize represent an adaptation to climate change. Indeed, genomic analysis of the Tularosa maize^{14,60} has shown that loci associated with drought tolerance (*dehyd1A*) and sugar content (*ae1* and *su1*) in the later cylinder-shaped cobs might have undergone episodes of selection between the earlier and later occupation phases at Tularosa, although other selective pressures, unrelated to environmental conditions, were also discussed. Archaeological evidence for the ways in which New Mexico farmers might have adapted their practice and crops to drought is less forthcoming although mitigation through enhanced irrigation during the later, drier occupation could be envisaged.

Here, we use paleometabolomics approaches to investigate the extractable metabolome of maize cobs from Tularosa Cave. The paper has two primary objectives: firstly, to examine differences in the extractable metabolomes of the two maize populations using principal components analysis (PCA) and to examine and attempt to characterise those features, if any, which are most

responsible for differentiating the two populations; and secondly, to examine known drought-related metabolites and assess their differences in abundances across the two morphological varieties of maize.

5.3 Results

5.3.1 Untargeted Metabolomic Analysis of Ancient Maize Extractable Metabolomes Reveals Variation Between Maize Phenotypes

Twenty-eight maize cobs from Tularosa Cave were sampled (examples in Appendix 1), 14 from each morphological group. Nine of the Tularosa maize samples have been radiocarbon dated and the dates suggest that the maize falls into two temporally distinct periods: older (1830 - 1719 BP, 95.4% CI) and younger (771 - 681 BP, 95.4% CI)^{14,193} (henceforth referred to as 1800 BP and 700 BP). Fourteen samples come from the 1800 BP period and a further fourteen from the 700 BP period. The older maize is ancestral to the younger¹⁴.

An untargeted study of methanol:water-soluble¹⁹⁴ maize metabolites was performed to identify features that are different across the two archaeological maize populations. Two datasets of full-scan positive- and negative-ion-mode LC–MS data were recorded, using a T3 reversed-phase column, chosen to retain as broad a range of metabolite polarities as possible in the same separation. For positive-ion-mode data, LC-MS data were recorded using an FTICR mass spectrometer (Bruker solarix XR 9.4T). In negative-ion-mode the data were collected using a ThermoTM OrbitrapTM FusionTM mass spectrometer. The data were de-zeroed to 50% to reduce instances of false positives, and feature intensities with a CoV of greater than 30 % were removed from the analysis. The data were also QC corrected¹¹⁹.

Figure 5.1 shows the PCA plots for positive and negative mode data. For both positive and negative mode data the PCA shows that the age and associated morphology of the maize sample accounts for the highest variance in the samples as described by PC1 (16.42 % and 20.83 % in positive and negative modes respectively). Multivariate analysis also showed clustering of QC samples (not shown), which indicates that the differences between the metabolomes of the samples account for the differentiation between groups rather than instrumental variation over the course of the multi-sample analysis. Clustering is not tight within groups, possibly due to biological variation, or diagenetic effects; PC1 offers the only differentiation between groups.

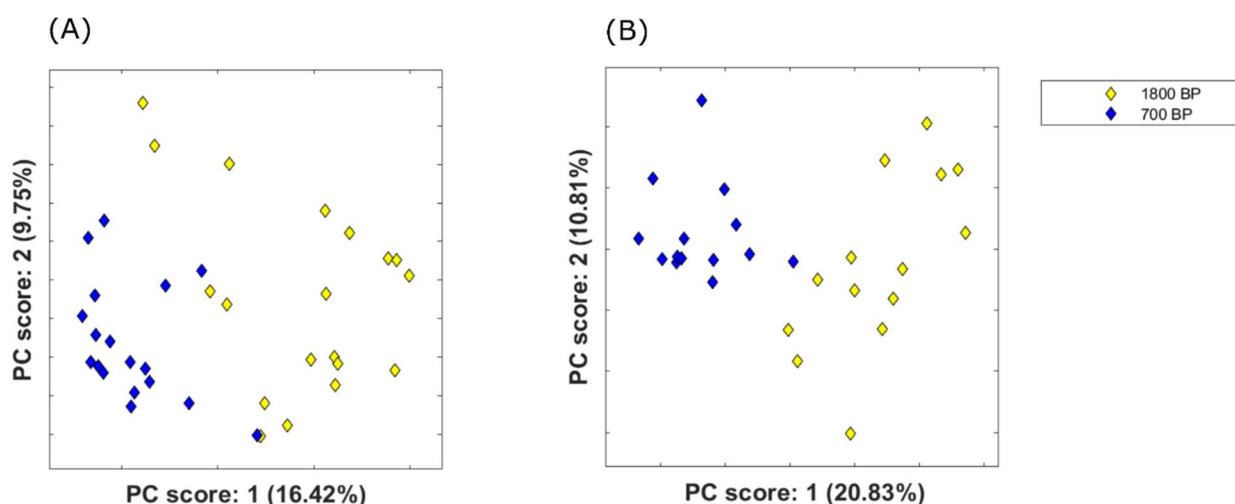


Figure 5.1: PCA plots showing the scores for the first two principal components obtained using untargeted metabolomic analysis of *Zea mays* cob extracts coloured by sample age (yellow and blue represent 1800 BP and 700 BP respectively) (A) for the positive-ion-mode; (B) and for the negative-ion-mode datasets. The data have been scaled to unit variance and QC corrected.

Figure 5.2 shows a volcano plot of the log fold change (between morphological maize groups) against $-\log$ of the adjusted p-values of the metabolites detected in negative-ion-mode (chosen as more featured were

detected in negative-ion-mode). The green dots show metabolites that have a significant p -value (less than 0.05) and a fold change between morphological groups of maize cobs greater than 1.5. A total of 7426 features (22 % of the total detected) show a statistically significant difference in their relative intensities between morphological groups, with 4467 (13%) of those showing elevated expression in the 700 BP group and 2959 (9%) showing elevated expression in the 1800 BP group. The plot shows there is high metabolic diversity between 1800 BP and 700 BP groups (green dots).

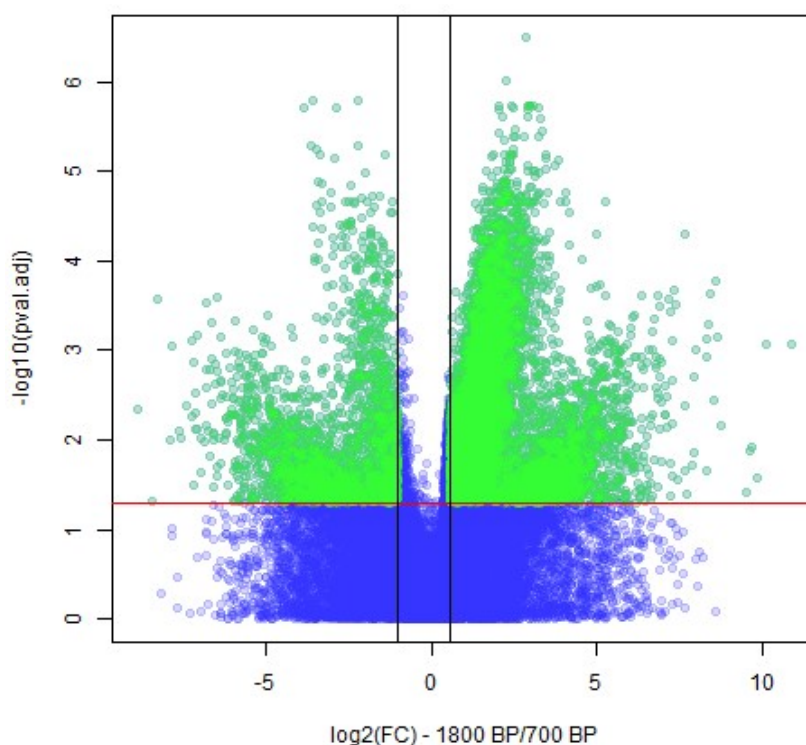


Figure 5.2: Volcano plot, green dots show features (i.e. metabolites) with significant adjusted p -values (<0.05) and fold change > 1.5 between 700 BP and 1800 BP Tularosa maize extracts. Blue dots show metabolites with non-significant adjusted p -values. Red lines to show adjusted p -value cut-off of 0.05, and black lines show fold changes < 0.5 or > 1.5 .

Multivariate analysis shows that PC1 is characterised by maize age and morphology in both positive- and negative-ion-mode data. Therefore, the largest loadings of PC1 were investigated further. T-tests were conducted on peak intensities of features identified as having the largest loadings in PC1.

For negative-ion-mode data, molecular formulae were derived using Xcaliber software and cross-checked using Progenesis QI. For positive-ion-mode data, molecular formulae were obtained from the FTICR-MS data using the 'SmartFormula' function of Bruker's DataAnalysis software and cross-checked using Progenesis QI; their m/z , t_R , molecular formulae, and Mann-Whitney test p -values (p -val)) are presented in Appendix 11. Where possible, HCD product ion spectra were obtained for key features (in positive and negative mode datasets) using a Thermo™ Orbitrap™ Fusion™ instrument, and the fragmentation patterns were interrogated against compound databases (Metlin, LipidBlast, ChemSpider, Progenesis MetaScope) in order to propose identifications. Table 5.1 displays information about key features where an assignment has been proposed (if Progenesis fragmentation score was greater than 30). It is interesting to note that vitexin, a flavonoid, is contributing significantly to PC1. Flavonoids are known to protect plants against biotic and abiotic stress¹⁹⁵. Sucrose or trehalose was also found to be contributing to PC1. Soluble carbohydrates such as sucrose and trehalose and other osmolytes act as osmoprotectants when a plant is under abiotic stress, such as drought stress¹⁰⁹.

Table 5.1: Table showing features with the highest loadings in PC1. *Scaled data. All features are level 3 Schymanski identifications¹³⁰.

Scan Mode	<i>m/z</i>	<i>t_R</i>	Molecular Species	MF	ppm	<i>p</i> -val	Possible Identification	Fragmentation Score
N	237.0766	7.20	[M-H ₂ O-H] ⁻	C ₁₂ H ₁₆ O ₆	-0.52	1.02 x10 ⁻⁵	Glyceraldehyde 3- phosphate (P-Gal)	59.8
N	377.0853	1.17	[M+Cl] ⁻ , [2M-H] ⁻ , [M+FA-H] ⁻ , [M-H] ⁻	C ₁₂ H ₂₂ O ₁₁	-0.86	4.1x10 ⁻³	Sucrose or trehalose	34
N and N*	413.0871	9.34	[M-H ₂ O-H] ⁻ , [M+FA-H] ⁻	C ₂₁ H ₂₀ O ₁₀	-1.73	7.95x10 ⁻⁵	Isovitexin/vitexin	64.5
N and N*	209.0091	5.97	[M-H] ⁻	C ₉ H ₆ O ₆	-0.17	8.21x10 ⁻⁶	Trimesic Acid	47.5
N*	291.0509	8.44	[M-H] ⁻ , [M+FA-H] ⁻	C ₁₃ H ₁₀ O ₅	-0.49	4.90x10 ⁻⁵	Pimpinellin	29.6
N*	273.0403	9.24	[M-H] ⁻	C ₁₄ H ₁₀ O ₆	-0.38	1.02x10 ⁻⁵	Athyriol	
P*	383.1125	12.81	[M+H] ⁻	C ₂₁ H ₁₈ O ₇	-0.19	8.06x10 ⁻⁵	Deoxy-aklanonic acid	55
P*	521.1434	12.55	[2M+H] ⁺	C ₁₄ H ₁₂ O ₅	0.02	1.33x10 ⁻³	Methoxy-stypandrone	38

5.3.2 Osmoprotectant disaccharides were revealed in archaeological maize

The m/z value of 377.085 corresponds to a hexose disaccharide, such as sucrose, trehalose, lactose, maltose and cellobiose which are known osmoprotectants¹⁰⁹. In negative-ion-mode data, the feature with m/z 377.085 was identified and investigated further. Lactose, maltose and cellobiose are reducing disaccharides, while sucrose and trehalose are non-reducing. Reducing and non-reducing oligosaccharides can be distinguished using product ion analysis; the product ion spectrum of the feature with m/z 377.085 is consistent with a non-reducing oligosaccharide. Hydrophilic interaction chromatography (HILIC) is a liquid chromatography (LC) technique that uses a polar stationary phase (for example, silica or a polar bonded phase), and allows retention and separation of polar molecules¹⁹⁶. Using this technique to analyse archaeological samples we observed two peaks with m/z 377.085, which eluted with the same retention times as authentic standards of trehalose and sucrose (Appendix 12). Abundances of the feature in the T3 LC-MS data can be seen in Figure 5.3. The feature is mostly absent from the data from the older samples (yellow diamonds) and present with high variability but higher average level in the more modern sample data (blue diamonds). This observation is notable due to evidence from a previous genetic study¹⁴ which found diversity at *su1* was found to be reduced more than 60 % between the 1800 year old samples and the 700 year old samples at Tularosa Cave. The gene *su1* is responsible for the storage of non-structural starches as soluble low molecular mass carbohydrates and the reduction in diversity would indicate that the gene has been selected for, possibly in response to climate conditions.

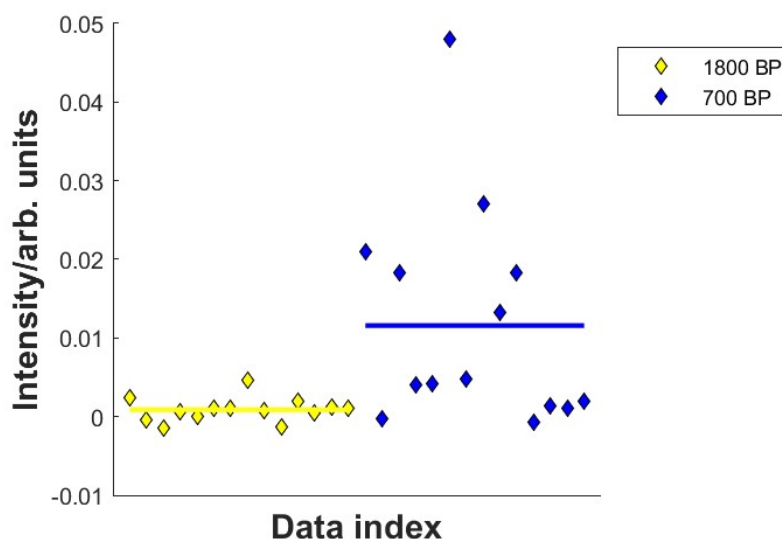


Figure 5.3: Figure showing the relative abundances of the feature with m/z 377.085 for the two maize varieties, where yellow and blue diamonds refer to 1800 BP and 700 BP samples respectively. Lines indicate averages across sample groups. Level 1 Schymanski identification¹³⁰.

5.3.3 Features with High Identity Scores were Investigated by Compound Class

A further analysis was conducted of metabolites from the negative-ion-mode dataset which had fragmentation scores greater than 75 (peak width ≥ 0.15 , isotope similarity ≤ 95 and $-1 \leq \text{ppm} \leq 1$). Negative-ion-mode was chosen for further analysis as more features were detected in this mode and higher quality database matches were found. The compound class of these metabolites was assigned using the KEGG database and information on these metabolites can be found in Appendix 13. Figure 5.4a shows a heatmap of the abundance of metabolites (log transformed) aggregated by class and Figure 5.4b shows boxplots of the same information. The biggest variation appears to be across carbohydrates, where they are more likely to be in greater abundances in the more modern samples. This could be due to an

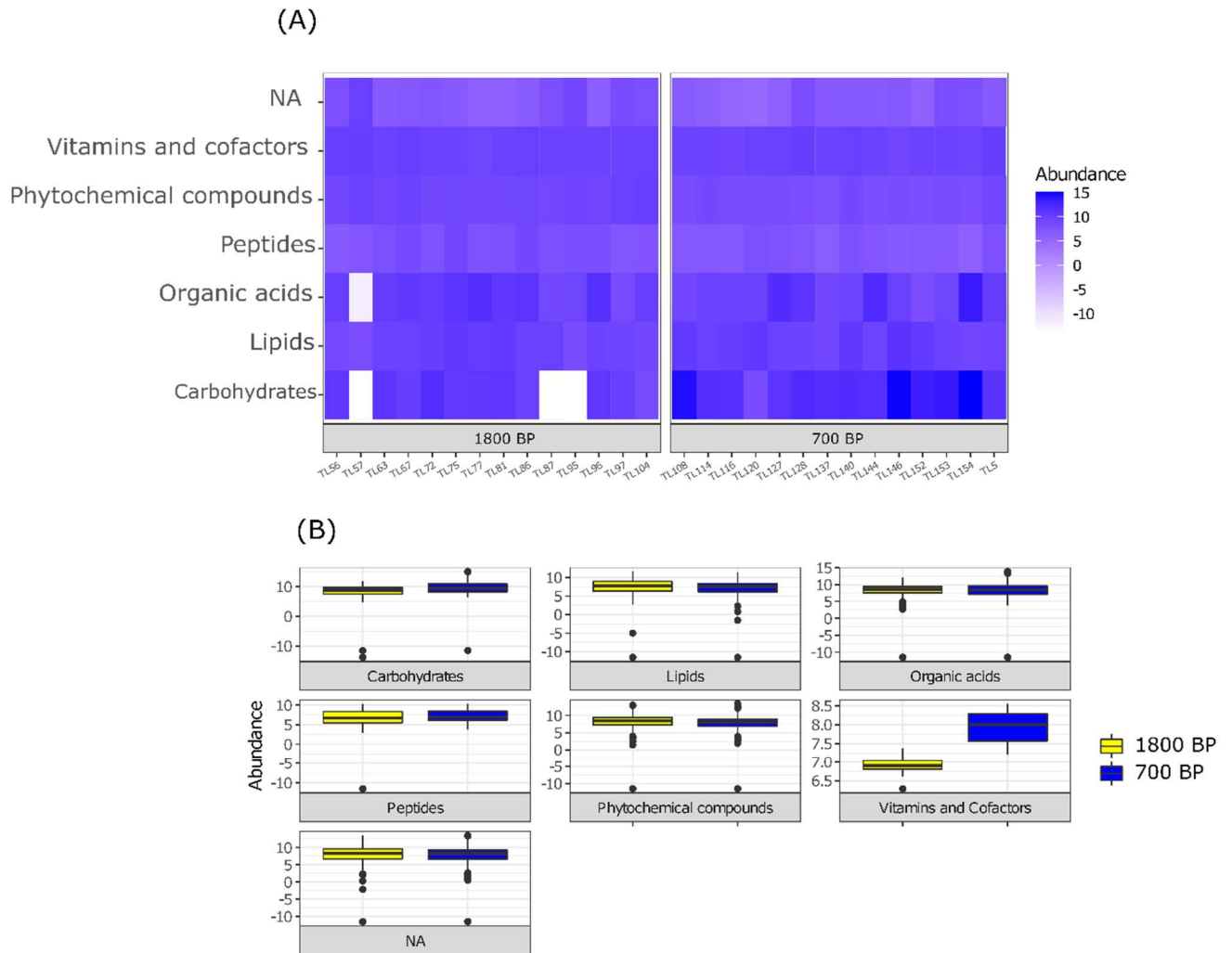


Figure 5.4: (A) Heatmap of the abundance of metabolites (log transformed) aggregated by compound class. (B) Boxplots of abundances of different compound classes of metabolites (carbohydrates, lipids, organic acids, peptides, phytochemicals, vitamins and cofactors and unidentified (NA)). 1800 BP and 700 BP groups are coloured yellow and blue respectively.

adaptation to drought stress. Alternatively, this could reflect diagenetic effects (see chapter 6 for more data and discussion of this topic) that are more evident in the older population where the carbohydrates have been converted to Maillard products or they may have been lost to the environment due to humid conditions. We were unable to confidently identify Maillard products in this analysis.

5.3.4 Drought-Related Metabolites Were Revealed in the Metabolome of Archaeological Samples

The prevalence of known drought metabolites was also investigated in the negative-ion-mode data. The m/z values of known drought metabolites were searched for in our LC-MS datasets using the Progenesis 'Identify Compounds' function. Identifications of those features with matching m/z values were proposed on the basis of their HCD spectra and a fragmentation score of over 50 (Table 5.2) and a peak width of greater than 0.15 mins. The PCA biplot (Figure 5.5) shows that the data from the older maize sample extracts cluster more closely together than the data from the younger maize extracts, which are more spread out. This means that there is higher variance within the younger sample data, with one notable outlier (TUL116). Along PC1 (26.3 %) the variance is due to the age and morphology of the samples. The features are labelled in the biplot and it can be seen that dihydroxycoumarin, hydroxyferulic acid and trans-caffeic acid contributing to PC1 variance, with these metabolites having a higher abundance in the 1800 BP group. Dihydroxycoumarin and hydroxyferulic acid are derivatives of the metabolites coumaric acid and ferulic acid arising through oxidation. In these samples coumaric acid is present in higher abundance in the 700 BP than the 1800 BP samples. This could be due to the coumarin being exposed to oxidising conditions for a longer length of time in the older sample tissues. The remaining metabolites of all classes have higher abundances in the more modern samples (Appendix 14), suggesting an elevation in drought stress indicators in the newer samples.

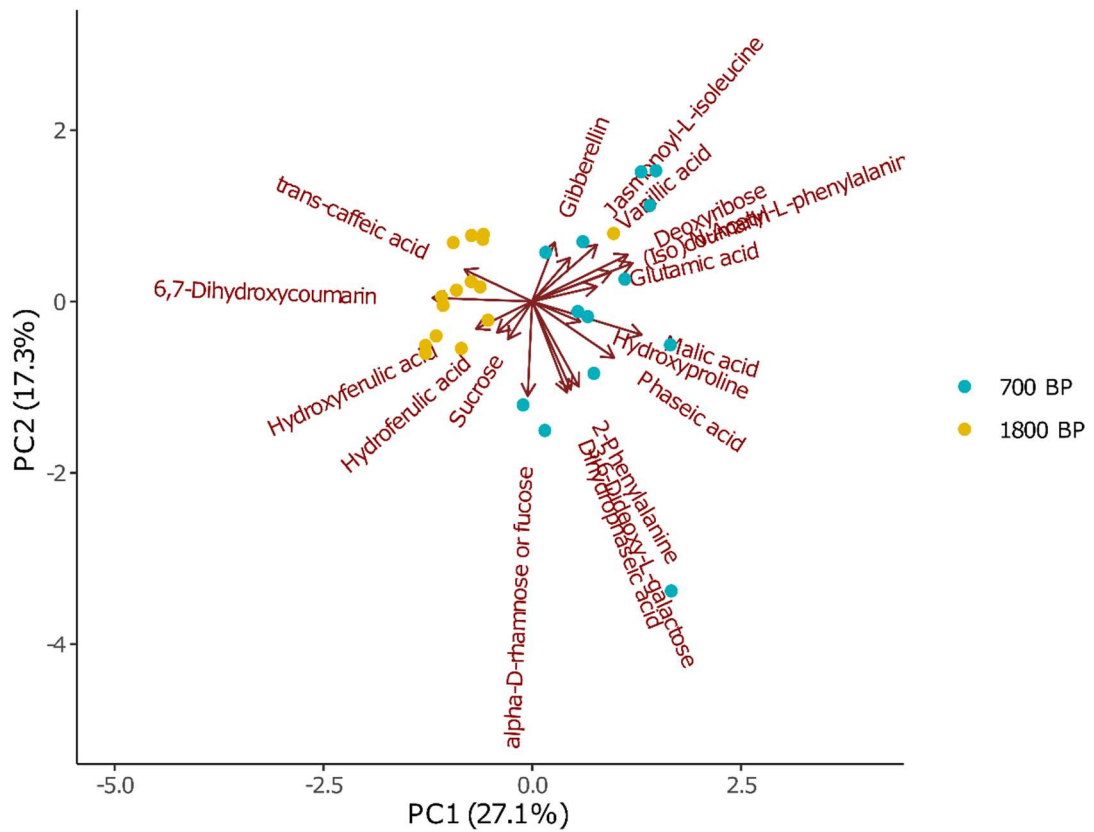


Figure 5.5: PCA biplot showing the scores for the first two principal components obtained for features with accurate m/z values corresponding to known drought related features selected from untargeted metabolomic analysis of archaeological *Zea mays*, coloured by age (yellow and blue represent 1800 BP and 700 BP respectively). Loadings of features are represented by red arrows, where the length of the arrow is proportional to the loading.

Table 5.2: Summary of data on all proposed identifications of drought-related biomarkers in archaeological maize extracts. Possible identifications were assigned using compound databases (Metlin, LipidBlast, ChemSpider, Progenesis MetaScope). The *p*-val between the 700 BP and 1800 BP maize are quoted. * Metabolite identification confirmed with a standard. FA = formic acid. All features are level 3 Schymanski identifications¹³⁰.

<i>m/z</i>	<i>t_R</i>	Molecular Species	MF	ppm	<i>p</i> -val	Possible Identification	Fragmentation Score
304.1917	9.52	[M-H ₂ O-H] ⁻	C ₁₈ H ₂₉ NO ₄	-0.44	4.31E-4	Jasmonoyl-L-isoleucine	62
261.1131	12.40	[M-H ₂ O-H] ⁻	C ₁₅ H ₂₀ O ₅	-0.49	1.42E-04	Hydroxyabscisic acid or phaseic acid	56.1
191.0350	9.25	[M-H ₂ O-H] ⁻	C ₁₀ H ₁₀ O ₅	0.15	1.04E-01	Hydroxyferulic acid	69.8
301.1040	1.68	[M+FA-H] ⁻	C ₁₁ H ₁₆ N ₂ O ₅	-0.47	2.99E-02	1-(β-D-Ribofuranosyl)-1,4-dihydronicotinamide	66.3
210.0771	4.09	[M+FA-H] ⁻	C ₉ H ₁₁ NO ₂	-0.24	1.48E-01	2-Phenylalanine	50.6
129.0557	3.25	[M-H] ⁻	C ₆ H ₁₂ O ₄	-0.15	8.51E-01	3,6-Dideoxy-L-galactose	60.3
223.0248	5.18	[M+FA-H] ⁻	C ₉ H ₆ O ₄	0.27	7.95E-05	6,7-Dihydroxycoumarin	57.9
145.0506	5.65	[M-H] ⁻	C ₆ H ₁₂ O ₅	0.01	9.61E-01	α-D-rhamnose or fucose	50.3
145.0295	8.78	[M-H] ⁻	C ₉ H ₆ O ₂	-0.03	1.01E-04	(Iso)coumarin	67.8

146.0459	1.68	[M-H] ⁻	C ₅ H ₉ NO ₄	0.38	6.26E-03	Glutamic acid	62.1
179.0562	1.19	[M+FA-H] ⁻	C ₅ H ₁₀ O ₄	0.66	1.01E-04	Deoxyribose	56.6
281.1393	10.08	[M-H] ⁻	C ₁₅ H ₂₂ O ₅	-0.55	2.09E-02	Dihydrophaseic acid	60.4
361.1289	7.11	[M+Cl] ⁻ , [M+FA-H] ⁻ , [M-H] ⁻	C ₁₉ H ₂₂ O ₇	-0.94	4.20E-01	Gibberellin	55.2
177.0557	10.56	[M-H ₂ O-H] ⁻	C ₁₀ H ₁₂ O ₄	0.08	2.02E-01	Hydroferulic acid	63
145.0295	8.78	[M-H] ⁻	C ₉ H ₆ O ₂	0.16	1.01E-04	(Iso)coumarin	67.1
164.0717	7.33	[M-H] ⁻	C ₁₁ H ₁₃ NO ₃	-0.20	1.48E-01	Phenylalanine	71.1
130.0510	1.78	[M-H] ⁻	C ₅ H ₉ NO ₃	-0.07	3.71E-01	Hydroxyproline	55
133.0142	1.55	[M-H] ⁻	C ₄ H ₆ O ₅	-0.09	2.37E-04	Malic acid	60.8
377.0853	1.17	[M+Cl] ⁻ , [2M-H] ⁻ , [M+FA-H] ⁻ , [M-H] ⁻	C ₁₂ H ₂₂ O ₁₁	-0.86	6.94E-02	Sucrose	33.8*
225.0404	6.59	[M+FA-H] ⁻	C ₉ H ₈ O ₄	-0.17	3.50E-03	Trans-caffeic acid	52.7
167.0351	6.02	[M-H] ⁻	C ₈ H ₈ O ₄	0.47	7.93E-01	Vanillic acid	61.4

5.4 Discussion

Metabolomic analysis can offer valuable insight into the physiological status of a biological system. Genomics can show us the potential of the biological system and proteomics shows us the tools by which these metabolic processes are carried out. However, metabolomics is direct evidence of the molecules produced in response to the genes mediated by the proteins. The metabolome is particularly sensitive to biotic and abiotic stressors^{197,198} and can hence be used to directly infer the biological status of a system. This chapter shows that the extractable maize metabolomes of two archaeological maize varieties grown in different climate conditions contain large numbers of metabolite features and that the metabolomes are distinguishable by PCA analysis.

The climate record shows that the more modern cobs experienced a period of pan-regional drought⁴, causing human population loss in this region. A previous study¹⁴ found diversity at the gene *su1* was reduced in the 700 year old samples by more than 60 % of that in the 1800 year old samples at Tularosa Cave which indicates that the gene was selected for, possibly in response to drought conditions. This gene is responsible for the storage of non-structural starches as soluble low molecular mass carbohydrates¹⁶¹. Low molecular mass carbohydrates such as sucrose, trehalose and fructose are implicated in osmotic regulation, which is important when water is scarce, helping to maintain the plant's structural integrity¹⁶². Da Fonseca *et al.* found that the *su1* gene was identified at higher frequency in the 700 BP samples suggesting that it had undergone selection since 1800 BP. Using metabolomics, we see evidence of this gene's expression directly through an increased abundance of sucrose in the 700 BP samples. An alternative hypothesis postulated¹⁴ is that *su1* was selected through culinary preferences as it is implicated in improving the pasting properties of the flour needed for

tortilla production. However, when the stable isotope measurements of maize cobs are also considered (Chapter 3), it is more likely that these genes were under selection at least largely as a consequence of the environmental conditions.

Other reducing monosaccharides, for example fucose, have also been identified as being expressed in the 700 BP samples. However, over time it is probable that reducing saccharides may be lost due to the Maillard reaction¹⁹⁹ taking place with amino acids, and we may expect to see some Maillard products as a result, however they could not be verifiably identified in this study. It is also possible that soluble saccharides have been lost preferentially post deposition in the more humid conditions of the 1800 BP period. It is possible that this could occur as a result of exposure to groundwater, however these samples were recovered in a stable cave environment, so this is unlikely. The effect of diagenesis on the metabolome as a whole must be considered. It is perfectly possible that a proportion of the variance across sample groups is due to diagenesis. However, the desiccated status of the samples and their depositional context within a cave means that we might expect the metabolome to be fairly well conserved. Lack of water in the plant material will inhibit enzymatic activity⁹⁴ and work by Gaffney *et al.*¹⁹⁴ has shown that the extractable maize metabolome can be well stabilised by lyophilisation (Chapter 4). The fact that most classes of metabolites do not vary in their levels significantly between the older and younger maize varieties (Figure 5.5) suggests that our observations are not just the result of general diagenesis. In addition, some metabolites were seen to decrease in the more recent maize variety while others increase (Section 5.3.3, Figure 5.4), again suggesting there is more than just general diagenesis occurring. Taken together with the genetic data from the same assemblage that are consistent with selection for stress resistance mechanisms, these observations argue against purely diagenetic effects being responsible for our

observations that drought stress markers specifically are observed in higher levels in the more recent, drought-grown maize.

To conclude, this work is a novel use of paleometabolomics. This approach can be used on well-preserved archaeological samples in order to assess biotic and abiotic stressors that were contemporary with the period when the archaeological plant material was grown.

5.5 Material and Methods

5.5.1 Archaeological Materials

The maize cobs used in this study were excavated from Tularosa Cave, New Mexico by Martin *et al.* (1952). Some of the samples used in this study have been radiocarbon dated (da Fonseca *et al.* 2015). The maize samples correspond to two temporally distinct occupations: older (1830 - 1719 BP, 95.4% CI, n=14) and younger (771 - 681 BP, 95.4% CI, n=14). The older samples have 'ovoid' morphology and the more modern samples have a 'cylinder' shaped morphology. The inner part of the cob was sampled for these analyses. Information about catalogue numbers and site context is provided in Appendix 15.

5.5.2 Metabolite Extraction Method

The method of Gaffney *et al.* (2021)²⁰⁰ was followed as described. The plant material (20 mg) was extracted with methanol:water (70:30, v/v, 100 µL). The extraction process consisted of shaking at 31 RCF for 30 min in the dark, followed by centrifugation at 28413 RCF for 10 min (M-24 Boeco centrifuge). The supernatant was transferred to a clean tube, dried using a vacuum concentrator (whilst kept cool) and reconstituted in methanol:water (70:30, v/v, 100 µL) and subsequently analysed using HPLC-FTICR-MS. All samples were extracted in a cold room (5 °C).

5.5.3 Data Collection

Samples were randomised and QCs composed of a pooled aliquot of 5 μ L from each sample were injected at the start of the experiment (20 injections) to equilibrate the column. A QC and a blank were injected after every five sample injections.

5.5.4 LC-MS-Based Analysis of Metabolome

5.5.4.1 *Liquid Chromatography Separation Method*

HPLC–MS was carried out using an Agilent 1200 HPLC fitted with an Atlantis® T3 column (Waters, cortecs 2.7 μ m, 3 \times 150 mm); the column temperature was maintained at 25 °C. The HPLC was coupled to an electrospray FTICR mass spectrometer (Bruker solariX XR 9.4T). The mobile phase was composed of water (A) and acetonitrile (B) both with 0.1% (v/v) formic acid, and the following gradient was used: 5% B increasing linearly to 95% over 22 min and held for 2 min. B was then returned to 5% over 0.33 min and held for 5.33 min to allow column equilibration. The flow rate was 300 μ L/min and the injection volume was 5 μ L.

5.5.4.2 *HILIC Separation Method*

HILIC-MS was carried out using Agilent 1200 HPLC fitted with a HILIC column (Cortecs HILIC Column, 90 Å, 2.7 μ m, 2.1 mm X 150 mm); the column temperature was maintained at 25 °C. The HPLC was coupled to an electrospray Orbitrap™ Fusion™ Tribrid™ mass spectrometer. The mobile phase was composed of water (A) and acetonitrile (B) both with 0.2% (v/v) formic acid, and the following gradient was used: 5% A increasing linearly to 50% over 20 min and held for 2 min. B was then returned to 5% over 0.33 min

and held for 5.33 min to allow column equilibration. The flow rate was 0.5 mL/min and the injection volume was 5 μ L.

5.5.5 Mass Spectrometry Methods

Positive-ion-mode: The LC methods are as described in Section 4.4.4.1. A Bruker solarix XR 9.4T mass spectrometer was operated over the m/z range 57.75–2000.00 with an ESI source. Analytes were detected in the positive-ion-mode using the following MS parameters: the dry gas flow was 7.0 L/min; the dry gas temperature was 200 °C, the source voltage was 4000 V and the nebuliser gas pressure was 2.0 bar.

Negative-ion-mode: The LC methods are as described in Section 4.4.4.1. An Orbitrap™ Fusion™ Tribrid™ mass spectrometer was operated in the negative-ion-mode over the m/z range 57.75–1000.00 using an ESI source. Analytes were detected in the negative-ion-mode using the following MS parameters: the ion transfer temperature was 325 °C; the vaporiser temperature was 350 °C; the sheath gas was 50 (arb); the aux gas was (arb) 10; time between master scans was 1 s; the isolation window was 1.6; the collisional energy was stepped and the HCD collision energies (%) were 20, 35, and 60.

5.5.6 LC-MS-MS

5.5.6.1 Mass Spectrometry Methods

The LC methods are as described in Section 4.4.4.1. An Orbitrap™ Fusion™ Tribrid™ mass spectrometer was operated in the positive-ion-mode or the negative-ion-mode with the following parameters. The m/z range was 85–1000, and the instrument was fitted with an ESI source (heated electrospray ionisation, Easy-Max NG). Analytes were detected in the positive-ion-mode using the following MS parameters: the ion transfer temperature was 325 °C; the vaporiser temperature was 350 °C; the sheath gas was 50 (arb); the aux

gas was (arb) 10; time between master scans was 1 s; the isolation window was 1.6; the collisional energy was stepped and the HCD collision energies (%) were 20, 35, and 60.

5.5.6.2 *Data Handling and Analysis*

Progenesis QI (Waters, Milford, MA, USA), a dedicated software package for processing LC–MS data, was used for alignment and peak picking. Bruker .d files were imported into Progenesis in centroid mode. The runs were aligned and alignment was accepted if within 80% of the reference run. Experimental groups were based on the age of the sample as described in Section 5.5.1 and Appendix 15.

At the peak picking stage, the following parameters were set to reduce the volume of data to allow the computer to process it. Peaks with a t_R of less than 1 min were excluded as being within the void and peaks with a t_R greater than 21 min were excluded on the basis of poor separation during the column wash phase. The list of expected charge-bearing species $[M]^+$, $[M+H]^+$, $[M+2H]^{2+}$, $[2M+H]^+$, $[M+K]^+$ and $[M+Na]^+$ for the positive-ion-mode and $[M-H]^-$, $[M+Cl]^-$, $[M-2H]^{2-}$, $[M+FA-H]^-$, $[2M-H]^-$ and $[M-H_2O-H]^-$ for the negative-ion-mode were chosen for consideration, as the same compound can ionise with more than one charge-bearing species. In the raw data 47,180 and 62,089 features were identified in the positive and negative-ion-modes, respectively. Features with a coefficient of variation greater than 30% in QC injections were excluded from further analysis.

5.5.6.3 *Statistical Analysis*

Statistical tests were conducted using the programming environment language 'MATLAB (Mathworks, Natick, MA, USA)' using the package 'metabolab'. The data were normalised using the total ion count, de-zeroed at

a rate of 50% and QC corrected¹¹⁵. 18,707 and 33,174 features were included in the analysis (positive and negative-ion-modes, respectively). Data were scaled to unit variance (the data for each variable were mean centered and then divided by the standard deviation of the variable). For each feature, the non-parametric Mann-Whitney test was used to test the statistical significance of differences between groups with Benjamini–Hochberg adjustment to correct for multiple testing.

Chapter 6. Assessment of the Effect of Diagenesis on Archaeological Maize Samples: Artificial Ageing Experiments

6.1 Introduction

The focus of this chapter was firstly to assess the preservation of the Tularosa maize samples and secondly to test the effect of diagenesis on isotope ratios and the extractable metabolome. Having found changes in the isotope ratios (chapter 3) and the metabolomes (chapter 5) between earlier (1800 BP) and later (700 BP) Tularosa maize cobs and it was therefore needed to assess if these effects are due to diagenesis or if they are indeed due to biological or environmental effects. In the work described in this chapter the state of preservation of the maize cobs was assessed using Fourier-transform infrared spectroscopy and elemental analysis. Then amino acid composition analysis was conducted to assess protein levels in the two populations of Tularosa maize, and the effect of ageing on $\delta^{15}\text{N}_{\text{bulk}}$ and $\delta^{15}\text{N}_{\text{AA}}$ was considered. Finally, the effect of ageing on the maize metabolome was tested.

The word 'diagenesis' was originally used by geologists to describe the physical and chemical changes to sediment caused by water-rock interactions, microbial activity, and compaction after deposition.

Archaeologists adopted the word to describe ageing processes that affect bones and fossils²⁰¹. Ultimately, the word has come to be used to describe the modification of an object's chemical or physical structure due to chemical and biological processes²⁰².

In archaeobotanical samples, diagenesis begins as soon as the sample is deposited and continues to the discovery of an archaeological specimen and can be defined as 'post depositional change'²⁰². The processes that affect samples can include chemical decomposition, microbial degradation and groundwater leaching, and such processes begin immediately. These processes can cause the removal of certain portions of the organic matter, contamination, or replacement of organic matter by exogenous material.

All of these processes introduce the potential for changing the isotopic composition and the metabolomic signature of the residual organic matter. Different amino acids have different isotope values^{79,82} so that preferential removal of one amino acid would be expected to alter the bulk isotope ratio signature of the sample. Microorganisms preferentially metabolise amino acids that represent better carbon sources (i.e. those with large side-chains), such as phenylalanine and glutamate²⁰³. In charred samples, a considerable proportion of amino acids are converted to melanoids which are resistant to biological degradation due to their structure²⁰⁴. Furthermore, amino acids bound in Maillard reaction products are more resistant to hydrolysis than those associated with proteins and polypeptides⁸². Work by Fraser⁸² *et al.* has found that burial of grain and seeds has no effect on the $\delta^{15}\text{N}$ signature and Metcalfe and Mead⁸⁴ have found that uncharred plant remains retain their isotope signature. Metcalfe and Mead also found that considering %C, %N, and C/N are not effective approaches to evaluate isotopic alterations of ancient plants. However, attenuated total reflectance Fourier-transform infrared spectroscopy (ATR-FTIR) is a promising way to characterise diagenesis processes⁸⁴.

In a metabolomics study it is well understood that the metabolome must be stabilised immediately on harvesting plant material to preserve the metabolic status of the plant (see chapter 4). However the long term effects of deposition are less well understood. Burial environment can have a big impact on the rate and type of diagenesis²⁰⁵. For example, soil chemistry can impact what type of reactions are able to occur, as can whether the environment is oxygenated or anoxic. Similarly, if the samples are deposited within the water table or where ground water flows, we can expect that to have an impact on the metabolome.

Artificial ageing experiments of archaeobotanical remains often focus on the effects of charring. Therefore, it is common for samples to be heated for a

short period of time at very high temperatures (over 100 °C) in order to emulate charring effects^{82,199,206}. In food studies, the effects of shorter term ageing are often conducted at lower temperatures (50 °C) for several weeks^{207,208}. The samples from Tularosa Cave are not charred, however they far more significantly aged than the samples heated for food studies.

In this chapter the preservation of the samples from Tularosa Cave was assessed using EA and ATR-FTIR spectroscopy. Artificial ageing experiments were used to investigate the effect ageing has on the maize metabolome and isotope ratios, including the individual amino acid isotope ratios.

6.2 Results and Discussion

6.2.1 Assessing the Preservation of the Tularosa Maize

FTIR and elemental analysis were conducted on modern aged maize and archaeological maize from Tularosa cave. Samples were heated in an oven at 70 °C for 0, 1, 2, 4, 8, and 16 weeks, in order to artificially age the samples for comparison with the Tularosa maize. Heating at 70 °C was chosen emulate the effects of diagenesis experienced by the Tularosa maize. Heating at higher temperature (as often seen in archaeological ageing experiments^{82,199,206}) resulted in charring. Lower temperatures are often chosen for food studies^{207,208}; however the samples from Tularosa Cave are more significantly aged than the samples heated for food studies. 70 °C was chosen with exponential sampling points, as this was hoped to best reflect the ageing process of the desiccated samples.

6.2.1.1 *ATR-FTIR of Archaeological and Modern Aged Maize Shows Limited Changes on Comparison with Modern Unaged Maize*

ATR-FTIR spectra were taken of a modern lyophilised sample and samples that had been aged at 70 °C for 0, 1, 2, 4, 8 and 16 weeks. Figure 6.1 shows the ATR-FTIR spectra of samples heated for 0 and 16 weeks (1, 2, 4, and 8 week ATR-FTIR spectra are in Appendix 16). We might expect to see a reduction in CH₂ and C–O groups in aged samples, due to loss of organic carbon. Styring *et al.*¹⁹⁹ suggested reduced C–O peaks in charred cereal grains are due to conversion of starch into melanoidins during Maillard reactions. However, in these aged samples there is not a noticeable reduction in these signals (CH₂ and C–O stretches are labelled on in Figure 6.1).

If the high $\delta^{15}\text{N}$ values observed in the ancient maize from Tularosa (discussed in chapter 3) resulted from diagenetic alteration, we might expect the greatest changes in the ATR-FTIR spectra to be in the amide peaks of samples with the highest $\delta^{15}\text{N}$ values (samples from the 1800 BP time period), but this was not what was observed. As can be seen in Figure 6.2, FTIR spectra of the older Tularosa samples compared to younger showed negligible changes in the amide and CH₂ and C–O stretches. Therefore, we can tentatively conclude that the changes in $\delta^{15}\text{N}$ values are not due to diagenesis, consistent with the literature⁸⁴. Further examples of ATR-FTIR spectra of Tularosa maize can be found in Appendix 17.

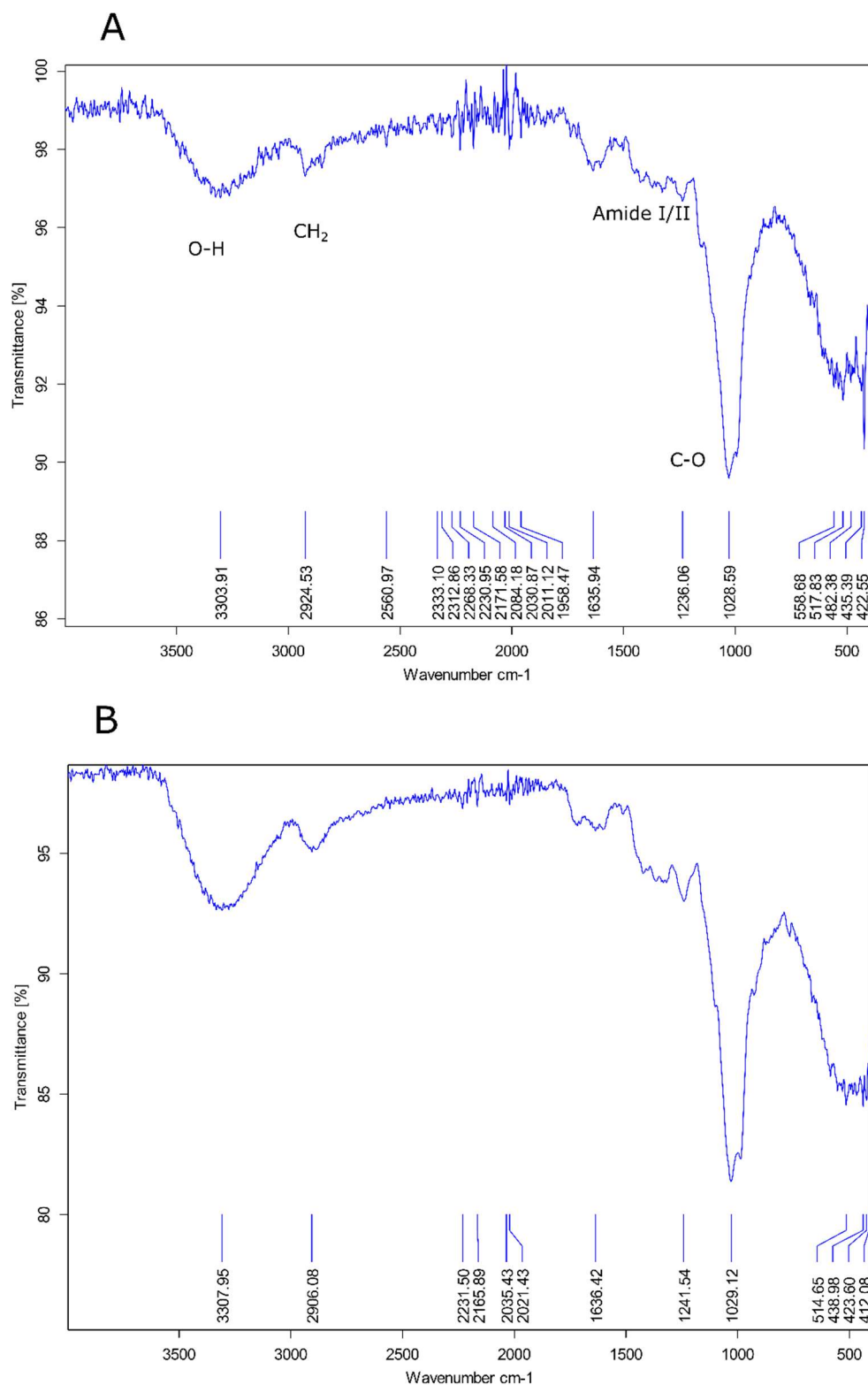


Figure 6.1: ATR-FTIR scans of (A) modern unheated sample (0 weeks) and (B) modern sample heated at 70 °C for 16 weeks.

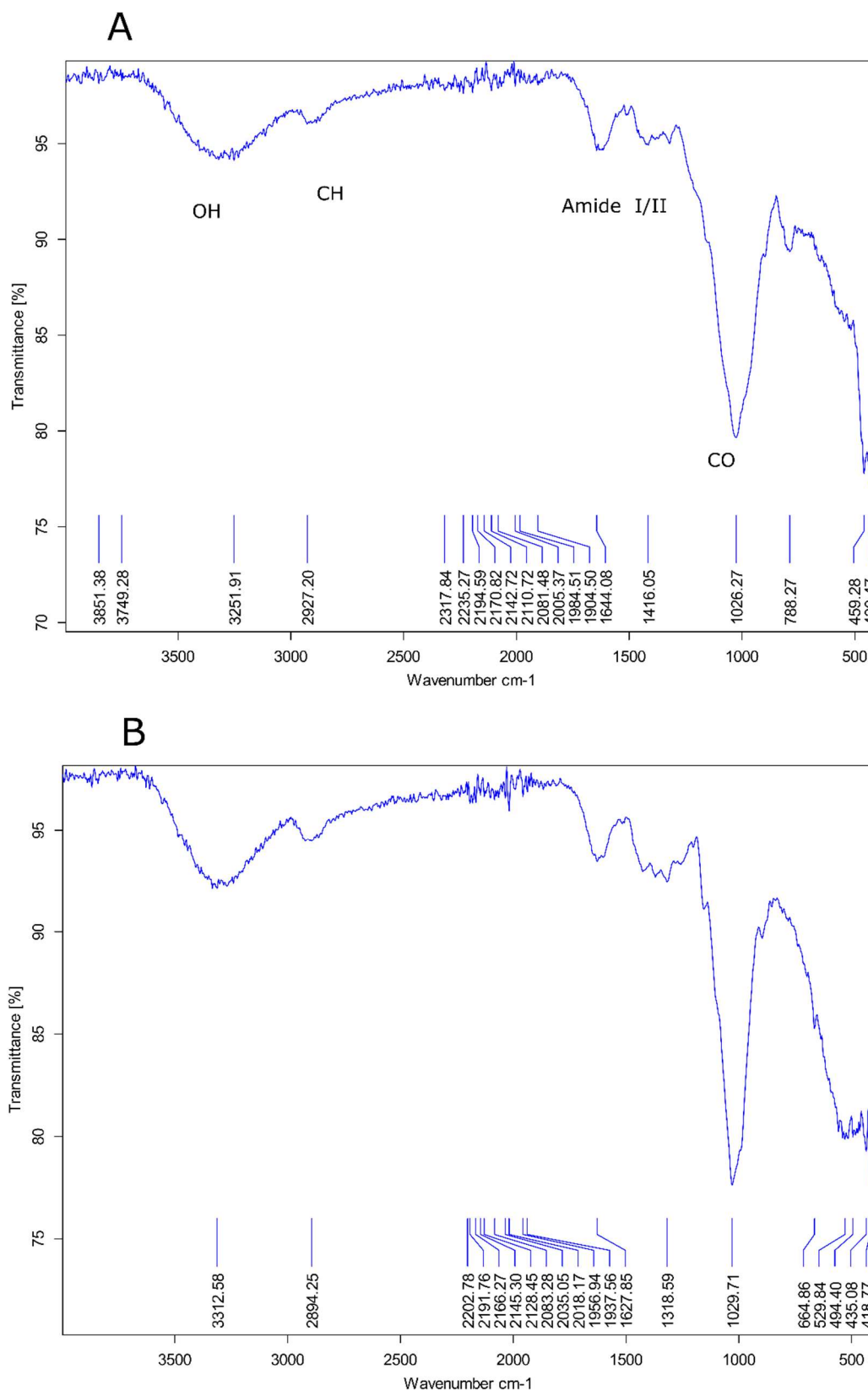


Figure 6.2: ATR-FTIR scans of Tularosa maize samples (A) 151, 700 BP and (B) 81, 1800 BP.

6.2.1.2 Elemental Analysis of Archaeological and Modern aged Maize Shows

Limited Changes Due to Ageing Processes

EA of carbon, hydrogen & nitrogen (CHN) was carried out on of archaeological maize from Tularosa Cave and on modern samples artificially aged by heating at 50 °C and 70 °C. The percentages of carbon, hydrogen and nitrogen were measured and the remaining material is assumed to be oxygen, as the compounds are mostly organic and inorganics are assumed to be in trace amounts. No statistical difference in O:C, H:C and C:N ratios (Table 6.1) was observed across archaeological age groups (700 BP and 1800 BP). Trends were not seen across the artificially aged modern experiments either. The C:N measurements are highly variable. This is either due to improper homogenisation prior to analysis, or because nitrogen percentages are so small that they could not be determined accurately (Appendix 18 contains all EA measurements).

Table 6.1: Table showing molar ratios (O:C, H:C, C:N) of archaeological maize and modern maize heated at 50 °C and 70 °C

Sample	Sample Type	Molar ratio O:C	Molar ratio H:C	Molar ratio C:N
81	Tularosa 1800 BP	0.85	1.53	71.26
91	Tularosa 1800 BP	0.94	1.68	75.08
82	Tularosa 1800 BP	0.98	1.45	51.03
123	Tularosa 700 BP	0.85	1.61	142.52
5	Tularosa 700 BP	0.89	1.71	84.28
140	Tularosa 700 BP	1.25	0.13	0.85
151	Tularosa 700 BP	0.91	1.46	74.47
1 day 55 °C	Modern control	0.91	1.65	202.51
2 days 55 °C	Modern control	1.19	1.73	107.70
5 days 55 °C	Modern control	0.89	1.71	84.99
19 days 55 °C	Modern control	0.93	1.68	75.08
40 days 55 °C	Modern control	0.91	1.68	64.61
0 weeks 70 °C	Modern control	0.87	1.55	35.06
1 weeks 70 °C	Modern control	0.76	1.71	91.56
2 weeks 70 °C	Modern control	0.83	1.41	42.21
4 weeks 70 °C	Modern control	0.77	12.16	49.53

8 weeks 70 °C	Modern control	0.80	1.58	104.77
16 weeks 70 °C	Modern control	0.79	1.60	72.79

In order to assess whether the highly variable C:N values are due to instrument error, the C:N were also determined using elemental analyser-IR-MS (EA-IR-MS). As can be seen in Table 6.2 the C:N measurement proved to be very unreliable and therefore should not be used to assess preservation. A study by Metcalf and Mead⁸⁴ also suggested that C:N values should not be used as an indicator of reliable $\delta^{15}\text{N}$ measurements because the natural variation in C:N in plants is too high to know if changes in this value reflect post depositional changes. However, Fraser *et al.*⁸² have found utility in the C:N method to assess $\delta^{15}\text{N}$ measurement reliability when it applies to charred samples.

Table 6.2: Table showing molar ratios of C:N of modern maize heated at 70 °C comparing two analysers.

Sample	Sample Type	Molar ratio C:N (thermal conductivity)	Molar Ratio (EA- IR-MS)
0 weeks 70 °C	Modern control	35.1	76.6
1 weeks 70 °C	Modern control	91.6	100.3
2 weeks 70 °C	Modern control	42.2	106.2
4 weeks 70 °C	Modern control	49.5	128.8
8 weeks 70 °C	Modern control	104.8	50.0
16 weeks 70 °C	Modern control	72.8	96.8

6.2.2 Bulk Isotope Ratios of Artificially Aged Samples

An enrichment of $\delta^{15}\text{N}_{\text{bulk}}$ was found in the 700 BP Tularosa maize cobs when compared with the 1800 BP Tularosa cobs (Chapter 3, Section 3.3.1). Whilst it is most likely that these effects are due to differences in the climate in the growing period for these samples, the effect of heating on modern maize was assessed to see if this could have an effect on the isotope ratios. Samples were heated at different temperatures (65, 70, 75 and 85 °C) and sampled periodically (0, 1, 2, 4, 8, and 16 weeks). As can be seen in Table 6.3 the

results are variable. However at each temperature there is, on average, an increase of 1.85 ‰ in $\delta^{15}\text{N}$ values between unheated samples those heated for 16 weeks. This is encouraging, as we might expect the older Tularosa maize (1800 BP) to be enriched due to diagenesis. Therefore, the enrichment seen in the 700 BP maize suggests this must be due to external factors.

Table 6.3: Table showing $\delta^{15}\text{N}$ and $\delta^{13}\text{C}$ values of artificially aged maize.

Weeks Heated	Temperature heated	$\delta^{15}\text{N}$	$\delta^{13}\text{C}$
0	65	-2.73	-11.78
1	65	-1.63	-11.43
2	65	-0.84	-10.58
4	65	-0.81	-11.32
8	65	-1.05	-10.95
16	65	-0.58	-10.73
0	70	2.01	-11.93
1	70	2.04	-11.96
2	70	1.01	-11.93
4	70	0.83	-12.03
8	70	2.89	-11.77
16	70	1.24	-12.02
0	75	-4.44	-11.50
1	75	-2.71	-11.64
2	75	-2.57	-11.65
4	75	0.13	-11.58
8	75	-2.42	-11.73
16	75	-1.33	-11.47
0	85	-4.22	-11.64
1	85	-3.79	-11.74
2	85	-2.49	-11.57
4	85	-2.84	-11.53
8	85	-1.82	-11.48
16	85	-1.29	-11.39

6.2.3 Amino Acid Composition Analysis

6.2.3.1 Amino acid Composition Analysis

In Chapter 3 (Section 3.3.3) the isotope ratios of individual amino acids were investigated in archaeological maize from Tularosa Cave. The N% levels (approximately 1%) of the Tularosa Cave were low suggesting low amounts of remaining protein. In order to check the levels of protein an amino acid composition analysis was carried out. Appendix 19 contains amino acid structural information. Acid hydrolysis to release free amino acids for analysis was carried out on samples of modern and ancient maize. Figure 6.3 shows the total amino acid content of a range of archaeological maize samples (1800 BP, yellow bars and 700 BP, blue bars).

Thirteen AAs were identified following separation by RP-HPLC (Figure 6.4). As can be seen in Figure 6.3 the total amino acid content does not appear to be affected by the age of the sample, suggesting similar protein levels.

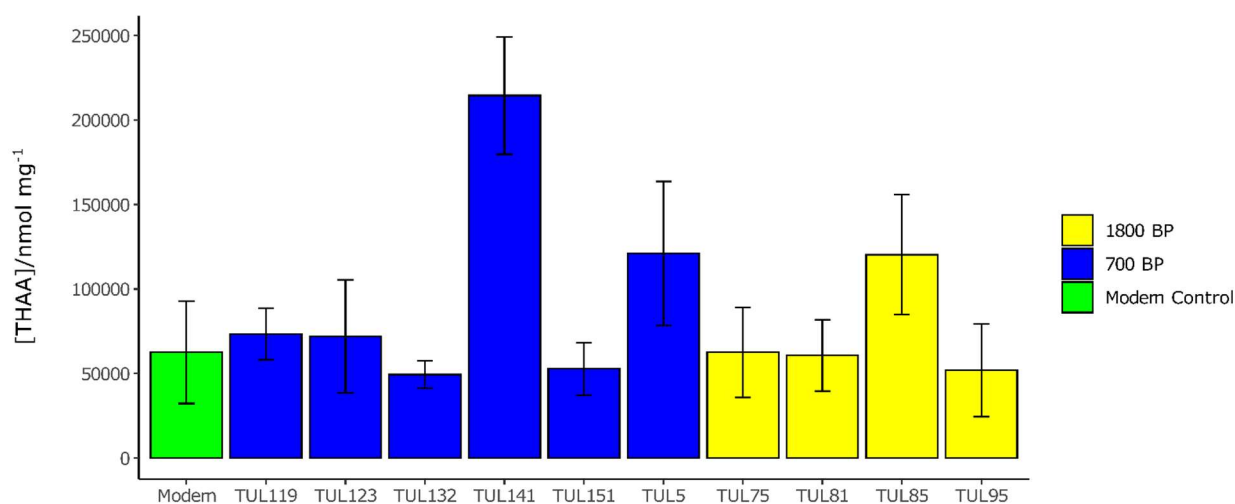


Figure 6.3: The amino acid concentrations of eight maize cobs found in Tularosa Cave. 1800 BP and 700 BP maize age groups are represented by yellow and blue coloured bars respectively. Green bar represents modern lyophilised maize samples. Error bars represent one standard deviation of triplicate experimental replicates.

The percentage contribution each AA makes to the total detectable amino acid composition is shown in Figure 6.4. The percentage contribution of each AA is relatively consistent across the archaeological samples of both age groups, again suggesting similar preservation of protein from which the AAs were released on acid hydrolysis. The percentage contributions are also similar to those obtained from modern lyophilised maize material. The aliphatic AAs Ala, Val, Leu and Ile make up over a third of the % composition with Gly making up around 20%. Ser, Thr, Arg, Tyr and Phe contribute 25% of the total AAs detected.

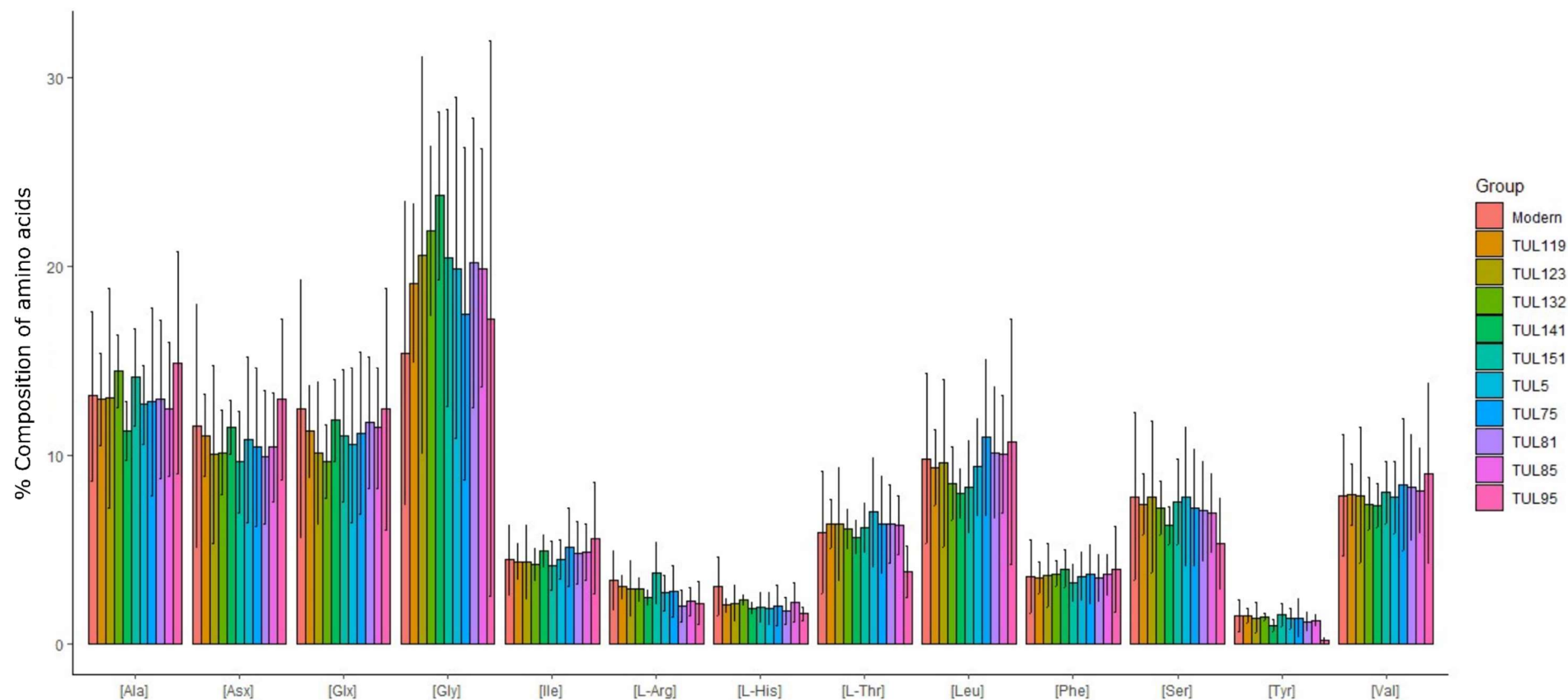


Figure 6.4: The AA % composition of eight Tularosa cave maize samples. Modern lyophilised maize in green. Error bars represent the standard deviation (1σ) of triplicate experimental replicates.

6.2.3.2 Amino Acid Racemisation Analysis of Tularosa Maize Shows Increased Asx D/L and Glx D/L with Age

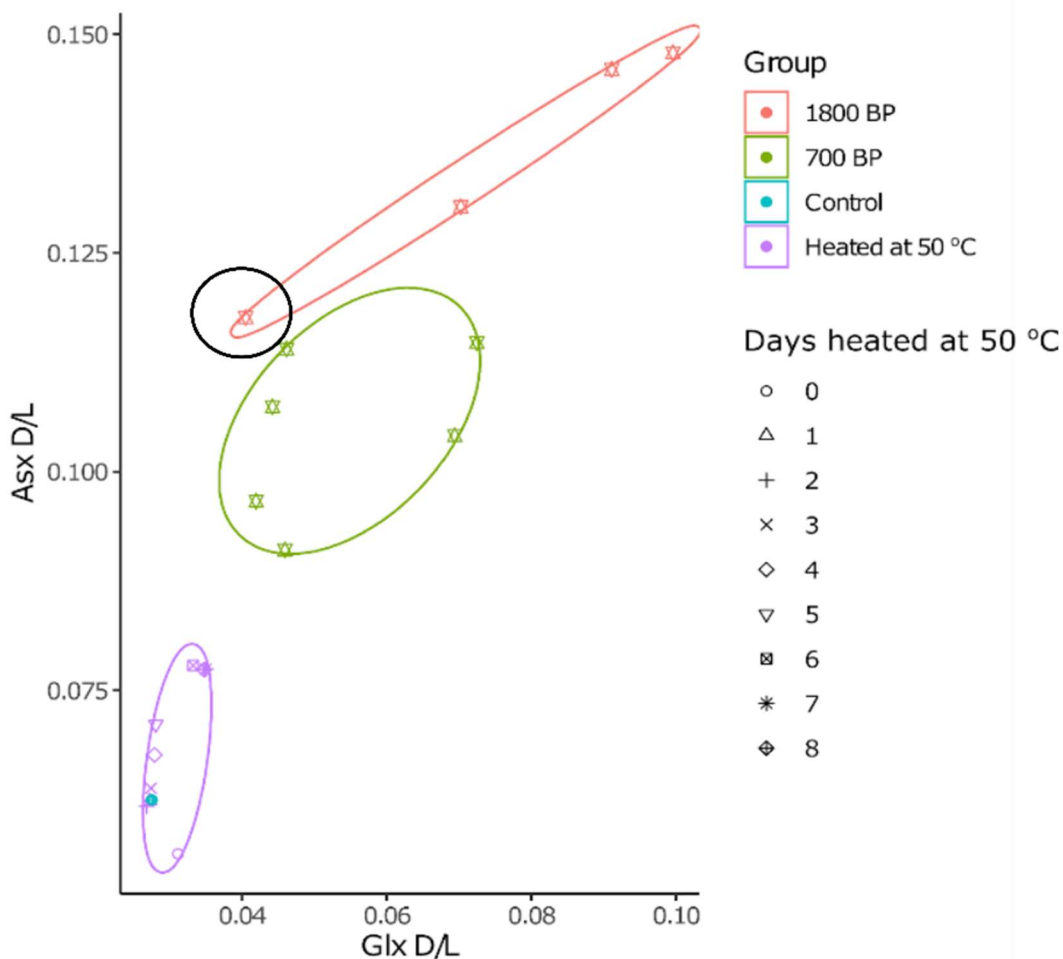


Figure 6.5: Figure plotting the racemisation of Asx D/L versus Glx D/L. Archaeological samples from Tularosa Cave (700 BP and 1800 BP) are marked as green circles and red squares respectively. Modern samples that were heated at 50 °C for 1, 2, 3, 4, 5, 6, 7, 8 days are marked as purple triangle, star, cross, circle, diamond and square respectively. Control sample (not heated) is marked in blue.

The racemisation of amino acids was investigated in artificially aged samples and in Tularosa maize. Some amino acids racemize over time more quickly than others (Asp/Asn > Glu/Gln > Ser > Ala)²⁰⁹. Figure 6.5 shows modern samples artificially aged between 0 and 8 days at 50 °C show increasing racemization of Asx (expressed as D/L^{209–211}) with increasing heating time,

but this is not observed for Glx. It is well documented²¹² that Glx takes longer to racemise than Asx, so this observation is not surprising. It was found that the Tularosa maize samples displayed an increased racemisation of both Asx and Glx with age, with one outlier in the 1800 BP group, indicated on Figure 6.5 with a black circle.

6.2.3.3 Artificially Aged Maize Samples Show No Change in Amino Acid Isotope Ratios Compared to a Modern Lyophilised Sample

The isotope ratios of individual amino acids were measured for a modern control and a modern sample which was heated at 70 °C for one week. The $\delta^{15}\text{N}_{\text{AA}}$ values were normalised to $\delta^{15}\text{N}_{\text{Glx}}$ and the results are displayed in Figure 6.6, which shows no statistical differences between the modern control and the heat aged sample. The standard deviation is high across triplicate measurements for most amino acids, but particularly for Phe in the aged sample. This gives us confidence that the $\delta^{15}\text{N}_{\text{AA}}$ values are resistant to some ageing effects and therefore that the $\delta^{15}\text{N}_{\text{AA}}$ values of archaeological maize are likely to be robust. Mean average $\delta^{15}\text{N}_{\text{AA}}$ values are provided in Appendix 20.

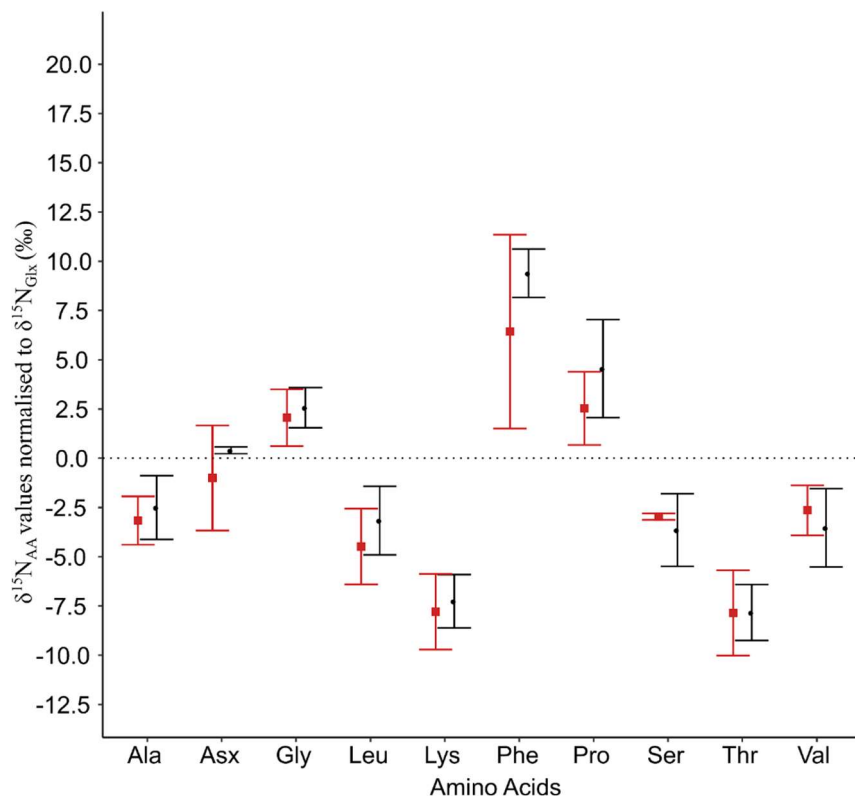


Figure 6.6: $\delta^{15}\text{N}_{\text{AA}}$ values normalised to $\delta^{15}\text{N}_{\text{Glx}}$ from maize inner cob samples. Red squares and black circles represent a sample aged at 70 °C for one week and a modern control. Black dotted line, $y=0$. Error bars represent the standard deviation associated with triplicate analytical measurements. Black dotted line, $y=0$.

6.2.4 The Effect of Ageing on the Extractable Maize Metabolome

To test the effect of ageing on the maize metabolome, maize was oven heated (70 °C) and sampled at several time points: 0, 1, 2, 4, 8, 16, 32 weeks. The maize was then stored at -80 °C prior to extraction. Two full-scan datasets were acquired for each sample extract (one in positive and one in negative mode). An untargeted study of methanol:water-soluble¹⁹⁴ maize metabolites was performed to identify features that are different across the aged maize samples. Two datasets of full-scan positive and negative-ion-mode LC–MS data were recorded, using a T3 reversed-phase column, chosen to retain as broad a range of metabolite polarities as possible. The data were de-zeroed to 50% to reduce instances of false positives, and features intensities with a CoV

of greater than 30 % were removed from the analysis. The data were also QC corrected¹¹⁹.

PC 1 shows the highest percent of total variance. Figure 6.7 shows the PCA plots for positive and negative mode data. In both positive and negative modes the PCA shows that any time spent in the oven versus fresh samples (0 weeks) accounts for the variance in PC1 (32.99 % and 33.12 % in positive and negative modes respectively). PC2 shows that that samples from weeks 1, 2 and 4 group together and samples from 8 and 16 weeks group together. This implies that key changes in the extracted metabolome occur after one week of heating and also between 4 and 8 weeks of heating at 70 °C.

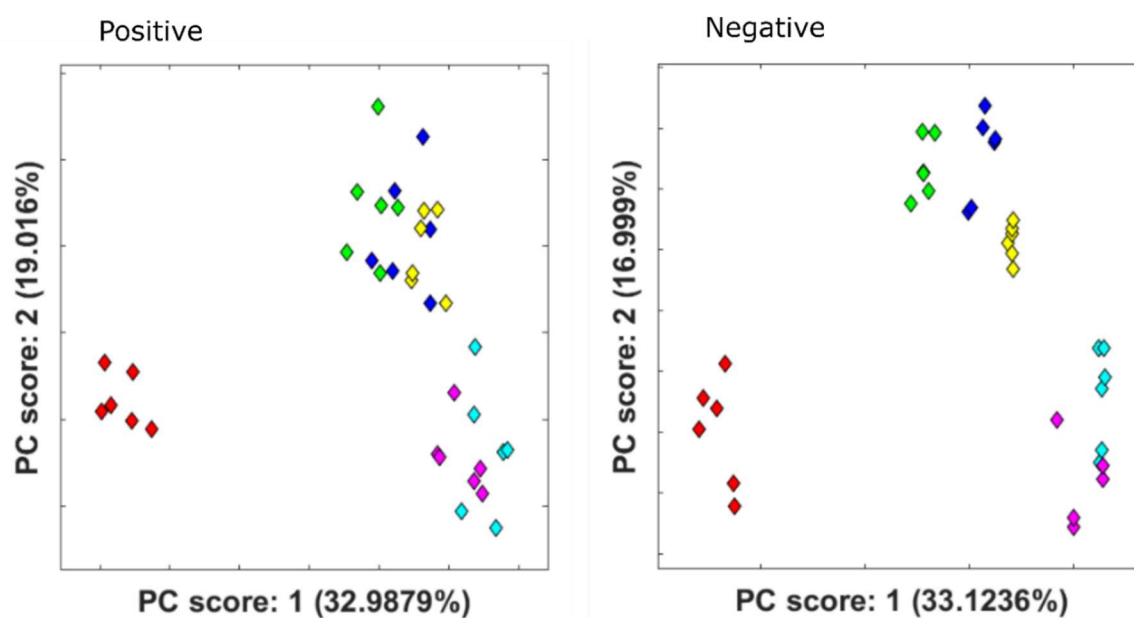


Figure 6.7: PCA plots showing the scores for the first two principal components obtained using untargeted metabolomic analysis of *Zea mays* cob extracts coloured by weeks spent in 70 °C oven. Red, green blue, yellow turquoise and purple diamonds represent 0, 1, 2, 4, 8, and 16 weeks respectively.

6.2.5 The Effect of Ageing on Drought-Related Metabolites was Investigated

In Chapter 5, drought-related metabolites found in archaeological maize samples were investigated. In this section, the results are described of investigating the effect of artificial ageing, as a proxy for diagenesis, on the drought markers. The drought-related metabolites were searched for in these datasets, based on retention time and accurate mass, in the negative-ion-mode data of the ageing experiment (Section 6.2.4). Negative-ion-mode only was used, as the negative-ion-mode data set was used in Chapter 5. Product ion information was obtained where possible using a Orbitrap™ Fusion™ Tribrid™ mass spectrometer. Metabolite identities were proposed on the basis of the product ion fragmentation score from the Progenesis QI 'Identify Compound' function (Table 6.4).

Table 6.4: Summary of data on proposed identifications of drought-related biomarkers in modern artificially aged maize. Proposed identifications were assigned using compound databases (Metlin, LipidBlast, ChemSpider, Progenesis MetaScope). All features are level 3 Schymanski identifications¹³⁰.

<i>m/z</i>	<i>t_R</i> (min)	Formula	Fragmentation Score	ppm	Isotope Similarity Score ^h	Description
225.0405	5.38	C ₉ H ₈ O ₄	44.5	1.19	97.26	Caffeic acid
252.0880	7.85	C ₁₁ H ₁₃ NO ₃	48.1	-0.44	96.24	Phenylalanine
267.0361	1.46	C ₄ H ₆ O ₅	32.4	-0.43	99.90	Malic acid
293.0988	1.33	-	-	-	-	Glutamic Acid
341.1457	2.29	C ₆ H ₁₂ O ₄	36.7	0.11	95.99	Dideoxy-L-galactose
465.1042	10.23	C ₁₀ H ₁₀ O ₅	15.2	-0.65	96.93	Hydroxyferulic acid
559.2546	10.37	C ₁₅ H ₂₀ O ₅	22	-0.22	95.84	Hydroxyabscisic acid or phaseic acid

^h Isotope similarity score compares the intensities of each isotope between observed and theoretical distributions. A total intensity difference of 0 gives a score of 100.

All Progenesis QI compounds abundance profiles can be found in Appendix 21. Dideoxy-L-galactose and ABA decreased with heating time. This suggests that their elevated abundances in the 700 BP age group of Tularosa maize is indeed due to elevated expression of these molecules in the metabolome and not an artifact of diagenesis. Hydroxyferulic acid, caffeic acid and phenylalanine all have negligible abundances when the maize has not been heated, but then elevated abundances following heating, suggesting they are released due to breakdown of other chemicals due to heating.

6.3 Conclusions

In this chapter the preservation of the archaeological maize was assessed using ATR-FTIR and EA. It was found that the amide and CH₂ and C-O stretches were not noticeably different between archaeological age groups, suggesting a similar level of preservation. It can be concluded that the samples retain a portion of organic material. This conclusion is also supported by the amino acid analysis data; total amino acid amounts released on acid hydrolysis of the different age samples are similar, as are the relative amounts of the different amino acids detected between archaeological age groups. As expected, racemization of Glx and Asx increased with the age of the samples (with one exception). Furthermore, comparison of the $\delta^{15}\text{N}_{\text{AA}}$ values of a modern sample and an aged sample showed that the $\delta^{15}\text{N}_{\text{AA}}$ value is resistant to diagenetic change.

Ageing appears to have a significant impact on the maize metabolome when heated at 70 °C for 1 week. A further key change occurs between 4 and 8 weeks. Unfortunately, only a limited number of metabolites were identified in this experiment; however, investigation of drought markers that could be

identified offered interesting insights. Dideoxy-L-galactose and ABA decreased with time spent being heated. This suggests that their elevated abundances in the 700 BP age group of Tularosa maize is indeed due to expression of these molecules in the metabolome and not to diagenesis. It is surprising that a photosensitive molecule such as ABA has survived in the maize cobs. Hydroxyferulic acid, caffeic acid and phenylalanine all have negligible abundances when the maize has not been heated, but then elevated abundances following heating, suggesting they are produced due to chemical reactions catalysed by heating. Malic acid and glutamic acid appear resistant to diagenetic effects from heating at least for a week.

To conclude, the Tularosa maize cobs are well preserved and offer a wealth of information. Here it was shown that increased $\delta^{15}\text{N}$ values in the more modern archaeological maize samples are most likely not due to diagenesis, as heating to simulate ageing increased rather than decreased $\delta^{15}\text{N}$ values. Furthermore, it was demonstrated that several drought metabolites are resistant to diagenesis and thus that their presence in the younger maize tissue extracts suggests that these are indeed indicative of a drought stress response in the ancient maize.

6.4 Material and Methods

6.4.1 Experimental Samples

B73 maize was sampled in 1 inch thick sections and heated in GC ovens at various temperatures (40, 60, 70, 75 and 85 °C) for 0, 1, 2, 4, 8, and 16 weeks. Samples were also heated at 55 °C for 0, 1, 2, 3, 4, 5, 6, 7, 8 days and 55 °C for 1, 2, 5, 19 and 40 days.

6.4.2 Archaeological Samples

Archaeological samples of Tularosa maize were investigated as described in Appendix 14.

6.4.3 Attenuated Total Reflectance Fourier-Transform InfraRed Spectroscopy

Bruker Alpha II InfraRed spectrometer was used. Approximately 1 gram of solid sample was placed on the Platinum Diamond-ATR QuickSnap Sampling Module attachment. Measurements were taken over the wavenumbers: 4000 - 400 cm^{-1} . The maximum resolution is 0.75 cm^{-1} using J-Stop cards and the wavenumber accuracy is $< 0.05 \text{ cm}^{-1}$.

6.4.4 LC-MS Metabolome Extraction

The method of Gaffney *et al.* (2021)¹⁹⁴ was followed as described. The plant material (10 mg) was homogenised and extracted with methanol:water (70:30, v/v, 100 μL). The extraction process consisted of shaking at 31 RCF for 30 min in dark conditions, followed by centrifugation at 28413 RCF for 10 min. The supernatant was transferred to a clean tube, dried using a vacuum concentrator (whilst kept cool) and reconstituted in methanol:water (70:30, v/v, 100 μL) and subsequently analysed using HPLC–FTICR–MS. All samples were extracted in a cold room (5 °C).

6.4.4.1 Data Collection

Three replicates of B73 maize heated at 70 °C were used per group (0, 1, 2, 4, 8, 16 weeks) and two technical replicates per sample. For analysis by LC–MS, the sample injections were separated into two semi-randomised batches containing one technical replicate from each extract. QCs composed of a pooled aliquot of 5 μL from each sample were injected at the start of the experiment (20 injections) to equilibrate the column. A QC and a blank were injected after every five sample injections.

6.4.5 LC–MS-Based Analysis of Metabolome

6.4.5.1 LC-MS Mass Spectrometry Methods

The LC methods are described in Section 4.4.4.1. A Bruker solariX XR 9.4T mass spectrometer was operated over the m/z range 57.75–2000.00 with an ESI source. Analytes were detected in the positive-ion-mode using the following MS parameters: the dry gas flow was 7.0 L/min; the dry gas temperature was 200 °C, the source voltage was 4000 V and the nebuliser gas pressure was 2.0 bar.

6.4.5.2 Data Handling and Analysis

Progenesis QI (Waters, Milford, MA, USA), a dedicated software package for processing LC–MS data, was used for alignment and peak picking. Bruker .d files were imported into Progenesis in centroid mode. The runs were aligned and alignment was accepted if within 80% of the reference run. Experimental groups were based on the age of the sample as described in Section 6.4.1.

At the peak picking stage, the following parameters were set to reduce the volume of data to allow the computer to process it. Peaks with a t_R of less than 1 min were excluded as being within the void and peaks with a t_R greater than 21 min were excluded on the basis of poor separation during the column wash phase. A minimum peak width of 0.05 min was set. The list of expected charge-bearing species $[M]^+$, $[M+H]^+$, $[M+2H]^{2+}$, $[2M+H]^+$, $[M+K]^+$ and $[M+Na]^+$ for the positive-ion-mode and $[M-H]^-$, $[M+Cl]^-$, $[M-2H]^{2-}$, $[M+FA-H]^-$, $[2M-H]^-$ and $[M-H_2O-H]^-$ for the negative-ion-mode were chosen for consideration, as the same compound can ionise in more than one way. In the raw data 34,718 and 20,440 features were identified in the positive and negative-ion-modes, respectively. Features with a CoV greater than 30% in QC injections were excluded from further analysis.

6.4.5.3 Statistical Analysis

Statistical tests were conducted using the programming environment language 'MATLAB (Mathworks, Natick, MA, USA)' using the package 'metabolab'. The data were normalised using the total ion count, de-zeroed at a rate of 50% and QC batch corrected¹¹⁹. 951 and 11,554 features were included in the analysis (positive and negative-ion-modes, respectively). Data were scaled to unit variance (the data for each variable is mean centered and then divided by the standard deviation of the variable). For each feature, the non-parametric Mann-Whitney test was used to test the statistical significance of differences between groups with Benjamini–Hochberg adjustment to correct for multiple testing.

6.4.6 LC–MS–MS

6.4.6.1 Mass Spectrometry Methods

The LC methods are as described in Section 4.4.4.1. An Orbitrap™ Fusion™ Tribrid™ mass spectrometer was operated in negative-ion-mode with the following parameters. The m/z range was 85–1000, and the instrument was fitted with an ESI source (heated electrospray ionisation, Easy-Max NG). Analytes were detected in the positive-ion-mode using the following MS parameters: the ion transfer temperature was 325 °C; the vaporiser temperature was 350 °C; the sheath gas was 50 (arb); the aux gas was (arb) 10; time between master scans was 1 s; the isolation window was 1.6; the collisional energy was stepped and the HCD collision energies (%) were 20, 35, and 60.

6.4.7 Amino acid analysis

6.4.7.1 Acid Hydrolysis and Amino Acid Recovery

Archaeological and modern maize inner cob powders (ca. 5 mg) were weighed and added to a sterile 2 mL glass hydrolysis vial. Vials were sealed

using a screw cap with silicon insert. HCl (6 M, 100 μ L) was added to the sample vial. Three vials were made for each cob, forming three experimental replicates for each cob. The vials were placed in an oven at 110 °C. The samples were removed from the oven after 24 h and allowed to cool to room temperature. The samples were evaporated to dryness using a centrifugal evaporator at room temperature for 24 h. Dry samples were rehydrated using rehydration fluid (100 μ L, 0.01 M HCl, 1.5 mM NaN₃, 0.01 mM L-homo-arginine) where the non-proteinogenic amino acid L-homo-arginine was used as an internal standard. Following rehydration, samples were vortexed (20 s) and centrifuged to separate remaining insoluble maize cob from solution. The supernatant (2.5 μ L aliquot) was transferred to a sterile autosampler vial with tapered insert and made up to 15 μ L using L-homo-arginine rehydration fluid (12.5 μ L) prior to analysis.

6.4.7.2 RP-HPLC of Amino Acids

The amino acid compositions of the samples were analysed by RP-HPLC using fluorescence detection following a modified method of Kaufman and Manley *et al.*²¹³. 2 μ L of sample solution was injected and mixed online with 2.2 μ L of derivatising reagent (260 mM N-iso-L-butyryl L-cysteine, 170 mM o-phthaldialdehyde in 1 M potassium borate buffer, adjusted to pH 10.4 with potassium hydroxide pellets). The amino acids were separated by RP-HPLC (Aligent 1100 series; HyperSil C18 BDS column: 250 mm length, 5 mm diameter, 5 μ m particle size) at 25 °C using a gradient elution of three solvents: sodium acetate buffer (solvent A: 23 mM sodium acetate trihydrate, 1.5 mM sodium azide, 1.3 μ M ethylenediaminetetraacetic acid, adjusted to pH 6.00 \pm 0.01 with acetic acid and sodium hydroxide), methanol (solvent C) and acetonitrile (solvent D). Initially 95% A and 5% C was used at a flow rate of 0.56 mL/min, and the composition gradient was increased to 50% C and 2% D after 95 minutes. Prior to the injection of the next sample, the column

was flushed with 95% C and D for 15 minutes, followed by equilibration of 95% A and 5% C for 5 minutes. The fluorescence detector uses a xenon-arc flash lamp at a frequency of 55 Hz, with a 280 nm cut-off filter and an excitation wavelength of 230 nm and emission wavelength of 445 nm.

6.4.8 Stable Isotope Ratio and EA (Carbon and Nitrogen) of Bulk Maize Cob Powder

Archaeological and modern maize inner cob powders were weighed in duplicate (2 mg) using an MT5 6dp micro balance (Mettler Toledo, Ohio, USA) into tin capsules, which were analysed by EA-IR-MS in a GSL analyser coupled to a 20-22 mass spectrometer (Sercon, Crewe, UK). An Exeter Analytical Inc. CE-440 analyser was also used for elemental analysis.

Chapter 7. Conclusions and Future Research

7.1 Summary

The overarching aim of this PhD project was to examine the effects of drought stress on the maize metabolome and the isotopic composition of maize. Specifically, both modern maize plants grown under experimentally-imposed watering conditions, as well as archaeological maize samples from Tularosa Cave were examined, as the latter offer a unique proxy for future droughts.

In summary, analysis of the ancient maize material by ATR-FTIR spectroscopy and EA showed that the archaeological maize is well preserved and retains a significant portion of organic material and nitrogen containing compounds. The amino acid composition analysis shows that total amino acid content was consistent across sample age groups, as was the percentage contribution each amino acid makes to the total. Since protein is the main source of nitrogen in the material, this gives confidence that nitrogen isotope ratios measurements are not significantly compromised due to loss of protein by diagenesis. Ageing experiments showed that compound specific $\delta^{15}\text{N}_{\text{AA}}$ values were also not altered due to heating.

It was found that nitrogen isotope ratios offer a novel way to infer drought stress conditions in both modern and archaeological samples. Climate records can show us that crops were cultivated during periods of drought but cannot tell us whether this stress was mitigated by anthropogenic practices such as irrigation. Measurements of bulk $\delta^{15}\text{N}$ can be used as a direct indicator that the plants experienced drought stress, but survived and adapted, and taken together with genetic adaptations, allow us build evidence for material having been subjected to drought. Measuring bulk $\delta^{15}\text{N}$ can therefore be used to monitor the effects of changing climatic conditions directly in well-preserved archaeobotanical remains. The $\delta^{15}\text{N}_{\text{bulk}}$ measurements were reflected in the compound specific $\delta^{15}\text{N}_{\text{AA}}$ values.

Understanding how humans have adapted their agricultural practices in the past, and how maize has responded genetically to past climate change, could contribute a vital perspective to present-day food security during the current climate crisis. Testing the oxygen and carbon isotope ratios of cellulose proved to be of limited value in this regard. However, when the source water isotope ratio of oxygen is known, then this could prove to be an interesting area of investigation.

This study has shown that lyophilising plant material is an effective way to stabilise the extractable plant metabolome in maize and extracting lyophilised material is as effective as extracting fresh material under liquid nitrogen. Lyophilisation is thus an adequate alternative to the more challenging, resource-intensive and potentially hazardous liquid nitrogen processing techniques. This observation has the potential to improve sample processing efficiencies which can be a bottle-neck in metabolomics workflows. However, the effect of desiccation on labile molecules such as phytohormones and the value of carrying out cold room extractions following lyophilisation require further study. The lyophilisation extraction technique also gave us useful information for application in our archaeobotanical studies where archaeological plant tissues were naturally preserved via desiccation.

Divergence in the metabolomic profiles of the experimentally drought-stressed maize studied here occurs with the onset of drought stress at the three-leaf stage. Drought stress at the grain-fill growth stage indicated a further divergence from the metabolome of well-watered plants. Differences in response to drought stress were also observed in two plant tissues, kernels and inner cob. It was shown that the drought-stress response was dominant across both tissue types and that inner cob material can be a useful source of information when no kernels are available. Untargeted metabolomic

profiling is clearly a powerful tool to better understand the biochemical mechanisms maize employs to cope with drought stress.

It was found that paleometabolomics can be used on well preserved archaeological samples in order to assess biotic and abiotic stressors that were contemporary with the period when the archaeological plant material was grown. Sucrose was found in higher abundance in the more modern Tularosa maize, which we suggest could be due to an adaptation to drought stress in the region. Ageing experiments showed that the most significant change in the extractable maize metabolome comes immediately after the samples are heated, within the first week. This leads us to suggest that the biggest changes in archaeological extractable metabolomes will occur rapidly after deposition. We infer that the changes in the extractable metabolomes of the different age groups of Tularosa maize samples are not due to diagenesis, but due to climate adaptations of the maize.

To conclude, this project has looked at the adaptations of ancient maize to historical drought to inform strategies that could be used to protect crops during modern day climate change. As temperatures are rising and parts of the world become increasingly vulnerable to drought events, the adaptations of our crops to historical drought events provide unique insights into protecting our crops from future droughts.

7.2 Recommendations for Future Research

7.2.1 Strategies to Protect Crops During Modern Day Climate Change

This PhD project has looked at the adaptations of ancient maize to historical drought to inform strategies that could be used to protect crops during

modern day climate change. Such strategies could include selective breeding to produce maize which exhibits traits resembling the drought adapted archaeological maize and breeding to produce the metabolites identified in this PhD.

7.2.2 Use of Oxygen and Carbon Cellulose Isotope Ratios to Test for Drought Stress

In the work outlined in Chapter 3 the effect of drought stress upon cellulose $\delta^{18}\text{O}$ values was found to be inconclusive. Previous studies^{17,54} have shown that the source water of ancient maize can be traced. If the source water was known, then smaller perturbations in the $\delta^{18}\text{O}$ values could perhaps then be attributed to climate. The results from chapter 3 also suggest $\delta^{13}\text{C}_{\text{bulk}}$ values are impacted by drought conditions, however further studies, including of individual amino acid carbon isotope measurements are needed to clarify this finding.

7.2.3 Control Experiments for Amino Acid Isotope Ratios

Fertiliser application causes an enrichment in $\delta^{15}\text{N}_{\text{bulk}}$ values^{70, 71}, which is similar to the effect of drought stress. In this study, climate data and archaeological context point towards drought stress being the reason that $\delta^{15}\text{N}_{\text{bulk}}$ values are higher.

in the later than the earlier Tularosa maize samples. However, thorough investigations of the effect of fertilisation on $\delta^{15}\text{N}$ values and the metabolome versus that of drought would help elucidate these issues in future studies.

7.2.4 Effect of Different Burial Environments on Archaeobotanical Metabolome and Isotope Ratios

In this work the effect of diagenesis was investigated using heating experiments. However, the burial environment of an archaeological sample also has an effect on the degradation processes. For example, whether the environment is anoxic or oxidising will affect the chemical processes of degradation. In this study, the samples were notably well preserved in a stable cave environment, so burial effects are minimised. A controlled study where samples are buried in different environments would help us to understand the effect this may have on the extractable metabolome and isotope ratios.

7.2.5 Effect of Different Cooking Techniques on Archaeobotanical Metabolome and Isotope Ratio Values

In this thesis the isotope ratios and metabolome were considered of maize, without consideration of any pre-depositional processes which may have occurred, such as cooking. Many of the archaeobotanical remains we are interested in are food crops; it is highly likely that some archaeobotanical remains have been cooked or pre-processed prior to deposition. It is advised that control experiments which consider the effects of cooking are carried out.

Often, samples are also found charred. Whilst charring will have a significant impact on the metabolome of the samples, interesting information may still be accessible if we are able to relate the charred signature by comparison with uncharred material. Control experiments where maize is charred or boiled could expand our understanding of paleometabolomics and isotope ratio studies.

7.2.6 Use of Metabolomics for Other Archaeobotanical Remains and Other Human/Animal Remains as a Complement to Other 'Omics Techniques

Paleometabolomics is a promising and novel way to analyse ancient organic remains which has the ability to discover stress responses of past organisms. This could have a very wide variety of applications including: assessing abiotic and biotic stressors of other ancient desiccated plant remains (similarly to the work described in this thesis); studying the metabolomes of human-manipulated objects such as timber, ivory and shells and studying well-preserved human remains. A previous study has used metabolomics to investigate the stomach contents of 'Iceman'¹⁰⁵; this approach could be applied to other mummified remains. It could be used to identify biomarkers of disease and stress in these individuals, and to identify dietary markers. Paleometabolomics is best utilised in combination with other 'omics techniques where it can be used to directly evidence ancient nucleic acid or paleoproteomic inferences.

Appendix

Appendix 1: left and right images are examples of 'ovoid' and 'cylindrical' shaped corn cobs respectively, from the 1800 ± 50 BP and 700 ± 50 BP occupations of Tularosa Cave.



Appendix 2: The %N and $\delta^{15}\text{N}$ values of B73 and B76 maize grown under different conditions. Moderate and severe drought equate to drought at the 3-leaf growing stage and drought at both the 3-leaf and grain-fill stages respectively.

Watering Regime	Sample Identification	Tissue Type	% N	$\delta^{15}\text{N}$ (‰)	
				Corrected Average	Sample Uncertainty
Well-Watered	B73 G	Inner cob	0.53	-6.47	0.37
Well-Watered	B73 J	Inner cob	0.28	-6.44	0.32
Well-Watered	B73 K	Inner cob	0.25	-6.24	0.29
Moderate Drought	B73 B	Inner cob	1.38	-4.14	0.26
Moderate Drought	B73 C	Inner cob	1.80	-3.70	0.26
Moderate Drought	B73 D	Inner cob	2.18	-2.78	0.30
Severe Drought	B73 E	Inner cob	3.22	-4.05	0.27
Severe Drought	B73 FA	Inner cob	3.22	-4.13	0.26
Severe Drought	B73 FB	Inner cob	3.04	-4.82	0.34

Well-Watered	B73 G	Kernel	1.67	-2.78	0.29
Well-Watered	B73 KA	Kernel	1.75	-1.95	0.27
Well-Watered	B73 KB	Kernel	1.70	-1.73	0.29
Moderate Drought	B73 B	Kernel	1.74	-3.07	0.29
Moderate Drought	B73 C	Kernel	1.79	-3.19	0.31
Moderate Drought	B73 D	Kernel	2.27	-3.66	0.36
Severe Drought	B73 E	Kernel	3.39	-4.24	0.28
Severe Drought	B73 FA	Kernel	3.39	-4.13	0.33
Severe Drought	B73 FB	Kernel	3.78	-4.63	0.43
Well-Watered	B76 G	Inner cob	1.51	-5.03	0.27
Well-Watered	B76HA	Inner cob	1.62	-4.58	0.39
Well-Watered	B76 HB	Inner cob	1.89	-3.04	0.31
Well-Watered	B76 I	Inner cob	2.38	-5.41	0.28
Moderate Drought	B76 D	Inner cob	1.79	-4.37	0.29

Moderate Drought	B76 EA	Inner cob	1.85	-3.26	0.29
Severe Drought	B76 A	Inner cob	1.75	-2.94	0.28
Severe Drought	B76 B	Inner cob	1.77	-3.10	0.25
Severe Drought	B76 CA	Inner Cob	3.11	-3.77	0.33
Severe Drought	B76 CB	Inner Cob	3.45	-2.36	0.30
Well-Watered	B76 G	Kernel	1.34	-5.24	0.41
Well-Watered	B76 H	Kernel	2.48	-3.65	0.32
Well-Watered	B76 I	Kernel	2.12	-4.26	0.35
Well-Watered	B76 J	Kernel	1.95	-1.43	0.25
Moderate Drought	B76 D	Kernel	2.34	-4.36	0.28
Moderate Drought	B76 EA	Kernel	2.05	-3.16	0.30
Moderate Drought	B76 EB	Kernel	2.75	-1.56	0.29
Severe Drought	B76 A	Kernel	1.57	-3.17	0.76
Severe Drought	B76 B	Kernel	2.40	-2.12	0.29

Severe Drought	B76 C	Kernel	1.97	-2.75	0.31
----------------	-------	--------	------	-------	------

Appendix 3: The %N and $\delta^{15}\text{N}$ values of Tularosa maize outer cob samples. The catalogue number, grid square and level are noted.

Cob Morphology	Sample Identification	Cat. No	Square	Level	% N	$\delta^{15}\text{N}$ (‰)	
						Corrected Average	Sample Uncertainty
ovoid	56	314984	2R2	14	4.06	4.25	0.22
ovoid	57	314984	2R2	14	2.57	4.14	0.20
ovoid	61	314984	2R2	14	1.19	1.93	0.23
ovoid	62	314980	2R1	13	1.18	3.72	0.51
ovoid	63	314981	2R1	13	0.82	2.67	0.19
ovoid	65	314924	2R1	12	0.74	4.32	0.19
ovoid	66	314924	2R1	12	0.76	4.297	0.25

ovoid	67	314940	2R1	12	1.01	5.70	0.31
ovoid	68	314940	2R1	12	0.83	1.40	0.33
ovoid	71	316025	2R1	13	1.90	3.47	0.19
ovoid	72	315043	2R1	13	1.94	3.14	0.43
ovoid	73	314924	2R1	12	2.02	3.70	0.19
ovoid	74	314940	2R1	12	1.11	2.36	0.26
ovoid	75	314980	2R1	13	0.67	3.10	0.28
ovoid	76	315264	3R2	11	4.06	6.24	0.21
ovoid	77	314924	2R1	12	0.77	4.67	0.35
ovoid	78	3 ¹⁵ 264	3R2	11	1.38	3.95	0.20

ovoid	79	3 ¹⁵ 043	2R1	13	2.22	2.78	0.54
ovoid	80	314940	2R1	12	0.98	2.97	0.20
ovoid	82	314980	2R1	13	1.19	3.73	0.23
ovoid	85	3 ¹⁵ 272	2R1	12	2.20	6.84	0.25
ovoid	86	314981	2R1	13	1.18	3.52	0.10
ovoid	87	3 ¹⁵ 043	2R1	13	2.21	4.35	0.27
ovoid	93	314982	2R1	13	1.46	4.37	0.38
ovoid	96	314982	2R1	13	1.03	4.97	0.23
ovoid	97	314982	2R1	13	1.48	1.94	0.30
ovoid	99	314982	2R1	13	0.90	3.80	0.19

ovoid	101	314940	2R1	12	1.00	2.84	0.38
ovoid	102	314924	2R1	12	0.72	3.89	0.23
ovoid	105	314043	2R1	13	1.00	4.61	0.18
ovoid	106	314043	2R1	13	0.98	1.31	0.24
cylindrical	114	315073	3R2	2	1.18	9.18	0.21
cylindrical	1 ¹⁵	315073	3R2	2	1.68	6.51	0.20
cylindrical	116	315073	3R2	2	1.48	5.09	0.21
cylindrical	119	315075	3R2	3	1.11	10.20	0.62
cylindrical	122	315076	3R2	3	1.75	9.30	0.19
cylindrical	123	315077	3R2	3	1.02	11.44	0.30

cylindrical	127	314742	2R1	1	1.02	8.87	0.25
cylindrical	128	314742	2R1	1	0.97	9.17	0.23
cylindrical	129	314742	2R1	1	2.08	9.33	0.17
cylindrical	131	314742	2R1	1	1.61	10.27	0.26
cylindrical	132	314750	2R1	1	0.95	8.65	0.53
cylindrical	133	314750	2R1	1	1.14	7.19	0.61
cylindrical	134	314750	2R1	1	1.53	4.88	0.28
cylindrical	135	314750	2R1	1	1.34	6.29	0.27
cylindrical	136	314731	2R2	2	1.10	6.29	0.27
cylindrical	137	314731	2R2	2	1.36	12.21	0. ¹⁵

cylindrical	138	314731	2R2	2	0.73	7.78	0.74
cylindrical	139	314731	2R2	2	0.92	6.10	0.20
cylindrical	141	314739	2R2	2	3.02	7.80	0.28
cylindrical	142	314739	2R2	2	0.83	8.83	0.18
cylindrical	143	314739	2R2	2	0.87	8.30	0.37
cylindrical	144	314739	2R2	2	0.99	10.22	0.20
cylindrical	145	314741	2R2	2	0.94	7.17	0.19
cylindrical	147	314741	2R2	1	3.64	9.16	0.58
cylindrical	148	314741	2R2	1	0.88	9.60	0.29
cylindrical	149	314741	2R2	1	0.93	12.80	0.28

cylindrical	150	314721	2R2	4	0.72	9.00	0.19
cylindrical	151	314721	2R2	4	1.24	5.73	0.21
cylindrical	152	314721	2R2	4	1.09	9.60	0.29
cylindrical	153	314721	2R2	4	1.00	12.80	0.28
cylindrical	154	314721	2R2	4	1.02	9.00	0.19
cylindrical	5	314984	2R2	14	1.08	5.73	0.21

Appendix 4: The %N and $\delta^{15}\text{N}$ values of Tularosa maize inner cob samples. The catalogue number, grid square and level are noted.

Inner Cob							
Cob	Sample	Cat. No	Square	Level	% N	$\delta^{15}\text{N}$ (‰)	
Morphology	Identification					Corrected Average	Sample Uncertainty
ovoid	56	314984	2R2	14	1.44	3.03	0.3
ovoid	57	314984	2R2	14	1.17	2.06	0.27
ovoid	61	314984	2R2	14	1.22	3.89	0.21
ovoid	62	314980	2R1	13	1.18	3.72	0.51
ovoid	63	314981	2R1	13	1.33	5	0.41
ovoid	65	314924	2R1	12	1	7.86	0.18
ovoid	66	314924	2R1	12	1.19	6.4	0.35

ovoid	68	314940	2R1	12	1.67	-6. ¹⁵	0.8
ovoid	69	314940	2R1	12	1.57	-2.09	0.35
ovoid	72	315043	2R1	13	1.75	2.31	0.2
ovoid	73	314924	2R1	12	2.3	-0.66	0.43
ovoid	74	314940	2R1	12	2.53	-4.01	0.33
ovoid	75	314980	2R1	13	0.73	4.19	0.23
ovoid	77	314924	2R1	12	1.05	7.49	0.17
ovoid	78	3 ¹⁵ 264	3R2	11	0.67	5.94	0.2
ovoid	79	315043	2R1	13	0.86	4.37	0.2
ovoid	80	314940	2R1	12	1.03	6.1	0.7

ovoid	81	314981	2R1	13	0.7	3.1	0.28
ovoid	82	314980	2R1	13	1.24	1.84	0.23
ovoid	84	314923	2R1	12	1.38	3.75	0.22
ovoid	85	315272	2R1	12	0.96	6.51	0.18
ovoid	86	314981	2R1	13	1.26	8.7	0.32
ovoid	87	315043	2R1	13	2.5	5.73	0.19
ovoid	88	314940	2R1	12	1.18	3.89	0.29
ovoid	90	314923	2R1	12	0.92	9.6	0.31
ovoid	93	314982	2R1	13	1.82	-0.74	0.26
ovoid	96	314982	2R1	13	1.03	4.96	0.23

ovoid	97	314982	2R1	13	1.11	2.47	0.33
ovoid	99	314982	2R1	13	0.82	4.2	0.24
ovoid	101	314940	2R1	12	4.35	-4.97	0.75
ovoid	102	314924	2R1	12	0.54	3.04	0.67
ovoid	103	314981	2R1	13	1.66	12.17	0.2
ovoid	105	314043	2R1	13	1	4.61	0.18
ovoid	106	314043	2R1	13	0.6	-0.9	0.35
cylindrical	114	315073	3R2	2	1.18	6.45	0.81
cylindrical	1 ¹⁵	315073	3R2	2	1.68	7.14	0.28
cylindrical	116	315073	3R2	2	1.11	4.16	0.23

cylindrical	119	315075	3R2	3	1.29	10.48	0.15
cylindrical	121	315076	3R2	3	1.75	9.18	0.21
cylindrical	123	315077	3R2	3	1.02	6.51	0.2
cylindrical	131	314742	2R1	1	2.24	17.15	1.42
cylindrical	132	314750	2R1	1	1.17	9.91	1.2
cylindrical	133	314750	2R1	1	0.82	14.7	0.97
cylindrical	134	314750	2R1	1	1.55	10.98	0.3
cylindrical	135	314750	2R1	1	1.42	14.2	0.7
cylindrical	136	314731	2R2	2	1.1	8.65	0.53
cylindrical	137	314731	2R2	2	1.36	7.19	0.61

cylindrical	138	314731	2R2	2	0.63	5.12	0.81
cylindrical	147	314741	2R2	2	3.92	7.9	0.16
cylindrical	151	314721	2R2	4	1.24	9.16	0.58
cylindrical	152	314721	2R2	4	1.09	9.6	0.29
cylindrical	154	314721	2R2	4	1.02	9	0.19
cylindrical	5	314984	2R2	14	0.9	6.42	0.22

Appendix 5: $\delta^{13}\text{C}_{\text{bulk}}$, $\delta^{13}\text{C}_{\text{cellulose}}$ and $\delta^{18}\text{O}_{\text{oxygen}}$ values for modern experimental samples, inner cob. %C is also provided.

Growing Conditions	Sample ID	% C	$\delta^{13}\text{C}_{\text{cellulose}} (\text{‰})$		$\delta^{18}\text{O}_{\text{cellulose}} (\text{‰})$	
			Corrected Average	Sample Uncertainty	Corrected Average	Sample Uncertainty
Well-Watered	B73G	4.36	-12.55	0.07	34.00	0.09
Well-Watered	B73J	0.18	-12.38	0.07	32.51	0.21
Well-Watered	B73K	0.36	-12.54	0.06	33.27	0.16
Moderate Drought	B73B	0.12	-14.38	0.13	30.03	0.15
Moderate Drought	B73C	0.11	-14.19	0.06	30.02	0.02
Severe drought	B73F	0.10	-14.46	0.07	30.01	0.19
Severe drought	B73E	-	-	-	30.86	0.13
Well-Watered	B76G	0.02	-13.01	0.06	32.32	0.11

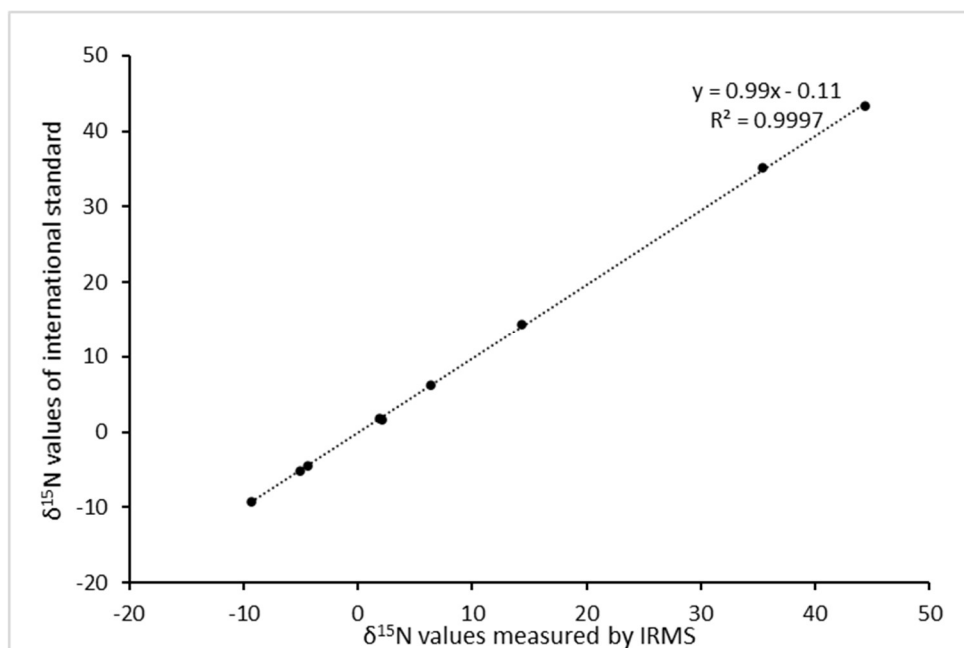
Well-Watered	B76I	0.07	-12.89	0.10	32.51	0.05
Moderate Drought	B76D	-	-	-	30.12	0.19
Moderate Drought	B76E	0.10	-14.37	0.06	31.91	0.09
Severe drought	B76B	0.23	-13.63	0.09	33.04	0.05
Severe drought	B76C	0.09	-13.68	0.09	33.99	0.18

Appendix 6: $\delta^{13}\text{C}_{\text{cellulose}}$ and $\delta^{18}\text{O}_{\text{oxygen}}$ values for archaeological samples. The catalogue number, grid square and level are noted. % C is also provided. TL indicates Tularosa Cave.

Cob Morphology	Sample ID	Cat. No	Square	Level	% C	$\delta^{13}\text{C}_{\text{cellulose}} (\text{‰})$		$\delta^{18}\text{O}_{\text{cellulose}} (\text{‰})$	
						Corrected Average	Sample Uncertainty	Corrected Average	Sample Uncertainty
Ovoid	TL61	314984	2R2	14	39.91	-8.41	0.16	31.00	0.04
Ovoid	TL75	314980	2R1	13	41.62	-8.89	0.09	30.28	0.22
Ovoid	TL81	314981	2R1	13	40.76	-8.72	0.09	31.44	0.04
Ovoid	TL85	3 ¹⁵ 272	3R2	11	40.88	-8.98	0.02	30.22	0.099
Ovoid	TL93	314982	2R1	13	41.12	-8.98	0.03	29.60	0.09
Cylindrical	TL108	315113	3R2	4	41.81	-	-	32.96	0.06
Cylindrical	TL119	315075	3R2	3	42.20	-8.54	0.01	30.29	0.08
Cylindrical	TL121	315076	3R2	3	40.02	-9.31	0.07	32.04	0.04

Cylindrical	TL123	315077	3R2	3	40.59	-8.62	0.08	26.30	0.26
Cylindrical	TL132	314750	2R2	1	41.51	-8.65	0.09	33.54	0.04
Cylindrical	TL140	314739	2R2	2	41.58	-9.24	0.08	33.84	0.19
Cylindrical	TL141	314739	2R2	2	40.41	-8.87	0.09	30.56	0.08
Cylindrical	TL145	314741	2R2	1	41.69	-9.05	0.08	31.92	0.07
Cylindrical	TL146	314741	2R2	1	41.63	-8.65	0.08	33.59	0.20
Cylindrical	TL ¹⁵¹	314721	2R2	4	40.74	-9.53	0.07	32.16	0.09
Cylindrical	TL5	314984	2R2	14	41.64	-9.75	0.07	30.79	0.08

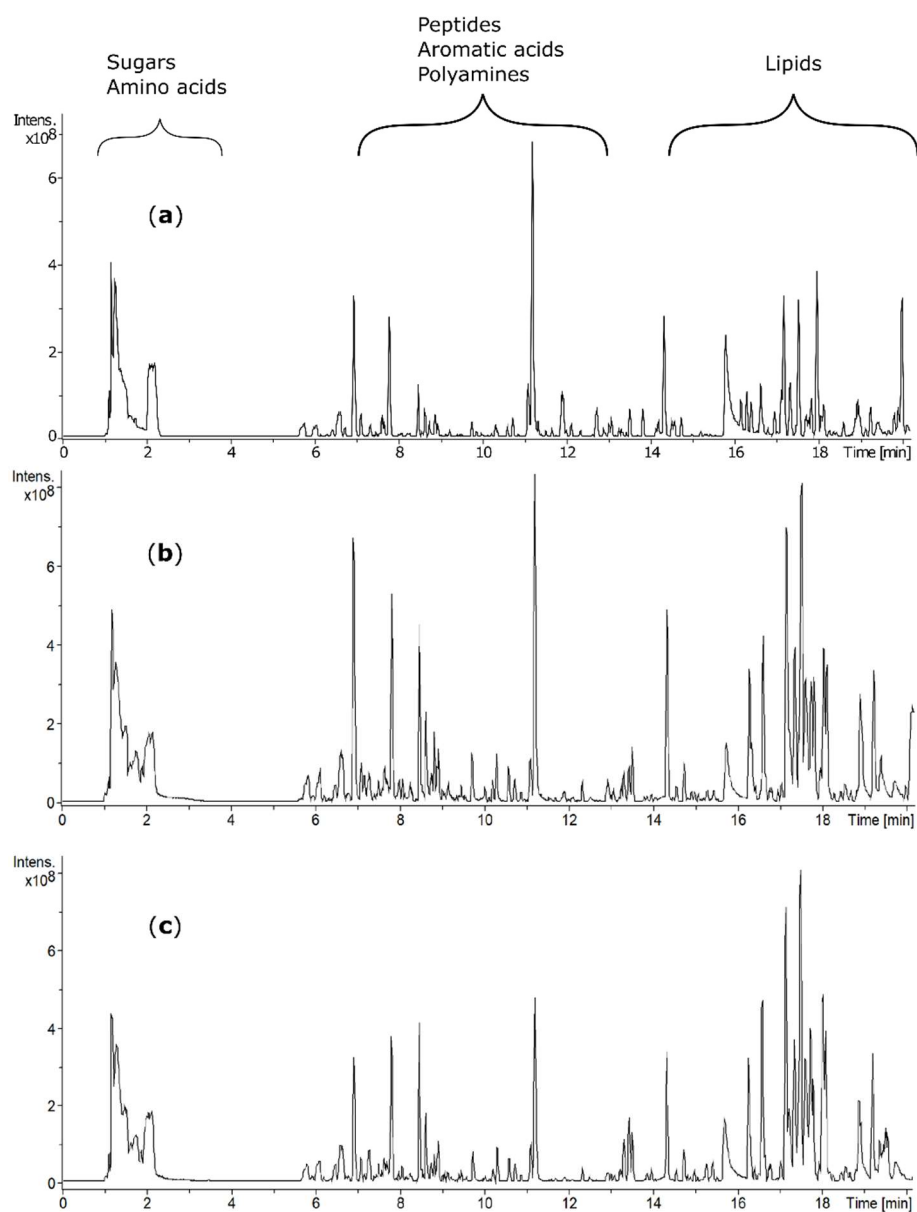
Appendix 7: Calibration curve of $\delta^{15}\text{N}_{\text{AA}}$ acid values.



Appendix 8: Table showing the moisture content of the maize used in the extraction condition experiment.

Sample	Fresh weight (g)	Dry weight (g)	Moisture content (%)
B73I	1.199	0.237	80
B73H	1.748	0.603	66
B73G	1.798	0.627	65
B73J	1.923	0.687	64

Appendix 9: Characteristic base peak ion chromatogram for (a) LNE (b) LC and (c) LRT samples obtained using a T3 column coupled to high resolution mass spectrometry (LC-HRMS) to allow the retention and separation of metabolites with a broad range of polarities.



Appendix 10: Summary of data on all possible drought related biomarkers of maize. Possible identifications were assigned using compound databases (Metlin, LipidBlast, ChemSpider, Progenesis MetaScope *Indicates the data were scaled. The adjusted ANOVA *p*-val is quoted. Where a possible identification is provided this indicates level 3 Schymanski identifications¹³⁰. Where no possible identification could be provided this indicates level 4.

Tissue Type	Scan Mode	m/z	<i>t</i> R	Molecular Species	MF	ppm	<i>p</i> -val	Possible Identification	Fragmentation Score
K	N*	279.1238	9.52	[M-H] ⁻	C ₁₅ H ₂₀ O ₅	-0.04	9.60E-15	Neophaseic Acid (neoPA)	50.1
K	N*	143.0349	3.88 and 3.89	[M-H] ⁻	C ₆ H ₈ O ₄	0.3	1.78E-14	Methyl itaconate	58.5
K	N*	129.0193	2.05	[M-H ₂ O-H] ⁻	C ₅ H ₈ O ₅	0.4	6.73E-14	Citramalic acid	29.4
K	N*	345.0827	2.8	[M-H] ⁻	C ₁₄ H ₁₈ O ₁₀	0.02	3.71E-9	No fragmentation information	-
K	N	423.2517	21.18	[M+FA-H] ⁻	C ₁₉ H ₃₉ O ₅ P	0.05	1.25E-10	No fragmentation information	-
K	N	447.2516	19.95	[M-H ₂ O-H]	C ₂₂ H ₄₃ O ₈ P	-0.32	8.07E-14	-	-
K	N	375.0570	3.88	[M-H] ⁻	C ₁₄ H ₁₆ O ₁₂	-0.24	1.85E-13	-	-
K	N	632.2858	11.88	[M-H] ⁻	C ₂₉ H ₄₈ NO ₁₂ P	-1.92	2.301E-3	-	-
K	N	735.2141	7.19	[M-H] ⁻	C ₃₄ H ₄₀ O ₁₈	0.09	3.19E-18	No fragmentation information	-

K	P*	480.3075	18.87	[M+H] ⁺	C ₂₃ H ₄₆ NO ₇ P	-0.21	1.19E-22	PE(18:1/0:0)	55.1
K	P*	260.1700	17.77	[M+2H] ²⁺	C ₂₃ H ₄₆ N ₆ O ₅ S	-0.5	4.86E-18	No fragmentation information	-
K	P	520.3398	17.75	[M+H] ⁺	C ₂₆ H ₅₀ NO ₇ P	-0.1	1.28E-18	PC(18:2/0:0)	88.8
K	P	634.3008	11.80	[M+H] ⁺	C ₃₆ H ₄₃ NO ₉	-0.35	4.55E-4	-	-
K	P	522.3556	18.99	[M+H] ⁺	C ₂₆ H ₅₂ NO ₇ P	-0.42	2.42E-16	PC(18:1/0:0)	78.4
K	P	478.2929	17.66	[M+H] ⁺	C ₂₃ H ₄₄ NO ₇ P	-0.26	9.06E-16	No fragmentation information	-
K	P	493.2810	8.07	[M+H] ⁺	C ₂₈ H ₃₆ N ₄ O ₄	-0.09	2.01E-5	No fragmentation information	-
IC	N*	538.1745	8.37	[M-H] ⁻	C ₂₄ H ₂₅ N ₇ O ₈	1.0	8.46E-26	-	-
IC	N*	559.1068	9.91	[M-H] ⁻	C ₁₉ H ₂₉ O ₁₇ P	-0.7	1.89E-14	-	-
IC	N*	491.1194	9.89	[M-H] ⁻	C ₂₃ H ₂₃ O ₁₂	0.3	2.81E-23	Aurantio-obtusin β-D-glucoside	35.4
IC	N	423.2514	21.18	[M+FA-H] ⁻	C ₁₉ H ₃₉ O ₅ P	-0.04	7.29E-16	No fragment info	-
IC	N	447.2517	19.95	[M-H ₂ O-H]	C ₂₂ H ₄₃ O ₈ P	-0.4	1.18E-5	-	-
IC	N	483.2729	19.32	[M-H] ⁻	C ₂₂ H ₄₅ O ₉ P	-0.91	3.04E-14	-	-
IC	N	571.2889	18.00	[M+FA-H] ⁻	C ₂₄ H ₄₇ O ₁₀ P	-0.05	8.75E-9	-	-
IC	N	540.3305	18.51	[M+FA-H] ⁻	C ₂₄ H ₅₀ NO ₇ P	0.37	1.81E-8	Lysolecithin	63.5
IC	P*	370.1131	6.54	[M+H] ⁺	C ₁₆ H ₁₉ NO ₉	0.46	6.59E-28	-	-

IC	P*	527.1550	12.71	[M+H] ⁺	C ₂₇ H ₂₆ O ₁₁	-0.35	8.17E-31	No fragment info	-
IC	P*	493.1340	9.84	[M+H] ⁺	C ₂₃ H ₂₄ O ₁₂	0.02	1.56E-28	No fragment info	-
IC	P*	540.1900	8.31	[M+H] ⁺	C ₂₇ H ₃₀ N ₃ O ₇ P	-0.5	4.23E-29	No fragment info	-
IC	P*	527.1537	13.05	[M+H] ⁺ ,	C ₂₇ H ₂₆ O ₁₁	0.2	8.17E-31	-	-
IC	P	441.2022	10.95	[M+H] ⁺	C ₂₄ H ₂₈ N ₂ O ₆	-0.31	3.60E-19	No fragment info	-
IC	P	903.3771	10.97	[M+H] ⁺	C ₄₉ H ₅₈ O ₁₆	0.2	3.72E-24	-	-
IC	P	265.1547	6.83	[M+H] ⁺	C ₁₄ H ₂₀ N ₂ O ₃	0.04	1.10E-28	Feruloyl putrescine	43.2
IC	P	411.1914	10.84	[M+H] ⁺	C ₂₃ H ₂₆ N ₂ O ₅	0.1	3.60E-19	No fragment info	-

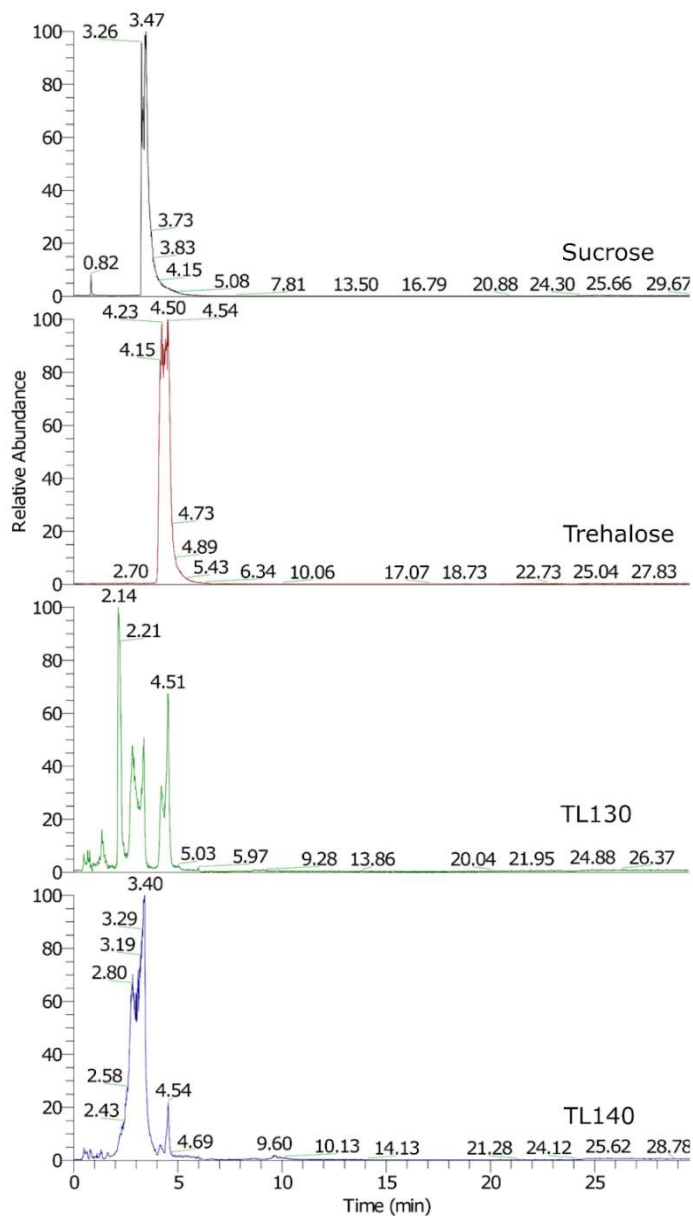
Appendix 11: Table showing features with the highest loadings of PC1. *Scaled data. Where a possible identification is provided this indicates level 3 Schymanski identifications¹³⁰. Where no possible identification could be provided this indicates level 4.

Scan Mode	m/z	tR	Molecular Species	MF	ppm	p-val	Possible Identification	Fragmentation Score
N	237.0766	7.20	[M-H ₂ O-H]-	C ₁₂ H ₁₆ O ₅	-0.52	1.02x10 ⁻⁵	P-Gal	59.8
N	439.1872	9.60	[M+Cl]-, [2M-H]-, [M+FA-H]-, [M-H]-	C ₂₄ H ₂₈ N ₂ O ₂		4.7x10 ⁻³	-	-
N	329.2328	11.30	[M+Cl]-, [2M-H]-, [M-H]-	C ₁₈ H ₃₄ O ₅	-1.2	4.7x10 ⁻³	Pinellic acid	12.3
N	413.1239	11.55	[M+Cl]-, [2M-H]-, [M+FA-H]-, [M-H]-	C ₂₂ H ₂₂ O ₈	-1.73	0.17	-	-
N	377.0853	1.17	[M+Cl]-, [2M-H]-, [M+FA-H]-, [M-H]-	C ₁₂ H ₂₂ O ₁₁	-0.86	4.1x10 ⁻³	Sucrose or trehalose	34
N and N*	413.0871	9.34	[M-H ₂ O-H]-, [M+FA-H]-	C ₂₁ H ₂₀ O ₁₀	-1.73	7.95 x10 ⁻⁵	Isovitexin or vitexin	64.5
N and N*	209.0091	5.97	[M-H]-	C ₉ H ₆ O ₆	-0.17	8.21 x10 ⁻⁶	Trimesic acid	47.5
N*	291.0509	8.44	[M-H]-, [M+FA-H]-	C ₁₃ H ₁₀ O ₅	-0.49	4.90x10 ⁻⁵	Pimpinellin	29.6
N*	399.0707	10.61	-	-	-	1.33x10 ⁻⁵	-	-
N*	273.0403	9.24	[M-H]-	C ₁₄ H ₁₀ O ₆	-0.38	1.02x10 ⁻⁵	Athyriol	

N*	347.0769	7.97	-	-		3.82x10-5	-	-
N*	483.1296	9.43	[M-H]-	C25H24O10		1.75 x10-5	-	-
P*	383.1125	12.81	[M+H]-	C21H18O7	-0.19	8.06x10-5	Deoxyaklanonic acid	55
P*	579.1863	13.31	-	-		4.82x10-4	-	-
P*	565.1699	13.05	-	-	-	3.93x10-4	-	-
P*	425.1204	11.26	-	-		3.13x10-4	-	-
P*	521.1434	12.55	[2M+H]+	C14H12O5	0.02	1.33x10-3	Methoxy- stypandrone	38
P*	565.1692	12.56	-	-	-	5.39x10-4	-	-
P*	631.1788	13.05	-	-	-	2.29x10-4	-	-
P*	127.7051	12.81	-	-	-	7.29x10-4	-	-
P*	509.1441	13.61	-	-	-	4.82x10-4	-	-
P*	577.1688	12.56	-	-	-	1.61x10-3	-	-
P*	577.1314	13.36	-	-	-	1.47x10-3	-	-
P*	535.1597	12.58	-	-	-	1.33x10-3	-	-
P*	537.1758	12.97	-	-	-	1.47x10-3	-	-

P*	399.1053	11.36	-	-	-	2.55x10-4	-	-
P*	551.1546	11.75	-	-	-	1.09x10-3	-	-

Appendix 12: Extracted ion chromatograms (m/z 377-378) of authentic sucrose and trehalose standards and archaeological samples: TL130 and TL140.



Appendix 13: Table showing features with fragmentation scores greater than 75 (peak width ≤ 0.15 , isotope similarity ≤ 95 and $-1 \leq \text{ppm} \leq 1$). The compound class of these metabolites was assigned using the KEGG database. Note: description shows database matches, whilst the stereochemistry cannot be assigned, the exact match is displayed.

Description	<i>m/z</i>	<i>t_R</i>	Fragmentation Score	Class
(1S,2R)-3-Methyl-3,5-				
Cyclohexadiene-1,2-diol	107.0501	6.56	66.3	NA
Ethyl maltol	121.0294	6.72	74	NA
1,4,5,6-Tetrahydro-6-oxonicotinic				
acid	122.0247	3.36	67.9	Organic acids
2,5-Dioxopentanoic acid	129.0193	3.27	66.1	Organic acids
Glutaric acid	131.035	2.67	73.6	Organic acids
Malic acid	133.0142	1.55	64.4	Organic acids
(1R,6S)-6-Amino-5-oxo-2-				
cyclohexene-1-carboxylic acid	136.0404	5.35	60.8	Peptides

(3E)-3-(Aminomethylene)-2H-pyran-2,6(3H)-dione	138.0197	2.72	63	Peptides
L-Fucono-1,5-lactone	143.035	2.45	69.9	Carbohydrates
5-Hydroxypiperic acid	144.0667	2.05	69	Organic acids
2-Formylbenzofuran	145.0295	7.20	68.6	NA
Coumarin	145.0295	8.78	67.3	Phytochemical compounds
(R)-4-Dehydropantoic acid	145.0506	5.65	67.8	Organic acids
Methylglutaric acid	145.0506	4.58	65.3	Organic acids
D-Xylonolactone	147.03	1.81	66.7	Carbohydrates
6-Imino-5-oxocyclohexa-1,3-dienecarboxylic acid	150.0197	6.88	61.9	Organic acids
Gallic acid	151.0038	7.58	60.8	Phytochemical compounds
1,6-Dihydroxy-2-methylcyclohexa-2,4-dienecarboxylic acid	151.0401	7.32	71	Organic acids
Menisdaurilide	151.0401	5.00	66.9	NA

1,6-Dihydroxy-4-methyl-2,4-cyclohexadiene-1-carboxylic acid	151.0401	6.13	77.5	Organic acids
3-Amino-5-hydroxybenzoic acid	152.0354	4.48	77.1	Organic acids
1-Carbapenem-3-carboxylic acid	152.0354	3.57	61.1	NA
5-Amino-5-deoxy-3-dehydroshikimic acid	152.0354	2.23	76.8	Organic acids
2-Hydroxyhepta-2,4-dienedioic acid	153.0194	6.54	72.4	Lipids
(-)-3-Dehydroshikimic acid	153.0194	5.88	69	NA
Suberic acid	155.0714	5.46	68.3	Lipids
5-Acetamidopentanoic acid	158.0824	3.41	60.2	NA
D-Galactono-1,5-lactone	159.03	1.34	60.7	Carbohydrates
2-Cyanophenol	164.0354	4.82	61.2	Organic acids
3-(Carboxyethyl)-3,5-cyclohexadiene-1,2-diol	165.0557	7.67	62.1	Organic acids

Pyridoxal	166.051	6.22	72.4	Vitamins and Cofactors
Dehydroacetic Acid	167.035	7.84	84.3	NA
Vanillic acid	167.0351	6.02	61.4	Organic acids
3-Methylpyrrole-2,4-dicarboxylic acid	168.0303	9.71	66.7	Organic acids
(S)-2,3-Dihydrodipicolinic acid	168.0303	3.39	60.1	Organic acids
(R)-3-[(R)-3-Hydroxybutanoyloxy]butanoic acid	171.0664	7.69	61.1	Organic acids
5-Deoxy-5-aminoshikimic acid	172.0617	2.02	62.2	NA
N-Acetyl-L-leucine	172.098	6.53	70.1	Peptides
4-Hydroxy-4-methylcyclohexanone	173.0819	7.41	60.1	NA
5,6-Dihydroxy-3-methyl-1,5,6-trihydroquinolin-2-one	174.0561	6.30	76.1	NA
Caffeoquinone	177.0194	6.53	66.5	Organic acids

(+)-Paeonilactone B	177.0557	10.56	64.7	NA
(3S,4R)-3,4-Dihydroxy-1,5-cyclohexadiene-1,4-dicarboxylic acid	181.0143	6.89	61.8	Organic acids
Maltol propionate	181.0507	7.58	63.5	Organic acids
2-Oxotetrahydrofuran-3,4-diyl diacetate	183.0299	5.02	67.6	NA
2-Hydroxy-5-methylquinone	183.0299	6.76	76.6	Organic acids
1,2-dihydro-3-ethylcatechol	185.0819	7.69	62	Organic acids
Allysine	190.0722	1.19	71.1	Peptides
Dehydro-D-arabinono-1,4-lactone	191.0198	1.27	68	Organic acids
2-Hydroxychromene-2-carboxylic acid	191.035	8.77	69.6	Organic acids
(2E)-5-Hydroxyferulic acid	191.035	9.25	69.8	Phytochemical compounds
(+)-Homotyrosine	194.0822	8.49	61.9	Peptides

(1S,4S)-4-Hydroxy-3-oxocyclohexanecarboxylic acid	203.0561	4.53	65.9	Organic acids
N-Carboxymethylisatin	204.0302	7.40	63.4	Organic acids
Indolelactic acid	204.0665	8.07	62.4	Organic acids
2-Hydroxy-8-methylchromene-2-Carboxylate	205.0506	7.71	61.9	Organic acids
3,4-Dihydro-1-benzoxepin-5(2H)-one	207.0662	6.08	60.5	NA
(E)-Ethyl caffeate	207.0662	8.70	70.7	Phytochemical compounds
6-Hydroxy-2-chromanone	209.0454	7.32	61.5	Phytochemical compounds
(S)-Betalamic acid	210.0408	6.51	68.4	Phytochemical compounds
Enicoflavine	210.0771	4.09	67.5	NA
1,4-Benzodioxan-2-methanol	211.0612	5.64	67.4	NA
Coixinden B	215.0713	11.45	62.1	NA
Butyryl-L-homoserine lactone	216.0877	3.41	66.9	Lipids

8-Acetyl-4-methylumbelliferone	217.0506	8.12	66.4	Phytochemical compounds
2'-Deoxynebularine	217.0729	4.08	64.5	NA
9-Oxononanoic acid	217.1081	7.25	60.9	Lipids
2-Hydroxyquinoline-3-carbaldehyde	218.0458	6.30	64.9	NA
8-METHOXYKYNURENIC ACID	218.0458	7.89	60.6	NA
2-(3-Carboxypropionyl)-6-hydroxy-cyclohexa-2,4-diene carboxylic acid	221.0455	8.78	69.8	Organic acids
7-Hydroxy-2-methyl-4H-chromen-4-one	221.0455	7.04	64.6	NA
Hymecromone	221.0455	9.17	67.4	Phytochemical compounds
Salsolinol	224.0928	12.31	68	Phytochemical compounds
Traumatic Acid	227.1289	10.86	62.3	Lipids
Bis-noryangonin	229.0505	8.26	71.7	NA

Pyriculol	229.0869	11.13	60.9	NA
Dodecanedioic acid	229.1444	13.97	62.1	Lipids
(S)-2-Acetamido-6-oxopimelic acid	230.067	1.70	66	Lipids
Homoaconitate	233.0302	1.26	61.9	Organic acids
Ramentaceone	233.0455	9.11	71.9	Phytochemical compounds
2-Hydroxycinchoninic acid	234.0407	6.54	62.8	Organic acids
2-Carboxy-2-hydroxy-8-carboxychromene	235.0247	5.90	66	NA
Ayapin	235.0247	5.32	63.4	Phytochemical compounds
4,8-Dimethyl-7-hydroxycoumarin	235.0612	8.05	65	NA
Methyl 4-(cyanomethoxy)benzoate	236.0564	6.46	65	NA
Scopoletin	237.0405	7.72	66.8	Phytochemical compounds
(3S)-3,6,8-Trihydroxy-3,4-dihydro-1(2H)-naphthalenone	239.056	5.69	71.1	NA

(R)-(-)-6-Hydroxymellein	239.0561	6.02	60.6	NA
Kakuol	239.0561	9.80	71.2	NA
Cnidilide	239.1288	10.87	61.8	NA
Dopaquinone	240.0513	1.67	69.4	Peptides
Isodictamnine	244.0615	5.85	61.9	Phytochemical compounds
5-Methylangelicin	245.0454	10.78	61.7	Phytochemical compounds
Isobergaptol	247.0247	6.99	62.5	NA
Monomethyl Azelate	247.1186	7.06	62	NA
Spirodilactone	249.0403	7.69	66.2	NA
2-O-Ethyl ascorbic acid	249.0615	1.22	66.3	Organic acids
Gentianamine	250.072	6.66	65.3	Organic acids
4-(Adamantan-1-ylamino)-4-oxobutanoic acid	250.1447	7.89	60.4	Organic acids
Eugenin	251.056	6.05	61.5	Phytochemical compounds

Acetylugenol	251.0925	12.18	62.8	Organic acids
Jasmonic acid	255.1237	7.67	60.7	Lipids
Ranunculin	257.0666	3.00	65.5	Phytochemical compounds
lactucin	257.0818	11.27	61.3	Phytochemical compounds
Cucurbitic acid	257.1395	9.83	67.8	Lipids
5-Decen-3-one, 9-hydroxy-2,2,9-trimethyl	257.1758	14.03	61.2	NA
2-Hydroxy-6-ketnonadienedioic acid	259.0458	3.08	60.5	NA
Mycosinol	259.0611	9.12	69.4	NA
Mannitol 1-phosphate	261.038	1.11	77.6	NA
Farinosin	261.1131	13.05	60.3	Phytochemical compounds
Ethyl 5-methoxy-1-benzofuran-2-carboxylate	265.0716	8.28	62.1	Organic acids
Polygonolide	265.0717	7.45	77.3	Phytochemical compounds

Metaxalone	266.1032	7.37	61.5	NA
2-Hydroxy-7-hydroxymethyl-2H- Chromene-2-carboxylic acid	267.0509	7.97	61	Organic acids
3-Deoxy-D-glycero-D-galacto-2- nonulosonic acid	267.0721	1.19	68.8	Carbohydrates
Blumenol A	269.1393	9.32	75.5	Organic acids
Murrayanine	270.0771	9.76	69.5	NA
Toralactone	271.0611	9.68	70.1	NA
Xanthyletin	273.0768	11.30	63.3	Phytochemical compounds
Desmethoxyyangonin	273.0768	11.53	67.7	NA
3-beta-D-Glucopyranuronosyloxy- 5-methylisoxazole	274.0568	1.22	62	Carbohydrates
3,4,6,7-Tetrahydro-2,5,8- benzotrioxacycloundecin-1,9-dione	281.0665	6.94	63.2	NA
Dihydrophaseic acid	281.1393	10.08	60.4	Lipids

Cypripedin	283.0611	16.16	68.1	NA
(S)-Hemiketal	285.0767	9.79	69.1	Organic acids
Navenone C	285.113	8.99	63.2	NA
Methylstyrylpyron	289.0717	9.69	62	Organic acids
Allamandin	289.0717	10.11	63.2	Phytochemical compounds
9-O-Acetylneuraminic acid	290.0881	1.57	76.2	Carbohydrates
2-(4-Hydroxyphenyl)-3-benzofuranyl methyl ketone	297.0766	10.40	75.4	NA
3,9-Dihydroxyptercarp-6a-en	299.056	9.09	67.1	Lipids
4-Hydroxy-3-[3-(2-hydroxy-5-methoxy-phenyl)-acryloyl]-6-methyl-pyran-2-one	301.0715	10.26	63	NA
1-(beta-D-Ribofuranosyl)-1,4-dihydronicotinamide	301.104	1.68	66.3	NA
(-)-Jasmonoyl-L-isoleucine	304.1916	16.39	61.2	Peptides

Rubrofusarin	307.0377	12.95	64.9	Phytochemical compounds
Paeonoside	309.0978	9.48	62.7	Carbohydrates
Furofoline I	310.0719	9.60	71.9	Phytochemical compounds
Isoxepac	313.0716	8.86	65.3	NA
Tolcapone	318.0617	11.88	60.4	NA
Carbestrol	319.1548	12.34	70.1	NA
Magellanine	320.1865	18.48	66.9	NA
Lycofawcine	322.2021	9.34	65.5	NA
(2Z)-3-[2-(beta-D-Glucopyranosyloxy)phenyl]acrylic acid	325.0926	7.11	60.7	NA
Kaempferol	331.0457	9.22	61.2	Lipids
Chlorogenoquinone	333.0613	7.66	68.6	NA
Platyphylline	336.1814	12.91	60.2	Phytochemical compounds

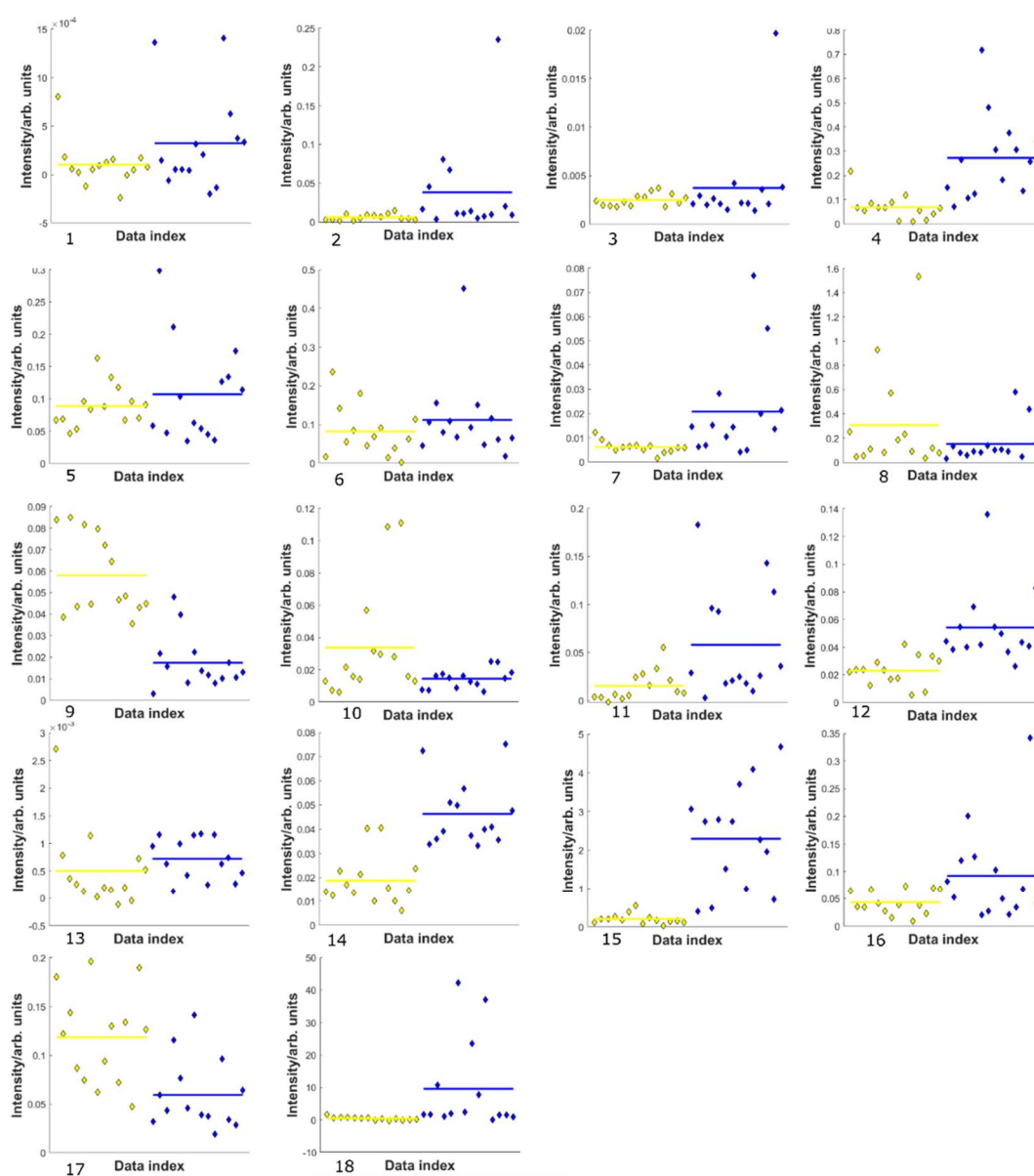
Cyclopentolate	336.1814	10.22	60.2	NA
Stealthin C	352.0824	8.88	63.8	NA
(5S,6S,10R,14aS,14bS)-6-Hydroxy- 10-methoxy-4,5,6- trimethyldodecahydro[1,6]dioxacy clododecino[2,3,4-gh]pyrrolizine- 2,7-dione	354.1919	12.35	61	NA
1-O-trans-Cinnamoyl-beta-D- Glucopyranose	355.1032	6.73	69.1	NA
Aflatoxin	357.0613	11.45	64.8	Lipids
(+)-Prosopinine	358.2596	17.78	65.6	Phytochemical compounds
6-Methoxyaromadendrin 3-O- acetate	359.0769	9.53	66.1	Phytochemical compounds
Neobyakangelicol	361.0926	7.58	68.6	NA
Coronatine	364.1763	13.59	64.9	NA

Homocapsaicin	364.2126	15.35	72.1	Phytochemical compounds
Dihexyverine	366.2647	18.33	78.1	NA
(5Z,9beta,11beta,13E,15S)-9,11,15-Trihydroxythromboxa-5,13-dien-1-oic acid	369.2279	9.65	86.4	Lipids
Methyl (2R)-4-hydroxy-6'-methoxy-6-methyl-3,4'-dioxo-3H-spiro[1-benzofuran-2,1'-cyclohexa[2,5]diene]-2'-carboxylate	375.0718	8.21	71	NA
Megastachine	376.2127	17.05	77.7	NA
Triflubazam	379.0909	5.99	64.3	NA
Erucic acid	383.3165	20.06	62.1	Lipids
(S)-Usnic acid	389.0876	10.50	68.3	Lipids
Eupatilin	389.0876	8.16	60.5	Lipids
Tetracenomycin M	401.0876	10.73	71.8	NA

(-)-Cubebin	401.1239	11.25	63.8	NA
(2S-3S)-Versiconal hemiacetal	403.0668	8.54	70.7	NA
5,8-Dihydroxy-3-(4-hydroxybenzyl)-7-methoxy-4-chromanone 8-acetate	403.1033	8.15	60.9	NA
Columbin	403.1395	9.34	61.4	Phytochemical compounds
Averantin	417.119	10.06	61.4	NA
(1S,2S,3S,5R,8R,11R,12S,13S,15S)-5-(3-Furyl)-12-hydroxy-3,11-dimethyl-6,14,16-trioxapentacyclo[10.3.2.0~2,11~.0~3,8~.0~13,15~]heptadecane-7,17-dione	419.1347	8.63	73.7	NA
Eupatundin	421.1504	6.61	67.2	Phytochemical compounds
1-O-Acetyl-alpha-maltose	429.125	1.68	66.8	Organic acids
Cleomiscosin A	431.0982	9.29	69.1	Phytochemical compounds

Glucosyloxyanthraquinone	431.0982	7.56	81.2	NA
(-)-Medicocarpin	431.1346	8.93	65.2	Lipids
Dromostanolone				
tetrahydropyranyl ether	433.2958	19.76	69.9	NA
Cassiaside	449.1088	8.39	71.5	NA
Methyl aklanonate	455.0982	11.84	61.2	Organic acids
Leiocarposide	613.1776	6.32	76.7	Carbohydrates
Plantamajoside	639.1934	7.19	75.8	Carbohydrates
Hellicoside	655.1885	6.27	66.7	Organic acids
Tricin 7-diglucuronoside	681.1312	7.48	65	Organic acids
Sucrose	377.0853	1.17	33.8	Carbohydrates

Appendix 14: Figure showing relative abundances of features from scaled data: 1 (m/z : 130.0510, t_R : 1.78), 2 (m/z : 261.1131, t_R : 12.0440), 3 (m/z : 129.0557, t_R : 3.25), 4 (m/z : 179.0562, t_R : 1.19), 5 (m/z : 145.0506265, t_R : 5.65), 6 (m/z : 361.1289, t_R : 7.11), 7 (m/z : 146.0459, t_R : 1.68), 8 (m/z : 146.0459, t_R : 10.56), 9 (m/z : 223.02478, t_R : 5.81), 10 (m/z : 191.0350, t_R : 9.25), 11 (m/z : 261.1131, t_R : 12.04), 12 (m/z : 145.0295, t_R : 8.78), 13 (m/z : 304.1917, t_R : 9.52), 14 (m/z : 133.0142, t_R : 1.55), 15 (m/z : 206.0822, t_R : 7.56), 16 (m/z : 210.0771, t_R : 4.09), 17 (m/z : 225.0404, t_R : 6.59), 18 (m/z : 167.0351, t_R : 6.02). Yellow and blue diamonds represent 1800 and 700 BP groups respectively.



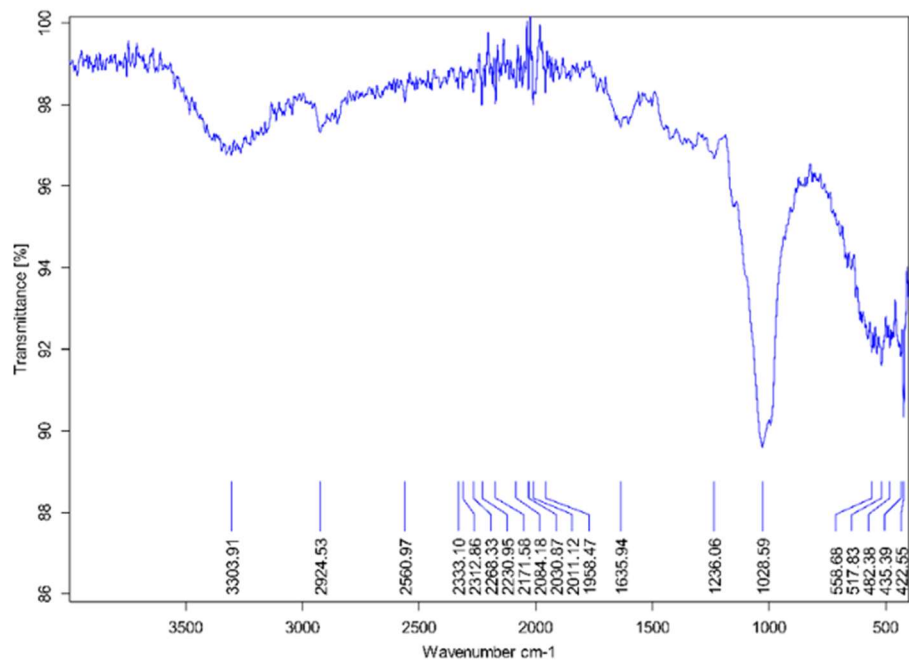
Appendix 15: The catalogue number, grid square and level of archaeological samples from archaeological maize from Tularosa Cave (Martin *et al.* 1952). TL indicates Tularosa Cave.

Cob Morphology	Sample ID	Cat. No	Square	Level
Ovoid	TL56	314984	2R2	14
Ovoid	TL57	314984	2R2	14
Ovoid	TL63	314981	2R1	13
Ovoid	TL67	314940	2R1	12
Ovoid	TL72	315043	2R1	13
Ovoid	TL75	314980	2R1	13
Ovoid	TL77	314924	2R1	12
Ovoid	TL81	314981	2R1	13
Ovoid	TL86	314981	2R1	13
Ovoid	TL87	315043	2R1	12
Ovoid	TL95	316025	2R1	13
Ovoid	TL96	314982	2R1	13
Ovoid	TL97	314982	2R1	13
Ovoid	TL104	314982	2R1	13
Cylindrical	TL108	315113	3R2	3

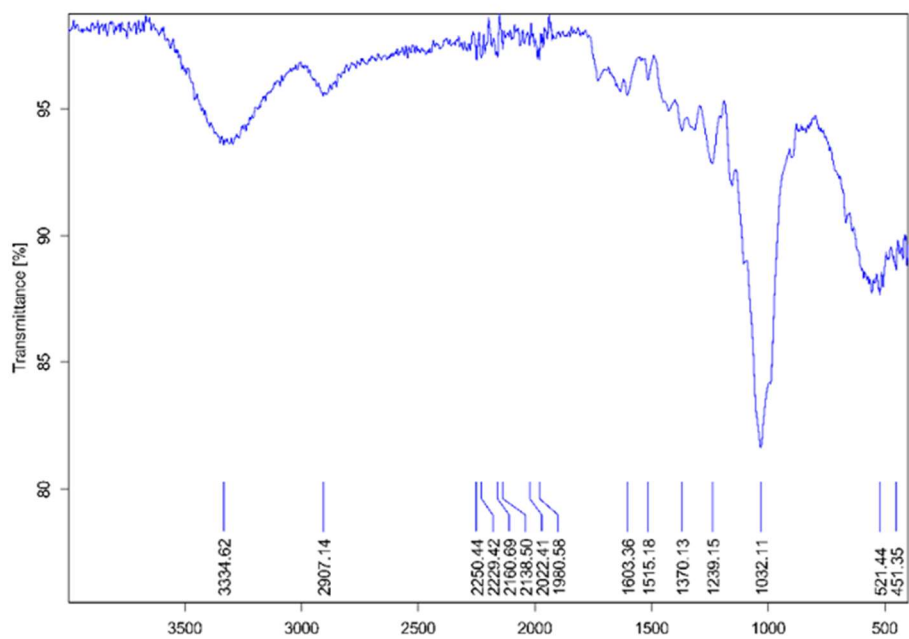
Cylindrical	TL114	315073	3R2	2
Cylindrical	TL116	315073	3R2	2
Cylindrical	TL120	315075	3R2	3
Cylindrical	TL127	314742	2R1	1
Cylindrical	TL128	314742	2R1	1
Cylindrical	TL137	314731	2R2	2
Cylindrical	TL140	314739	2R2	2
Cylindrical	TL144	314739	2R2	2
Cylindrical	TL146	314741	2R2	1
Cylindrical	TL152	314721	2R2	4
Cylindrical	TL153	314721	2R2	4
Cylindrical	TL154	314721	2R2	4
Cylindrical	TL5	314984	2R2	14

Appendix 16: ATR-FTIR scans of modern maize heated at 70 °C for 0, 1, 2, 4, 8 and 16 weeks.

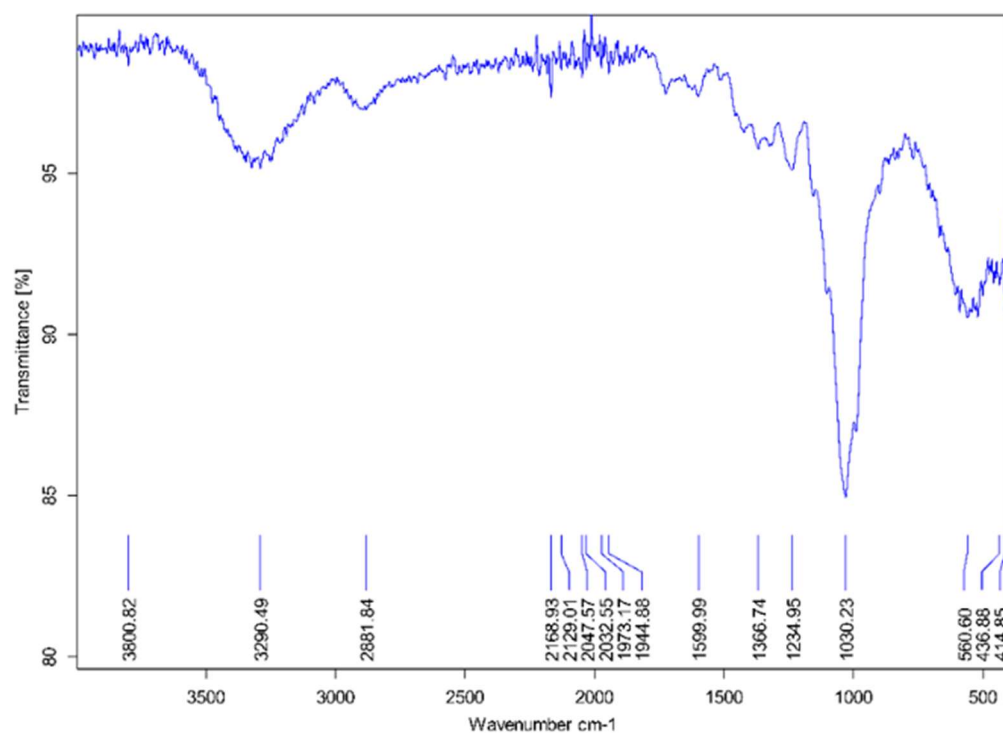
0 Weeks



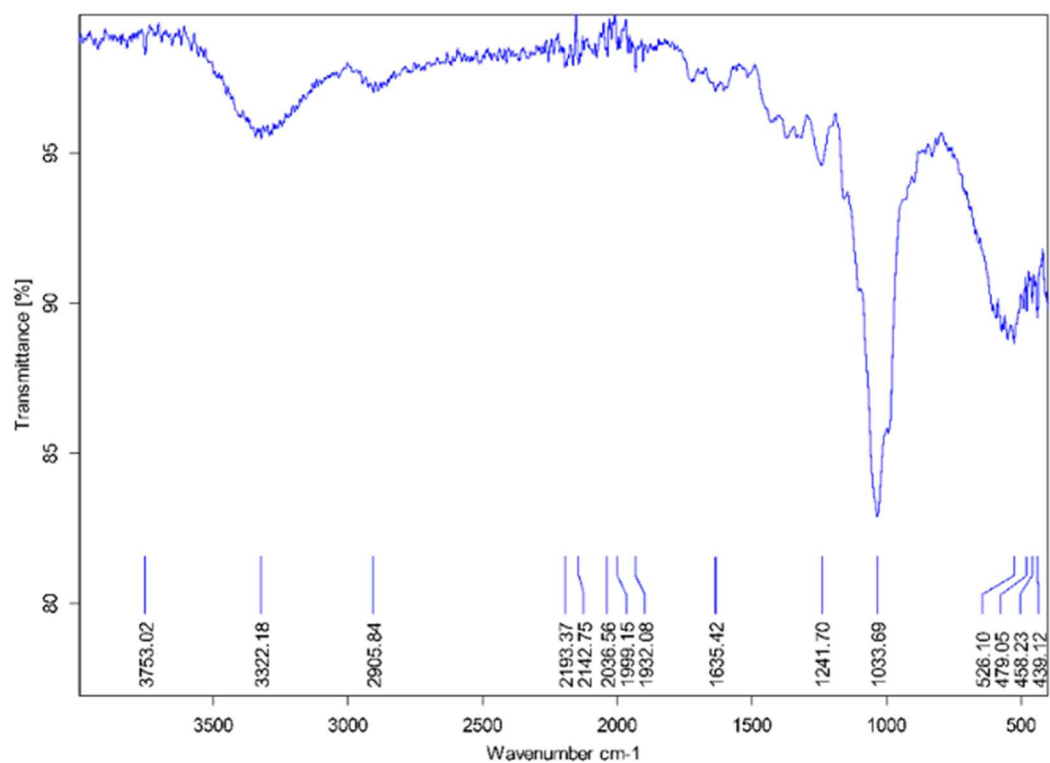
1 Week

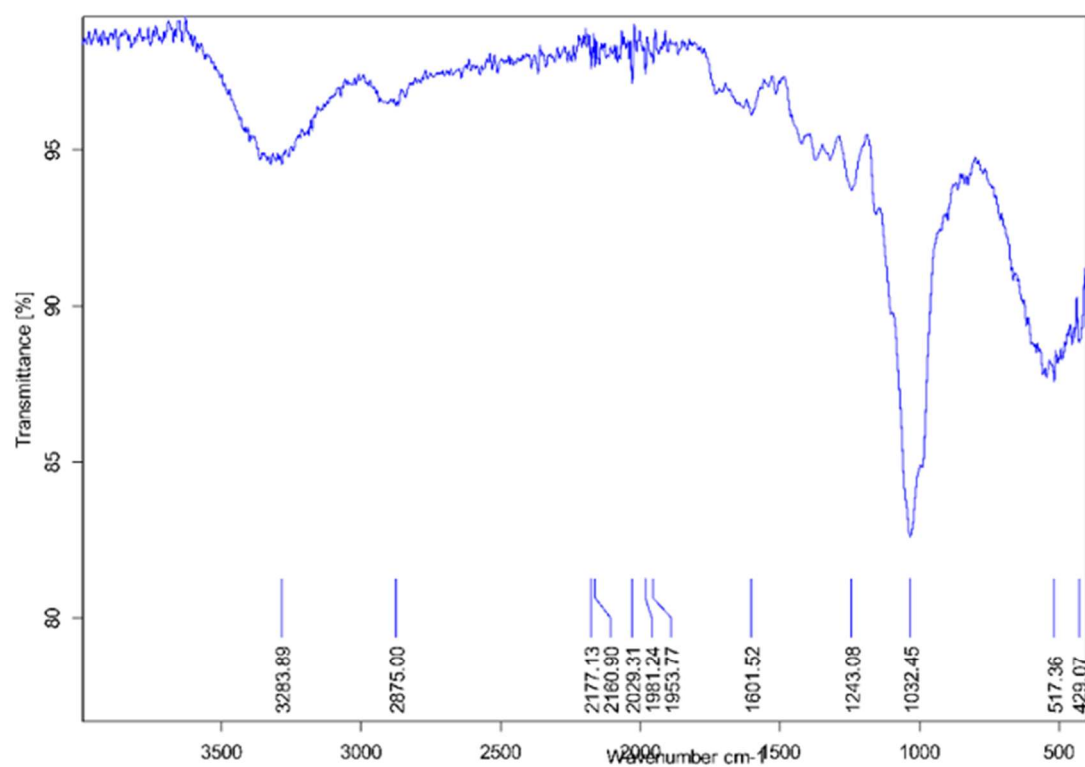


2 Weeks

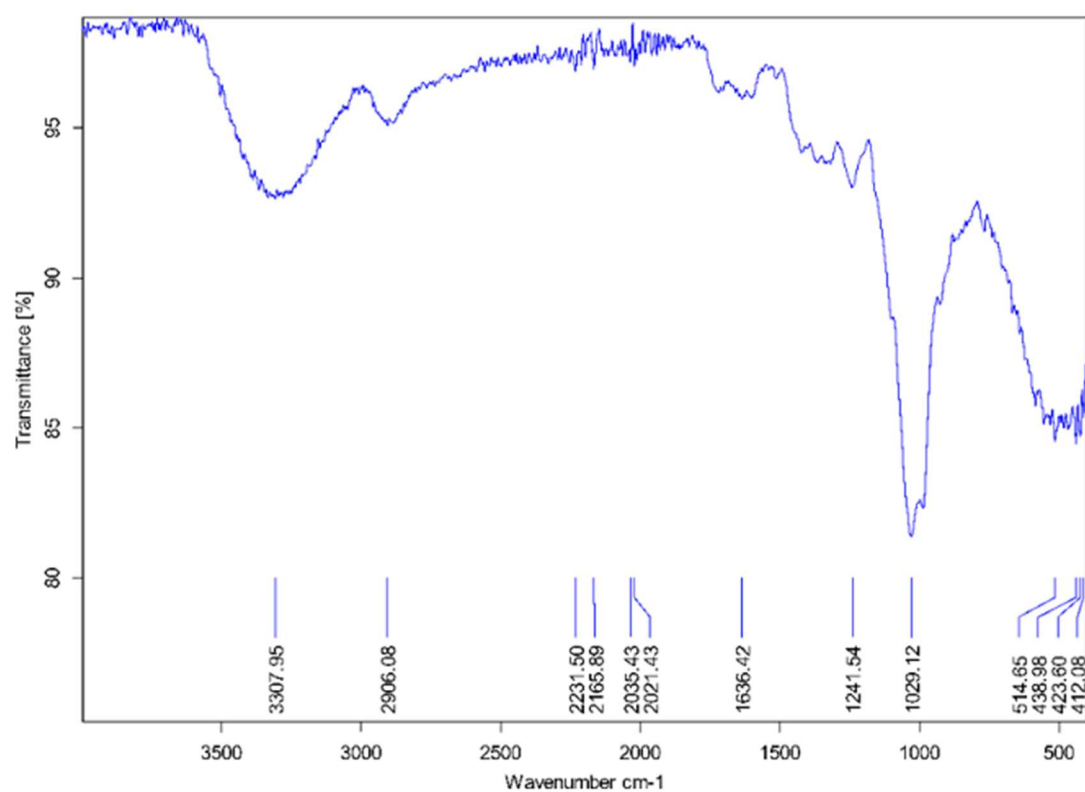


4 Weeks



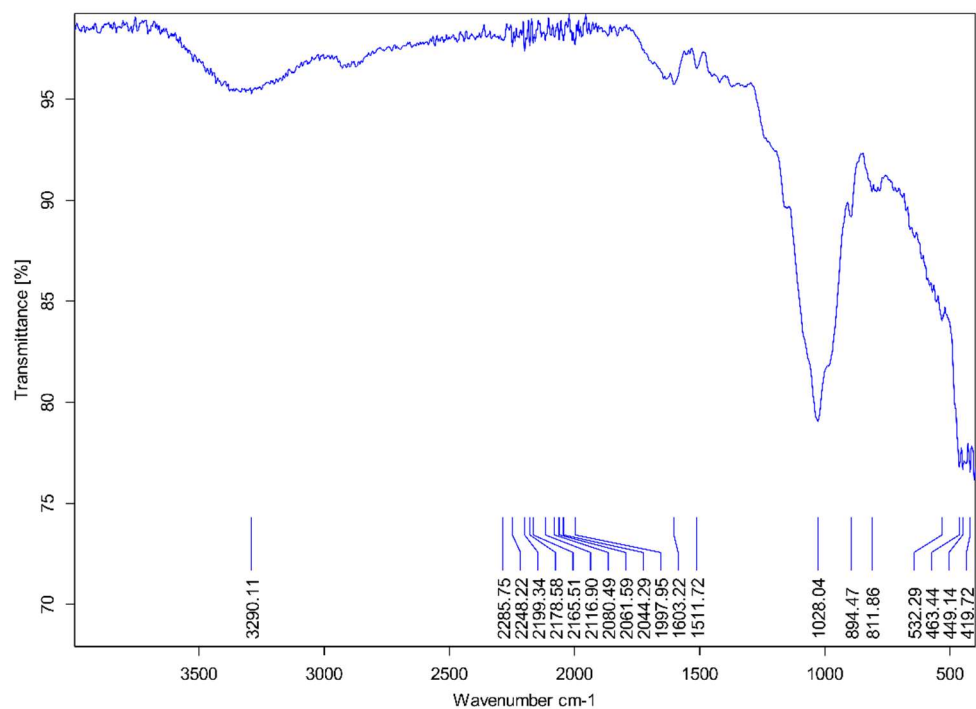


16 Weeks

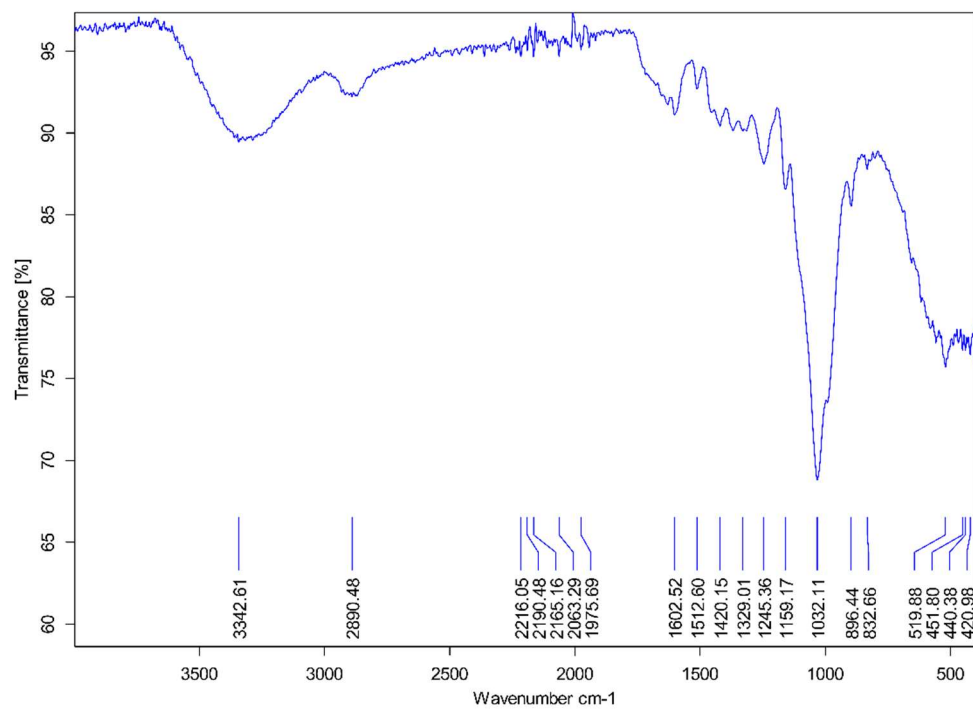


Appendix 17: ATR-FTIR scans of archaeological maize (123, 151, 81, 82)
TL indicates Tularosa Cave.

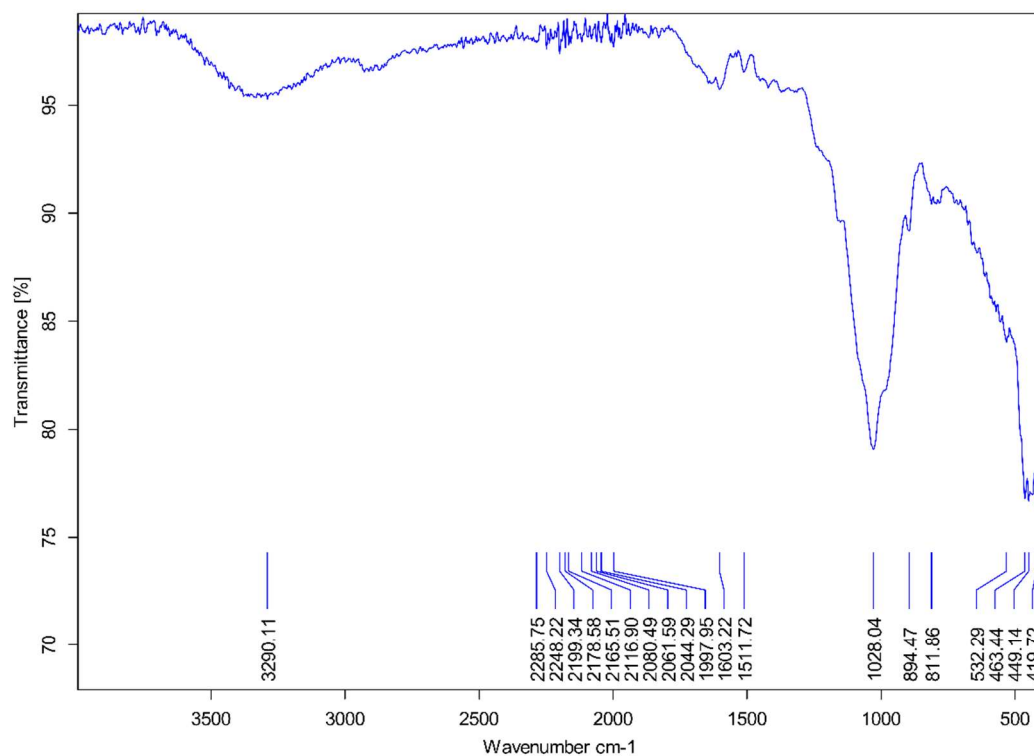
TL123



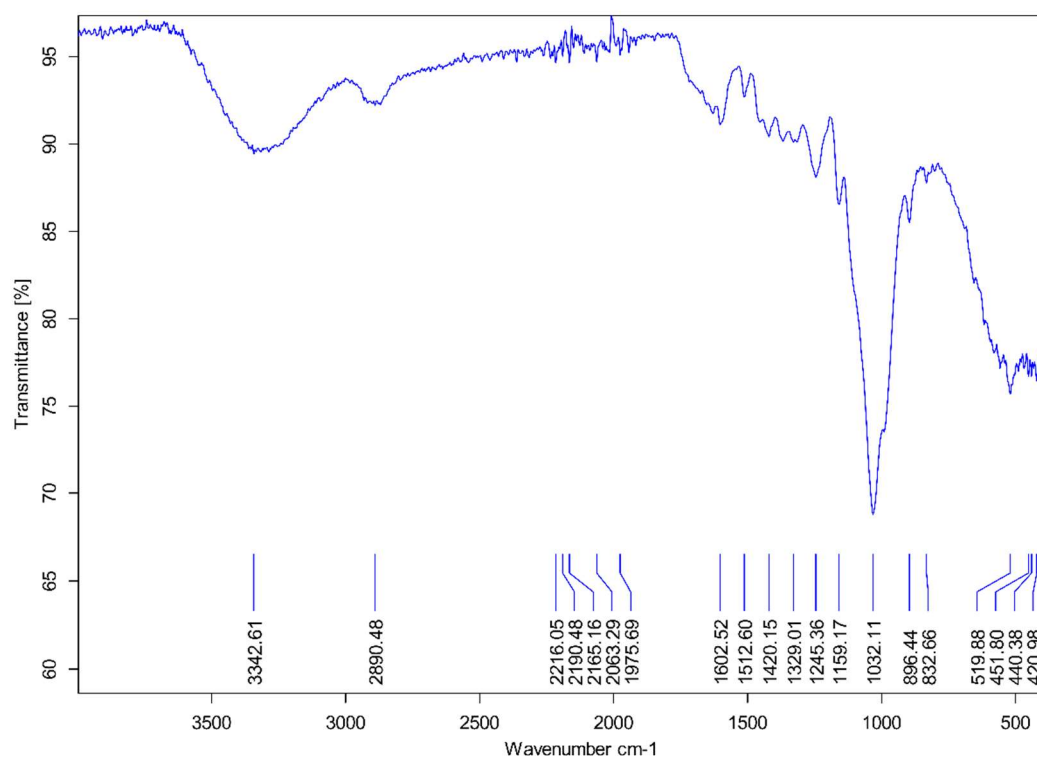
TL151



TL123



TL151



Appendix 18: Elemental analysis data of archaeological maize from Tularosa Cave and modern samples heated in the oven at 55 °C and 70 °C. TL indicates Tularosa Cave.

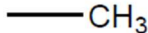
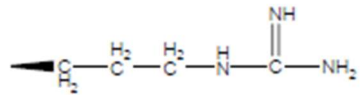
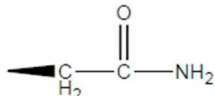
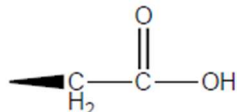
Sample	Element	C	H	N	Rest (assume all O)	Molar ratio O:C	Molar ratio H:C	Molar ratio C:N
TL81 1800 BP	Observed % MASS 1	43.93	5.58	0.67	49.32			
	Observed % MASS 2	44.03	5.73	0.77	49.48			
	Mean % MASS	43.98	5.66	0.72	49.65			
	SD of Mean % MASS	0.07	0.11	0.07	0.11			
	Mean molar ratio	3.66	5.61	0.05	3.10	0.85	1.53	71.26
TL91 1800 BP	Observed % MASS 1	42.19	5.92	0.58	51.31			
	Observed % MASS 2	41.50	5.90	0.72	51.88			
	Mean % MASS	41.85	5.91	0.65	51.60			
	SD of Mean % MASS	0.49	0.01	0.10	0.40			
	Mean molar ratio	3.48	5.86	0.05	3.22	0.94	1.68	75.08
TL82 1800 BP	Observed % MASS 1	39.79	4.85	0.98	54.38			
	Observed % MASS 2	42.04	5.12	0.89	51.95			
	Mean % MASS	40.92	4.99	0.94	53.17			
	SD of Mean % MASS	1.59	0.19	0.06	1.72			
	Mean molar ratio	3.41	4.95	0.07	3.32	0.98	1.45	51.03
TL123 700 BP	Observed % MASS 1	43.87	5.93	0.37	49.53			
	Observed % MASS 2	44.12	5.95	0.35	49.58			
	Mean % MASS	44.00	5.94	0.36	49.71			
	SD of Mean % MASS	0.18	0.01	0.01	0.04			
	Mean molar ratio	3.66	5.89	0.03	3.11	0.85	1.61	142.52
TL5 700 BP	Observed % MASS 1	43.46	6.17	0.55	49.82			
	Observed % MASS 2	41.81	6.10	0.62	51.47			
	Mean % MASS	42.64	6.13	0.59	50.65			

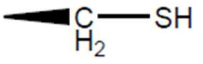
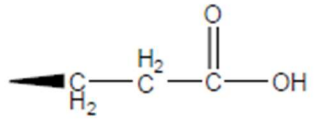
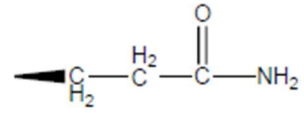

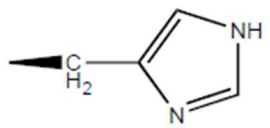
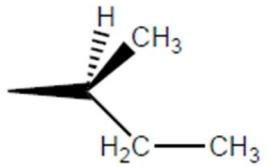
	SD of Mean % MASS	1.17	0.05	0.05	1.17			
	Mean molar ratio	3.55	6.08	0.04	3.17	0.89	1.71	84.28
TL140	Observed % MASS 1	42.02	5.75	0.46	51.77			
	Observed % MASS 2	41.44	5.40	0.22	52.95			
700 BP	Mean % MASS	41.73	5.57	0.34	52.36			
	SD of Mean % MASS	0.41	0.25	0.17	0.83			
	Mean molar ratio	3.45	5.53	0.02	3.27	1.25	0.13	0.85
TL151	Observed % MASS 1	42.10	5.20	0.49	52.21			
	Observed % MASS 2	42.83	5.18	0.84	51.15			
700 BP	Mean % MASS	42.47	5.19	0.67	51.68			
	SD of Mean % MASS	0.52	0.01	0.25	0.75			
	Mean molar ratio	3.54	5.15	0.05	3.23	0.91	1.46	74.47
1 day 55C oven	Observed % MASS 1	42.50	5.94	0.32	51.24			
	Observed % MASS 2	42.59	5.83	0.17	51.41			
	Mean % MASS	42.55	5.89	0.25	51.33			
	SD of Mean % MASS	0.06	0.08	0.11	0.12			
	Mean molar ratio	3.54	5.84	0.02	3.21	0.91	1.65	202.51
2 days 55C oven	Observed % MASS 1	35.97	5.27	0.46	58.30			
	Observed % MASS 2	36.99	5.31	0.33	57.37			
	Mean % MASS	36.48	5.29	0.40	57.84			
	SD of Mean % MASS	0.72	0.03	0.09	0.66			
	Mean molar ratio	3.04	5.25	0.03	3.61	1.19	1.73	107.70
5 days 55C oven	Observed % MASS 1	43.46	6.17	0.55	49.82			
	Observed % MASS 2	41.81	6.10	0.62	51.47			
	Mean % MASS	42.64	6.14	0.59	50.65			
	SD of Mean % MASS	1.17	0.05	0.05	1.17			
	Mean molar ratio	3.55	6.09	0.04	3.17	0.89	1.71	84.99

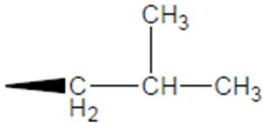
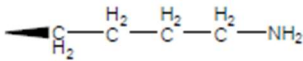
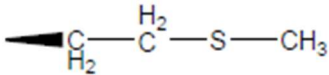
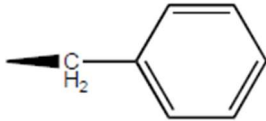
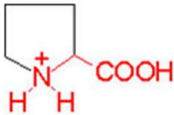
19 days 55C oven	Observed % MASS 1	42.19	5.92	0.58	51.31			
	Observed % MASS 2	41.50	5.90	0.72	51.88			
	Mean % MASS	41.85	5.91	0.65	51.60			
	SD of Mean % MASS	0.49	0.01	0.10	0.40			
	Mean molar ratio	3.48	5.86	0.05	3.22	0.93	1.68	75.08
40 days 55C oven	Observed % MASS 1	42.34	6.06	0.86	50.73			
	Observed % MASS 2	41.87	5.80	0.66	51.63			
	Mean % MASS	42.11	5.93	0.76	51.21			
	SD of Mean % MASS	0.33	0.18	0.14	0.64			
	Mean molar ratio	3.51	5.88	0.05	3.20	0.91	1.68	64.61
0 weeks 70	Observed % MASS 1	43.45	5.68	1.25	49.62			
	Observed % MASS 2	42.83	5.51	1.62	50.04			
	Mean % MASS	43.14	5.60	1.44	49.83			
	SD of Mean % MASS	0.44	0.12	0.26	0.30			
	Mean molar ratio	3.59	5.55	0.10	3.11	0.87	1.55	35.06
1 weeks 70	Observed % MASS 1	46.27	6.28	0.63	46.82			
	Observed % MASS 2	46.38	6.53	0.55	46.54			
	Mean % MASS	46.33	6.41	0.59	46.68			
	SD of Mean % MASS	0.08	0.18	0.06	0.20			
	Mean molar ratio	3.86	6.35	0.04	2.92	0.76	1.71	91.56
2 weeks 70	Observed % MASS 1	44.35	5.21	1.20	49.24			
	Observed % MASS 2	44.68	5.36	1.26	48.70			
	Mean % MASS	44.52	5.29	1.23	49.24			
	SD of Mean % MASS	0.23	0.11	0.04	0.38			
	Mean molar ratio	3.71	5.24	0.09	3.08	0.83	1.41	42.21
4 weeks 70	Observed % MASS 1	46.21	5.50	0.98	47.31			
	Observed % MASS 2	45.95	6.12	1.19	46.74			

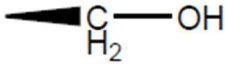
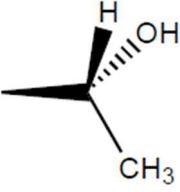
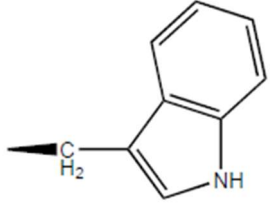
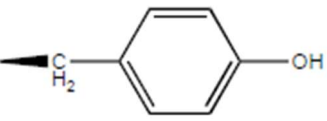
	Mean % MASS	46.08	5.81	1.09	47.03			
	SD of Mean % MASS	0.18	0.44	0.15	0.40			
	Mean molar ratio	3.84	5.76	0.08	2.94	0.77	12.16	49.53
8 weeks 70	Observed % MASS 1	44.69	6.00	0.56	48.75			
	Observed % MASS 2	46.05	6.01	0.45	47.49			
	Mean % MASS	45.37	6.01	0.51	48.12			
	SD of Mean % MASS	0.96	0.01	0.08	0.89			
	Mean molar ratio	3.78	5.96	0.04	3.01	0.80	1.58	104.77
16 weeks 70	Observed % MASS 1	45.56	6.11	0.94	47.39			
	Observed % MASS 2	44.32	5.99	0.50	49.19			
	Mean % MASS	44.94	6.05	0.72	47.39			
	SD of Mean % MASS	0.88	0.08	0.31	1.27			
	Mean molar ratio	3.74	6.00	0.05	2.96	0.79	1.60	72.79

Appendix 19: Table showing the properties of amino acids. R group is shown in black. And for proline the base structure is drawn in red. Hydrophobicity data obtained from Monera *et al*²¹⁴.

Amino acid	3 letter code	Molecular weight/ gmol ⁻¹	R group	Charge at pH7	Hydrophobicity index at pH 7
Alanine	Ala	89.1		0	41
Arginine	Arg	174.2		1	-14
Asparagine	Asn	132.1		0	-28
Aspartic acid	Asp	133.1		-1	-55

Cysteine	Cys	121.2		0	49
Glutamic acid	Glu	147.1		-1	-31
Glutamine	Gln	146.2		0	-10
Glycine	Gly	75.1		0	0
Histidine	His	155.2		1	8
Isoleucine	Ile	131.2		0	99

Leucine	Leu	131.2		0	97
Lysine	Lys	146.2		1	-23
Methionine	Met	149.2		0	74
Phenylalanine	Phe	165.2		0	100
Proline	Pro	115.1		0	-46

Serine	Ser	105.1		0	-5
Threonine	Thr	119.1		0	13
Tryptophan	Trp	204.2		0	97
Tyrosine	Tyr	181.2		0	63

- 239 -

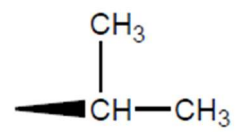
Valine

Val

117.2

0

76

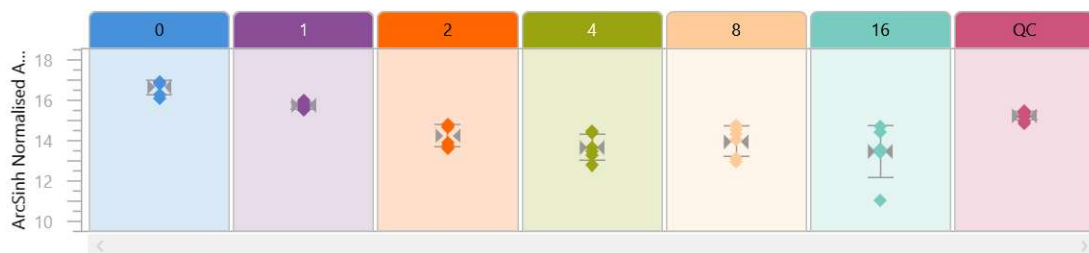


Appendix 20: Mean average AA $\delta^{15}\text{N}$ values from inner maize cob samples. Numbers in brackets represent one standard deviation associated with triplicate analytical replicate measurements for AA $\delta^{15}\text{N}$ values and replicate precision for duplicate experimental replicates of bulk $\delta^{15}\text{N}$ values.

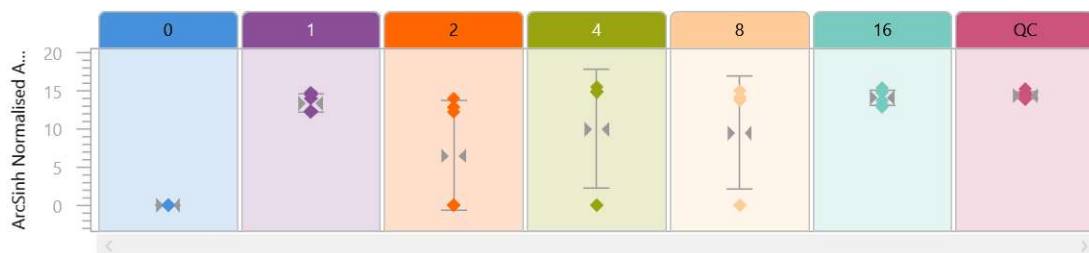
Sample Identification	AA $\delta^{15}\text{N}$ value (‰)													
	Gly	Ser	Glx	Ala	Asx	Pro	Hyp	Val	Leu	Ile	Thr	Lys	Phe	Bulk
Artificially aged sample	10.3 (1.4)	5.3 (0.2)	8.2 (1.0)	5.1 (1.2)	7.2 (2.7)	10.8 (1.9)	5.6 (4.8)	5.6 (1.3)	3.8 (1.9)	-1.0 (1.9)	0.4 (2.2)	0.4 (1.9)	14.7 (1.9)	5.0
Modern Reference	10.9 (1.0)	4.6 (1.8)	8.3 (1.5)	5.8 (1.6)	8.7 (0.2)	12.8 (2.5)	-0.6 (0.1)	4.8 (2.0)	5.1 (1.7)	-0.6 (0.1)	0.5 (1.4)	1.0 (1.4)	17.7 (1.2)	7.8

Appendix 21: Progenesis QI abundance profiles of known drought metabolites from artificially aged maize.

Abscisic Acid



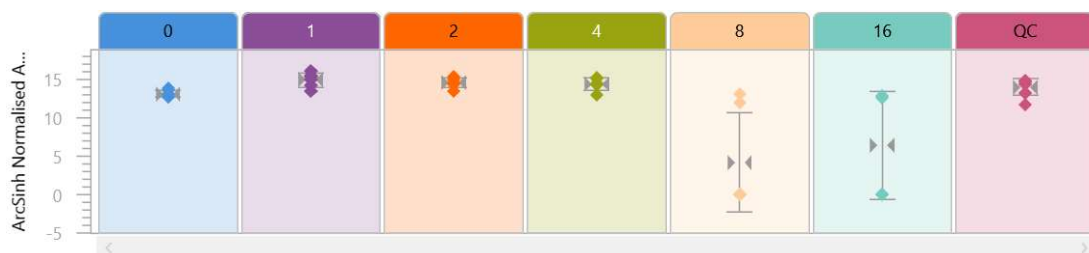
Caffeic Acid



Phenylalanine



Glutamic Acid



Hydroxyferulic Acid



Malic Acid



Dideoxy-L-galactose



List of Abbreviations

AA	Amino acid – each AA abbreviation given in appendix 19
ATR-IR	Attenuated total reflectance infrared spectroscopy
BBCH	Biologische Bundesanstalt, Bundessortenamt und Chemische Industrie
BP	Before present
CID	Collision induced dissociation
CoV	Coefficient of variation
CRM	Charge residue model
dc	Direct current
DCM	Dichloromethane
DNA	Deoxyribonucleic acid
EA	Elemental analysis
EIC	Extracted ion chromatogram
ESI	Electrospray ionisation
FTICR	Fourier transform ion cyclotron resonance
GC	Gas chromatography
GC-C-IR-MS	Gas chromatography-combustion-isotope ratio-mass spectrometry
GRIN	Germplasm resources information network
HCl	Hydrochloric acid
HCD	Higher-energy C-trap dissociation

HILIC	Hydrophilic interaction liquid chromatography
HPLC	High performance liquid chromatography
HRMS	High resolution mass spectrometry
IR	Isotope ratio
IEM	Ion evaporation model
IS	Internal standard
LC	Liquid chromatography
MS	Mass spectrometry
MS/MS	Tandem mass spectrometry
m/z	Mass-to-charge ratio
NaOH	Sodium hydroxide
PC	Principal component
PCA	Principal component analysis
PL-SDA	Partial least-squares discriminant analysis
RF	Radio frequency
RNA	Ribonucleic acid
ROS	Reactive oxygen species
RP	Reverse Phase
THAA	Total hydrolysable amino acid
t_R	Retention time
QC	Quality control

References

1. Shiferaw, B., Prasanna, B. M., Hellin, J. & Bänziger, M. Crops that feed the world 6. Past successes and future challenges to the role played by maize in global food security. *Food Security* **3**, 307 (2011).
2. Maitra, S. & Singh, V. Invited review on ‘maize in the 21st century’ Emerging trends of maize biorefineries in the 21st century: scientific and technological advancements in biofuel and bio-sustainable market. *J. Cereal Sci.* **101**, 103272 (2021).
3. Benson, L. V. & Berry, M. S. CLIMATE CHANGE AND CULTURAL RESPONSE IN THE PREHISTORIC AMERICAN SOUTHWEST. *Kiva* **75**, 87–117 (2009).
4. Bocinsky, R. K. & Kohler, T. A. A 2,000-year reconstruction of the rain-fed maize agricultural niche in the US Southwest. *Nat. Commun.* **5**, 5618 (2014).
5. Polyak, V. J. & Asmerom, Y. Late Holocene climate and cultural changes in the southwestern United States. *Science* **294**, 148–151 (2001).
6. Chaves, M. M., Maroco, J. P. & Pereira, J. S. Understanding plant responses to drought—from genes to the whole plant. *Funct. Plant Biol.* (2003).
7. Boyer, J. S. Plant productivity and environment. *Science* **218**, 443–448 (1982).
8. Lobell, D. B. *et al.* Prioritizing climate change adaptation needs for food security in 2030. *Science* **319**, 607–610 (2008).

9. Harrigan, G. G. *et al.* Impact of Genetics and Environment on Nutritional and Metabolite Components of Maize Grain. *Journal of Agricultural and Food Chemistry* vol. 55 6177–6185 (2007).
10. Wisser, R. J. *et al.* The Genomic Basis for Short-Term Evolution of Environmental Adaptation in Maize. *Genetics* **213**, 1479–1494 (2019).
11. Cabrera-Bosquet, L., Sánchez, C. & Araus, J. L. Oxygen isotope enrichment ($\Delta^{18}\text{O}$) reflects yield potential and drought resistance in maize. *Plant, Cell & Environment* vol. 32 1487–1499 (2009).
12. Jones, P. G. & Thornton, P. K. The potential impacts of climate change on maize production in Africa and Latin America in 2055. *Global Environmental Change* (2003) doi:10.1016/S0959-3780(02)00090-0.
13. Schmidhuber, J. & Tubiello, F. N. Global food security under climate change. *Proc. Natl. Acad. Sci. U. S. A.* **104**, 19703–19708 (2007).
14. Da Fonseca, R. R. *et al.* The origin and evolution of maize in the Southwestern United States. *Nature Plants* **1**, 14003 (2015).
15. Martin, P. S., Bluhm, E., Cutler, H. C., Grange, R. T. & Rinaldo, J. B. Mogollon cultural continuity and change; the stratigraphic analysis of Tularosa and Cordova Caves / [by] Paul S. Martin, Chief Curator, Department of Anthropology, et al. (1952) doi:10.5962/bhl.title.5156.
16. Woodhouse, C. A., Russell, J. L. & Cook, E. R. Two Modes of North American Drought from Instrumental and Paleoclimatic Data. *J. Clim.* **22**, 4336–4347 (2009).
17. Williams, D. G., Coltrain, J. B., Lott, M., English, N. B. & Ehleringer, J. R. Oxygen isotopes in cellulose identify source water for archaeological maize in the American Southwest. *J. Archaeol. Sci.* **32**, 931–939 (2005).

18. Cabrera-Bosquet, L., Sánchez, C. & Araus, J. L. Oxygen isotope enrichment ($\Delta^{18}\text{O}$) reflects yield potential and drought resistance in maize. *Plant Cell Environ.* **32**, 1487–1499 (2009).
19. Monneveux, P., Sheshshayee, M. S., Akhter, J. & Ribaut, J.-M. Using carbon isotope discrimination to select maize (*Zea mays* L.) inbred lines and hybrids for drought tolerance. *Plant Sci.* **173**, 390–396 (2007).
20. Shulaev, V., Cortes, D., Miller, G. & Mittler, R. Metabolomics for plant stress response. *Physiol. Plant.* **132**, 199–208 (2008).
21. Esau, K. *Anatomy of Seed Plants*. (Wiley, 1977).
22. Sage, R. F. The evolution of C_4 photosynthesis. *New Phytol.* **161**, 341–370 (2004).
23. Kistler, L. *et al.* Multiproxy evidence highlights a complex evolutionary legacy of maize in South America. *Science* **362**, 1309–1313 (2018).
24. Stitzer, M. C. & Ross-Ibarra, J. Maize domestication and gene interaction. *New Phytol.* **220**, 395–408 (2018).
25. Doebley, J. The Genetics of Maize Evolution. *Annu. Rev. Genet.* **38**, 37–59 (2004).
26. Doebley, J., Stec, A. & Gustus, C. teosinte branched1 and the origin of maize: Evidence for epistasis and the evolution of dominance. *Genetics* (1995).
27. Project MUSE - Maya Creation Myths.
<https://muse.jhu.edu/book/776>.
28. Piperno, D. R., Ranere, A. J. & Holst, I. Starch grain and phytolith evidence for early ninth millennium BP maize from the Central Balsas River Valley, Mexico. *Proceedings of the* (2009).

29. Matsuoka, Y. *et al.* A single domestication for maize shown by multilocus microsatellite genotyping. *Proc. Natl. Acad. Sci. U. S. A.* **99**, 6080–6084 (2002).
30. Van Heerwaarden, J. & Doebley, J. Genetic signals of origin, spread, and introgression in a large sample of maize landraces. *Proceedings of the* (2011).
31. Yamasaki, M., Wright, S. I. & McMullen, M. D. Genomic screening for artificial selection during domestication and improvement in maize. *Ann. Bot.* **100**, 967–973 (2007).
32. Hufford, M. B. *et al.* The genomic signature of crop-wild introgression in maize. *PLoS Genet.* **9**, e1003477 (2013).
33. Hufford, M. B. *et al.* Comparative population genomics of maize domestication and improvement. *Nat. Genet.* **44**, 808–811 (2012).
34. Yang, C. J. *et al.* The genetic architecture of teosinte catalyzed and constrained maize domestication. *Proc. Natl. Acad. Sci. U. S. A.* **116**, 5643–5652 (2019).
35. Merrill, W. L. *et al.* The diffusion of maize to the southwestern United States and its impact. *Proc. Natl. Acad. Sci. U. S. A.* **106**, 21019–21026 (2009).
36. Cairns, J. E. *et al.* Adapting maize production to climate change in sub-Saharan Africa. *Food Security* **5**, 345–360 (2013).
37. Southworth, J. *et al.* Consequences of future climate change and changing climate variability on maize yields in the midwestern United States. *Agriculture, Ecosystems and Environment* (2000) doi:10.1016/S0167-8809(00)00223-1.
38. Borlaug, N. Feeding a hungry world. *Science* **318**, 359 (2007).

39. Maroco, J. P., Pereira, J. S. & Manuela Chaves, M. Growth, photosynthesis and water-use efficiency of two C4Sahelian grasses subjected to water deficits. *J. Arid Environ.* **45**, 119–137 (2000).
40. Jackson, R. B., Sperry, J. S. & Dawson, T. E. Root water uptake and transport: using physiological processes in global predictions. *Trends Plant Sci.* **5**, 482–488 (2000).
41. O'Brien, M. J., Leuzinger, S., Philipson, C. D., Tay, J. & Hector, A. Drought survival of tropical tree seedlings enhanced by non-structural carbohydrate levels. *Nat. Clim. Chang.* **4**, 710–714 (2014).
42. Shabala, S. N. & Lew, R. R. Turgor regulation in osmotically stressed *Arabidopsis* epidermal root cells. Direct support for the role of inorganic ion uptake as revealed by concurrent flux and cell turgor measurements. *Plant Physiol.* **129**, 290–299 (2002).
43. Yang, L. *et al.* Deciphering drought-induced metabolic responses and regulation in developing maize kernels. *Plant Biotechnol. J.* **16**, 1616–1628 (2018).
44. Wang, B. *et al.* Effects of maize organ-specific drought stress response on yields from transcriptome analysis. *BMC Plant Biol.* **19**, 335 (2019).
45. Benson, L. & Berry, M. S. *Climate Change and Cultural Response In The Prehistoric American Southwest*. <https://digitalcommons.unl.edu/usgsstaffpub/725> (2009).
46. Periman, R. D. The influence of prehistoric Anasazi cobble-mulch agricultural features on northern Rio Grande landscapes. *Tech Coords. Desired Future Conditions for Southwestern Riparian Ecosystems: Bringing Interests and Concerns Together* 181–188 (1996).

47. Huckleberry, G. & Rittenour, T. Combining radiocarbon and single-grain optically stimulated luminescence methods to accurately date pre-ceramic irrigation canals, Tucson, Arizona. *J. Archaeol. Sci.* **41**, 156–170 (2014).
48. Doolittle, W. E. Agriculture in north America on the eve of contact: A reassessment. *Ann. Assoc. Am. Geogr.* **82**, 386–401 (1992).
49. Smoak, G. E. The Native West before 1700. in *The World of the American West* 70–101 (Routledge, 2010).
50. Nash, S. & Koons, M. Preliminary Results of AMS Radiocarbon Dating of Sandals from Tularosa Cave, NM. *Collected Papers from the 18th Biennial Mogollon Archaeology Conference*.
51. Rasmussen, J. B. T., Polyak, V. J. & Asmerom, Y. Evidence for Pacific-modulated precipitation variability during the late Holocene from the southwestern USA. *Geophys. Res. Lett.* **33**, L08701 (2006).
52. Tieszen, L. L. & Fagre, T. Carbon Isotopic Variability in Modern and Archaeological Maize. *J. Archaeol. Sci.* **20**, 25–40 (1993).
53. Benson, L. V. *et al.* Development and evaluation of geochemical methods for the sourcing of archaeological maize. *J. Archaeol. Sci.* **35**, 912–921 (2008).
54. Benson, L. V. Development and application of methods used to source prehistoric Southwestern maize: a review. *J. Archaeol. Sci.* **39**, 791–807 (2012).
55. Benson, L. *et al.* Ancient maize from Chacoan great houses: where was it grown? *Proc. Natl. Acad. Sci. U. S. A.* **100**, 13111–13115 (2003).
56. Johnson, K. D., Wright, D. R. & Terry, R. E. Application of carbon isotope analysis to ancient maize agriculture in the Petexbatún region of Guatemala. *Geoarchaeology* **22**, 313–336 (2007).

57. Webb, E. A., Schwarcz, H. P. & Healy, P. F. Detection of ancient maize in lowland Maya soils using stable carbon isotopes: evidence from Caracol, Belize. *Journal of Archaeological Science* vol. 31 1039–1052 (2004).
58. Webb, E. A. *et al.* Stable carbon isotope signature of ancient maize agriculture in the soils of Motul de San José, Guatemala. *Geoarchaeology* **22**, 291–312 (2007).
59. COP26-Presidency-Outcomes-The-Climate-Pact.pdf.
60. Jaenicke-Després, V. *et al.* Early allelic selection in maize as revealed by ancient DNA. *Science* **302**, 1206–1208 (2003).
61. Kennett, D. J. *et al.* High-precision chronology for Central American maize diversification from El Gigante rockshelter, Honduras. *Proc. Natl. Acad. Sci. U. S. A.* **114**, 9026–9031 (2017).
62. Fordyce, S. L. *et al.* Deep Sequencing of RNA from Ancient Maize Kernels. *PLoS One* **8**, e50961 (2013).
63. Das, S. S., Karmakar, P., Nandi, A. K. & Sanan-Mishra, N. Small RNA mediated regulation of seed germination. *Front. Plant Sci.* **6**, 828 (2015).
64. Miller, A. J. & Cramer, M. D. Root nitrogen acquisition and assimilation. *Plant Soil* **274**, 1–36 (2005).
65. Strong, D. T. & Fillery, I. R. P. Denitrification response to nitrate concentrations in sandy soils. *Soil Biol. Biochem.* **34**, 945–954 (2002).
66. Meng, L. *et al.* Arbuscular mycorrhizal fungi and rhizobium facilitate nitrogen uptake and transfer in soybean/maize intercropping system. *Front. Plant Sci.* **6**, 339 (2015).
67. Craine, J. M. *et al.* Ecological interpretations of nitrogen isotope ratios of terrestrial plants and soils. *Plant and Soil* vol. 396 1–26 (2015).

68. Craine, J. M. *et al.* Global patterns of foliar nitrogen isotopes and their relationships with climate, mycorrhizal fungi, foliar nutrient concentrations, and nitrogen availability. *New Phytol.* **183**, 980–992 (2009).
69. Amundson, R. *et al.* Global patterns of the isotopic composition of soil and plant nitrogen. *Global Biogeochem. Cycles* **17**, (2003).
70. Robinson, D. $\delta^{15}\text{N}$ as an integrator of the nitrogen cycle. *Trends Ecol. Evol.* **16**, 153–162 (2001).
71. Szpak, P. Complexities of nitrogen isotope biogeochemistry in plant-soil systems: implications for the study of ancient agricultural and animal management practices. *Front. Plant Sci.* **5**, 288 (2014).
72. Kriszan, M. *et al.* Revealing N management intensity on grassland farms based on natural $\delta^{15}\text{N}$ abundance. *Agric. Ecosyst. Environ.* **184**, 158–167 (2014).
73. Hogberg, P. Tansley Review No. 95. ^{15}N natural abundance in soil-plant systems. *New Phytol.* **137**, 179–203 (1997).
74. Szpak, P., Longstaffe, F. J., Millaire, J.-F. & White, C. D. Stable isotope biogeochemistry of seabird guano fertilization: results from growth chamber studies with maize (*Zea mays*). *PLoS One* **7**, e33741 (2012).
75. Subramanian, K. S. & Charest, C. Arbuscular mycorrhizae and nitrogen assimilation in maize after drought and recovery. *Physiol. Plant.* **102**, 285–296 (1998).
76. Ortiz, N., Armada, E., Duque, E., Roldán, A. & Azcón, R. Contribution of arbuscular mycorrhizal fungi and/or bacteria to enhancing plant drought tolerance under natural soil conditions: effectiveness of autochthonous or allochthonous strains. *J. Plant Physiol.* **174**, 87–96 (2015).
77. Styring, A. K. *et al.* Practical considerations in the determination of compound-specific amino acid $\delta^{15}\text{N}$ values in animal and plant tissues by

gas chromatography-combustion-isotope ratio mass spectrometry, following derivatisation to their N-acetylisopropyl esters. *Rapid Commun. Mass Spectrom.* **26**, 2328–2334 (2012).

78. Styring, A. K., Fraser, R. A., Bogaard, A. & Evershed, R. P. The effect of manuring on cereal and pulse amino acid $\delta^{15}\text{N}$ values. *Phytochemistry* **102**, 40–45 (2014).

79. Styring, A. K., Fraser, R. A., Bogaard, A. & Evershed, R. P. Cereal grain, rachis and pulse seed amino acid $\delta^{15}\text{N}$ values as indicators of plant nitrogen metabolism. *Phytochemistry* **97**, 20–29 (2014).

80. Ehleringer, J. R. & Dawson, T. E. Water uptake by plants: perspectives from stable isotope composition. *Plant, Cell and Environment* (1992) doi:10.1111/j.1365-3040.1992.tb01657.x.

81. Roden, J. S., Lin, G. & Ehleringer, J. R. A mechanistic model for interpretation of hydrogen and oxygen isotope ratios in tree-ring cellulose. *Geochim. Cosmochim. Acta* (2000) doi:10.1016/S0016-7037(99)00195-7.

82. Fraser, R. A. *et al.* Assessing natural variation and the effects of charring, burial and pre-treatment on the stable carbon and nitrogen isotope values of archaeobotanical cereals and pulses. *J. Archaeol. Sci.* **40**, 4754–4766 (2013).

83. DeNiro, M. J. & Hastorf, C. A. Alteration of $^{15}\text{N}/^{14}\text{N}$ and $^{13}\text{C}/^{12}\text{C}$ ratios of plant matter during the initial stages of diagenesis: Studies utilizing archaeological specimens from Peru. *Geochim. Cosmochim. Acta* **49**, 97–115 (1985).

84. Metcalfe, J. Z. & Mead, J. I. Do Uncharred Plants Preserve Original Carbon and Nitrogen Isotope Compositions? *Journal of Archaeological Method and Theory* 1–29 (2018).

85. Fiehn, O. Metabolomics - The link between genotypes and phenotypes. *Plant Mol. Biol.* (2002) doi:10.1023/A:1013713905833.
86. George G. Harrigan, *† *et al.* Metabolite Analyses of Grain from Maize Hybrids Grown in the United States under Drought and Watered Conditions during the 2002 Field Season. *J. Agric. Food Chem.* **55**, 6169–6176 (2007).
87. Röhlig, R. M., Eder, J. & Engel, K.-H. Metabolite profiling of maize grain: differentiation due to genetics and environment. *Metabolomics* **5**, 459 (2009).
88. Witt, S. *et al.* Metabolic and phenotypic responses of greenhouse-grown maize hybrids to experimentally controlled drought stress. *Mol. Plant* **5**, 401–417 (2012).
89. Richter, J. A., Erban, A., Kopka, J. & Zörb, C. Metabolic contribution to salt stress in two maize hybrids with contrasting resistance. *Plant Sci.* **233**, 107–115 (2015).
90. Sun, C., Gao, X., Fu, J., Zhou, J. & Wu, X. Metabolic response of maize (*Zea mays* L.) plants to combined drought and salt stress. *Plant and Soil* vol. 388 99–117 (2015).
91. Shen, Q. *et al.* Multi-omics analysis reveals molecular mechanisms of shoot adaption to salt stress in Tibetan wild barley. *BMC Genomics* **17**, 889 (2016).
92. Liu, F., Marshall, R. S. & Li, F. Understanding and exploiting the roles of autophagy in plants through multi-omics approaches. *Plant Sci.* **274**, 146–152 (2018).
93. Kopka, J., Fernie, A., Weckwerth, W., Gibon, Y. & Stitt, M. Metabolite profiling in plant biology: platforms and destinations. *Genome Biol.* **5**, 109 (2004).

94. Kim, H. K. & Verpoorte, R. Sample preparation for plant metabolomics. *Phytochemical Analysis* (2010) doi:10.1002/pca.1188.
95. Hamid, S. S., Wakayama, M., Soga, T. & Tomita, M. Drying and extraction effects on three edible brown seaweeds for metabolomics. doi:10.1007/s10811-018-1614-z.
96. Oikawa, A. *et al.* Effects of freeze-drying of samples on metabolite levels in metabolome analyses. *J. Sep. Sci.* **34**, 3561–3567 (2011).
97. Irchhaiya, R. *et al.* Metabolites in plants and its classification. *World Journal of Pharmacy and Pharmaceutical Sciences (WJPPS)* **4**, 287–305 (2015).
98. Yang, L. *et al.* Response of Plant Secondary Metabolites to Environmental Factors. *Molecules* **23**, (2018).
99. Hussein, R. A. & El-Anssary, A. A. Plants Secondary Metabolites: The Key Drivers of the Pharmacological Actions of Medicinal Plants. in *Herbal Medicine* (ed. Builders, P. F.) (IntechOpen, 2019).
100. viva. 12 Difference Between Primary And Secondary Metabolites With Examples. <https://vivadifferences.com/primary-vs-secondary-metabolites/> (2019).
101. Rai, V. K. Role of amino acids in plant responses to stresses. *Biol. Plant.* **45**, 481–487 (2002).
102. Wilkinson, S. & Davies, W. J. ABA-based chemical signalling: the co-ordination of responses to stress in plants. *Plant Cell Environ.* **25**, 195–210 (2002).
103. Srivastava, L. M. *Plant Growth and Development: Hormones and Environment*. 139–140 (Academic Press, 2002).
104. Cruz de Carvalho, M. H. Drought stress and reactive oxygen species: Production, scavenging and signaling. *Plant Signal. Behav.* **3**, 156–165 (2008).

105. Maixner, F. *et al.* The Iceman's Last Meal Consisted of Fat, Wild Meat, and Cereals. *Curr. Biol.* **28**, 2348-2355.e9 (2018).
106. Brownstein, K. J., Tushingham, S., Damitio, W. J., Nguyen, T. & Gang, D. R. An Ancient Residue Metabolomics-Based Method to Distinguish Use of Closely Related Plant Species in Ancient Pipes. *Front Mol Biosci* **7**, 133 (2020).
107. Zimmermann, M. *et al.* Metabolomics-based analysis of miniature flask contents identifies tobacco mixture use among the ancient Maya. *Sci. Rep.* **11**, 1590 (2021).
108. Sehgal, A. *et al.* Drought or/and Heat-Stress Effects on Seed Filling in Food Crops: Impacts on Functional Biochemistry, Seed Yields, and Nutritional Quality. *Front. Plant Sci.* **9**, 1705 (2018).
109. Ahmad, F., Singh, A. & Kamal, A. Osmoprotective role of sugar in mitigating abiotic stress in plants. *Protective Chemical Agents in the Amelioration of Plant Abiotic Stress* 53–70 (2020)
doi:10.1002/9781119552154.ch3.
110. Hall, R. *et al.* Plant metabolomics: the missing link in functional genomics strategies. *Plant Cell* **14**, 1437–1440 (2002).
111. Yadav, B., Jogawat, A., Rahman, M. S. & Narayan, O. P. Secondary metabolites in the drought stress tolerance of crop plants: A review. *Gene Reports* **23**, 101040 (2021).
112. Kalampokis, I. F. *et al.* Untargeted metabolomics as a hypothesis-generation tool in plant protection product discovery: Highlighting the potential of trehalose and glycerol metabolism of fungal conidiospores as novel targets. *Metabolomics* **16**, 79 (2020).

113. Naz, S., Vallejo, M., García, A. & Barbas, C. Method validation strategies involved in non-targeted metabolomics. *J. Chromatogr. A* **1353**, 99–105 (2014).
114. De Vos, R. *et al.* Untargeted large-scale plant metabolomics using liquid chromatography coupled to mass spectrometry Identification of metabolites View project metabolomics and metabolism View project Untargeted large-scale plant metabolomics using liquid chromatography coupled to mass spectrometry. (2007) doi:10.1038/nprot.2007.95.
115. Broadhurst, D. *et al.* Guidelines and considerations for the use of system suitability and quality control samples in mass spectrometry assays applied in untargeted clinical metabolomic studies. *Metabolomics* **14**, 72 (2018).
116. Gika, H. G., Theodoridis, G. A., Wingate, J. E. & Wilson, I. D. Within-day reproducibility of an HPLC-MS-based method for metabonomic analysis: application to human urine. *J. Proteome Res.* **6**, 3291–3303 (2007).
117. Sangster, T., Major, H., Plumb, R., Wilson, A. J. & Wilson, I. D. A pragmatic and readily implemented quality control strategy for HPLC-MS and GC-MS-based metabonomic analysis. *Analyst* **131**, 1075–1078 (2006).
118. Cubbon, S. J. LC-MS for the metabonomic study of human urine samples.
119. Rusilowicz, M., Dickinson, M., Charlton, A., O’Keefe, S. & Wilson, J. A batch correction method for liquid chromatography-mass spectrometry data that does not depend on quality control samples. *Metabolomics* **12**, 56 (2016).
120. Cubbon, S., Bradbury, T., Wilson, J. & Thomas-Oates, J. Hydrophilic Interaction Chromatography for Mass Spectrometric Metabonomic Studies of Urine. *Analytical Chemistry* vol. 79 8911–8918 (2007).

121. Kirkland, J. J. Development of some stationary phases for reversed-phase HPLC. *J. Chromatogr. A* **1060**, 9–21 (2004).
122. Chester, T. L. Recent developments in high-performance liquid chromatography stationary phases. *Anal. Chem.* **85**, 579–589 (2013).
123. Zhang, X. *et al.* Chromatographic evaluation of octadecyl-bonded SiO₂/SiO₂-based stationary phase for reversed-phase high performance liquid chromatography. *J. Inorg. Organomet. Polym. Mater.* **23**, 1445–1450 (2013).
124. Hemström, P. & Irgum, K. Hydrophilic interaction chromatography. *J. Sep. Sci.* **29**, 1784–1821 (2006).
125. Chang, Y. *et al.* A simultaneous extraction method for metabolome and lipidome and its application in cry1Ac and sck-transgenic rice leaf treated with insecticide based on LC–MS analysis. *Metabolomics* **10**, 1197–1209 (2014).
126. Alden, B. A. *et al.* Improvements in reversed-phase HPLC columns designed for polar compound retention: Introducing Atlantis T3 columns. <https://www.waters.com/content/dam/waters/en/app-notes/2006/WA43235/WA43235-ko.pdf>.
127. Yamashita, M. & Fenn, J. B. Electrospray ion source. Another variation on the free-jet theme. *J. Phys. Chem.* **88**, 4451–4459 (1984).
128. Kind, T. *et al.* Identification of small molecules using accurate mass MS/MS search. *Mass Spectrom. Rev.* **37**, 513–532 (2018).
129. Blaženović, I., Kind, T., Ji, J. & Fiehn, O. Software Tools and Approaches for Compound Identification of LC-MS/MS Data in Metabolomics. *Metabolites* **8**, (2018).

130. Schymanski, E. L. *et al.* Identifying Small Molecules via High Resolution Mass Spectrometry: Communicating Confidence. *Environ. Sci. Technol.* **48**, 2097–2098 (2014).
131. Progenesis QI. <https://www.nonlinear.com/progenesis/qi/>.
132. Kim, H.-Y. Analysis of variance (ANOVA) comparing means of more than two groups. *Restor. Dent. Endod.* **39**, 74–77 (2014).
133. Kao, L. S. & Green, C. E. Analysis of variance: is there a difference in means and what does it mean? *J. Surg. Res.* **144**, 158–170 (2008).
134. Saccenti, E., Hoefsloot, H. C. J., Smilde, A. K., Westerhuis, J. A. & Hendriks, M. M. W. B. Reflections on univariate and multivariate analysis of metabolomics data. *Metabolomics* (2014) doi:10.1007/s11306-013-0598-6.
135. Cambiaghi, A., Ferrario, M. & Masseroli, M. Analysis of metabolomic data: tools, current strategies and future challenges for omics data integration. *Brief. Bioinform.* **18**, 498–510 (2017).
136. Ludwig, C. & Günther, U. L. MetaboLab--advanced NMR data processing and analysis for metabolomics. *BMC Bioinformatics* **12**, 366 (2011).
137. Worley, B. & Powers, R. Multivariate Analysis in Metabolomics. *Current Metabolomics* **1**, 92–107 (2013).
138. Shahaf, N., Aharoni, A. & Rogachev, I. A Complete Pipeline for Generating a High-Resolution LC-MS-Based Reference Mass Spectra Library. *Methods Mol. Biol.* **1778**, 193–206 (2018).
139. Bruins, A. P. Mechanistic aspects of electrospray ionization. *J. Chromatogr. A* **794**, 345–357 (1998).
140. Nguyen, S. & Fenn, J. B. Gas-phase ions of solute species from charged droplets of solutions. *Proc. Natl. Acad. Sci. U. S. A.* **104**, 1111–1117 (2007).

141. Fernandez de la Mora, J. Electrospray ionization of large multiply charged species proceeds via Dole's charged residue mechanism. *Anal. Chim. Acta* **406**, 93–104 (2000).
142. Marshall, A. G., Hendrickson, C. L. & Jackson, G. S. Fourier Transform Ion Cyclotron Resonance Mass Spectrometry. in *Encyclopedia of Analytical Chemistry* (John Wiley & Sons, Ltd, 2006).
143. Paul, W. Electromagnetic traps for charged and neutral particles. *Rev. Mod. Phys.* **62**, 531–540 (1990).
144. Hecht, E. S., Scigelova, M., Eliuk, S. & Makarov, A. Fundamentals and advances of orbitrap mass spectrometry. *Encyclopedia of Analytical Chemistry* 1–40 (2019) doi:10.1002/9780470027318.a9309.pub2.
145. Olsen, J. V. *et al.* Higher-energy C-trap dissociation for peptide modification analysis. *Nat. Methods* **4**, 709–712 (2007).
146. Prathap, B., Dey, A., Srinivasa, R. G. H., Johnson, P. & Arthanariswaran, P. A Review - Importance of RP-HPLC in Analytical Method Development. *IJNTPS* **3**, 15–23 (2013).
147. Bigeleisen, J. Chemistry of Isotopes: Isotope chemistry has opened new areas of chemical physics, geochemistry, and molecular biology. *Science* **147**, 463–471 (1965).
148. Hofmann, A. E. *et al.* Using Orbitrap mass spectrometry to assess the isotopic compositions of individual compounds in mixtures. *Int. J. Mass Spectrom.* **457**, 116410 (2020).
149. Darragh, A. J., Garrick, D. J., Moughan, P. J. & Hendriks, W. H. Correction for amino acid loss during acid hydrolysis of a purified protein. *Anal. Biochem.* **236**, 199–207 (1996).
150. Silverman, S. N. *et al.* Practical considerations for amino acid isotope analysis. *Org. Geochem.* 104345 (2021).

151. Fonseca, R. R. da *et al.* The origin and evolution of maize in the Southwestern United States. *Nature Plants* vol. 1 (2015).
152. Grissino-Mayer, H. D. The rare, old-aged conifers of El Malpais-- Their role in understanding climatic change in the American Southwest
Henri D. Grissino-Mayer, Thomas W. Swetnam, and Rex K. Adams. *New Mexico Bureau of Mines & Mineral Resources, Bulletin* **156**, 155 (1997).
153. Stahle, D. W., Fye, F. K., Cook, E. R. & Griffin, R. D. Tree-ring reconstructed megadroughts over North America since a.d. 1300. *Clim. Change* **83**, 133–149 (2007).
154. Amundson, R. *et al.* Global patterns of the isotopic composition of soil and plant nitrogen. *Global Biogeochem. Cycles* **17**, (2003).
155. Chen, J., Xu, W., Velten, J., Xin, Z. & Stout, J. Characterization of maize inbred lines for drought and heat tolerance. *J. Soil Water Conserv.* **67**, 354–364 (2012).
156. Below, F. E., Cazetta, J. O. & Seebauer, J. R. Carbon/nitrogen interactions during ear and kernel development of maize. in *Physiology and Modeling Kernel Set in Maize* 15–24 (Crop Science Society of America and American Society of Agronomy, 2015).
157. Hirel, B., Martin, A., Terce-Laforgue, T., Gonzalez-Moro, M.-B. & Estavillo, J.-M. Physiology of maize I: A comprehensive and integrated view of nitrogen metabolism in a C₄ plant. *Physiol. Plant.* **124**, 167–177 (2005).
158. Takada, M., Niu, R., Minami, E. & Saka, S. Characterization of three tissue fractions in corn (*Zea mays*) cob. *Biomass Bioenergy* **115**, 130–135 (2018).
159. Benson, L. V. Factors Controlling Pre-Columbian and Early Historic Maize Productivity in the American Southwest, Part 1: The Southern Colorado Plateau and Rio Grande Regions. *Journal of Archaeological Method and Theory* **18**, 1–60 (2011).

160. Liu, S. *et al.* Genome-Wide Analysis of ZmDREB Genes and Their Association with Natural Variation in Drought Tolerance at Seedling Stage of *Zea mays* L. *PLoS Genet.* **9**, e1003790 (2013).
161. Schultz, J. A. & Juvik, J. A. Current models for starch synthesis and the sugary enhancer1 (se1) mutation in *Zea mays*. *Plant Physiol. Biochem.* **42**, 457–464 (2004).
162. Halford, N. G., Curtis, T. Y., Muttucumaru, N., Postles, J. & Mottram, D. S. Sugars in crop plants. *Ann. Appl. Biol.* **158**, 1–25 (2011).
163. Zhang, C. *et al.* Mechanisms for the relationships between water-use efficiency and carbon isotope composition and specific leaf area of maize (*Zea mays* L.) under water stress. *Plant Growth Regul.* **77**, 233–243 (2015).
164. Dercon, G., Clymans, E., Diels, J., Merckx, R. & Deckers, & J. Differential ¹³ C isotopic discrimination in maize at varying water stress and at low to high nitrogen availability. doi:10.1007/s11104-006-0001-8.
165. Lancashire, P. D. *et al.* A uniform decimal code for growth stages of crops and weeds. *Annals of Applied Biology* vol. 119 561–601 (1991).
166. Corr, L. T., Berstan, R. & Evershed, R. P. Optimisation of derivatisation procedures for the determination of delta¹³C values of amino acids by gas chromatography/combustion/isotope ratio mass spectrometry. *Rapid Commun. Mass Spectrom.* **21**, 3759–3771 (2007).
167. Azubuike, C. P., Rodríguez, H., Okhamafe, A. O. & Rogers, R. D. Physicochemical properties of maize cob cellulose powders reconstituted from ionic liquid solution. *Cellulose* **19**, 425–433 (2012).
168. Staff, R. A., Reynard, L., Brock, F. & Ramsey, C. B. Wood Pretreatment Protocols and Measurement of Tree-Ring Standards at the Oxford Radiocarbon Accelerator Unit (ORAU). *Radiocarbon* **56**, 709–715 (2014).

169. Godfray, H. C. J. *et al.* Food security: The challenge of feeding 9 billion people. *Science* vol. 327 812–818 (2010).
170. Harrigan, G. G. *et al.* Impact of environmental and genetic factors on expression of maize gene classes: Relevance to grain composition. *J. Food Compost. Anal.* **22**, 158–164 (2009).
171. Yancey, P. H. Organic osmolytes as compatible, metabolic and counteracting cytoprotectants in high osmolarity and other stresses. *J. Exp. Biol.* **208**, 2819–2830 (2005).
172. Vishwakarma, K. *et al.* Absciscic Acid Signaling and Abiotic Stress Tolerance in Plants: A Review on Current Knowledge and Future Prospects. *Front. Plant Sci.* **8**, 161 (2017).
173. Jogawat, A. *et al.* Crosstalk between phytohormones and secondary metabolites in the drought stress tolerance of crop plants: A review. *Physiol. Plant.* **172**, 1106–1132 (2021).
174. Savchenko, T. *et al.* Functional convergence of oxylipin and abscisic acid pathways controls stomatal closure in response to drought. *Plant Physiol.* **164**, 1151–1160 (2014).
175. Fountain, J. C. *et al.* Oxidative stress and carbon metabolism influence *Aspergillus flavus* transcriptome composition and secondary metabolite production. *Sci. Rep.* **6**, 38747 (2016).
176. Dunn, W. B. & Ellis, D. I. Metabolomics: Current analytical platforms and methodologies. doi:10.1016/j.trac.2004.11.021.
177. Fu, J. H., Sun, X. H., Wang, J. D., Chu, J. F. & Yan, C. Y. Progress in quantitative analysis of plant hormones. *Chinese Science Bulletin* vol. 56 355–366 (2011).
178. Cubbon, S., Antonio, C., Wilson, J. & Thomas-Oates, J. Metabolomic applications of HILIC-LC-MS. *Mass Spectrom. Rev.* **29**, 671–684 (2010).

179. Marti, G. *et al.* Metabolomics reveals herbivore-induced metabolites of resistance and susceptibility in maize leaves and roots. *Plant Cell Environ.* **36**, 621–639 (2013).
180. Zhu, D., Kebede, B., Chen, G., McComb, K. & Frew, R. Impact of freeze-drying and subsequent storage on milk metabolites based on ¹H NMR and UHPLC-QToF/MS. *Food Control* **116**, 107017 (2020).
181. Cheng, K., Brunius, C., Fristedt, R. & Landberg, R. An LC-QToF MS based method for untargeted metabolomics of human fecal samples. *Metabolomics* **16**, 46 (2020).
182. Zhou, R. *et al.* A New Absciscic Acid Catabolic Pathway. *Plant Physiol.* **134**, 361–369 (2004).
183. Santiago Da Silva, C. M., Habermann, G., Marchi, M. R. R. & Zocolo, G. J. *The role of matrix effects on the quantification of abscisic acid and its metabolites in the leaves of Bauhinia variegata L. using liquid chromatography combined with tandem mass spectrometry.* vol. 24 223–232 (2012).
184. Korovetska, H., Novák, O., Turečková, V., Hájíčková, M. & Gloser, V. Signalling mechanisms involved in the response of two varieties of *Humulus lupulus* L. to soil drying: II. changes in the concentration of abscisic acid catabolites and stress-induced phytohormones. *Plant Growth Regul.* **78**, 13–20 (2016).
185. Gigon, A., Matos, A. R., Laffray, D., Zuily-Fodil, Y. & Pham-Thi, A. T. Effect of drought stress on lipid metabolism in the leaves of *Arabidopsis thaliana* (Ecotype Columbia). *Ann. Bot.* **94**, 345–351 (2004).
186. Laxalt, A. M. & Munnik, T. Phospholipid signalling in plant defence. *Current Opinion in Plant Biology* vol. 5 332–338 (2002).
187. Xue, H. W., Chen, X. & Mei, Y. Function and regulation of phospholipid signalling in plants. *Biochemical Journal* vol. 421 145–156 (2009).

188. Kamara, A. Y., Menkir, A., Badu-Apraku, B. & Ibikunle, O. The influence of drought stress on growth, yield and yield components of selected maize genotypes. *J. Agric. Sci.* **141**, 43–50 (2003).
189. Markova, G., Baas, S., Conforti, P., Ahmed, S. & Others. 2017: the impact of disasters and crises on agriculture and food security. *2017: the impact of disasters and crises on agriculture and food security.* (2018).
190. Wang, J., Vanga, S. K., Saxena, R., Orsat, V. & Raghavan, V. Effect of Climate Change on the Yield of Cereal Crops: A Review. *Climate* **6**, 41 (2018).
191. Harrigan, G. G. *et al.* Metabolite analyses of grain from maize hybrids grown in the United States under drought and watered conditions during the 2002 field season. *J. Agric. Food Chem.* **55**, 6169–6176 (2007).
192. Xu, G. *et al.* Evolutionary Metabolomics Identifies Substantial Metabolic Divergence between Maize and Its Wild Ancestor, Teosinte. *Plant Cell* **31**, 1990–2009 (2019).
193. Nash, S. Koons and Nash AMS Tularosa Sandals 2015.
194. Gaffney, I., Sallach, J. B., Wilson, J., Bergström, E. & Thomas-Oates, J. Metabolomic Approaches to Studying the Response to Drought Stress in Corn (*Zea mays*) Cobs. *Metabolites* **11**, (2021).
195. Abdullah, F. I., Chua, L. S. & Rahmat, Z. Prediction of C-glycosylated apigenin (vitexin) biosynthesis in *Ficus deltoidea* based on plant proteins identified by LC-MS/MS. *Front. Biol.* **12**, 448–458 (2017).
196. Buszewski, B. & Noga, S. Hydrophilic interaction liquid chromatography (HILIC)--a powerful separation technique. *Anal. Bioanal. Chem.* **402**, 231–247 (2012).
197. Piasecka, A., Kachlicki, P. & Stobiecki, M. Analytical Methods for Detection of Plant Metabolomes Changes in Response to Biotic and Abiotic Stresses. *Int. J. Mol. Sci.* **20**, (2019).

198. Dawid, C. & Hille, K. Functional Metabolomics—A Useful Tool to Characterize Stress-Induced Metabolome Alterations Opening New Avenues towards Tailoring Food Crop Quality. *Agronomy* **8**, 138 (2018).
199. Styring, A. K. *et al.* The effect of charring and burial on the biochemical composition of cereal grains: investigating the integrity of archaeological plant material. *J. Archaeol. Sci.* **40**, 4767–4779 (2013).
200. Gaffney, I., Sallach, J. B., Wilson, J., Bergström, E. & Thomas-Oates, J. Metabolomic Approaches to Studying the Response to Drought Stress in Corn (*Zea mays*) Cobs. *Metabolites* **11**, (2021).
201. Hedges, R. E. M. Bone diagenesis: an overview of processes. *Archaeometry* **44**, 319–328 (2002).
202. Wilson, L. & Pollard, A. M. Here today, gone tomorrow? integrated experimentation and geochemical modeling in studies of archaeological diagenetic change. *Acc. Chem. Res.* **35**, 644–651 (2002).
203. Balzer, A. *et al.* In vitro decomposition of bone collagen by soil bacteria: The implications for stable isotope analysis in archaeometry. *Archaeometry* **39**, 415–429 (1997).
204. Almendros, G. & Dorado, J. Molecular characteristics related to the biodegradability of humic acid preparations. *Eur. J. Soil Sci.* **50**, 227–236 (1999).
205. Nielsen-Marsh, C. M. & Hedges, R. E. M. Patterns of Diagenesis in Bone I: The Effects of Site Environments. *J. Archaeol. Sci.* **27**, 1139–1150 (2000).
206. Hartman, G. *et al.* Post-charring diagenetic alteration of archaeological lentils by bacterial degradation. *J. Archaeol. Sci.* **117**, 105119 (2020).
207. Xin, X. *et al.* Proteome analysis of maize seeds: the effect of artificial ageing. *Physiol. Plant.* **143**, 126–138 (2011).

208. McDonough, C. M., Floyd, C. D., Waniska, R. D. & Rooney, L. W. Effect of accelerated aging on maize, sorghum, and sorghum meal. *J. Cereal Sci.* **39**, 351–361 (2004).
209. McCudden, C. R. & Kraus, V. B. Biochemistry of amino acid racemization and clinical application to musculoskeletal disease. *Clin. Biochem.* **39**, 1112–1130 (2006).
210. Ohtani, S. & Yamamoto, K. Age estimation using the racemization of amino acid in human dentin. *J. Forensic Sci.* **36**, 792–800 (1991).
211. Ohtani, S. & Yamamoto, T. Age estimation by amino acid racemization in human teeth. *J. Forensic Sci.* **55**, 1630–1633 (2010).
212. Grishin, D. V., Zhdanov, D. D., Pokrovskaya, M. V. & Sokolov, N. N. D-amino acids in nature, agriculture and biomedicine. *All Life* **13**, 11–22 (2020).
213. Kaufman, D. S. & Manley, W. F. A new procedure for determining dl amino acid ratios in fossils using reverse phase liquid chromatography. *Quat. Sci. Rev.* **17**, 987–1000 (1998).
214. Monera, O. D., Sereda, T. J., Zhou, N. E., Kay, C. M. & Hodges, R. S. Relationship of sidechain hydrophobicity and alpha-helical propensity on the stability of the single-stranded amphipathic alpha-helix. *J. Pept. Sci.* **1**, 319–329 (1995).